Development and Study of the Microfluidic Open Interface Coupled with Solid-phase Microextraction for Rapid Analysis

by

Emir Nazdrajić

A thesis

presented to the University of Waterloo

in fulfillment of the

thesis requirement for the degree of

Doctor of Philosophy

in

Chemistry

Waterloo, Ontario, Canada, 2022

Examining Committee Membership

The following served on the Examining Committee for this thesis. The decision of the Examining Committee is by majority vote.

External examiner	Dr. Robert B. Cody Principal Scientist JEOL USA, Inc.
Supervisor	Prof. Janusz Pawliszyn University Professor and Canada Research Chair Department of Chemistry, University of Waterloo
Internal Member	Prof. Shirley Tang Professor and Associate Dean of Science Department of Chemistry, University of Waterloo
Internal Member	Prof. Germán Sciaini Associate Professor and Canada Research Chair Department of Chemistry, University of Waterloo
Internal-external Member	Prof. Sushanta Mitra University Professor Department of Mechanical and Mechatronics Engineering, Physics and Astronomy

Author's Declaration

This thesis consists of material all of which I authored or co-authored: see Statement of Contributions included in the thesis. This is a true copy of the thesis, including any required final revisions, as accepted by my examiners.

I understand that my thesis may be made electronically available to the public.

Statement of Contributions

Chapter 2 is not published, but the material is being prepared for submission to the Journal of American Society for Mass Spectrometry special edition "High-throughput in Mass Spectrometry." Khaled Murtada has prepared the slurries used for the coating of SPME devices. Hernando Rosales has assisted in operating Thermo TSQ Vantage and Thermo TSQ Quantiva and setting up MS methods. Daniel Rickert assisted with experiments and running the microfluidic open interface coupled to SCIEX API 4000 MS. Victor Galievsky assisted in incorporating the photointerrupter into the design of the microfluidic open interface. Parts of the microfluidic open interface (building all electronic components and machining components for the microfluidic open interface design) have been made in the University of Waterloo Science Technical Services. Emir Nazdrajić has performed coating of all SPME fibers, has built prototype software for the operation of the microfluidic open interface, has adjusted the designs of the electrospray capillary assemblies and other ionization source adjustments required for coupling microfluidic open interface to different MS instruments, has run all experimental work with Shimadzu LCMS 8060. Emir Nazdrajić also did all data processing while Janusz Pawliszyn assisted data interpretation. Janusz Pawliszyn supervised the whole MOI development.

The content of **Chapter 3** has been published as a research article: Nazdrajić, E.; Murtada, K.; Pawliszyn, J.B. The Effect of Sorbent Particles in a Binder on the Mass Transfer Kinetics in Separation Media: *in-silico* Study and Experimental Verification. *Anal. Chem.* **2021**, *93, 44*, 14764 - 14772. (https://doi.org/10.1021/acs.analchem.1c03373) The content of this research article has been reprinted with permission of ACS Publications, and it follows ACS Publications and University of Waterloo policies.

In **Chapter 3**, Emir Nazdrajić and Khaled Murtada contributed approximately equally by participating in all aspects from experimental design, conduction of experiments, data processing, data interpretation, and manuscript writing. Emir Nazdrajić did all COMSOL modeling. Janusz Pawliszyn assisted in data interpretation and supervision of the whole project.

The content of **Chapter 4** has been published as a research article: Nazdrajić, E.; Tascon, M.; Rickert, D.A.; Gómez-Ríos, G.A.; Kulasingam, V.; Pawliszyn, J.B. Rapid Determination of Tacrolimus and Sirolimus in Whole Human Blood by Direct Coupling of Solid-phase Microextraction via Microfluidic Open Interface. *Anal. Chim. Acta* **2021**, *1144*, 53-60. (https://doi.org/10.1016/j.aca.2020.11.056) The content of this research article has been reprinted with the permission of Elsevier, and it follows Elsevier and University of Waterloo policies.

The contribution of Marcos Tascon was project design, conduction of the initial experiment, *i.e.*, imprecision of the calibration plot slopes, and assistance in data interpretation. Daniel A. Rickert contributed to the project design and assisted in data interpretation. German A. Gómez-Ríos contributed to the project design and assisted in data interpretation. The contribution of Vathany Kulasingam was project design, assisted in data interpretation, and kindly provided residual whole blood samples of patients undergoing immunosuppression therapy at University Health Network, Toronto, Ontario, Canada. The rest of the experimental work, project design, data processing, data interpretation, and manuscript writing were completed by Emir Nazdrajić.

The content of **Chapter 5** has not yet been published yet. The work is being prepared for submission to an academic journal. Daniel Rickert has assisted Emir Nazdrajić with experimental design, preparation for the experiments, performing experiments, and analysis using the microfluidic open interface. Daniel Rickert and Janusz Pawliszyn assisted Emir Nazdrajić in data interpretation. Janusz Pawliszyn supervised the whole project.

The content of **Chapter 6** is not published yet; however, the goal is to publish it soon with a few additional experiments. The University of Waterloo Science Technical Services constructed the homemade electronic circuits. Victor Galievsky assisted in incorporating photointerrupters into the MOI design, assembling the electronic circuit around NI-DAQ, and fitting the optical fibers into standardized nuts for a four-way chromatographic tee. The rest, which includes SPME fiber coating, prototype software development,

experimental procedure, analysis, and data processing have been done by Emir Nazdrajić. Janusz Pawliszyn assisted Emir Nazdrajić in data interpretation. Janusz Pawliszyn supervised the whole project.

Abstract

Analytical chemistry mainly aims to identify and quantify analytes in matrices of interest. Analytical chemistry is an indispensable part of chemistry (and other scientific fields) because identification and quantification rely on repeatable and accurate measurements. Today's gold-standard systems for trace analysis are mainly chromatographic systems (liquid chromatography or gas chromatography) coupled to mass spectrometry. These methods attained the gold-standard status because of the overall method sensitivity and selectivity abilities. However, the main weakness of these systems is that they often require extensive sample preparation to reach outstanding performance regarding selectivity and sensitivity.

Nevertheless, the chromatography step can be lengthy when selectivity is needed. Mass spectrometry has improved over the years, encouraging researchers to introduce samples directly to mass spectrometry, thus circumventing chromatographic separation. This field became known as direct-to-mass spectrometry. One of the main aims of this field is to avoid lengthy chromatography time and practically have real-time monitoring or high-throughput/rapid analysis of analytes at trace levels with little or no (laborious) sample preparation. However, these approaches serve only as the first line of study (rapid screening step), after which positive samples are submitted for thorough analysis using a gold-standard method. One of the main disadvantages of direct-to-mass spectrometry analysis is susceptibility to matrix effects (due to lack of separation), which internal standards can somewhat mitigate. Another disadvantage is instrument contamination resulting from inadequate or no sample preparation that is sacrificed for the overall rapid analysis. The most suitable sample preparation for direct-to-mass spectrometry analysis is solid-phase microextraction. It is a method developed to perform sampling and sample preparation in a single cohesive step. One of the advantages of this method is the non-exhaustive enrichment. The main advantages of this sample preparation method include using matrix-compatible coating, which offers analyte enrichment with minimal or no matrix interference co-enrichment.

Additionally, the open-bed enrichment of solid-phase microextraction offers avenues for high-throughput sample preparation steps that minimize the overall analytical workflow time. When such analysis is used for the direct-to-mass spectrometry analysis, the general analytical workflow time is reduced by avoiding chromatography. Solid-phase microextraction has been coupled directly to mass spectrometry in many ways. One of the ways solid-phase microextraction can be coupled directly to the mass spectrometry is via a microfluidic open interface. The microfluidic open interface system coupled to mass spectrometry comprises a suction component (created by the ionization source of a mass spectrometer), an inflow component (pumping system), and a desorption chamber. All three components connect to a three-way chromatographic tee. The main requirement is that the suction component is constant. The liquid level in the desorption chamber can be introduced to the mass spectrometer by changing the inflow. Solid-phase microextraction devices (after the enrichment step) are then introduced to the very low-volume desorption chamber for analysis. The inflow stops after a short desorption time (e.g., 5 s). The suction component aspirates the volume of the desorption chamber, thus injecting the solution into the mass spectrometer for the analysis. The main highlights of the microfluidic open interface coupled to a mass spectrometer are desorption in a flow-isolated system and desorption into a low volume, which provides a tall Gaussian peak.

The overall objective of this thesis is to redesign the microfluidic open interface system to demonstrate automation of the analysis workflow and make it suitable for rapid analysis.

Firstly, **Chapter 2** identifies the disadvantages of the existing microfluidic open interface system, which are used to improve the next design. The new system contains commonly available material to make the system approachable. Additionally, all system components are automated (by writing a homemade program from scratch), reducing the error from the manual operation. Nevertheless, this chapter depicts how the solid-phase microextraction coating design is essential for optimal desorption and analysis sensitivity. **Chapter 3** expands on the fundamental idea raised towards the end of **Chapter 2** by quantifying the mass transfer resistance in separation media. The effect of sorbent in matrix-compatible binders is crucial to understand for some applications. The extraction (or the desorption) of analytes will be controlled by the

effective diffusion coefficient in the coating rather than at the interface or boundary layer, as it was a most common assumption before. The following two chapters, **Chapter 4** and **Chapter 5**, contain applications that utilize the two designs of the microfluidic open interface for the analysis of immunosuppressive drugs and fentanyl analytes from the whole blood, respectively. For both works, the sample preparation is done in a high-throughput fashion. After the analysis with a microfluidic open interface, the overall method times (per sample) are substantially lower than gold-standard methods reported in the literature while maintaining similar detection and quantification limits compared to state-of-the-art reported methods. Therefore, solid-phase microextraction coupled directly to mass spectrometry via a microfluidic open interface offers a suitable replacement for a gold-standard method. **Chapter 6** contains an alternative and simplified use of the microfluidic open interface coupled to the homemade ultraviolet-visible light detection system. Finally, **Chapter 7** encompasses the main findings and offers a future perspective on using solid-phase microextraction with a microfluidic open interface coupled directly to mass spectrometry or an alternative detector, such as ultraviolet-visible light detection.

Acknowledgments

I would like to take this opportunity to express my appreciation to all who have supported and assisted me in completing the degree.

Firstly, I would like to express my deepest gratitude to my supervisor, Professor Janusz Pawliszyn, for allowing me to work in his research group. I am sincerely grateful for being allowed to join his research group directly from my B.Sc. degree, for having been involved in many exciting projects, and for having been allowed to participate in scientific meetings. Thank you for constructive criticism, academic guidance, and endless support.

Secondly, I would like to extend my gratitude to my committee members, Professor Shirley Tang and Professor Germán Sciaini, for the time and effort invested in my thesis development, guidance, and advice. I would also like to extend this gratitude to Professor Terry B. McMahon. Finally, I would also like to thank the external examiner, Dr. Robert B. Cody, and the internal-external examiner, Prof. Sushanta Mitra, for accepting the invitation to evaluate my work and for the time and effort spent on this thesis.

Furthermore, I would like to express my gratitude to Pawliszyn Research Group colleagues who have helped tremendously in different ways during the program including (alphabetically listed) Dr. Diana Marcela Cárdenas-Soracá, Dr. Victor Galievsky, Dr. Chiranjit Ghosh, Dr. German Augusto Gómez-Ríos, M. Sc. Dominika Gruszecka, Dr. Mohammad Huq, Dr. Sofia Lendor, Dr. Nikita Looby, Dr. Khaled Murtada, M. Sc. Paola Alejandra Ortiz Suarez, M. Sc. Daniel Rickert, Mr. Hernando Fabian Alonso Rosales Solano, Dr. Varoon Singh, Dr. Kanchan Sinha Roy, Dr. Marcos Tascon, M. Sc. Milaan Thirukumaran, and Dr. Tijana Vasiljević, and others.

Additionally, I am grateful to the University of Waterloo Science Technical Services, especially to Mr. Krunomir Dvorski and Mr. Hiruy Haile, for the great help and guidance provided during the degree. Finally, I would like to extend my gratitude to Ms. Catherine Van Esch and Ms. Kim Rawson, graduate

administrative coordinators of the Department of Chemistry, for their assistance and support during the degree.

Nevertheless, I would like to thank (industrial/academic) collaborators for crucial project discussions, including (listed alphabetically) Dr. Yohei Arao, Dr. Achille Cappiello (and his research group), Dr. Vathany Kulasingam, Dr. Nishimura Masayuki, Dr. Tairo Ogura, and Dr. Olga Shimelis (and her team at Millipore Sigma).

Lastly, I would like to extend my deepest gratitude to my parents, Ševko and Fika Nazdrajić, and siblings, Belma, Amar, and Benjamin, for their endless love, support, and motivation.

Dedication

I dedicate this thesis to

my parents; Fika and Ševko Nazdrajić

my siblings; Belma, Amar, and Benjamin

and my family and friends that have always supported me

for their love, understanding, and support throughout my career.

Ex nihilo nihil fit

Table of Contents

List of Figures

List of Tables

List of Abbreviations

ADE-OPI – acoustic droplet ejection open port interface

CBS – coated blade spray

CMIA – chemiluminescent microparticle immunoassay

CYC – cyclosporine A

DART – direct analysis in real time

DBDI – dielectric barrier discharge

DESI – desorption electrospray ionization

direct-to-MS – direct introduction to mass spectrometry

DI-SPME – direct immersion format solid-phase microextraction

ESI – electrospray ionization

EVE - everolimus

FEP – fluorinated ethylene propylene

FID – flame ionization detection

GC – gas chromatography

HLB – hydrophilic-lipophilic balance

HS-SPME – headspace format solid-phase microextraction

ISD – immunosuppressive drugs

LC – liquid chromatography

LLE – liquid-liquid extraction

LOD – limit of detection

LOQ – limit of quantitation

LPME – liquid-phase microextraction

MS – mass spectrometry

MS/MS – tandem mass spectrometry

MOI – microfluidic open interface

nanoESI – nano electrospray ionization

OPSI – open port sampling interface

PAN - polyacrylonitrile

PBS – phosphate buffer saline

PDMS - polydimethylsiloxane

PDMS-CAR – polydimethylsiloxane carboxen mixed-phase sorbent

PDMS-CWR – polydimethylsiloxane carbon wide-range mixed-phase sorbent

PDMS-DVB – polydimethylsiloxane divinylbenzene mixed-phase sorbent

PEEK – polyether ether ketone

PESI – probe electrospray ionization

PS – paper spray

PTFE – polytetrafluoroethylene

PVDF – polyvinylidene fluoride

QC – quality control

SBSE – stir bar sorptive extraction

SCX – strong cation exchange

SGGS – standard gas generating system

SIR - sirolimus

SLPM – standard liters per minute

SPE – solid-phase extraction

SPME – solid-phase microextraction

TAC – tacrolimus

TWA – time-weighted average

List of Symbols

a – SPME device support thickness, [m]

b – SPME device total thickness, [m]

C^0 – initial concentration, [mol m^{-3}]

C_E – analyte extraction phase concentration, [mol m^{-3}]

C_P – analyte concentration in the sorbent, [mol m^{-3}]

C_{PDMS} – analyte concentration in PDMS, [mol m^{-3}]

C_S – analyte sample phase concentration, [mol m^{-3}]

d – diameter, [m]

D – analyte diffusion coefficient, [m^2 s^{-1}]

D_E – analyte diffusion coefficient in the extraction phase, [m^2 s^{-1}]

D_{eff} – analyte effective diffusion coefficient, [m^2 s^{-1}]

D_S – analyte diffusion coefficient in the sample phase, [m^2 s^{-1}]

k – phase capacity, [unitless]

K_{ES}, K_{FS} – analyte distribution constant between extraction phase and sample phase, [unitless]

$K_{P/PDMS}$ – analyte distribution constant between sorbent phase and PDMS, [unitless]

L, l – length, [m]

M – arbitrary parameter, [m s^{-1}]

M_∞– the amount of analyte extracted at equilibrium, [mol]

M_t – the amount of analyte at time = t, [mol]

n – the amount of analyte, [mol]

n_P – the amount of analytes in the sorbent phase, [mol]

n_{PDMS} – the amount of analytes in PDMS, [mol]

P – pressure, [Pa]

Q – volumetric flow rate, [$m^3\ s^{-1}$]

q_n – arbitrary parameter [unitless]

r – radius, [m]

Re – Reynolds number, [unitless]

t – time, [s]

t_e – time at equilibrium, [s]

u – sample phase velocity, [$m\ s^{-1}$]

V_F – the volume of the fiber, [m^3]

V_{PDMS} – the volume of the PDMS, [m^3]

V_S – the volume of the sample phase, [m^3]

α – arbitrary parameter, [unitless]

δ – boundary layer thickness, [m]

μ - dynamic viscosity, [Pa s]

ρ – solution density, [$g\ m^{-3}$]

σ – mean squared displacement, [m]

Chapter 1: Introduction

1.1. Analytical chemistry and analytical workflow

Analytical chemistry concerns quantitative and qualitative measurements of analytes in matrices of interest.[1] It is an integral part of chemistry and other science areas because all scientific progress relies on accurate and reproducible data measurements compiled for results and further interpretation. Analytical chemistry spawns the analysis of everyday samples such as foods (*e.g.*, determine protein or fat content), blood (e.g., assess alcohol content), and soil (*e.g.*, break down soil composition on planet Mars). Some applications require speedy (rapid) analysis because knowing the results in real-time or as soon as possible can be crucial. The analysis process (or the analytical workflow) consists of several steps: sampling, sample preparation, separation, quantitation, statistical evaluation, and decision making.[2] Each of these steps is vital in the overall process. The sampling process is obtaining a small amount of material whose composition represents the bulk of the sampled material.[1] The objective of sample preparation is to isolate and enrich analytes from the sample matrix because most instrumentation cannot directly handle very dirty and complex samples.[2] This step is critical also because analytes must be concentrated to satisfactory levels to be analyzed quantitatively or qualitatively. The next step, separation (chromatography), aims to isolate components of complex extracts so that the analytes during the analysis are free of interferences.[2] Other steps include quantitation (determination of the amount of analytes present), statistical evaluation (assessment of data obtained and process into meaningful results into interpretation), and finally, the decision-making step.[2] As described, the analytical workflow consists of several steps that must be completed sequentially. The subsequent step cannot begin without finishing the previous step; therefore, the slowest step in the whole process determines the overall speed. Many efforts have been put into speeding up different parts of the analytical workflow to make the overall analysis process rapid. Instrumental analysis using mass spectrometry is one of the effort areas where improvements have been made. A lot of advancements in mass spectrometry have been made since their invention. Instruments have been simplified even to portable versions. Due to mass spectrometry's characteristics, it gained a unique position among

analytical methods because of its unequaled sensitivity, detection limits, speed, and diversity of applications.[3] However, a separation step is required to maintain their sensitivity and have analysis free of interferences. The classical separation methods (*e.g.*, liquid and gas chromatography coupled to mass spectrometry) can take 10 and 30 minutes to analyze a sample.[4] Newer separation methods can be reduced to as low as the range of 0.5 and 5 min while having a decent degree of separation.[5–7] Although the separation times of some chromatography methods have decreased, some separation between analytes and interferences is obtained. Moreover, internal standards (isotopically labeled analogs) can be used to correct (up to some degree) the overall matrix effects because internal standards will experience the same degree of *interference* during the analysis.

1.2. Direct-to-mass spectrometry analysis: avenues of rapid analysis

Chromatographic systems coupled to mass spectrometry are the gold standard methods due to overall sensitivity and selectivity capabilities. The main disadvantage of these methods is the lengthy chromatography time. Typically, analysis sequences need to include calibration standards, blanks, quality controls, and samples. They might require very laborious sample preparation before the separation step, which ensures desired chromatographic selectivity, sensitivity, and compatibility with the mass spectrometry (MS).[8,9] On the other hand, there have been improvements and attempts in direct-to-mass spectrometry (direct-to-MS) analysis which has gained popularity in many fields. These fields include metabolomics, forensics, pharmaceutical drug development, etc.[10] These approaches aim to circumvent lengthy chromatography time and practically have real-time monitoring or high-throughput/rapid analysis of analytes at trace levels with little or no (laborious) sample preparation. The simplest method for introducing samples to the mass spectrometer is a dilute-shoot method, where a diluted sample (if compatible with MS) is introduced directly via flow-injection analysis.[11] On the other hand, a sub-field of direct-to-MS analysis termed ambient MS has become very popular.[12–14]

Since the invention of desorption electrospray ionization (DESI) in 2004, researchers across the world have invested their efforts into becoming creative in introducing samples directly to MS.[15] In general, ambient-

MS methods can be divided into a couple of categories according to the desorption/ionization mechanisms: solvent, laser, vibrational, acoustic, thermal, and plasma.[13] Liquid-based desorption/ionization mechanisms include methods like DESI and paper spray (PS) that have been very popular. DESI has seen the most success with analyses of surfaces because it is performed by spraying solution onto a surface from which nebulized droplets (into which surface analytes extract) bounce off towards the MS inlet.[16] This method allows for (sectional) tissue analysis, and the concentration of analytes in different parts of the tissue (or any other flat surface sample) can be analyzed. On the other hand, PS works by depositing and allowing a sample to dry onto a piece of triangular paper, after which a spray solvent is added, and voltage is applied to introduce analytes into MS.[17] This method is very susceptible to introducing interfering species (e.g., salts), thus compromising the signal. However, an isotopically labeled standard can be added to a spray solution and produce quantitative analysis. An alternative popular desorption/ionization mechanism is plasma desorption. The first plasma-based ambient ionization technique is direct analysis in real time (DART) which operates by exciting heated carrier gas (typically He, Ar, or N_2) which ionizes molecules thermally desorbed from device or sample placed in front of the MS inlet..[18] Although simple in principle, this method is suitable for volatile compounds at a narrow molecular mass range.[13] An alternative to this design includes dielectric barrier discharge (DBDI), which generates an electric discharge between two electrodes separated by an insulating material.[19] The most significant advantage of this design is that the sample does not require to be positioned between plasma and the MS inlet, which simplifies the method and makes it more suitable for *in-vivo* or fieldable applications. A notable direct-to-MS technology developed in recent years is acoustic droplet ejection coupled to open-port interface (ADE-OPI) coupled directly to MS.[20] It operates by acoustically ejecting nanoliter-scale droplets from plates (up to 1536 well plate format) into OPI that leads directly to the MS.[20] The ejection rate can be as high as 6 Hz for standards prepared in a variety of matrices which allows for analysis of 1152 samples in 63 s at full-width at half maximum of 105 ms and relative standard deviation of 8 %.[21] A technology like this is an enormous improvement in terms of rapid or high-throughput analysis; however, it can lack sample preparation which

will hinder quantitative analysis. It seems to be one of the best technologies invented for qualitative research.

On the other hand, some direct-to-MS or ambient-MS methods are not comparable to the gold standard analytical methods because of lack of selectivity, sensitivity, automation, inadequate quantitation, and possible instrument contamination.[10] In terms of selectivity, direct-to-MS methods lack the separation step capable of separating isomers or isobars.[22] A technology/field capable of addressing this issue is differential ion mobility, where ionized species are separated in the gas phase according to their mobility through a separation cell. Unlike the conventional gas/liquid chromatography (separation), the separation herein occurs within a second, thus still allowing high-throughput/rapid analysis.[23] In terms of lack of automation, many ambient technologies are operated manually, which often poses an issue to laboratories that require running many samples daily. This problem is emphasized when specific laboratories require to train technicians about technologies that need to be utilized, which is counterproductive.[24] They would instead use an automated technology that is more *fool-proof* and user-friendly. These other issues mentioned above (inadequate sensitivity, degree of quantitation, and susceptibility to instrument contamination) arise mainly because of the presence of matrix effects because of insufficient sample preparation and ionization under ambient conditions. Regardless, some degree of sample preparation is required for a method to avoid matrix effects. Unfortunately, sample preparation remains one area of the analytical workflow with tedious and complicated procedures, thus often becoming a bottleneck in the overall analysis.[2,25].

1.3. Overview of sample preparation methods for direct-to-MS introduction

Although the direct-to-MS methods aim to simplify the overall workflow, analytical workflow simplification with little sample preparation backfires regarding resulting analysis sensitivity. Sample preparation methods can be classified into three main groups: 1) flow through equilibrium and pre-equilibrium, 2) batch equilibrium and pre-equilibrium, and 3) steady-state exhaustive and non-exhaustive.[2] Some of these methods are summarized in **Table 1.1.**

Table 1.1. Classification of extraction techniques with an example of each method included.[2]

Flow-Through Equilibrium and Pre-equilibrium		**Batch Equilibrium and Pre-equilibrium**		**Steady-state Exhaustive and Non-exhaustive**
Exhaustive	*Non-exhaustive*	*Exhaustive*	*Non-exhaustive*	-
Solid-phase extraction	In-tube solid-phase microextraction	Liquid-liquid extraction	Solid-phase microextraction	Membrane

One of the examples of sample preparation coupled used with DESI-MS is performing solid-phase extraction (SPE) where retained analyte on the cartridge was eluted onto a closing frit, evaporated, then the DESI spray was used to introduce the analytes to the MS.[26] This method allows preconcentration of 1 L volume into 1 mm circular spot, thus yielding up to six orders of magnitude, provided the sample volume is sufficient.[26] An alternative strategy involves a modified extraction using a liquid membrane whose side opposite to the sample is sprayed with DESI and introduced to the MS.[27] The highlight of this approach is an analysis time of about 11 s per sample.[27] Using a similar method as with SPE-DESI mentioned above, SPE was used for selective extraction of analytes that were subsequently eluted to the paper substrate used for the PS-MS analysis.[27] This overall method allowed for increased detection limits by a factor of 14 – 70, depending on the analyte.[27] Excellent enrichment factors were achieved (100 – 700-fold) when single drop liquid-phase microextraction (LPME) was used to enrich analytes from a complex sample.[28] This was achieved by lowering 2 µL of xylene into the aqueous solution while attached to a syringe. After the extraction, it was withdrawn back into the syringe and deposited onto the paper substrate for PS. Similar simple liquid extraction approach was coupled to DART, where the methanol-water solution was used to enrich illegal synthetic drugs from herbal dietary supplements.[29] After extraction, a tip was dipped and placed between the DART source and the MS for the analysis in less than 10 seconds.

In comparison to liquid-based methods, SPE methods are more cost-effective, environmentally friendly, and preferable. Polydimethylsiloxane (PDMS) coated stir bar was used for a stir bar sorptive extraction (SBSE) method for the extraction of analytes, and then it was positioned between the DART source and the

MS for analysis where part-per-trillion detection limits were obtained.[30,31] Besides all these attempts, the research community started shifting towards miniaturizing the sample preparation techniques.[32] Some noteworthy attempts include a RapidFire system where (partial) online sample preparation method extracted analytes from a complex matrix were introduced to an SPE system and then directly to the MS. This method provides runtimes below 15 seconds, which is an enormous achievement.[33] The disadvantage of this work is the inadequate sample preparation as whole blood was mixed with required reagents, then the solution was mixed and centrifuged. Subsequently, the supernatant was used for injection. Open-bed sample preparation technologies are inevitably better for coupling them to an online system.

Adequate sample preparation for this is solid-phase microextraction (SPME), a sample preparation method developed by Arthur and Pawliszyn that merges sampling and sample preparation into one cohesive step.[34] It is a non-exhaustive sample preparation method in which analytes, in a free-form, equilibrate with the extraction phase and provide sensitive and quantitative information.[2] Instead of being optimized for maximum enrichment of analytes (like SPE or liquid-liquid extraction, LLE), it is optimized to extract less than 1 % of free analyte concentration, which does not disturb the sample environment. This is extremely important for *in-vivo* analysis.[35] This way, SPME provides a snapshot of the system being studied, thus the amount of all sample components being extracted is very small, which leads to minimal instrument contamination. Although it extracts a very small amount of analytes compared to exhaustive methods, it makes up in contrast to other sample preparation methods by being coupled with appropriate mechanisms for desorption to eliminate the overall dilution factor.[36]

1.4. Solid-phase microextraction as ideal sample preparation for direct-to-mass spectrometry analysis

An adequate sample preparation technique for direct-to-MS analysis is SPME. It can address the challenges of mainstream sample preparation methods like SPE or LLE. SPME devices typically consist of inert support coated with polymer responsible for the analyte enrichment.[2] Up to today, SPME devices have been used in different formats (fiber, tube, vessel, suspended particles, stirrer, disk, etc.).[37,38] The extraction

process is done by exposing an SPME device to the sample either in direct or in membrane-protected format for low volatility analytes and in headspace format for semi-volatile and volatile analytes, as shown in **Figure 1.1.**[2]

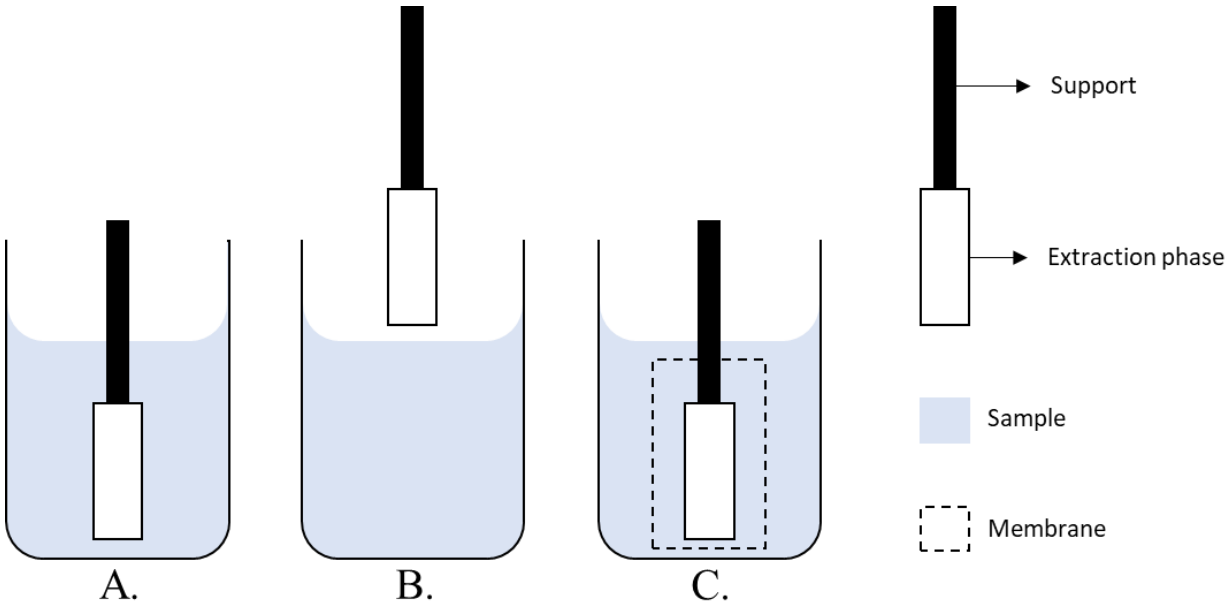

Figure 1.1. Different extraction modes using SPME: (**A**) direct immersion, (**B**) headspace, and (**C**) membrane-protected format.[2]

The analyte desorption is done by thermal or solvent exposure, where those fluids are subsequently introduced into the instrument for analysis.[2] Recently, SPME devices have been exposed to a light source for spectrophotometric desorption.[2,39] The advantage of SPME, when coupled directly to MS, is the use of a matrix-compatible SPME devise composed of high-capacity sorbent bound to support with polyacrylonitrile (PAN).[40] The high-capacity sorbent is well embedded in (PAN) so that the matrix components (often those that interfere with the overall analysis) do not get coextracted due to PAN's small pore size. In the end, a sufficient amount of analytes is extracted to provide a sufficient instrument response while reducing the coextraction of contaminations and interferences in comparison to other methods. Another advantage of SPME is the ability of the extraction phase to have balanced coverage of analytes in very complex matrices.[41] Briefly, sample components that do not interact with the sample matrix are present in very high amounts and typically have a low affinity for the extraction phase, K_{FS}, so these analytes'

(absolute) recovery is very low. On the other hand, sample components interacting with the sample matrix are in very small concentrations and tend to have high affinities for the extraction phase, K_{FS}; therefore, their absolute recoveries will be larger. Overall, balanced coverage of all sample components is obtained.

1.5. Review of solid-phase microextraction coupled to mass spectrometry approaches

Direct couplings of SPME to MS can be organized according to the degree of "ambiance," ionization strategy, and desorption strategy.[35] Herein, the SPME-MS method will be divided into categories that show what kind of peak will be produced. This way, all SPME-MS can be classified into categories that produce Gaussian and "square-wave-like" signals. **Figure 1.2.** shows designs of several direct-to-MS methods coupled with SPME with signals that they make.

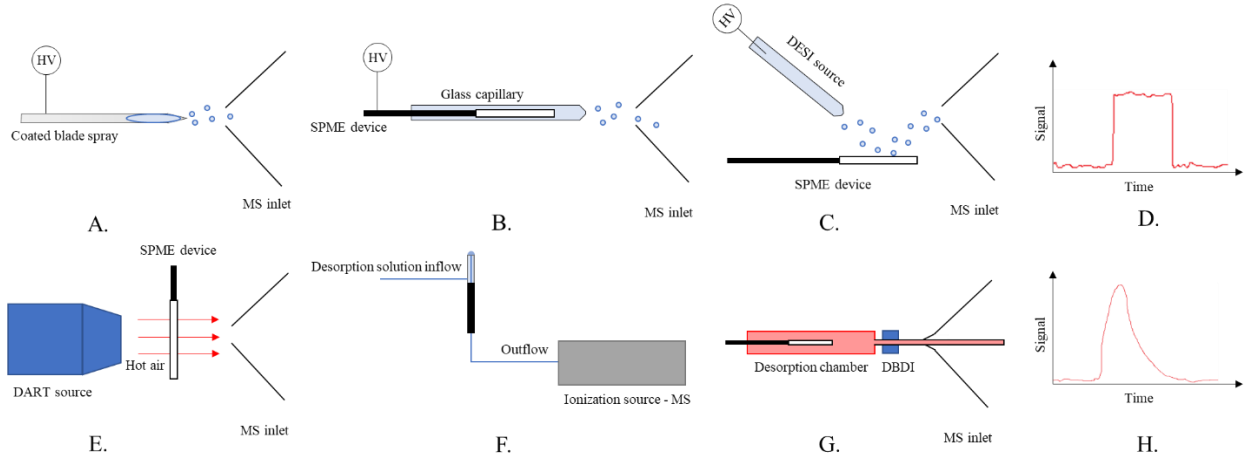

Figure 1.2. Schematic designs of several direct-to-MS techniques coupled with SPME and the peak shape they produce. Coated blade spray (**A**), nanoESI (**B**), and DESI (**C**) produce "square-wave-like" signals (**D**), while DART (**E**), OPSI (**F**), and DBDI (**G**) produce Gaussian-like signals (**H**).[35,42]

The "square-wave-like" signal methods can perform analysis over (relatively) longer periods. In other words, large sets of analytes can fit into the analysis, and more complex analysis can be performed, requiring longer analysis time per analyte (*e.g.*, n^{th} multiple reaction monitoring). Some of these methods include coated blade spray (CBS),[43,44] nanoelectrospray ionization (nanoESI),[45,46] and DESI.[47–49] Some of these methods have their disadvantages. For example, DESI-MS includes a very short-time stable signal as

analytes are quickly desorbed from the coating surface. The signal starts dropping because it takes some time for analytes to migrate from deeper parts of the coating to the surface, which can be observed in the literature.[47–49] Additionally, nanoESI suffers from possible clogging due to spray capillaries' very narrow inner diameter. When dry SPME devices are introduced for desorption, bubbles will likely appear that will cause electrospray instability.[45,46] Out of these, CBS is a method that provides the greatest robustness. The technology has been advanced, and in terms of rapid analysis, it is capable of breaching the 10-second analysis barrier for a large set of analytes[44], and when sample preparation is run high-throughput fashion, the analysis time per sample can be as low as 3 min.[50] Some of CBS's (minor) disadvantages include ionization at ambient conditions (which need to be well controlled) and small signal-to-noise ratios produced when extracting extremely low analyte concentrations.

Some methods that produce Gaussian peaks are DART, open probe sampling interface (OPSI), DBDI, and microfluidic open interface (MOI), while DART can produce square-wave like signals as well.[51] Although the generated signal width can be very low for these methods, the MS instruments have advanced to the point where one ms dwell time can be used,[44] thus allowing these methods to analyze (relatively) larger sets of analytes. DART and DBDI use thermal desorption to release enriched analytes from SPME devices and are more suitable for analyzing volatile and semi-volatile analytes (headspace format SPME, HS-SPME). On the other hand, OPSI uses solvent desorption, which is the most ideal for non-volatile analyte analysis (direct immersion SPME, DI-SPME format). One characteristic of these three direct-to-MS approaches is that the analytes are introduced to the instrument as soon as they are desorbed from the SPME devices. For the case of applications where the desorption time is relatively long (*i.e.*, the desorption of the analyte is slow), very shallow and vast Gaussian peaks will be generated that will compromise the signal-to-noise ratios.[52] MOI is a direct-to-MS approach that addresses this disadvantage by having a flow-isolated desorption region (where SPME devices are introduced and analytes are desorbed) while the solution is continuously supplied to the ESI, thus not introducing any interruptions.[53] Therefore, when the analyte

desorption is done, the low volume (~ 7 µL) concentrated plug of analytes is introduced at once, which offers a great sensitivity.

1.6. Solid-phase microextraction coupled to mass spectrometry via microfluidic open interface

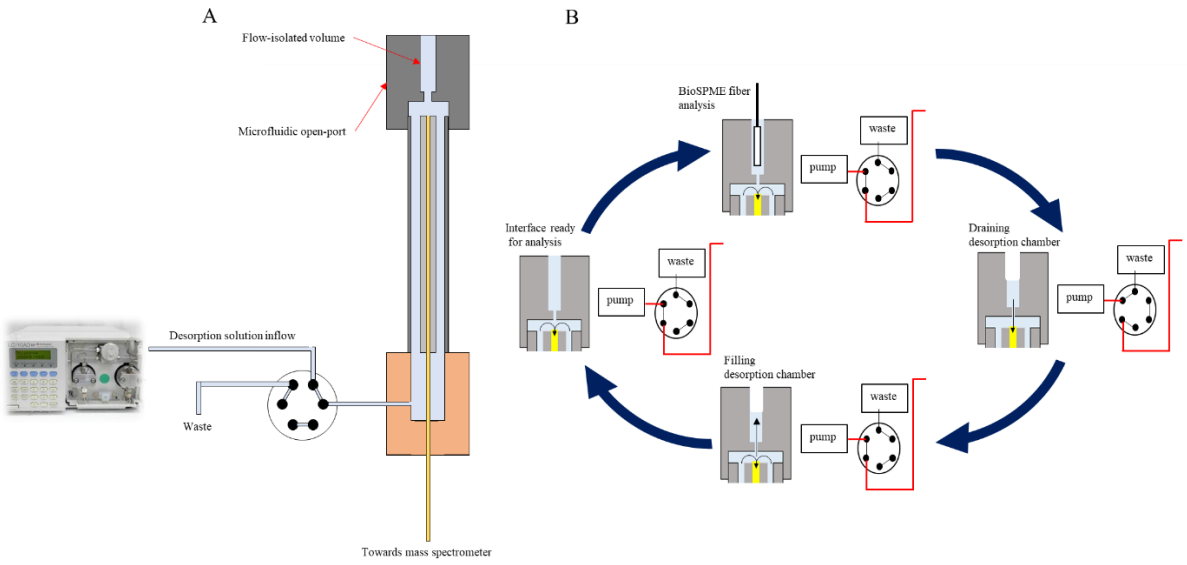

Figure 1.3. Schematic/simplistic design of MOI setup (**A**) and operational workflow (**B**). Objects/parts are not in relative size to one another.[53]

The MOI design is described in **Figure 1.3.** It has been inspired by the OPSI design[53–55], and it is composed of a Teflon cylinder with a diameter of the upper side is 1 mm and 10 mm deep, while the lower side has a 3.18 mm diameter. These two sections are connected by a 0.5 mm diameter that is 2 mm long, which acts as a flow restriction in the system. This dead volume makes the desorption chamber of the MOI. This Teflon cylinder sits on two tubes in the coaxial configuration where the outer tube (304 stainless steel) with dimensions of 1.75 mm inner diameter x 3.18 mm outer diameter x 9 cm length. The inner capillary tube has a 254 µm inner diameter x 361 µm outer diameter x 20 cm length. The desorption solution inflow is provided through the gap between inner and outer tubes that meets a junction that connects this outer gap with the Teflon cylinder and the most inner path of the coaxial tube design. This path leads to electrospray

(ESI) ionization through the 150 µm inner diameter stainless steel capillary. A six-port valve is positioned before the coaxial tubes that has the purpose of *artificially* stopping the pumping system, allowing the instrument to aspirate the volume from the MOI desorption chamber via pressure differential created by the nebulization gas.

The operational workflow, shown in **Figure 1.3.B.,** consists of several steps. In the first step, the whole system is put into equilibrium, meaning that the inflow is the same as the aspiration flow rate. At this stage, the volume in the desorption chamber is stagnant, and microfluidic flow layers do not disturb the desorption volume. This has been verified with a computational model.[53] The second step in the workflow, **Figure 1.3.B-2.**, is the placement of the SPME fiber into the desorption chamber for a set amount of time. When SPME fiber is removed, the six-port valve is switched to another position, **Figure 1.3.B-3.**, so that the volume in the desorption chamber is being aspirated. Finally, just before the whole volume is aspirated from the desorption chamber, previously predetermined, the inflow is increased to fill the desorption chamber, **Figure 1.3.B-4.**, and to reset the system to the step shown in **Figure 1.3.B-1.**

Some highlights of SPME-MOI-MS/MS include the use of a matrix-compatible extraction phase, minimal coextraction of matrix interferences, and desorption into low volume flow-isolated region (*i.e.*, desorption chamber).[52,53,56] So far, there hasn't been any direct comparison of SPME-MOI with some other direct-to-MS technologies coupled with SPME (CBS, DART, DESI, nanoESI, etc.), which makes comparison or highlighting MOI a little bit difficult. However, comparing these has been done considering each methodology's theoretical advantages and disadvantages.[35,46] The main advantage of MOI over technologies producing a "square-wave" is that the greater signal-to-noise ratios are obtained when the instrument signal is squeezed into a (Gaussian) peak. Nevertheless, the main disadvantage of nanoESI includes sprayer clogging and bubble production during ESI spray, while DESI is more suitable for qualitative analysis of surfaces. DBDI, and OPSI have the characteristic of continuous desorption that doesn't allow the introduction of concentrated analyte plug. Nevertheless, the MOI offers more easy capability for automation as it is easier to develop an automated system that would lower SPME fibers into

desorption chambers. While work in this area has been done for the CBS, the main disadvantage remains running the whole set of 96 blades in automated fashion.[44] SPME-MOI is very attractive technology as dispersed (magnetic) particle format has been successfully coupled with it.[56] In theory, slight modifications to the desorption chamber will allow coupling flat surface format of SPME devices. The flexibility of the SPME format allows for a variety of applications to be coupled with SPME-MOI that require unique SPME device formats (*e.g.*, small cylindrical format for *in-vivo* brain analysis,[57] dispersed (magnetic) particle format for very low sample volumes,[56] or flat surface for greater sensitivity in general[56]).

For SPME-MOI-MS/MS to gain better traction, the method needs to have many advantages over traditional methods (*e.g.*, LC-MS). The most significant advantage SPME-MOI-MS/MS has over liquid chromatography coupled to mass spectrometry (LC-MS) is the analysis time, as separation steps can be lengthy. Additionally, the SPME component allows for high-throughput sample preparation, significantly reducing the overall sample preparation required. Therefore, it is essential to consider theoretical aspects of SPME to enable SPME-MOI-MS/MS to perform rapid and (completely) automated analysis.

1.7. Solid-phase microextraction: Theoretical considerations for rapid analysis

SPME can address the disadvantages of mainstream (exhaustive) sample preparation techniques and the need for rapid and automated analysis both in the laboratory and *in-situ* analysis.[35]

The successful implementation of SPME as a sample preparation method depends on a good understanding of the equilibrium dynamics. When the coating is exposed to the sample, analytes will start partitioning into the coating according to their distribution constant (K_{FS}) described by the **Equation 1.1.**[2]

$$K_{FS} = \frac{C_{\text{extraction phase}}}{C_{\text{sample phase}}} \tag{1.1.}$$

The most significant feature of SPME is that it is non-exhaustive analyte enrichment, which means that the analyte concentration in the sample phase will not be disturbed during the extraction process.[2] This can only be achieved by using a very small extraction phase compared to the sample volumes.[36] The amount

extracted using an SPME device with absorptive (liquid coatings – *e.g.*, polydimethylsiloxane) can be calculated with **Equation 1.2.**:[2]

$$n = \frac{K_{FS} V_F V_S}{K_{FS} V_F + V_S} C_0 \tag{1.2.}$$

where n is the amount extracted [ng], V_F is the coating volume [mL], V_S is the sample volume [mL], and C_0 is the initial concentration [ng mL^{-1}]. In such cases where sample volume is sufficiently large to overcome the product of distribution constant and extraction phase volume, *i.e.*, $K_{FS}V_F << V_S$ (*e.g.*, *in-situ* analysis), **Equation 1.2.** can be simplified into **Equation 1.3.**:[2]

$$n = K_{FS} V_F C_0 \tag{1.3}$$

The **Equation 1.3.** can be used to calculate initial sample concentration at extraction equilibrium, using the amount extracted, the volume of the extraction phase, and the distribution constant. In some applications, analytes require a very long time to reach equilibrium with the extraction phase (because of high K_{FS}), but extraction times must be very short for the overall method to be rapid. In that case, several calibration approaches have been explored in the pre-equilibrium regime of an extraction time profile (**Figure 1.4.**).[58]

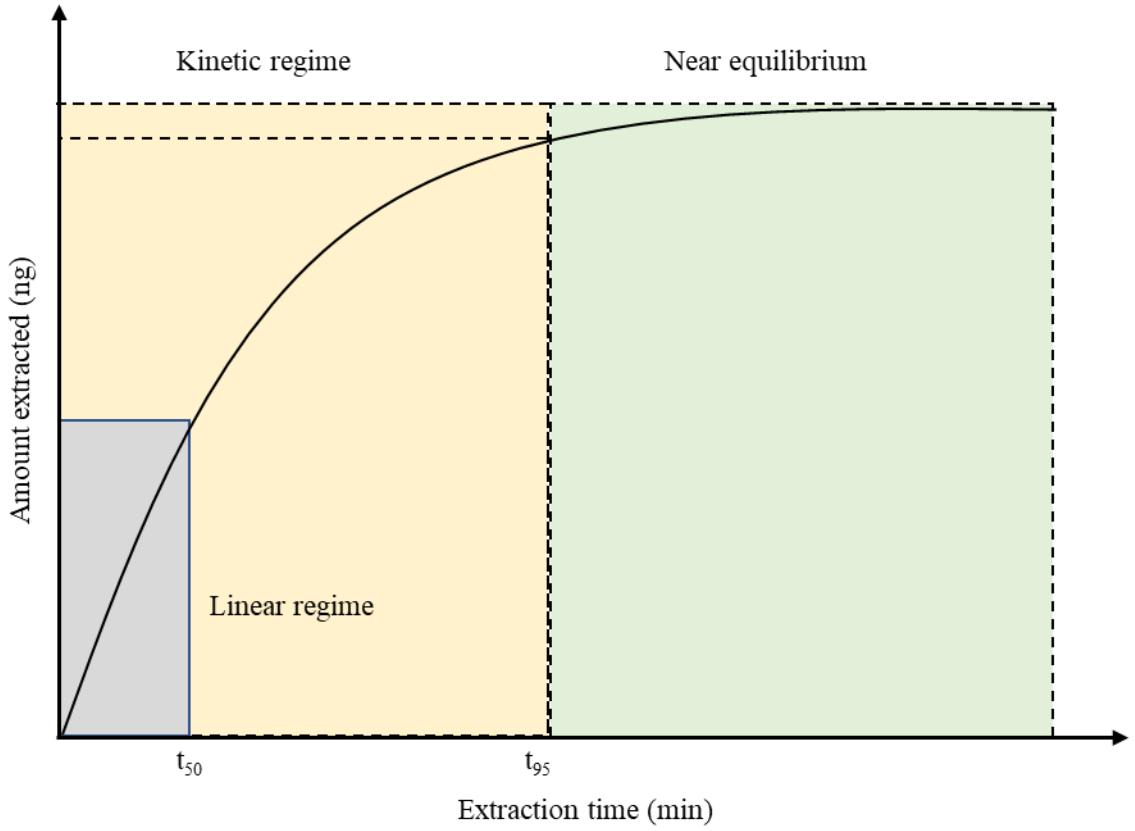

Figure 1.4. SPME extraction time profile and identification of linear, kinetic, and equilibrium. The t_{50} represents the time point at which 50 % of analytes are extracted, while t_{95} stands for the time point at which 95 % of analytes are extracted.[58]

Figure 1.4. shows that in the kinetic regime, the rate of change of extracted analytes with respect to the extraction time is very high early, so the greatest irreproducibility and inaccuracy can be associated with extractions at this period. Therefore, it is vital to control system conditions (e.g., temperature, pH, solution composition, etc.) to ensure that the K_{FS} value does not change. It is essential to clarify that the stirring rate plays a significant role in controlling the equilibration time in the SPME, shown indirectly by **Equation 1.4.** below:[2]

$$t_e = 3\frac{\delta K_{FS}(b-a)}{D_S} \qquad (1.4.)$$

where t_e is the equilibration time [s], b is the total extraction phase thickness [m], a is SPME device support thickness [m], D_S is the analyte diffusion coefficient in the sample phase [m^2 s^{-1}], and δ is the boundary layer thickness [m]. A boundary layer is a very thin fluid layer immediate to the object exposed to agitation in the sample environment.[59] The boundary layer is seen as the Achille's heel of direct immersion SPME format because analytes have very low D_S in liquid and semi-solid samples, which decreases t_e (according to **Equation 1.4.** For headspace SPME format, D_S is much higher in gaseous samples than liquid and semi-solid samples, and the gas viscosities are much lower, yielding much lower equilibration times.[36,60]

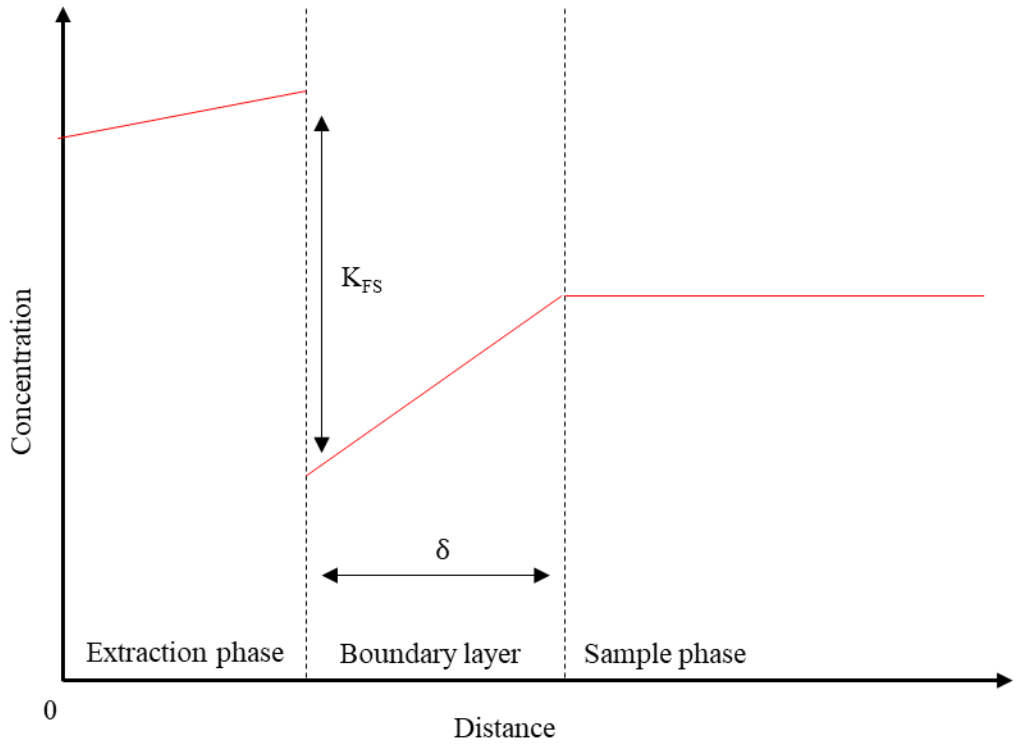

Figure 1.5. The concentration profiles of analytes (shown in red) at some extraction time show the concentration differences in the sample phase, boundary layer, and extraction phase.[2]

Providing agitation to relatively viscous samples forces molecules around an object (*i.e.*, SPME extraction device) to move, thus reducing the δ and t_e. Increasing agitation speed does not affect the amount extracted. An exception to this case could be seen when sonication is applied for sample agitation. Because of vigorous sample agitation, the heating is inevitable, leading to a change in K_{FS}.[61] Over time, sample preparation instrumentation has been improved, capable of controlling mentioned critical factors (*e.g.*, temperature,

stirring rate, etc.). A fully automated high-throughput sample preparation system for SPME devices known as Concept96 system has been developed at (PAS Technologies, Magdala, Germany) which allows reproducible analyte enrichments onto SPME devices, and it has been applied for many applications.[52,62–68]

Two more situations can influence the extraction time in SPME. In one of the scenarios, the extraction time can be negatively impacted (lowered) by the very low analyte diffusivity in the coating[60], which can be avoided with very thin coatings. The other scenario considers extractions performed from complex samples where the analyte-matrix complexes are present in the vicinity of the SPME device (*i.e.*, boundary layer). The analyte-matrix complexes release analytes into free concentration, thus maintaining a high concentration gradient and speeding up the extraction kinetics, shown in **Figure 1.5.**[69,70] It is important to clarify here that the SPME extracts via free concentrations, and in such situations, only the free concentration will equilibrate with the coating.[71] **Figure 1.6.** depicts that the analyte release from the analyte-matrix complex into free concentration will highly depend on the reverse rate constant and the depletion of free concentration in the boundary layer.

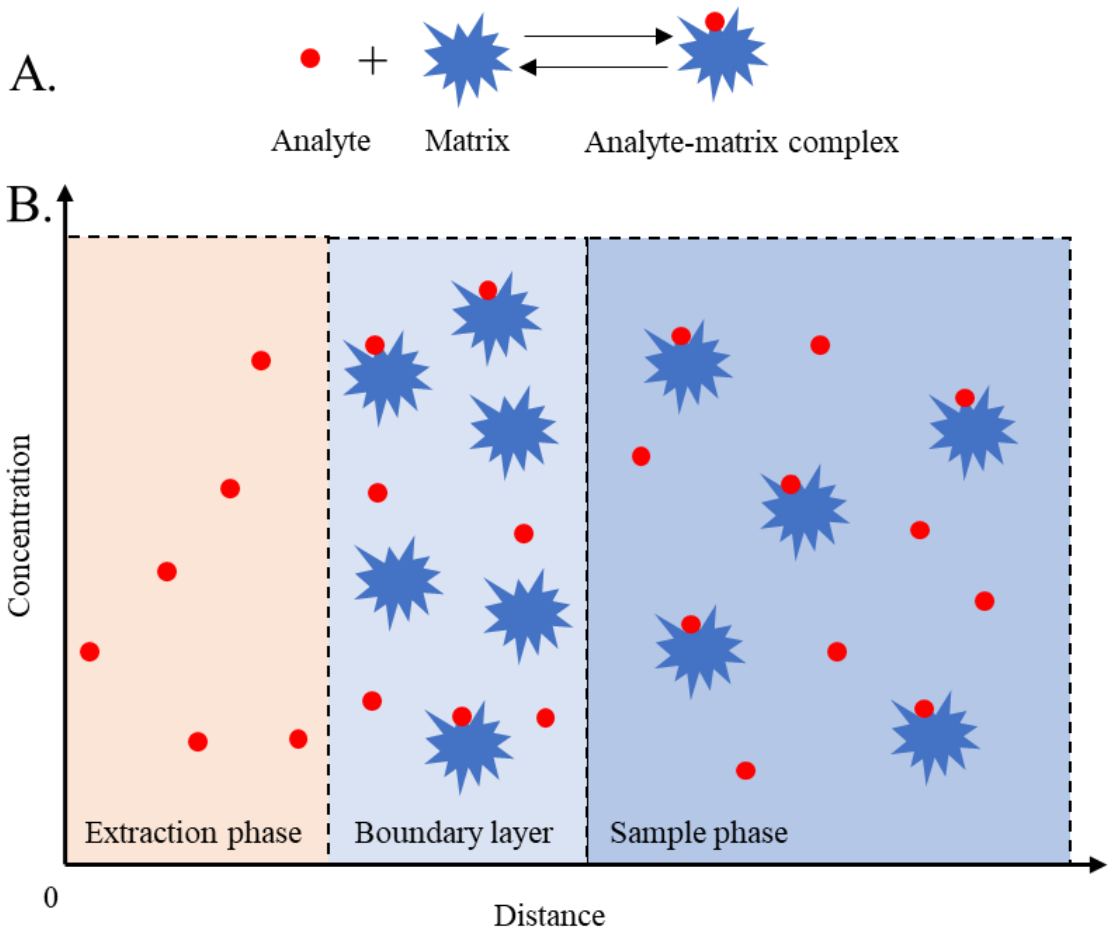

Figure 1.6. The schematic representation of analyte and matrix behavior in the extraction phase, boundary layer, and sample phase.[71]

The abovementioned aspects can be manipulated to control extraction kinetics, and equilibrium extractions are unnecessary if sufficient analyte amounts are extracted in pre-equilibrium regimes. Therefore, SPME is a non-exhaustive and equilibrium-based sample preparation method, capable of being termed with rapid analysis, especially when using high-throughput systems that decrease the average sample preparation protocol time for a set of 96 samples by a factor of 96.

1.8. Microfluidics: Theoretical considerations

Microfluidics, a subdiscipline of fluid mechanics, is the discipline on studying fluids at micro- and nanometer scales.[72] A system is referred to as microfluidic when dimensions through which fluids flow is on a sub-millimeter scale because, at these levels, fluid turbulence and gravitational forces are often

negligible.[72] MOI system in all previous publications flow path is restricted to sub-millimeter scale;[52,53,56] therefore, it can be assumed that the predominant flow profiles are laminar.[72] Laminar flow (profile) is when a fluid flows in laminae or layers; there is no mixing of adjacent fluid layers.[73] This flow can be characterized by the Reynolds equation (for flow in pipe) shown below in **Equation 1.5.**:[73]

$$\mathrm{Re} = \frac{\rho u d}{\mu} \tag{1.5.}$$

where Re represents the Reynolds number [unitless], d prepresents diameter [m], ρ represents the fluid density [kg m^{-3}], u represents fluid linear flow velocity [m s^{-1}], and μ represents fluid (dynamic) viscosity [Pa s]. Under normal conditions, the transition from laminar to turbulent (mixing of adjacent fluids) flow in pipes occurs at Re ≈ 2300.[73] The characteristic of laminar flows is that they can be mathematically expressed with great accuracy, unlike the turbulent flow; therefore, the Hagen-Poiseuille law can be used to describe the laminar flow using the **Equation 1.6.**:[73]

$$\mathrm{Q} = \frac{\pi \Delta \mathrm{P} r^4}{128 \mu \mathrm{L}} \tag{1.6.}$$

where Q represents the fluid volumetric flow rate [m^3 min^{-1}], ΔP represents pressure differential between two points in the fluid path [Pa], r represents the radius of the pipe [m], and L represents the fluid flow length in the pipe [m]. Herein it is briefly described that for a given pressure differential that produces a certain suction flow rate in some systems, the two most critical components will be the radius of the pipe flow path and the length of the fluid flow path. From these two factors, the radius of the flow path is the most critical as $Q \sim r^4$.

Hence, from a microfluidic point of view, **Equation 1.6.** can be used to identify the MOI design's limitations shown in **Figure 1.3.** The MOI performance can be improved by increasing the suction flow rate to create more narrow Gaussian peaks, which could improve the signal-to-noise ratios by decreasing the length of tubes used or using slightly wide inner diameters. Also, due to parabolic profiles of the laminar flow, it is suggested to avoid any turns/kinks in the flow path so that there is minimum contribution to concentrated

analyte plug diffusion along the fluid flow path. Furthermore, some consideration should be given to mixing MS-compatible solvents that make the desorption solution used for the MOI system because certain mixtures can change μ and thus affect the suction flow rate. The current design also has unnecessarily long tube lengths through which analytes diffuse along the flow path resulting in peak broadening.

1.9. Research objectives

Direct-to-MS methods are becoming more popular because of the rapid, practically real-time analysis they can provide. However, a big challenge remains that they struggle to beat systems where chromatography is coupled to MS because of the separation it provides. In addition, direct-to-MS methods require a reasonable degree of sample cleanup and overall system automation to overtake the prevalence of chromatography-MS methods. One promising area is using SPME as sample preparation because of its cleanup; however, SPME-MS methods are not fully automated, although they possess a high degree of full automation compatibility as sample preparation is already automated.

Therefore, the overall research objective of this thesis is to redesign the MOI system to demonstrate automation of the full analytical workflow and make it suitable for rapid analysis. This overall objective will be supported by 1) redesign of the MOI according to the microfluidic suggestions, 2) redesign of the MOI to allow fool-proof usage (*i.e.*, system simplification and automation), and 3) theoretical study of the extraction kinetics in the coatings of SPME with the focus on conditions required for the rapid analysis.

This thesis supports the overall research objective through chapters that make its content. **Chapter 2** describes the redesign of the MOI system. This redesigning/development considers microfluidic considerations (changing tubing length and diameter sizes), overall design simplification (getting rid of a switch valve), and automation (incorporation of photointerrupters, Visual Basic program that controls fluid and MOI operational workflow). **Chapter 3** describes the theoretical study that quantifies the mass transfer resistance in the coatings of SPME devices. The outcomes of this work, published in Analytical Chemistry, are used to provide considerations for SPME coating design that would be suitable for rapid analysis, among other conclusions. **Chapter 4** describes an application where matrix-compatible SPME coatings have been

used to extract immunosuppressive drugs from whole blood and then directly coupled to the previous design of MOI. Although this thesis focuses on the redesign and improvement of the MOI, this chapter aims to show that previous design can be competitive in terms of rapid analysis. Furthermore, the overall method turnaround time for high-throughput analysis is well under the turnaround time desired for clinical applications for daily adjustments. However, the main disadvantage of that MOI design is the lack of automation.

Furthermore, **Chapter 5** describes the application of matrix-compatible SPME fibers (generously provided by Millipore Sigma) and coupling them to a new and improved MOI design to extract fentanyl, its analogs, and a common fentanyl precursor from whole blood. The results of this work show that the method is comparable with the most sensitive LC-MS/MS methods in the literature. At the same time, the overall turnaround time is significantly faster in comparison. Nevertheless, **Chapter 6** describes the coupling of MOI to an alternative detection system, ultraviolet-visible light. The whole system is controlled by the software written in Visual Basic. This chapter's main highlight is that MOI does not necessarily require a mass spectrometer as a detector and can be coupled to any other detection system.

Chapter 2: Coupling of Solid-phase Microextraction Directly to Mass Spectrometry via Improved Microfluidic Open Interface

2.1. Preamble

This chapter is not published, but the material is being prepared for submission to the Journal of American Society for Mass Spectrometry special edition "High-throughput in Mass Spectrometry." Khaled Murtada has prepared the slurries used to prepare the SPME fibers. Hernando Rosales has assisted with running microfluidic open interface experiments on Thermo TSQ Vantage and Thermo TSQ Quantiva and setting up MS methods. Daniel Rickert assisted with experiments and running of the MOI coupled to SCIEX API 4000 MS. Victor Galievsky assisted in incorporating the photointerrupter into the design of the microfluidic open interface. Parts of the MOI (building all electronic components and machining components for the MOI design) have been made in the University of Waterloo Science Technical Services. Emir Nazdrajić has performed coating of all SPME fibers used herein, has built prototype software for the operation of the microfluidic open interface, and has adjusted the designs of the electrospray capillary assemblies and other ionization source adjustments required for coupling MOI to different MS instruments. Emir Nazdrajić also did all data processing while Janusz Pawliszyn assisted data interpretation. Janusz Pawliszyn supervised the whole MOI development.

2.2. Introduction

Mass spectrometry is a powerful technology for the qualitative and quantitative analysis of samples applied in food, environmental, forensic, and biological analysis, among other fields.[74] Thus, chromatographic techniques (*e.g.*, LC) coupled with mass spectrometry became a gold standard for quantitative and qualitative analysis of various complex samples. The outstanding performance of LC-MS can be achieved with adequate sample preparation and a separation step.[75] Due to recent improvements in the MS, they can analyze complex samples directly to mass spectrometry without chromatography, even under ambient conditions.[74] Their most significant advantage of direct mass spectrometry over chromatography coupled

to mass spectrometry is the circumvention of the typically lengthy separation step that does not allow for high-throughput or rapid analysis. Recent direct mass spectrometry applications include the analysis of in-vivo,[76] biological,[77] pharmaceutical,[78] food samples[79], and other fields. The disadvantage of directly introducing samples to mass spectrometry for the analysis of complex samples is the introduction of the enormous amount of matrix components that can interfere with or suppress the analyte's signal. Hence, coupling an appropriate sample preparation method to the overall workflow is crucial for the sensitivity of the overall direct-to-MS analysis and the mass spectrometer stability and cleanliness.

Thus, according to the abovementioned needs for minimizing the matrix effects, the SPME is the most appropriate sample preparation method for direct-to-MS application. It is a versatile and non-exhaustive sample preparation technique that combines sampling, isolation, and enrichment into a single consolidated step.[35] The main reason SPME is the best sample preparation technique for direct-to-mass spectrometry applications is its matrix-compatible coatings and non-exhaustive enrichment. The matrix-compatibility context herein is mainly seen through the inertness of the complex matrix components towards the coatings of SPME devices, where matrix components may cause fouling of devices or can cause ionization matrix effects.[35] Matrix-compatible coatings are composed of high-capacity sorbents (depending on the analyte of interest) and a polyacrylonitrile binder. Regarding non-exhaustive enrichment, all matrix components equilibrate with the extraction phase according to their distribution constants, resulting in minimal amounts extracted. On the other hand, exhaustive sample preparation counterparts (*e.g.*, solid-phase extraction or micro solid-phase extraction) extract a large amount of all matrix components; thus, the overall SPME extracts introduced to the mass spectrometer are cleaner. The equilibration of the analyte with the coating is the most significant disadvantage of the SPME. The maximum amount extracted is at equilibrium, and some applications may require very long equilibration times. This way, one is either forced to extract for a very long time or forced to be satisfied with mediocre recovery. However, SPME devices can easily be coupled to instrumentation that can run a high-throughput analytical workflow (*e.g.*, Concept96), reducing the average runtime per single device.[80–82]

Matrix-compatible SPME coatings for sampling biological matrices have been successfully coupled directly to MS via different approaches. Some of these approaches are probe electrospray ionization (PESI),[83] DESI,[48,49] nanoESI,[84] OPSI,[54] MOI,[53] DART,[85] substrate spray,[86] and CBS.[87] These coupling approaches can be divided into two categories based on the type of peak they produce: Gaussian or square.[46] The most significant advantage of ionization technologies that create a square peak (*e.g.*, CBS, nanoESI) is the ability to have a long and stable spray over a relatively long time, allowing the ability to fit many scans and ions monitored. On the other hand, ionization technologies that provide Gaussian peak (*e.g.*, OPSI) counter square peak technologies because all desorbed analytes are introduced relatively simultaneously, thus offering higher signal-to-noise ratios. The disadvantage of these technologies can be the ability to perform many scans for many ions monitored because the Gaussian peak width limits the analysis time; however, this is very specific scenario based on the type of mass spectrometer used.MS technologies have advanced in the area of polarity switching and dwell time. This advancement allows newer mass spectrometry instrumentation to offer Gaussian peak technologies to fit more ion transitions and scans, thus an avenue to be superior to ionization technologies that produce square peaks. An example of this application is SPME-PESI-MS/MS, where the mass spectrometry method dwell time was 1 ms and each of the scans of single pick-and-spray cycles was 1 s.[83] However, the disadvantage of PESI is the relatively narrow (single) peak width which limits the number of transitions that can be monitored (regardless of MS advancements) and the disadvantage of OPSI methods is the production of relatively large peaks as analytes are continuously introduced to the mass spectrometer as analytes are desorbing from the coating which leads to peak broadening (on the right side). One technology capable of producing perfect Gaussian peaks is the MOI. The analytes are desorbed from the SPME device in a flow-isolated desorption chamber, then a narrow analyte plug is introduced to the instrument, resembling a low microliter injection. This interface has been published numerous times for a variety of applications.[52,53,56] The disadvantages of this setup is that it uses unnecessarily long suction tubing (10+ cm long)[53] which limits the suction flow rate according to the **(1.6.** Another disadvantage is that it uses a custom-made Teflon cylinder which those interested

utilizing this interface could see as a roadblock. Additionally, fluidics in the interface was controlled manually that can lead to some irreproducibility.

Therefore, this chapter aims to redesign the interface design using appropriate tubing type, inner/outer diameter, and tubing lengths, allowing optimal suction and rapid analyte introduction to the mass spectrometer. Additionally, the overall design will be simplified by incorporating a certain degree of automation by adding photointerrupters to the desorption chamber capable of monitoring air/water interface changes and thus sending information to the computer, which will adjust the inflow flow rate accordingly.

2.3. Experimental

2.3.1 Chemicals and materials

Acetaminophen, acetylfentanyl, amphetamine, buprenorphine, lorazepam, morphine, and propranolol were purchased from Cerilliant®. Phosphate-buffered (PBS) solution (0.01 M) used for the experiments was prepared using phosphate-buffered saline powder purchased from Millipore Sigma. PAN (molecular mass 150 000), polyvinylidene difluoride (PVDF, molecular weight 180 000), polytetrafluoroethylene amorphous fluoroplastics (PTFE AF 2400), dimethylformamide, divinylbenzene, N-vinylpyrrolidone, 2-azobisisobutyronitrile, monosodium phosphate monohydrate, disodium phosphate heptahydrate, and formic acid were purchased from Millipore Sigma. Methanol, acetonitrile, and isopropanol were purchased from Fisher Scientific. Perfluoro compounds FC72™ was purchased from Acros Organics. Water used in this experiment has been produced by MilliQ® ultrapure water system purification system with 18.2 MΩ cm resistivity at 25 °C and total organic content < 5 ppb. The human whole blood K_2EDTA gender pooled was purchased from BioIVT. The custom-made PAN-C_8-SCX SPME fibers (~ 40 µm thickness) were kindly provided by Millipore Sigma. Nitinol wire used as the support for the SPME devices was purchased from Nitinol Devices & Components (Fremont, CA, USA). Hydrophilic-lipophilic balance (HLB) particles used in this work were synthesized according to the procedure reported elsewhere.[88]

2.3.2 Preparation of PAN-HLB, PVDF-HLB, and Teflon-HLB extraction phases

The matrix-compatible polyacrylonitrile (PAN) binder was prepared by dissolving 5.0 g of PAN in 72.5 mL of dimethylformamide at 90 °C for 1 hour. The solution was occasionally mixed (every 15 min), and the resulting solution was pale yellow. The PAN-HLB slurry was prepared by mixing 0.6 g of HLB particles and 6.0 g of PAN. The resulting solution was probe sonicated and left to stir for a few days at 900 rpm until a homogeneously dispersed mixture was prepared. Once the homogenous mixture was prepared, the nitinol wire was cut into 6.0 cm pieces to dip-coat the extraction phase. The nitinol wire (SPME device support) was lowered in the PAN-HLB slurry at 5 mm s^{-1} until 1 cm of the wire was submerged. Then it was withdrawn up at 1 mm s^{-1} and placed into an oven for 1 min at 90 °C. The dipping process is repeated until the wanted coating thickness is reached. This procedure is also described elsewhere.[89]

The matrix-compatible polyvinylidene fluoride (PVDF) solution was prepared by dissolving 5.0 g of PVDF in 36.75 mL of dimethylformamide at 90 °C for 1 hour. The solution was occasionally mixed (every 15 min), and the resulting solution was pale yellow. To 6.0 g of the resulting solution, 0.6 g of HLB particles were added. The slurry was sonicated for 2 min and then left for a few days to stir at 900 rpm. Once the composition was homogenized, the 6.0 cm nitinol wire was dip-coated. The lowering speed was 5 mm $s^{-1,}$ and the withdrawing speed was 1 mm s^{-1}. After the withdrawing process, the SPME fiber was placed in the oven for 1 min at 90 °C. The dip-coating process was repeated until the desired thickness was reached.

For the preparation of matrix-compatible Teflon (PTFE AF 2400)-HLB SPME fibers, the slurry was prepared by mixing 0.04 g of HLB particles in 0.93 mL of FC-72 solvent. Then the solution was sonicated for 10 min, followed by the addition of 0.04 g of Teflon. The solution is vortexed at 1200 rpm overnight to achieve a homogeneous slurry. Once the composition was homogenized, the 6.0 cm nitinol wire was dip-coated. The lowering speed was 5 mm $s^{-1,}$ and the withdrawing speed was 1 mm s^{-1}. After the withdrawing process, the SPME fiber was placed in the oven for 1 min at 90 °C. The dip-coating process was repeated until the desired thickness was reached.

Table 2.1. Dimensions of the SPME fiber devices (thin and thick versions) for PAN-HLB, PVDF-HLB, and Teflon-HLB coatings (1 cm coating length). Sizes are measured using an Olympus SZX10 stereomicroscope system equipped with an SC30 digital camera (Olympus, Japan).

SPME fiber	Average support diameter (µm)	Average total diameter (µm)	Average coating thickness (µm)
PAN-HLB (thick)	208	234	13
PAN-HLB (thin)	208	212	2
PVDF-HLB (thick)	208	236	14
PVDF-HLB (thin)	208	214	3
Teflon-HLB (thick)	208	228	10
Teflon-HLB (thin)	208	222	7

2.3.3 Sample preparation

The standard stock mixture was prepared at 10 µg mL^{-1} in methanol and kept at -80 °C until the experiments. This stock was used to spike PBS, urine, or whole blood samples.

For all experiments, all SPME fibers were cleaned in 1:1:1 = methanol:acetonitrile:isopropanol (V:V:V) solution for 30 min to remove any compounds from the extraction phase. After this, the SPME fibers were conditioned in 1:1 = methanol:water (V:V) solution for 30 min to wet the extraction phase surface and activate the extraction phase.

The PBS solution (pH = 7.4, 0.1 M) was prepared by mixing 0.28 g of monosodium phosphate monohydrate and 2.14 g of disodium phosphate heptahydrate with 100 mL of MilliQ water. For extractions from this PBS solution, the PBS was spiked with analytes (50 ng mL^{-1}) and vortexed for 1 min. Then it was aliquoted (1 mL) into wellplates, and SPME fibers were placed into the well using Concept96 (PAS Technology) agitating at 1200 rpm. Following the extraction, the SPME fibers were washed in MilliQ water for 5 s at 1200 rpm.

For extractions from urine, the second-morning urine was collected from a volunteer. The urine was spiked with analytes (50 ng mL^{-1}) and was left for 60 min for equilibration. Then the urine was aliquoted (1.0 mL)

into wellplates, and SPME fibers were placed into the well using Concept96 (PAS Technology) agitating at 1200 rpm. Following the extraction, SPME fibers were washed in MilliQ water for 5 s at 1200 rpm.

For extractions from whole blood, the thawed whole blood was spiked (50 ng mL^{-1}) and left overnight at 4 °C for equilibration. The following day it was used for the extractions. The 200 µL spiked whole blood aliquot was mixed with 800 µL of PBS (pH = 6.0) in a 2 mL wellplate, and SPME fibers were placed into the well using Concept96 agitating at 1200 rpm. After the extraction, SPME fibers were washed in MilliQ water for 5 s at 1200 rpm.

2.3.4 Description of the improved microfluidic open interface

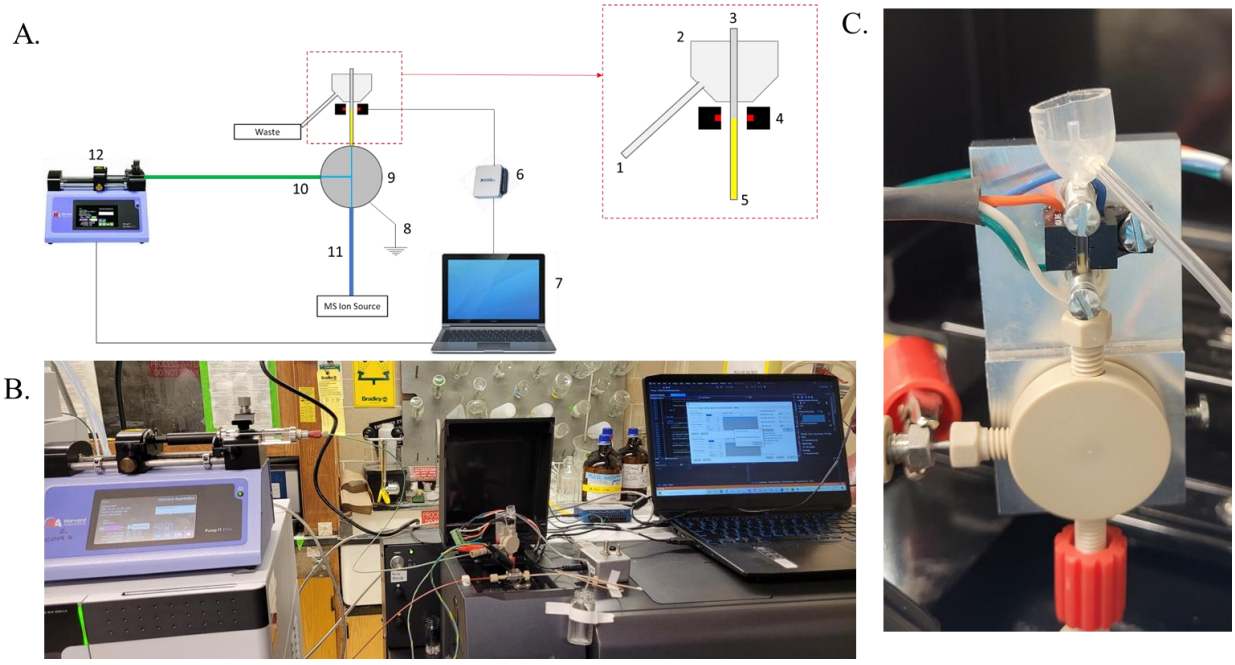

Figure 2.1. (**A**) Schematic of the improved Microfluidic Open Interface System. 1) Tubing leading overfilled desorption solution to the waste. 2) Collection/waste tube. 3) Desorption chamber, transparent PTFE tubing (0.0625 in outer diameter, 0.03125 in inner diameter). 4) Photointerrupter. 5) Yellow PEEK tubing (0.03125 in outer diameter, 0.007 in inner diameter). 6) National Instruments data acquisition device – NI 6002. 7) Laptop that controls the system with the program written in Visual Studio 2019. 8) Upstream electrospray ground. 9) Metal three-way chromatographic tee, 1 mm bore. 10). Green PEEK tubing (0.0625 in outer diameter, 0.030 in inner diameter). 11) Short blue PEEK tubing (5 cm, 0.0625 in outer diameter, 0.010 in inner diameter). 12) Programmable syringe pump equipped with 10 mL gastight syringe. (**B**) Overall real-life view of all components that make the MOI-MS system. (**C**) Close up of the desorption chamber, chromatographic tee, and waste line.

As shown in **Figure 2.1.**, the improved MOI system consists of a couple of sections that communicate to the home-written software in Microsoft Visual Studio Community 2019, version 16.9.4, described in **Section 2.3.3.** One side of the three-way chromatographic tee (1 mm bore, VICI) is connected to the ion source of the mass spectrometer via a short blue polyether ether ketone (PEEK) tube (5 cm, 0.0625 in outer diameter, 0.010 in inner diameter, Millipore Sigma). The ionization source produces suction flow by the venturi effect. The suction flow rate of the desorption solution in the MOI system depends on a couple of factors: viscosity of the desorption solution, inner diameters of the plumbing connections used, and the lengths of those connections. The Blue PEEK (5 cm, 0.0625 in outer diameter, 0.010 in inner diameter) tube has been selected for optimum flow rate capable of yielding rapid analysis.

Additionally, as with the previous MOI design, the electrospray capillary has been replaced with a wider 316 stainless steel capillary (360 µm outer diameter, 150 µm inner diameter, McMaster-Carr) for optimum suction flow rate. Another side of the three-way chromatographic tee is connected to the 10 mL gastight syringe (Hamilton) via a green PEEK tube (0.0625 in outer diameter, 0.030 in inner diameter, Millipore Sigma). For accurate desorption solution volumetric inflow from the syringe, it is essential to have rigid walls (*e.g.*, green PEEK) that do not expand/compress when the desorption solution flow rate changes. Finally, the last side of the three-way chromatographic tee is connected to the desorption chamber made of two pieces of tubing. The inner tubing is yellow PEEK (0.03125 in outer diameter, 0.007 in inner diameter, Cole-Parmer), serves as the flow restrictor, and is positioned inside the transparent fluorinated ethylene-propylene (0.0625 in outer diameter, 0.03125 in inner diameter, McMaster-Carr) tubing which is 10 mm longer than the yellow PEEK tubing to match SPME device coating length. The extra length makes the flow isolated volumetric portion (5.0 µL) where SPME fiber is desorbed for the analysis. The MOI operates so that suction flow is constant and the inflow is varied. When inflow is greater, equal to, or smaller than suction, then the desorption solution level (in the desorption chamber) increases, is stable, or decreases, respectively. Outside the bottom of the 10 mm channel, a photointerrupter (i.e., micro switch, HOA1870-031, Honeywell) constantly monitors air/liquid changes in the MOI system. It communicates to home-

written software through the National Instruments DAQ device, USB-6002 NI (National Instruments). The software gives further commands to the programmable syringe pump to adjust its inflow parameters.

2.3.5 Software development

The home-written code used to create the software that controls the MOI system is in **Appendix A.** The software comprises several tabs: MS Flow Control, COM Port Settings, Sends Commands Separately, and Methods.

MS Flow Control tab is shown in **Figure 2.2.** It contains parts that collect the data from the photointerrupter and the National Instruments Data Acquisition (NI DAQ). The data collected determines the difference between air/liquid interface and sends the information to the syringe pump to adjust the inflow accordingly. Also, there are inputs for desorption time (ms), desorption volume (µL), wash flow rate (µL min^{-1}), and wash time (ms). Additionally, there is an option to save/load these parameters into a method.

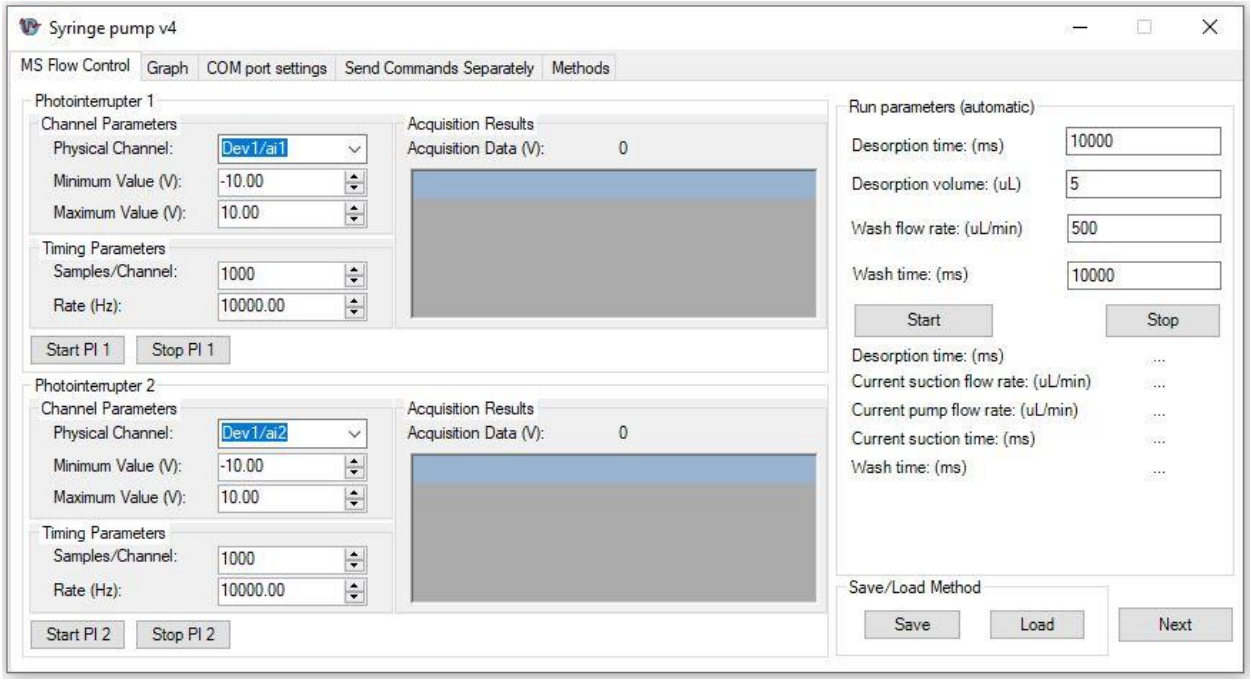

Figure 2.2. MS Flow Control tab of the home-written software in Microsoft Office Visual Studio 2019.

The next tab, Graph, is shown in **Figure 2.3.** and it contains plots that graphically show the data collected from the photointerrupters, thus offering a tool for manual control/check of the photointerrupters before running the MOI.

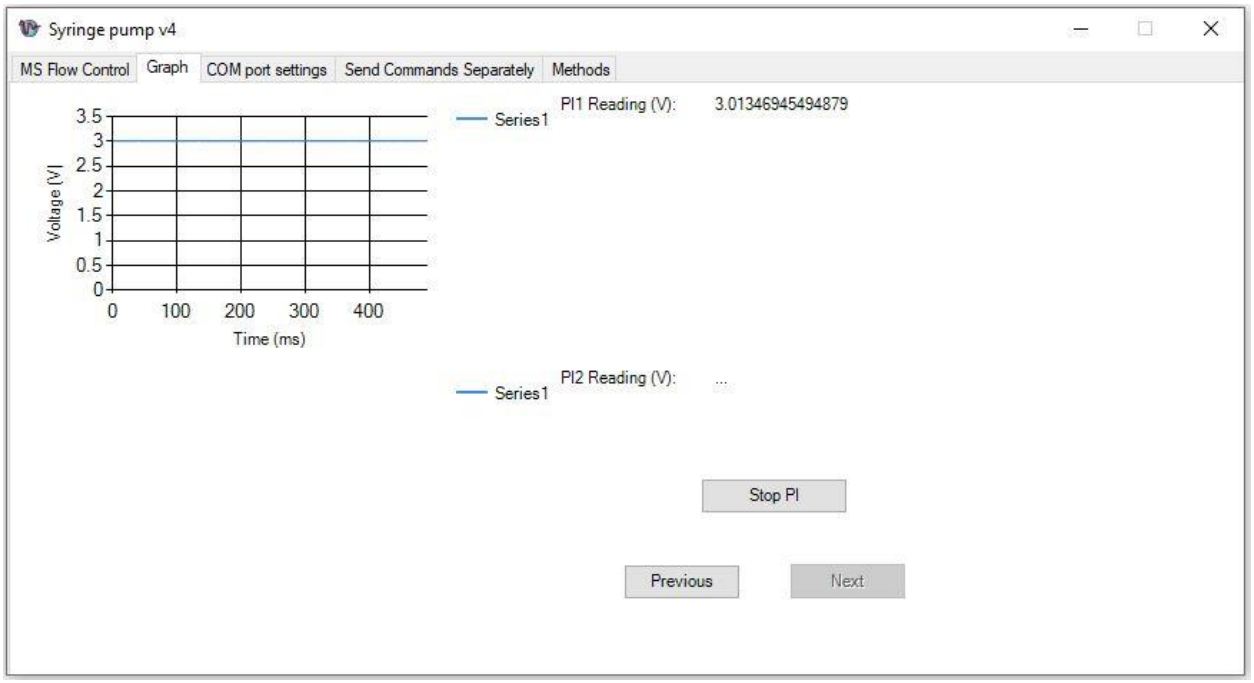

Figure 2.3. Graph tab of the home-written software in Microsoft Office Visual Studio 2019 showing data collection from the photointerrupter 1, for testing purposes.

The next tab, COM Port Settings, is shown in **Figure 2.4.** and it shows the window when the software is started. Next, it offers access to the communication ports of the computer used. Once connected, it displays basic information (baud rate, stop bits, data bits, parity, handshake, and read timeout) of the port through which it established the communication.

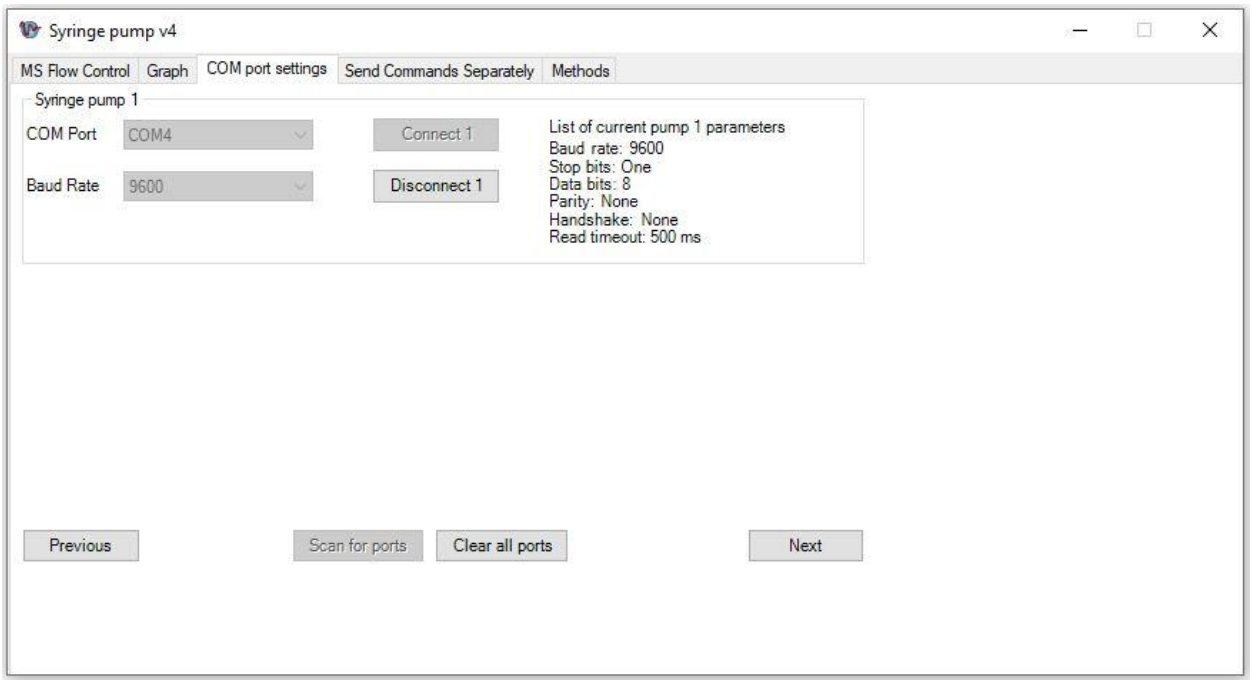

Figure 2.4. COM port settings tab of the home-written software in Microsoft Office Visual Studio 2019 shows a connected syringe pump with its parameters.

The next tab, Sends Commands Separately, is shown in **Figure 2.5.** and it offers a way to communicate with the syringe pump once connected. It is mainly used to test the pump communication before running.

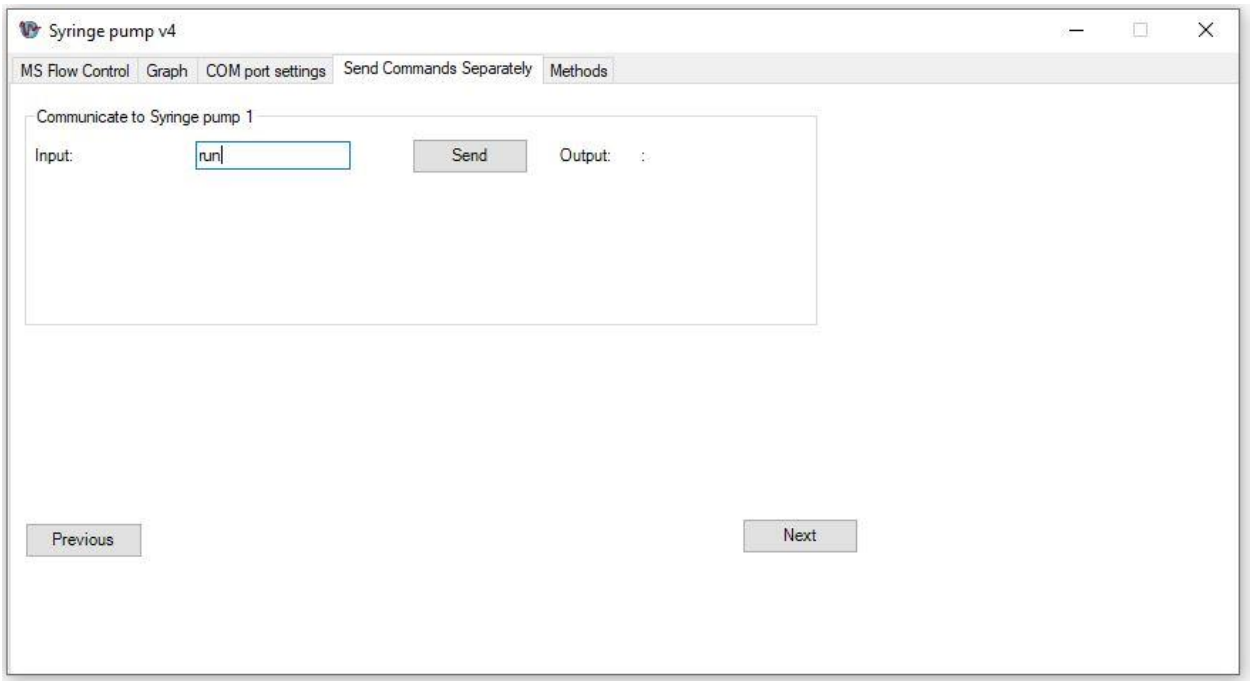

Figure 2.5. Sends commands separately tab of the home-written software in Microsoft Office Visual Studio 2019 with the purpose of testing syringe pump connection by running a simple command (*e.g.*, run).

The last tab is Methods, shown in **Figure 2.6.** It offers a way to save/load/edit methods specific to the syringe pump. These methods contain infuse/withdraw direction information, syringe selection, force setting, flow rate, and target volume.

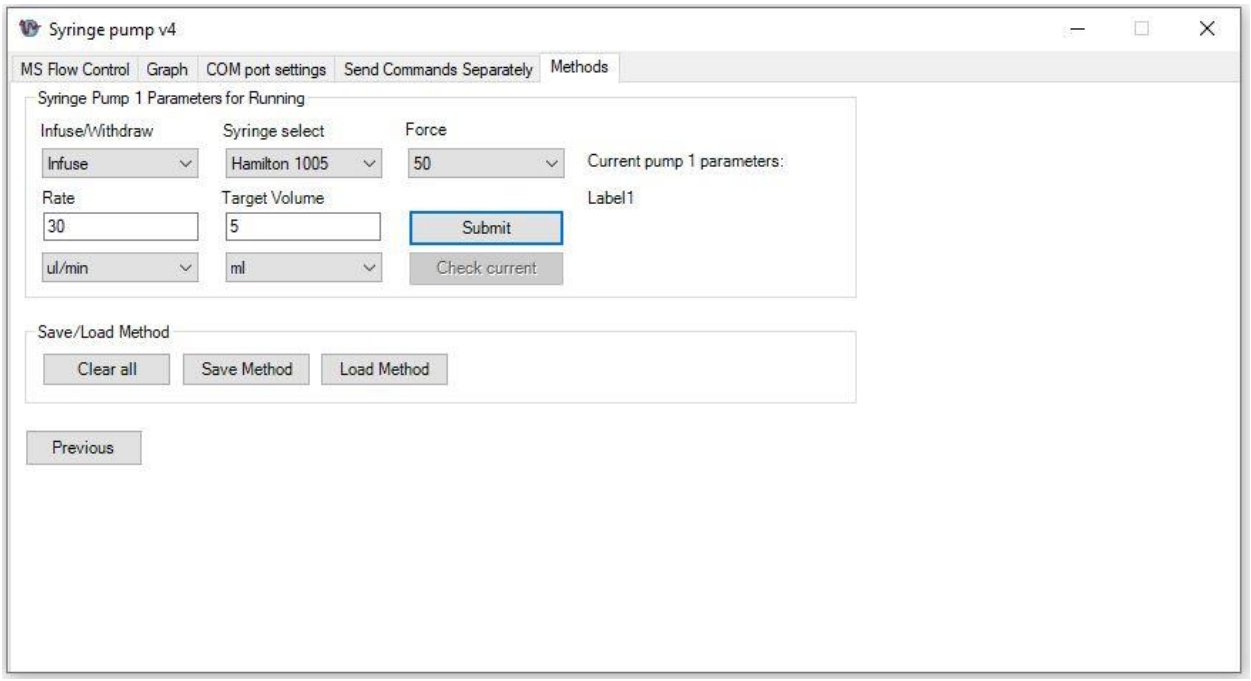

Figure 2.6. Methods tab of the home-written software in Microsoft Office Visual Studio 2019 shows the options to save/load syringe and syringe pump parameters.

2.3.6 Microfluidic open interface operational workflow

Overall, the analysis of SPME fiber with the MOI consists of a couple of stages. Firstly, consider the desorption chamber empty. The inflow of desorption solution is increased to fill the desorption chamber. Next, the mass spectrometer method is manually started. Then, the SPME fiber is placed into the flow isolated region of the desorption chamber for short desorption (*e.g.*, 5 s). This desorption step is timed, and the software turns off the inflow flow rate after it expires. Next, the SPME fiber is removed. When the air/liquid interface triggers the photointerrupter, the software starts the syringe pump with two times the flow rate to flush the leftover analyte contaminated desorption solution from the dead volume out of the MOI into the wash container placed outside of the desorption chamber. This dead volume is equal to the tubing volume between the desorption chamber and the three-way chromatographic tee (approximately 0.7 µL). The complete residual volume must be expelled. If all desorption volume is sucked to the instrument for the analysis, an air bubble will be introduced to the electrospray process, interrupting the signal.

Flushing everything out for a predetermined period (*e.g.*, 15 s) is enough to clean the system from the analyte. Then after this process, the software sets back the actual inflow flow rate to keep the level in the desorption chamber level. Then, another suction process is repeated to ensure that there is no trace amount of analyte in the system that might cause the carryover.

2.3.7 Instrumental analysis

For a set of experiments performed on API 4000, the instrumental parameters are shown in **Table 2.2.**

Table 2.2. Instrumental/tuning parameters for acetylfentanyl on SCIEX API 4000 triple quadrupole mass spectrometer.

Analyte	Acetylfentanyl
Precursor Ion (m/z)	323.0
Product Ion (m/z)	188.2
Dwell Time (ms)	50
Declustering Potential (V)	102.2
Entrance Potential (V)	10.0
Collision Energy (V)	32.7
Collision Exit Potential (V)	14.1

The source conditions for the API 4000 are listed below in **Table 2.3.**

Table 2.3. Ionization source conditions for MOI coupled to SCIEX API 4000 mass spectrometer.

Curtain gas (psi)	20
Ion Source Gas 1 (psi)	90
Ion Source Gas 2 (psi)	70
Ion Spray Voltage (V)	5000
Temperature (°C)	300

For a set of experiments performed on Thermo TSQ Vantage, the instrumental parameters are shown in **Table 2.4.**

Table 2.4. Instrumental/tuning parameters for lorazepam on Thermo TSQ Vantage triple quadrupole mass spectrometer.

Analyte	Lorazepam
Precursor Ion (m/z)	321.0
Product Ion (m/z)	274.9
Dwell time (ms)	50
Collision Energy (V)	22
S-Lens (V)	73

The source conditions for the Thermo TSQ Vantage are listed below in **Table 2.5.**

Table 2.5. Ionization source conditions for MOI coupled to Thermo TSQ Vantage triple quadrupole mass spectrometer.

Positive mode ionization voltage (V)	3000
Sheath gas	40
Auxiliary gas	10
Sweep gas	1
Ion transfer capillary	275

For a set of experiments performed on Thermo TSQ Quantiva, the instrumental parameters are shown in

Table 2.6.

Table 2.6. Instrumental/tuning parameters for lorazepam on Thermo TSQ Quantiva triple quadrupole mass spectrometer.

Analyte	Lorazepam
Precursor Ion (m/z)	321.1
Product Ion (m/z)	275.0
Collision Energy (V)	24
RF Lens (V)	69
Dwell Time (ms)	10

The source conditions for the Thermo TSQ Quantiva are listed below in **Table 2.7.**

Table 2.7. Ionization source parameters for Thermo TSQ Quantiva triple quadrupole MS for optimum performance of the microfluidic open interface operation.

Positive mode ionization voltage (V)	3500
Sheath gas	50
Auxiliary gas	10
Sweep gas	1
Ion transfer capillary (°C)	325
Vaporization temperature (°C)	30

For the set of experiments done on Shimadzu LCMS-8060, the instrumental parameters are shown in **Table 2.8.**

Table 2.8. Instrumental/tuning parameters for analytes on Shimadzu LCMS-8060 triple quadrupole mass spectrometer.

Analyte	**Precursor Ion (m/z)**	**Product Ion (m/z)**	**Dwell Time (ms)**	**Q1 Pre Bias (V)**	**Collision Energy (V)**	**Q3 Pre Bias (V)**
Amphetamine	136.2	91.1	10	-10	-21	-16
Acetaminophen	152.2	110.1	10	-16	-19	-11
Buprenorphine	468.3	55.1	10	-13	-51	-22
Morphine	286.1	152.1	10	-13	-55	-30
Lorazepam	320.9	275.0	10	-16	-16	-21
Propranolol	260.2	116.2	10	-12	-19	-12

The ionization source conditions for the Shimadzu LCMS-8060 are listed below in

Table 2.9.

Table 2.9. Ionization source parameters for Shimadzu LCMS-8060 triple quadrupole MS for optimum performance of the microfluidic open interface operation.

Nebulizing gas flow (L min^{-1})	3.0
Drying gas flow (L min^{-1})	Off
Heating gas flow (L min^{-1})	Off
Interface voltage (V)	4000
Interface temperature (°C)	Off
DL Temperature (°C)	250
Heat block temperature (°C)	400

Table 2.10. Physicochemical properties and structures of analytes accessed from Chemicalize (https://chemicalize.com/app/calculation, 7. June 2022.). (**a**) stands for acidic pKa while (**b**) stands for basic pKa.

Analyte	pKa	LogP	Molar mass (g mol^{-1})	Structure
Amphetamine	10.0	1.8	135.2	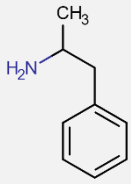
Acetaminophen	9.5	0.9	151.1	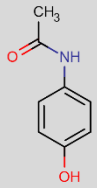
Buprenorphine	9.6 (a) 10.4 (b)	3.6	467.7	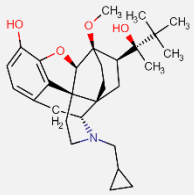
Morphine	10.3 (a) 9.1 (b)	0.9	285.3	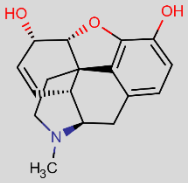
Lorazepam	10.6	3.5	321.1	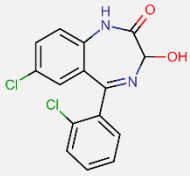

Propranolol	14.1 (a) 9.7 (b)	2.6	259.4	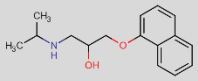

2.4. Results and Discussion

2.4.1. Initial development

The **Figure 2.7.** shows the comparison of peaks obtained by the two MOI designs. The peak width of the new MOI design is about 0.1 min (6 s), while the peak width of the previous version is about 0.2 min (12 s).

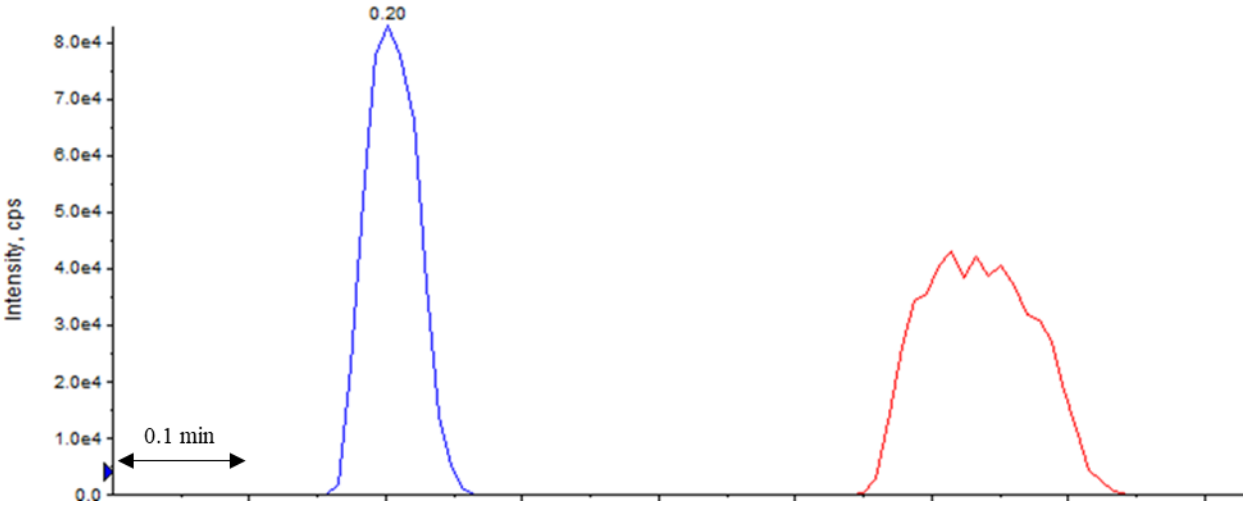

Figure 2.7. The comparison/overlay of the peak shape generated by the two designs of the MOI. The blue peak represents the improved design (described in **Section 2.3.3.** and manually operated, without software, NI DAQ device, and photointerrupter), and the red peak represents the previous design (described in **Section 1.6.**). This experiment was performed on SCIEX API 4000 triple quadrupole MS. The peaks represent 15 min extraction of acetylfentanyl from urine (1 ng mL^{-1}) with HLB-PAN SPME fiber.

A fair comparison between these two designs is difficult because the desorption chamber volumes are different (new design: 5.0 µL, previous design: 7.8 µL) because of the inner diameter differences. Additionally, the new design is improved by reducing the distance between the desorption chamber, which

offers less suction resistance, thus yielding that the new design has a higher suction flow rate (about 50 %). A higher suction flow rate can naturally squeeze the analyte plug and provide higher intensity. However, the blue peak is twice as high, but the red peak is about twice broad. Hence, it can be concluded that the area of these two peaks is the same; thus, the new design of MOI does not contribute to any analyte signal (in terms of area counts) increase/decrease.

The advantage of the sharper Gaussian peak produced is that it offers the ability to have a higher signal-to-noise ratio, thus the ability to reach lower LOQ/LOD levels. On the other hand, such a sharp peak will reach the MS detector saturation at lower concentrations than a broader Gaussian peak, thus limiting the higher operational concentration.

The next step was to show that this improved version of the MOI could be reproducible.

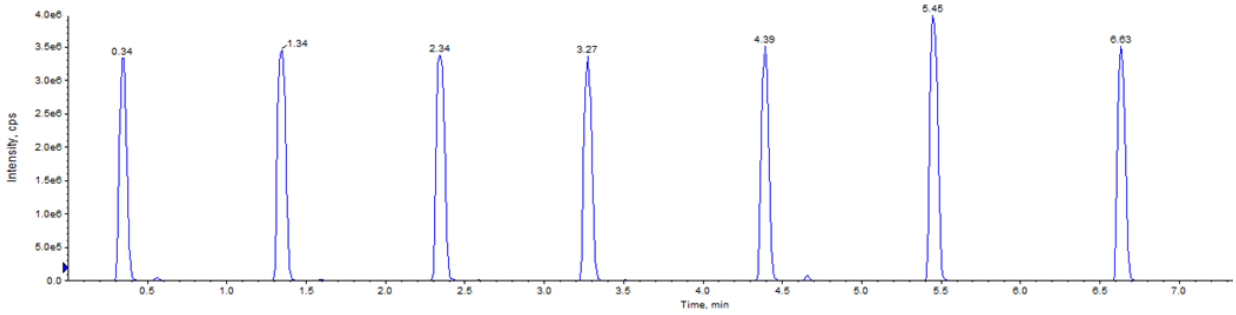

Figure 2.8. The introduction of multiple (n = 7) replicates of HLB-PAN SPME fibers was used to extract acetylfentanyl from urine (50 ng mL^{-1}) for 15 min. The improved design of the MOI was operated manually (described in **Section 2.3.6.** and manually operated without software, NI DAQ device, and photointerrupter). The experiment was performed on SCIEX API 4000. The area counts relative precision is 8%.

Figure 2.8. shows that the improved design of the MOI is indeed reproducible, even though when operated manually. Therefore, the next step in the design is to perform (semi-)automation of the MOI system because the peaks did not elute at regular intervals. Also, the (semi-)automation of the MOI system allows for fewer errors, as manual operation can lead to errors. Nevertheless, manual control would provide a steep learning curve if this interface was ever introduced to others.

2.4.2. Automation

The **Table 2.11.** shows the relative precision of raw area counts when MOI has been used manually (described in **Section 2.3.4.** and manually operated, without software, NI DAQ device, and photointerrupter) versus the MOI system with automation (described in **Section 2.3.6.**). The differences between the two ways of using the MOI mostly come from slight differences in volumes *injected* from the desorption chamber to the MS instrument. When analytes are desorbed in very small volume (*e.g.*, 5 µL), a minimal volume injection variation (in case of manual operation) will cause relatively high differences in MS response because of the high amount of analytes that are present.

Table 2.11. The relative precision difference of raw area counts before and after the automation. Analytes, spiked at 20 ng mL^{-1}, were extracted from the whole blood (n = 4) for 60 min using PAN-C_8-SCX SPME fiber agitated at 1200 rpm. For this experiment, Shimadzu LCMS-8060 has been used.

Analyte	Before automation	After automation
4-ANPP	21	8
Acetylfentanyl	28	14
Alfentanil	26	15
Carfentanil	24	9
Fentanyl	28	12
Sufentanil	24	5

2.4.3. Adapting MOI for other mass spectrometer manufacturers

Figure 2.9. shows the schematic design of the most critical parts for proper MOI operation coupled to the ionization sources of SCIEX's turbo spray, Thermo's ion max, and Shimadzu's ion source. Briefly, the suction flow in the MOI interface is created by the Venturi effect caused by the nebulization/sheath gas running along the electrospray capillary. The negative pressure aspirates the liquid from the interface. For the optimum suction flow rate, the inner diameter and length of the tubings are critical as the viscosity of the solution. Methanol is MS compatible solvent that offers the best performance in terms of low viscosity and the ability to desorb analytes from the SPME coating. The problem can appear when the temperature

of the suction flow path comes close/reaches the boiling point of the desorption solution (primarily methanol-based). Then, methanol evaporates, and bubbles are created in the narrow electrospray capillaries (100 – 150 µm inner diameter), which will cause a lot of resistance and slow the suction flow rate. Furthermore, this will widen the narrow plug of analytes introduced to the instrument, and the signal-to-noise ratio will suffer.

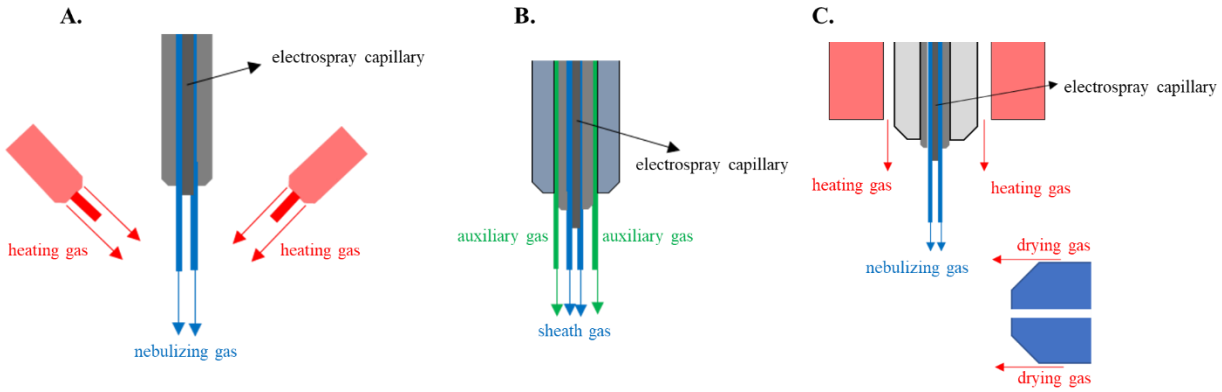

Figure 2.9. Schematic representation of critical parts of SCIEX (A), Thermo (B), and Shimadzu (C) ionization sources for the MOI. Essential parts include nebulization, heating, drying, sheath, auxiliary gas source, and direction with respect to electrospray capillary.

The use of heating gas for the electrospray can have a negative influence on the MOI function. Briefly, and in simple words, once the nebulizing gas has dispersed the liquid into tiny droplets, a heating gas is applied to evaporate the excess solvent of those droplets. Then, the number of charged species in the droplets keeps increasing as the solvent evaporates, which leads to droplet bursts into smaller droplets. This process keeps going until the ion is almost entirely desolvated. This process occurs as the droplet is being introduced to the MS.[3]

The best ionization source for the MOI seems to be designed by the SCIEX, where the heating gas, which has the purpose of enhancing the solvent evaporation during electrospray ionization, is aimed at the nebulized droplets that have exited the electrospray capillary; thus no bubbles are created in the electrospray capillary. On the other hand, it is built differently where the heating gas runs along the electrospray capillary. This way, the eluent from the electrospray capillary is heated as it elutes. This way is not optimal

for the proper functioning of the MOI. One way to avoid this is not to use heating gas (use regular ESI instead of heated-ESI format). The Thermo MS has a heated transfer capillary at the MS inlet, providing enough heating to evaporate excess solvent surrounding the ions.

Furthermore, Shimadzu runs with a similar design as the Thermo. They also have heating gas running along the axis of the electrospray capillary, which heats it, thus producing unwanted bubbles. The best way to use it is to turn off the temperature. Interface temperature is also turned off. Shimadzu MS inlet has a desolvation line (analogous to Thermo transfer capillary) heated to a very high temperature (normal use 250 °C). On top of this, it also has a heat block heated at 400 °C (see

Table 2.9.) which helps dry the ions before they enter the MS. Shimadzu MS also has a drying gas, a hot gas that can come outside of the MS to assist in desolvation, but it is turned off, so it does not heat the tip of the electrospray capillary. These MS have slightly different MS and ionization source designs and are compatible with the MOI under the right conditions.

Another essential aspect for the optimal use of the MOI is the electrospray capillary assembly design. **Figure 2.10.** shows the electrospray capillary assemblies used for different ionization sources. For MOI to have optimal conditions suction flow rate of 100 – 150 µL min^{-1} is required. For SCIEX to reach this operating suction flow rate, the electrospray capillary assembly of the SCIEX ionization source needed to be modified. The regular 100 µm inner diameter stainless steel capillary is replaced with the 150 µm inner diameter 316 stainless steel (McMaster-Carr), and a PEEK tubing was cut to serve as a sleeve for the fitting (0.0625 in outer diameter, 0.016 in inner diameter, IDEX). One of the reasons for this is the relatively long electrospray capillary which creates more suction resistance. The Thermo uses a unique ferrule design, and

the standard electrospray capillary had to be used for the Thermo ionization source. Even though the standard electrospray capillary offers a suction flow rate of 85 µL min^{-1}, it is sufficient to create sharp peaks.

Moreover, the electrospray capillary assembly used in the Shimadzu ionization source seems the best. Their standard capillary can be replaced with a modified one (150 µm inner diameter 316 stainless steel + 0.0625 in outer diameter, 0.016 in inner diameter PEEK tubing was cut to serve as a sleeve for the fitting). The length is very short, more than two times shorter than SCIEX-one.

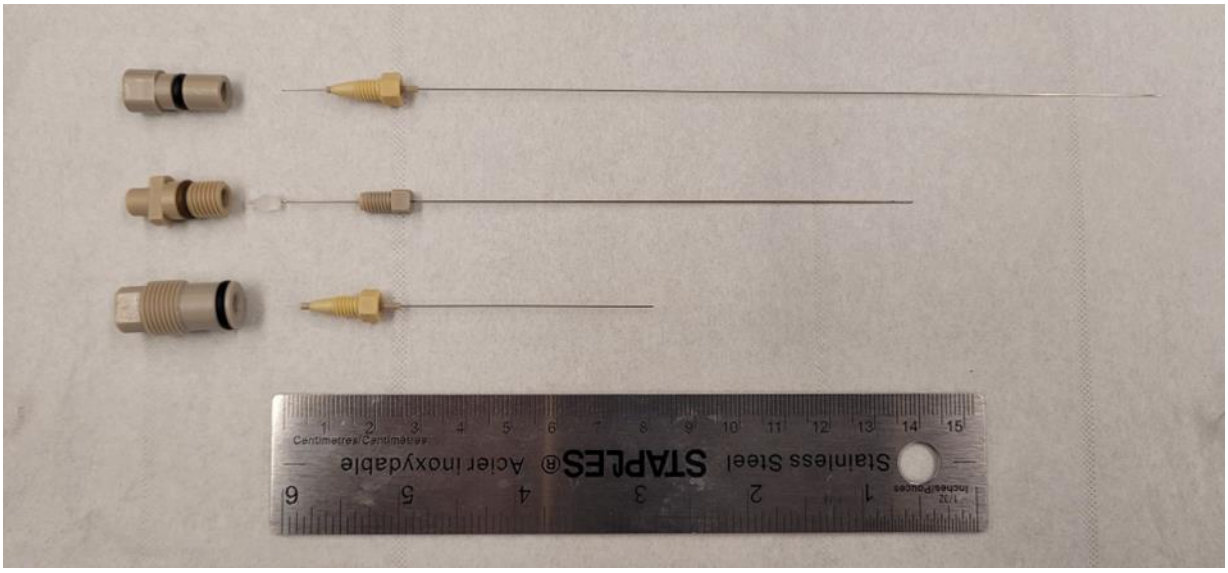

Figure 2.10. Electrospray capillary assemblies used for different ion source designs for coupling microfluidic open interface to different mass spectrometers. Electrospray capillary assemblies for the ion sources created by SCIEX, Thermo, Shimadzu (top to down).

Considering all three ionization-MS designs, the Shimadzu one seems the best because its electrospray capillary design can be easily modified. A short design produces little suction resistance, and the heated MS inlet dries the excess solvent even though the heating gas is turned off.

2.4.4. Comparison of peak shapes of MOI when coupled to mass spectrometers of different manufacturers and carryover assessment

Since the desorption chamber of the MOI is not in the desorption solution flow path the whole time, the design is susceptible to carryover in the desorption chamber. When the concentration of the analyte plug (after desorption) is ready to be introduced to the MS for analysis, there can be an amount of desorption

solution droplets containing analytes stuck in the pockets created by sharp corners. During the analysis, the whole desorption volume can't be introduced to the MS because air will enter the electrospray capillary; thus, it will cause signal instability.

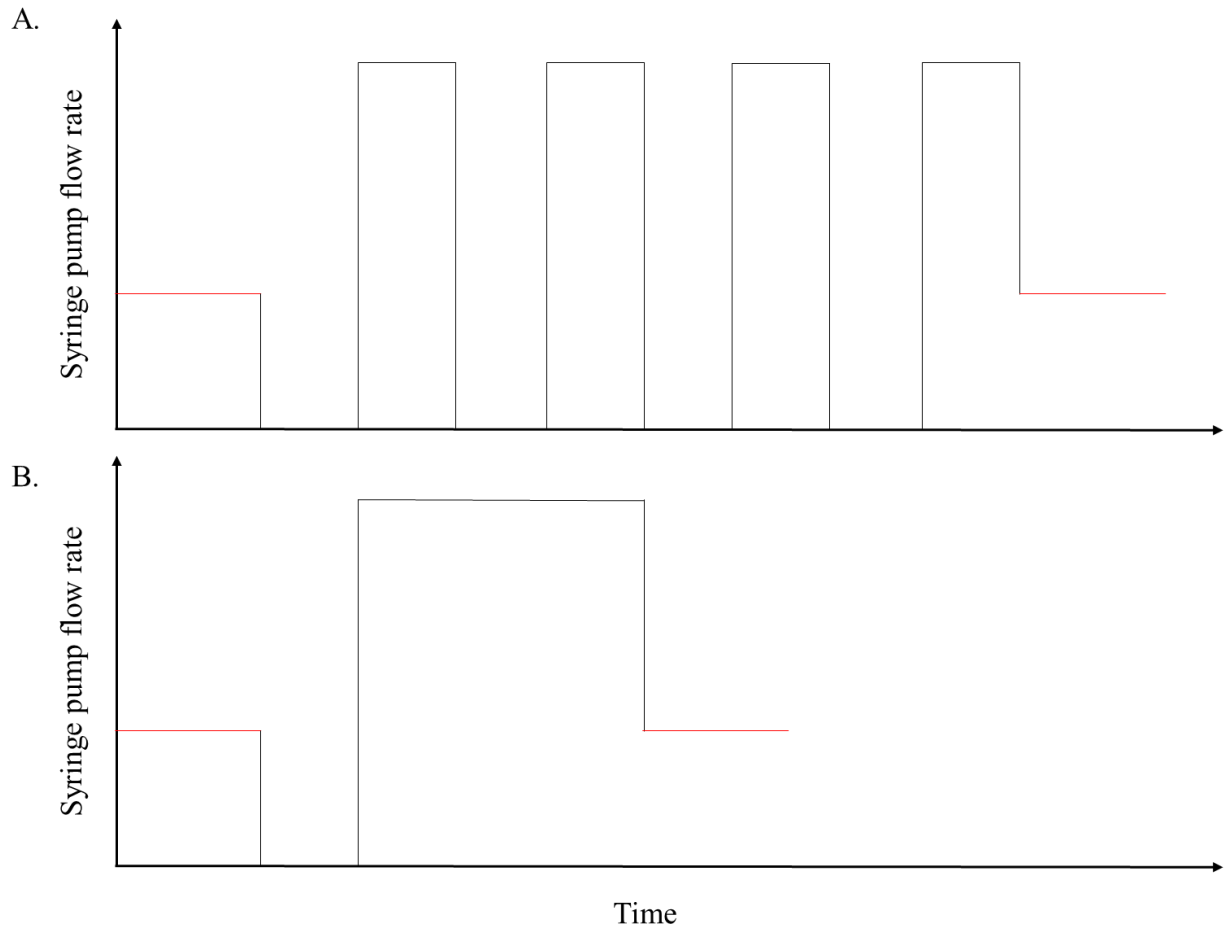

Figure 2.11. (A) The inflow syringe pump profile to address the carryover. (B) Alternative inflow syringe pump profile to address the carryover. The red line on both parts of the figure represents the suction flow rate.

The carryover can be minimized by repeating the introduction of analytes to the instrument a couple of times until a baseline signal is obtained. This is shown in **Figure 2.12.**, where the carryover after consecutive injections is monitored. The carryover has been removed (addressed) by repeating the *injection* process at least three more times to recover the baseline signal. This process adds additional analysis time, which counters the idea of rapid analysis.

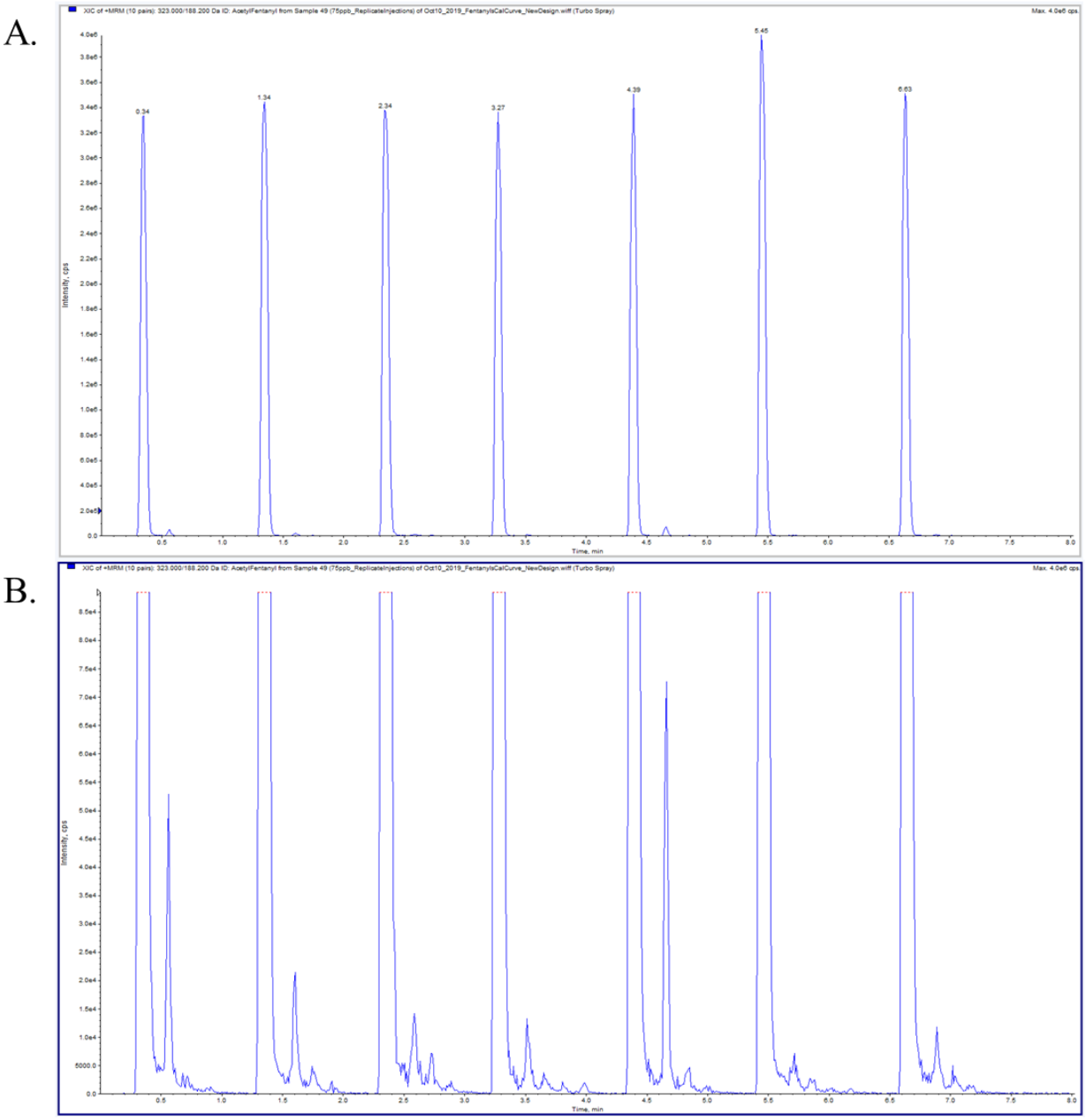

Figure 2.12. (A) The introduction of multiple (n = 7) replicates of HLB-PAN SPME fibers were used to extract acetylfentanyl from urine (50 ng mL^{-1}) for 15 min. The improved design of the MOI was operated manually (described in **Section 2.3.4.** and manually operated without software, NI DAQ device, and photointerrupter). (B) Zoomed in version. The peaks on the right-hand side are consecutive injections of analytes to the instrument, indicating the carryover. After three additional injections, the baseline signal is recovered.

Alternatively, the carryover can be dealt with by expelling the leftover from the desorption volume out through the open port into a collection chamber. This way, shown in **Figure 2.13., Figure 2.14.**, and **Figure**

2.15., the amount of carryover is pretty much non-existent when analyzed on different triple quadrupole mass spectrometers (Shimadzu LCMS 8060, Thermo Quantiva, and Thermo Vantage; respectively).

Additionally, **Figure 2.13.**, **Figure 2.14.**, and **Figure 2.15.** show the injection of lorazepam and peak shapes produced by the MOI. As discussed in **Section 2.4.3.,** the optimum interface design is created by the Shimadzu, which results in having the (slightly) more narrow baseline peak shape compared to other manufacturers.

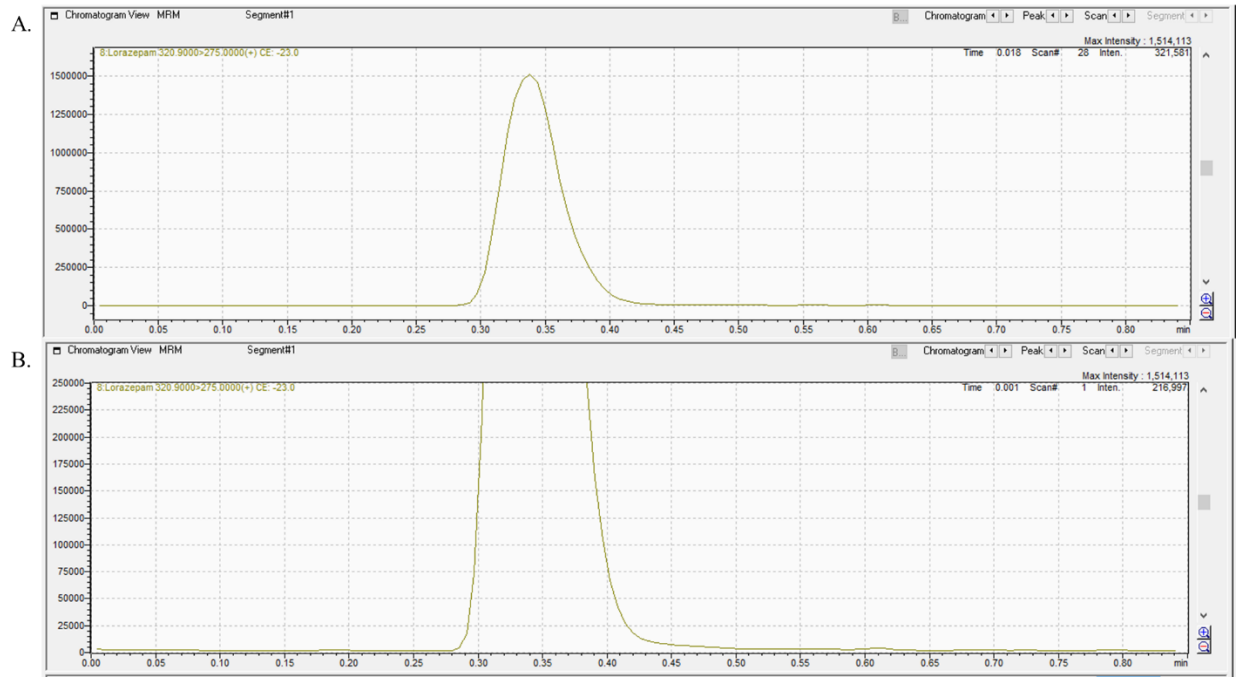

Figure 2.13. The analysis of lorazepam after extraction from PBS spiked at 50 ng mL^{-1} using PAN-HLB SPME fiber for 60 minutes at 1200 rpm. The desorption conditions were 10 s in methanol:acetonitrile:water = 7:2:1 (V:V:V) with 0.1 % formic acid. This analysis is run on the Shimadzu LCMS 8060 triple quadrupole mass spectrometer. (A) shows the full view, while (B) shows the zoomed-in version at about 15 % of the maximum intensity. The x-axis represents time (min) while the y-axis represents raw intensity.

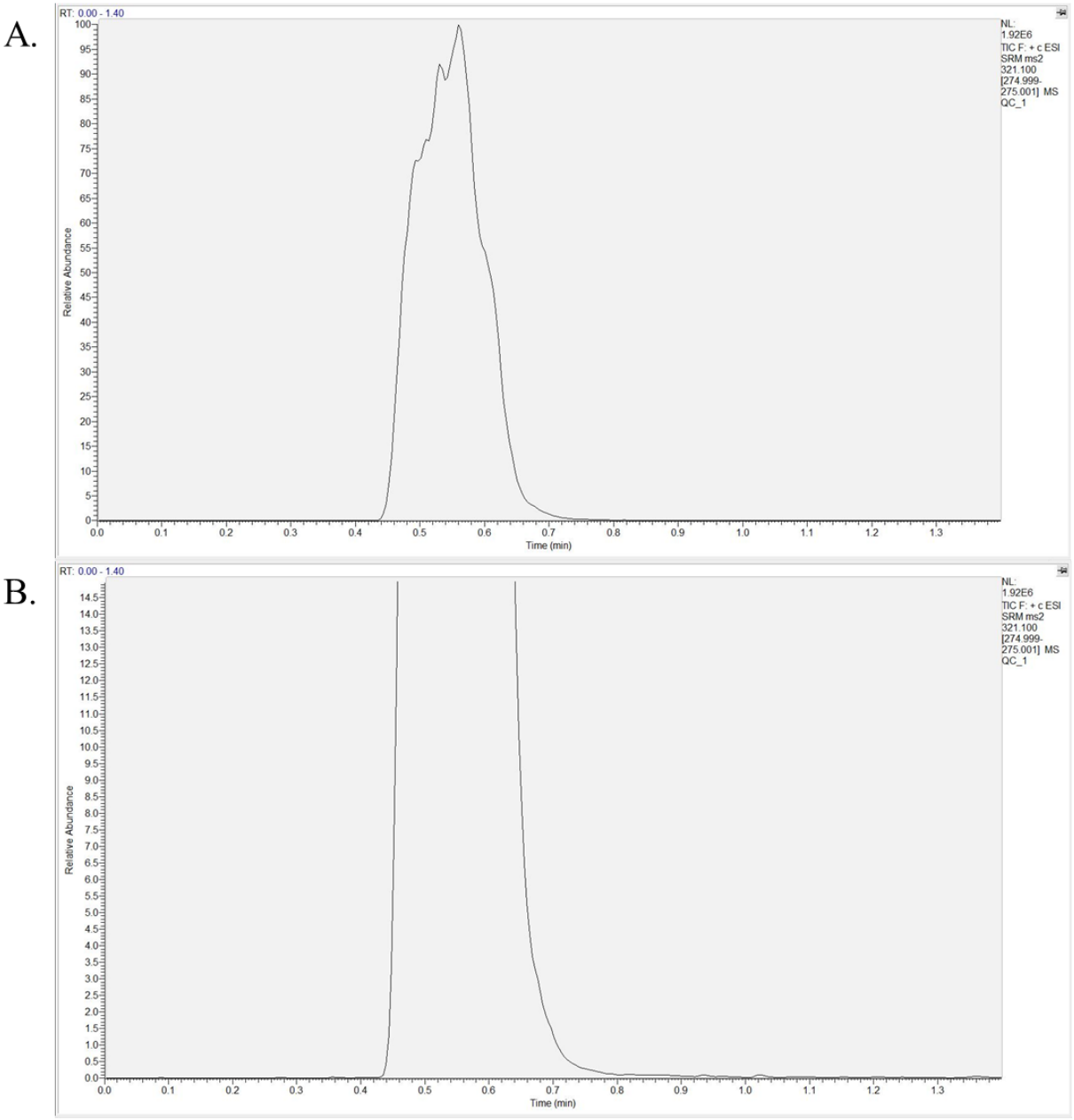

Figure 2.14. The analysis of lorazepam after extraction from PBS spiked at 50 ng mL^{-1} using PAN-HLB SPME fiber for 60 minutes at 1200 rpm. The desorption conditions were 10 s in methanol:acetonitrile:water = 7:2:1 (V:V:V) with 0.1 % formic acid. This analysis is run on the Thermo Quantiva triple quadrupole mass spectrometer. (A) shows the full view, while (B) shows the zoomed-in version at about 15 % of the maximum intensity. The x-axis represents time (min) while the y-axis represents relative intensity.

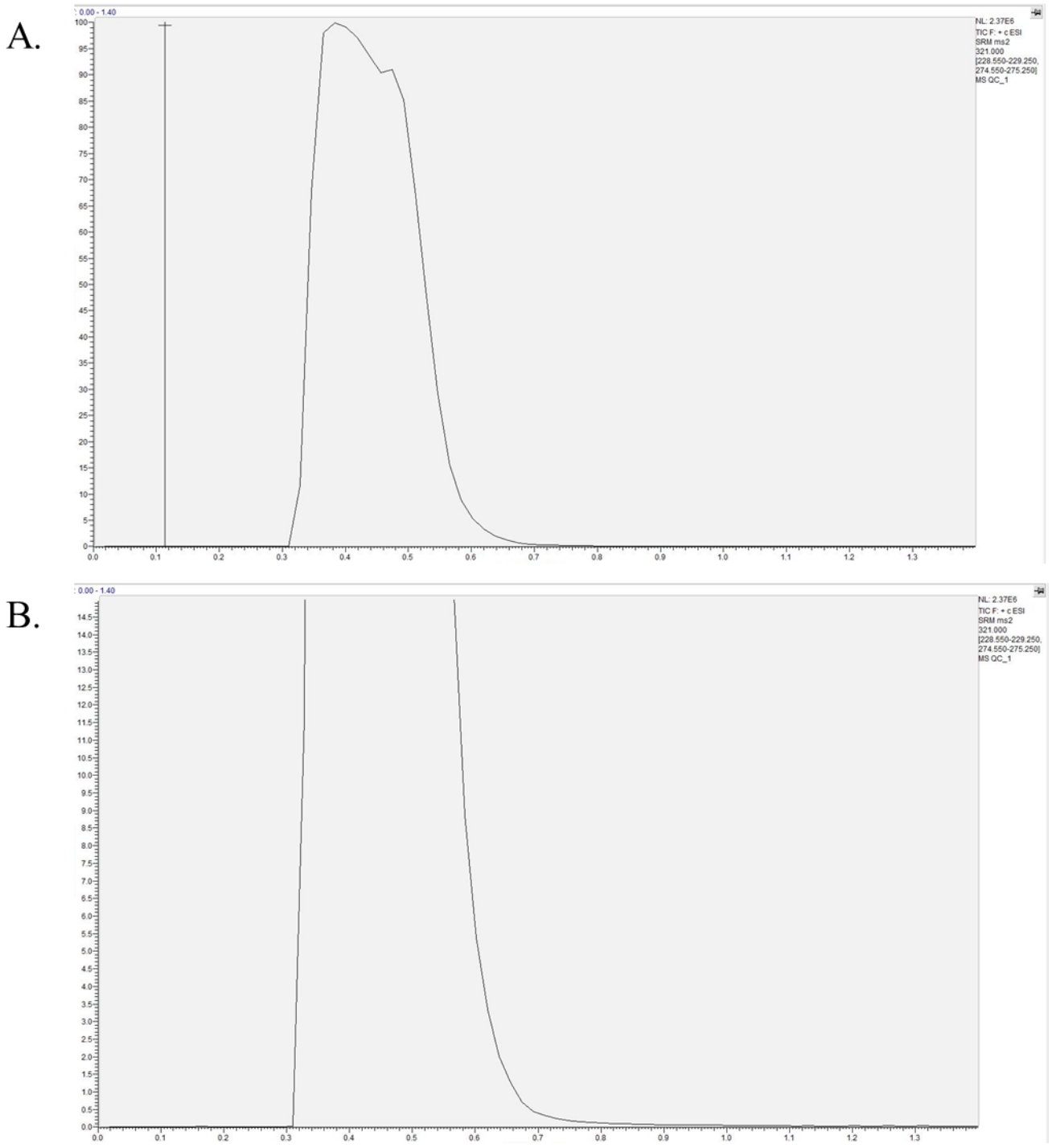

Figure 2.15. The analysis of lorazepam after extraction from PBS spiked at 50 ng mL^{-1} using PAN-HLB SPME fiber for 60 minutes at 1200 rpm. The desorption conditions were 10 s in methanol:acetonitrile:water = 7:2:1 (V:V:V) with 0.1 % formic acid. This analysis is run on the Thermo Vantage triple quadrupole mass spectrometer. (A) shows the full view, while (B) shows the zoomed-in version at about 15 % of the maximum intensity. The x-axis represents time (min) while the y-axis represents relative intensity.

2.4.5. Extraction time profiles of selected analytes for the evaluation of the MOI

Several analytes were selected to be used to evaluate the MOI for direct coupling with mass spectrometry. Namely, those analytes are amphetamine, acetaminophen, buprenorphine, morphine, lorazepam, and propranolol. These analytes are selected due to differences in the affinity for the extraction phase and differences in the polarity. Physicochemical properties and analyte structures are listed in **Table 2.10.** The evaluation considers different thicknesses of the PAN-HLB, PVDF-HLB, and Teflon-HLB coatings, to compare what coating thickness (Table 2.1.) is suitable for the analysis with MOI. The main reason is that the desorption time to maintain rapid analysis status is very short. **Figure 2.16.** shows the optimum extraction time using both types of PAN-HLB SPME fibers is about 60 minutes. Notably, the amount of acetaminophen introduced to the mass spectrometer decreases throughout the extraction period because this analyte is susceptible to displacement. The polar analytes equilibrate quicker with the extraction phase (because of the low distribution constant). Then as the extraction proceeds, the more nonpolar analytes (with higher distribution constant) can displace that compound from the extraction phase.[90]

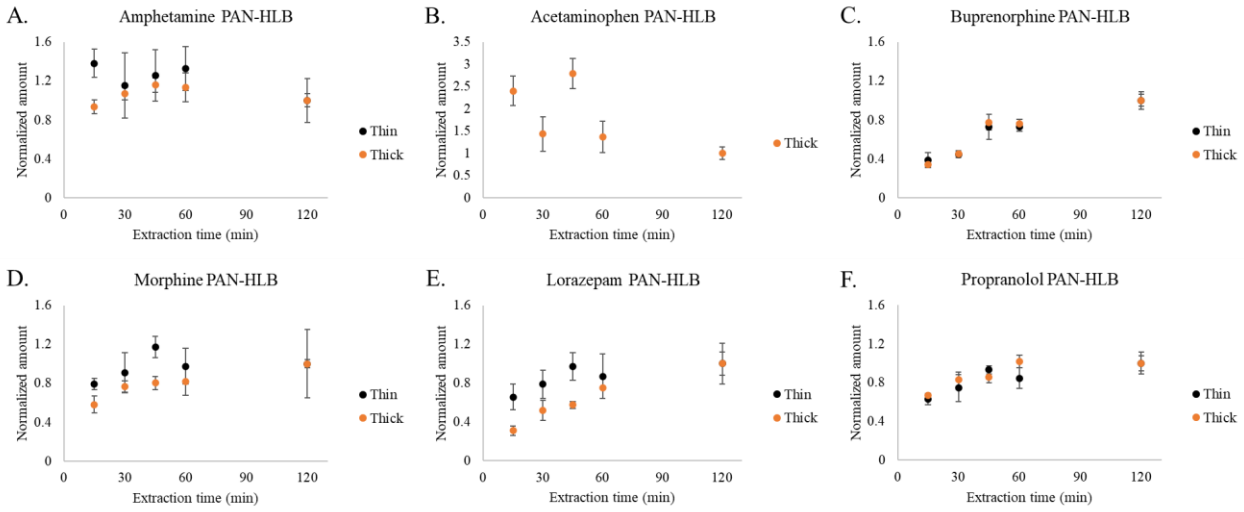

Figure 2.16. Extraction time profile of amphetamine (A), acetaminophen (B), buprenorphine (C), morphine (D), lorazepam (E), and propranolol (F) using 1 cm long PAN-HLB coating. The points in black represent thinner coating (coating thickness of 2 µm), while the points in orange represent thicker coating (coating thickness of 13 µm). The extractions were performed from PBS, where all analytes were spiked at 50.0 ppb for 60 minutes at 1200 rpm using Concept96. Data for acetaminophen extraction using thin PAN-HLB is missing because the amount introduced to the mass spectrometer is below limit of quantitation.

Figure 2.17. shows that the suitable equilibration time for PVDF-PAN SPME fibers is 60 minutes (as for PAN-HLB), but the interesting detail is that acetaminophen is not displaced. The lack of displacement herein is likely because more analytes with higher distribution constant (e.g., buprenorphine) are still in the linear extraction regime after two hours.

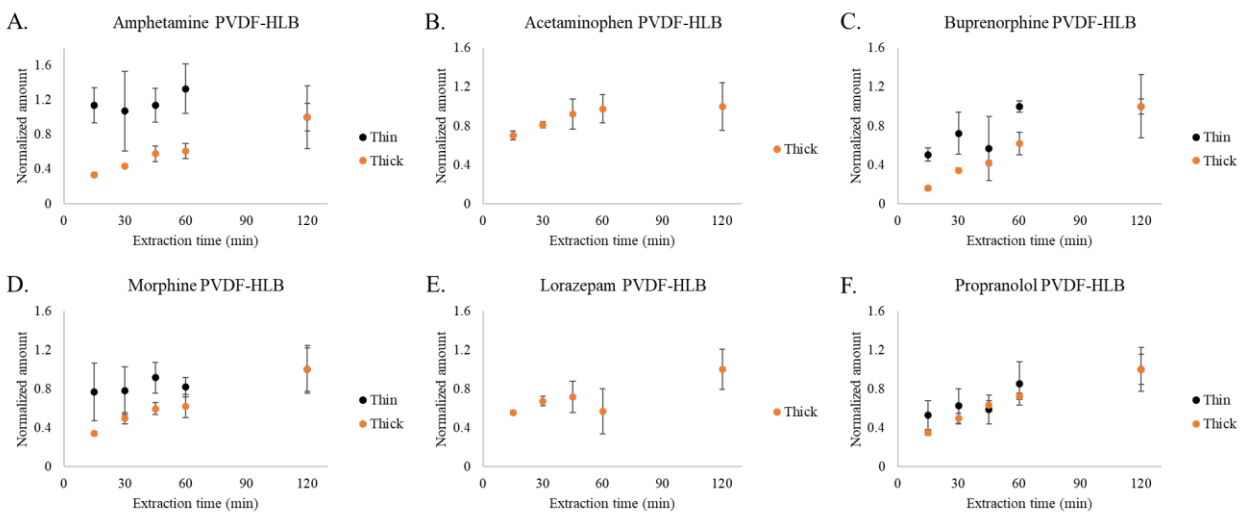

Figure 2.17. Extraction time profile of amphetamine (A), acetaminophen (B), buprenorphine (C), morphine (D), lorazepam (E), and propranolol (F) using 1 cm long PVDF-HLB coating. The points in black represent thinner coating (average coating thickness of 3 µm), while the points in orange represent thicker coating (average coating thickness of 14 µm). The extractions were performed from PBS, where all analytes were spiked at 50.0 ppb for 60 minutes at 1200 rpm using Concept96. Acetaminophen and Lorazepam extractions using thin PVDF-HLB coating are missing because the amount introduced to the mass spectrometer was below the limit of quantitation.

Figure 2.18. shows look a little bit different because Teflon-HLB SPME fiber does not seem very good in the extraction of half of the analytes in this study. Moreover, the suitable extraction time herein is 45 minutes, but because of simplicity in the experimental part, 60 minutes is the optimal extraction time for all SPME fibers.

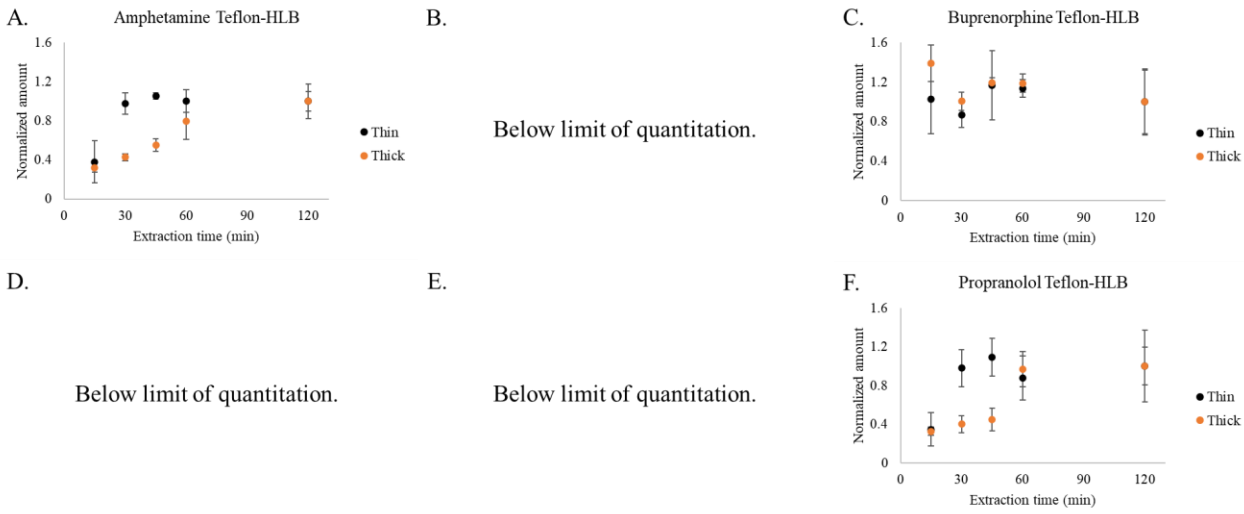

Figure 2.18. Extraction time profile of amphetamine (A), acetaminophen (B), buprenorphine (C), morphine (D), lorazepam (E), and propranolol (F) using 1 cm long Teflon-HLB coating. The points in black represent thinner coating (average coating thickness of 7 µm), while the points in orange represent thicker coating (average coating thickness of 10 µm). The extractions were performed from PBS, where all analytes were spiked at 50.0 ppb for 60 minutes at 1200 rpm using Concept96. Data for acetaminophen, morphine, and lorazepam are missing because the amount of analytes introduced to the mass spectrometer were below limit of quantitation.

2.4.6. Desorption time profiles of selected analytes for the evaluation of the MOI

The next important step for the MOI-MS method is to find the most suitable desorption time for studied analytes. Since different coating compositions (and thicknesses) were used, other desorption times will be ideal for each SPME fiber type. **Figure 2.19.** shows the desorption time profile of analytes from thick and thin PAN-HLB fibers. The optimum desorption time for thin PAN-HLB SPME fiber is 5 s, while up to 10 s are required for the thicker PAN-HLB SPME fibers to reach desorption equilibrium. Noteworthy, the amount of acetaminophen introduced to the mass spectrometer using thin PAN-HLB SPME fiber was not above the limit of quantitation.

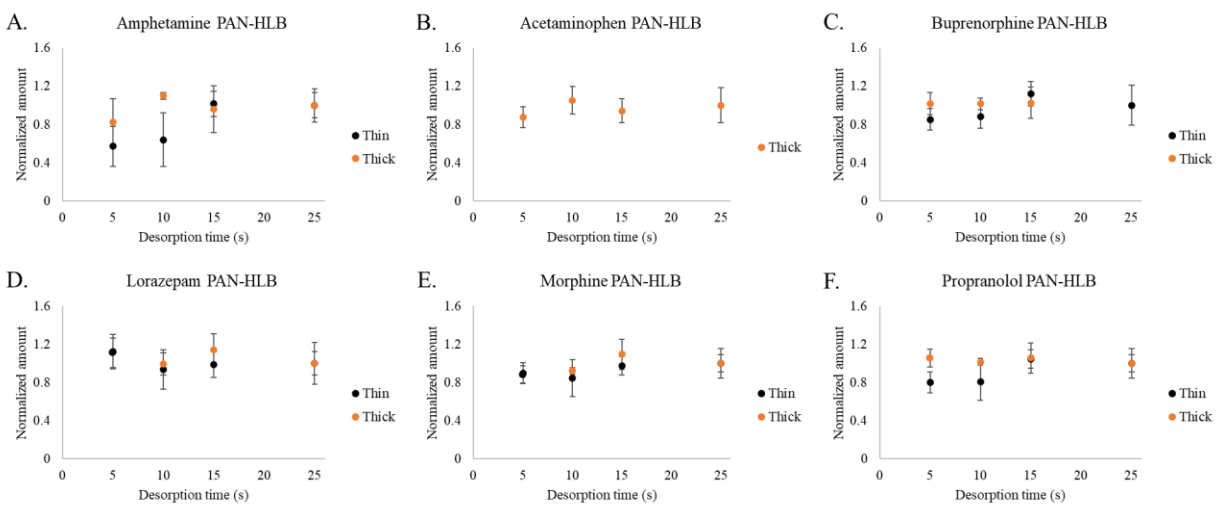

Figure 2.19. Desorption time profile of amphetamine (A), acetaminophen (B), buprenorphine (C), morphine (D), lorazepam (E), and propranolol (F) using 1 cm long PAN-HLB coating. The points in black represent thinner coating (average coating thickness of 2 µm), while the points in orange represent thicker coating (average coating thickness of 13 µm). The desorption solution was methanol:acetonitrile:water (7:2:1 = V:V:V) with 0.1 % formic acid. Data for acetaminophen desorption using thin PAN-HLB coating is missing because the amount of analytes introduced to the mass spectrometer were below the limit of quantitation.

On the other hand, the optimum desorption time for the PVDF-HLB SPME fiber (both thin and thick) is selected to be 15 s (shown in **Figure 2.20.**).

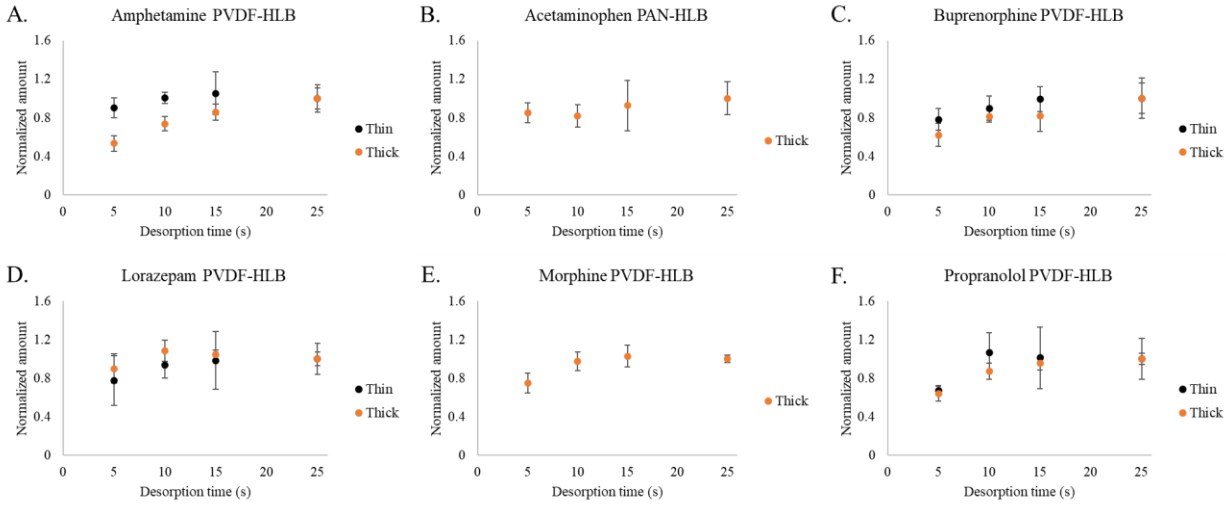

Figure 2.20. Desorption time profile of amphetamine (A), acetaminophen (B), buprenorphine (C), morphine (D), lorazepam (E), and propranolol (F) using 1 cm long PVDF-HLB coating. The points in black represent thinner coating (average coating thickness of 3 µm), while the points in orange represent thicker coating (average coating thickness of 14 µm). The desorption solution was methanol:acetonitrile:water

(7:2:1 = V:V:V) with 0.1 % formic acid. Data for acetaminophen and lorazepam using thin PVDF-HLB coating are missing because the amount introduced to the mass spectrometer was below the limit of quantitation.

Nevertheless, the optimum desorption time selected for the Teflon-HLB SPME fibers was 25 s.

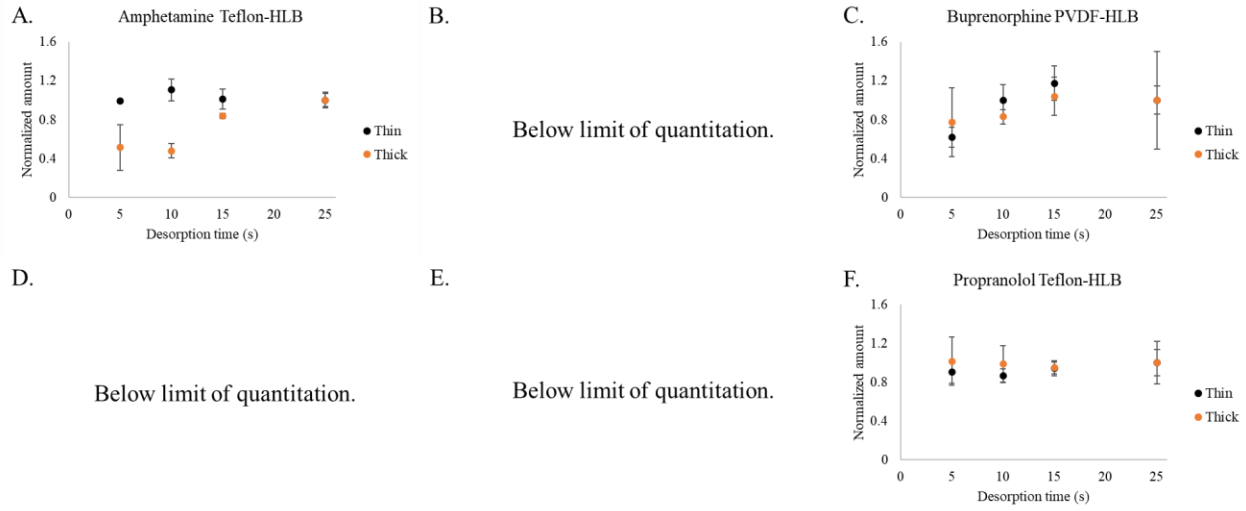

Figure 2.21. Desorption time profile of amphetamine (A), acetaminophen (B), buprenorphine (C), morphine (D), lorazepam (E), and propranolol (F) using 1 cm long Teflon-HLB coating. The points in black represent thinner coating (average coating thickness of 7 µm), while the points in orange represent thicker coating (average coating thickness of 10 µm). The desorption solution was methanol:acetonitrile:water (7:2:1 = V:V:V) with 0.1 % formic acid. Data for acetaminophen, morphine, and lorazepam are missing because the amount of analytes introduced to the mass spectrometer were below limit of quantitation.

2.4.7. Repeated desorptions of selected analytes for the evaluation of the MOI

Typically for the SPME applications, desorption times (from SPME fibers) is in the range of 20 – 30 minutes. The idea of coupling SPME to MOI is to desorb analytes rapidly. The desorption of analytes using the MOI reaches equilibration (or apparent equilibration) for a fraction of 1 minute. It is hard to believe that in MOI, the analytes can be desorbed more rapidly than for the regular SPME applications. Therefore, repeated (consecutive) desorptions are attempted from the same SPME fiber device to assess the amount of the carryover on the SPME fiber.

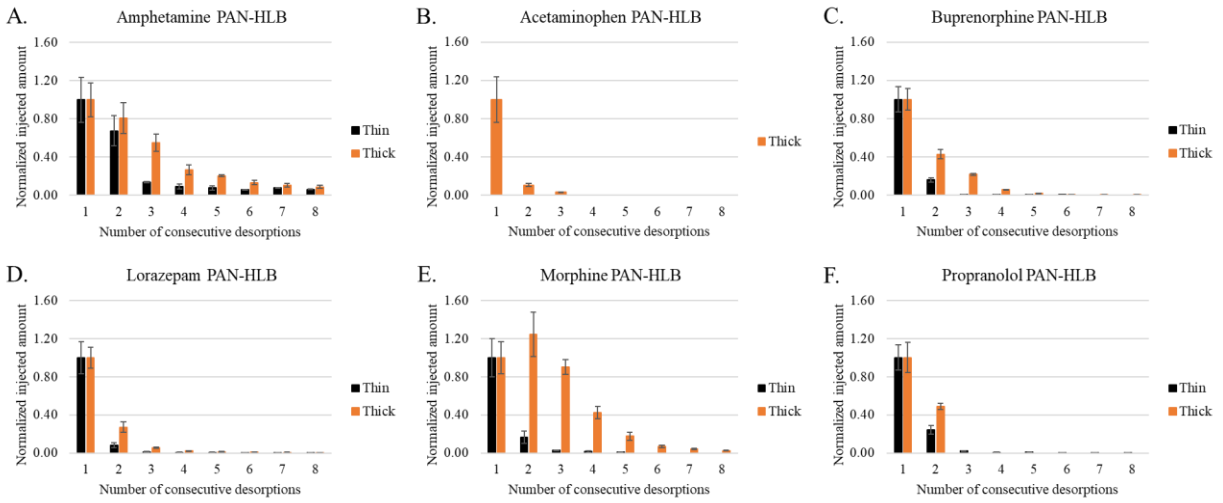

Figure 2.22. Repeated/consecutive desorptions, using the same SPME fiber, of amphetamine (A), acetaminophen (B), buprenorphine (C), morphine (D), lorazepam (E), and propranolol (F) using 1 cm long PAN-HLB coating. The points in black represent thinner coating (average coating thickness of 2 µm), while the points in orange represent thicker coating (average coating thickness of 13 µm). The desorption solution was methanol:acetonitrile:water (7:2:1 = V:V:V) with 0.1 % formic acid for 10 s. Data for acetaminophen desorption using thin PAN-HLB coating is missing because the amount of analytes introduced to the mass spectrometer were below the limit of quantitation.

On the other hand, the situation with the PVDF-HLB SPME fiber is very different from the PAN-HLB. For both thin and thick coatings, the analytes require more consecutive desorptions to be depleted from the SPME fibers, regardless of desorption equilibration shown in **Figure 2.20.**

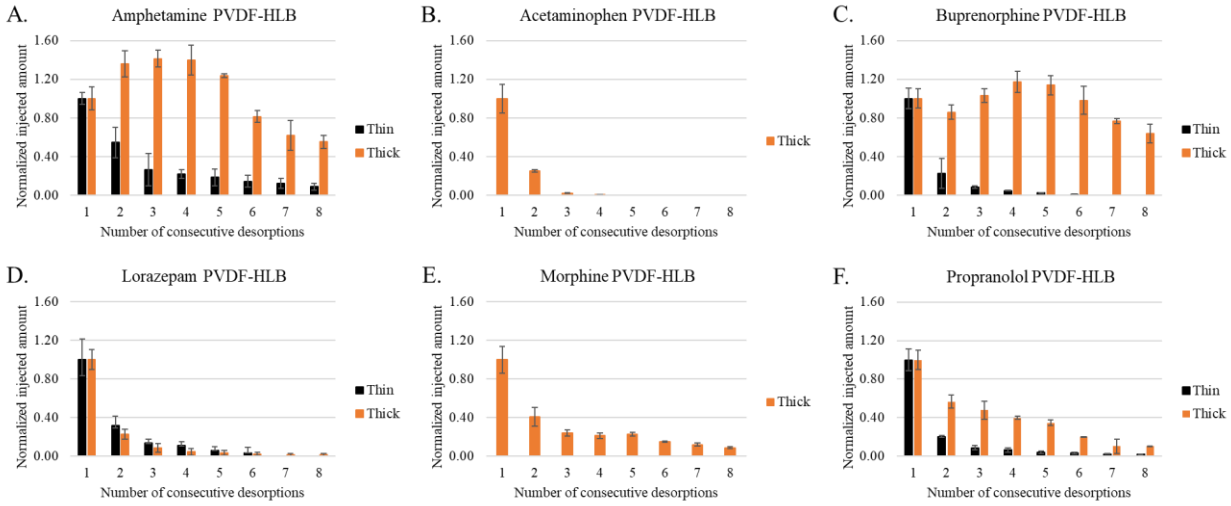

Figure 2.23. Repeated/consecutive desorptions, using the same SPME fiber, of amphetamine (A), acetaminophen (B), buprenorphine (C), morphine (D), lorazepam (E), and propranolol (F) using 1 cm long

PVDF-HLB coating. The points in black represent thinner coating (average coating thickness of 3 µm), while the points in orange represent thicker coating (average coating thickness of 14 µm). The desorption solution was methanol:acetonitrile:water (7:2:1 = V:V:V) with 0.1 % formic acid for 15 s. Data for acetaminophen and lorazepam using thin PVDF-HLB coating are missing because the amount introduced to the mass spectrometer was below the limit of quantitation.

Lastly, for the Teflon-HLB SPME fiber, for three analytes whose amount introduced is above the limit of quantitation, the analytes get depleted from the coating rather rapidly, for both thin and thick coatings (shown in **Figure 2.24.**).

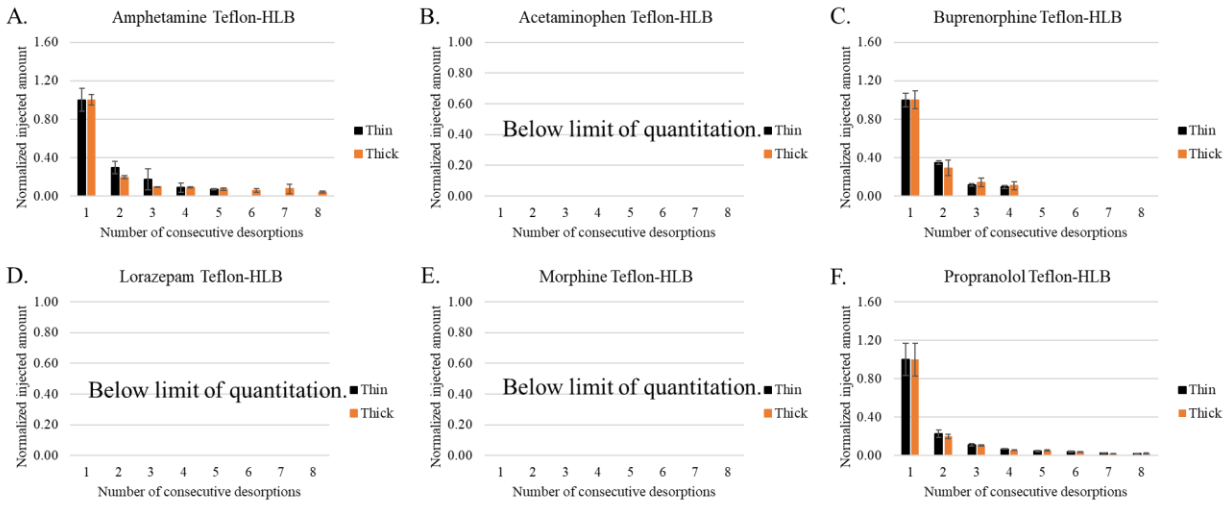

Figure 2.24. Repeated/consecutive desorptions, using the same SPME fiber, of amphetamine (A), acetaminophen (B), buprenorphine (C), morphine (D), lorazepam (E), and propranolol (F) using 1 cm long Teflon-HLB coating. The points in black represent thinner coating (average coating thickness of 7 µm), while the points in orange represent thicker coating (average coating thickness of 10 µm). The desorption solution was methanol:acetonitrile:water (7:2:1 = V:V:V) with 0.1 % formic acid for 25 s. Data for acetaminophen, morphine, and lorazepam are missing because the amount of analytes introduced to the mass spectrometer were below the limit of quantitation.

Considering that these three coating compositions above have different behavior of analyte depletion from the SPME devices, it becomes evident that this is a crucial aspect to pay attention to for future work. These results suggest that the analytes extracted with the Teflon-HLB SPME fibers seem to be extracted only on the surface since the depletion rate is the same for thin and thick coatings. However, the analyte depletion from the PVDF-HLB and PAN-HLB offers something that fundamentally needs to be investigated (**Chapter 3**). Nevertheless, it is essential to emphasize that the amount of analytes extracted is higher with thicker coatings, as it contains more HLB particles. Therefore, some applications in the future might require

somewhat acceptable desorption efficiency, but if the limits of detection/quantitation are satisfied, it is a success. Lastly, this only poses importance for the SPME-MOI that the optimization and careful study of the binder-sorbent interaction is crucial.

2.5. Conclusions

SPME is one of the best sample preparation methods for direct coupling to mass spectrometry. Non-exhaustive enrichment yields a small amount of analytes and interferences to be introduced to instruments, reducing contamination risks. In other words, only a fraction of analytes are introduced with solid-phase microextraction, which maintains the instrument clean. SPME has been coupled to mass spectrometry using a variety of sampling interfaces, but MOI is one of the best for trace analysis. Analytes extracted from SPME devices are desorbed into very low volume and introduced to the MS in the very narrow plug, thus providing tall Gaussian peaks. The MOI interface herein has been simplified. The previous design consisted of unnecessarily long tubes and a manual system that was relatively tricky to handle. Herein, the design is simplified, it is made of (mostly) commercially available parts, and the analysis process is (semi)automated. Full automation of the MOI system is crucial for this technology to be represented in trace analysis laboratories worldwide because know-how offers a steep learning curve.

Nevertheless, the simplicity of the design has been demonstrated by coupling to different manufacturers of mass spectrometers (Thermo, SCIEX, Shimadzu). Lastly, compared to the traditional SPME protocol, the desorption performance has been evaluated for several coating compositions, yielding results that call for careful study of the binder and sorbent interactions in the coating. More about this topic is discussed in the following **Chapter 3**.

Chapter 3. The Effect of Sorbent Particles in Binder on the Mass Transfer Kinetics in Separation Media: *In-silico* Study and Experimental Verification

3.1. Preamble

The content of this chapter has been published as a research article: Nazdrajić, E.; Murtada, K.; Pawliszyn, J.B. The Effect of Sorbent Particles in a Binder on the Mass Transfer Kinetics in Separation Media: *in-silico* Study and Experimental Verification. *Anal. Chem.* **2021**, *93, 44,* 14764 - 14772. (https://doi.org/10.1021/acs.analchem.1c03373) The content of this research article has been reprinted with permission of ACS Publications, and it follows ACS Publications and University of Waterloo policies.

Emir Nazdrajić and Khaled Murtada contributed approximately equally by participating in all aspects from experimental design (assisted by Janusz Pawliszyn), conduction of experiments, data processing, data interpretation (assisted by Janusz Pawliszyn), and manuscript writing (assisted by Janusz Pawliszyn). In addition, Emir Nazdrajić did all COMSOL modeling.

3.2. Introduction

SPME is based on the underlying principle of equilibration between the analytes and the extraction phase; thus, the mass transfer resistance of analytes plays a vital role in the extraction kinetics of SPME.[38] A number of extraction phases have been developed for routine use that include single-phase absorbents (*e.g.*, PDMS) and mixed-phase sorbents (*e.g.*, polydimethylsiloxane/divinylbenzene (PDMS/DVB), carbon-wide range/polydimethylsiloxane (PDMS/CWR), and carboxen/polydimethylsiloxane (PDMS/CAR)).[91] Extraction phase optimization involves analyzing essential parameters such as thickness, length, and the amount of sorbent used. As prior experimental results have shown, greater extraction phase thickness increases the amount of analyte extracted and the equilibration time. Thus, optimizing the thickness of the extraction phase to find the best balance between analyte extraction and equilibration time is important.[2]

An understanding of extraction kinetics is critical in applications based on pre-equilibrium extraction. The mass transfer of analytes from the matrix to the extraction phase can be described using Fick's second law,[92,93] which is a second-order partial differential equation that can be solved with initial and boundary conditions representing the system of interest. Furthermore, it is important to emphasize that the overall mass transfer resistance is comprised of the mass transfer resistance in the sample phase (analyte diffusion across the boundary layer), at the interface (if complete contact between the sample matrix and extraction phase is not made), and in the extraction phase (analyte diffusion in the extraction phase). The most efficient mass transfer (i.e., the fastest equilibration) is obtained when the overall resistance is controlled by the mass transfer in the sample matrix. Researchers have explored various ways of reducing mass transfer resistance in the sample phase by decreasing the size of the boundary layer.[2,52,59,94] In contrast, resistance at the interface can be reduced by ensuring that the extraction phase is fully wetted (conditioned) before the extraction. Researchers have also attempted to describe the mass transfer resistance in the extraction phase, but these efforts have only yielded limited outcomes.[92] Furthermore, findings have shown that, in some cases, mass transfer is not improved by increasing agitation at the sample phase. This is especially true for gaseous samples where analytes are extracted using high-adsorption-capacity material (e.g., CAR/PDMS).[60] In another study, Xu et al. described a mathematical model for SPME kinetics in semisolid samples matrices, which yielded several key findings. Specifically, in semisolid samples, mass transfer resistance increases during extraction, preloaded analytes' extraction and desorption are isotropic, and analytes with higher distribution constants deviate more significantly from the first-order kinetics.[95] Chao et al. utilized Fick's second law to estimate the effective diffusion coefficients for benzene and toluene in PDMS-coated SPME fibers for gaseous and aqueous samples. In addition, Chao et al. also detailed how sample concentration and stirring speed affect the diffusion coefficient, but they failed to discuss whether the mass transfer resistance from outside of the extraction phase contributes to the overall mass transfer resistance, thus potentially skewing the results.[96]

The fundamental ideas of mass transfer into liquid PDMS binder are well understood. In this manuscript, we utilize the finite element analysis software, COMSOL Multiphysics (v.5.6), to develop numerical models that will provide a better understanding of how sorbents in PDMS binder impact extraction kinetics, thereby resolving any misunderstandings regarding the mass transfer process. Furthermore, the numerical approach allows solutions that consider practical extraction conditions, unlike analytical solutions that frequently impose impractical assumptions. This work elucidates how extraction phase thickness and parameters associated with the PDMS binder and sorbent influence extraction using benzene and o-xylene as model analytes. We further use SPME as an experimental tool to evaluate the effect of the sorbent particles in the sorbent/binder composite, as this tool has previously been used to determine the physicochemical properties of various coatings.[97] The findings of this research offer insight into how the migration of chemicals can be controlled using composite separation media comprised of binder and sorbent(s).

3.3. Theoretical Considerations

Previous numerical models computed by COMSOL Multiphysics for the simulation of SPME mass transport have mainly considered the extraction phase as either a liquid (e.g., PDMS) or a solid porous surface (*e.g.*, CAR/PDMS).[36,59,60,69,71,98,99] The porosity and concentration of sorbent in the extraction phase are required parameters for modeling; however, it is often not possible to obtain these values for commercially available SPME devices, as such information is proprietary. Despite this limitation, it is possible to numerically model mass transport by considering the whole extraction phase as a liquid phase where the extraction phase diffusion coefficient is taken as the effective diffusion coefficient (D_{eff}). This is described by **Equation 3.1.,** which is adopted from mass transfer in porous media and chromatographic theories:[100]

$$D_{eff} = \frac{D_E}{1 + k} \tag{3.1.}$$

where D_E represents the diffusion coefficient [m^2 s^{-1}] in the binder (*e.g.*, PDMS) and k represents the phase capacity, or the ratio of analytes extracted by the mixed-phase sorbent (*e.g.*, CAR/PDMS) and the PDMS-only extraction phase. One assumption here is that, in mixed-phase sorbents, most analytes are enriched on the sorbent and not in the binder, which is demonstrated by the difference in their respective distribution constants. Another assumption is that the restriction factor associated with the presence of the particles in the extraction phase is unity since the amount of sorbent in the extraction phase is very low. In chromatographic theoretical equations, the restriction factor of unity corresponds to open tubular columns; typically, a well-packed column will have a restriction factor of 0.8.[100] The phase capacity, also known as the retention factor, can be used to calculate the volumetric ratio of particle to binder **Equation 3.2.**:[25]

$$k = \frac{n_P}{n_{PDMS}} = \frac{C_P V_P}{C_{PDMS} V_{PDMS}} = K_{P/PDMS} \frac{V_P}{V_{PDMS}} \quad (3.2.)$$

where n_P and n_{PDMS} represent the amounts of analyte on the particle and in the PDMS of the extraction phase; C_P and C_{PDMS} represent the concentrations of a specific analyte on the particle and in the PDMS of the extraction phase; V_P and V_{PDMS} represent volumes of the particles and the PDMS in the extraction phase; and $K_{P/PDMS}$ represents the partition ratio of a given analyte between the particle and the PDMS. Thus, a very high phase capacity ($k >> 1$) will decrease D_{eff}, which is the case for very strong adsorbents or larger particle/binder volumetric ratios.

The diffusion coefficients of benzene and o-xylene in PDMS have been determined in numerous studies.[101–104] However, variations in PDMS composition may cause these values to fluctuate slightly. The extraction phase diffusion coefficient of benzene and o-xylene can be estimated using a Crank's analytical solution for mass transfer from a homogenous solution with limited volume.[105] Crank also devised an analytical solution for cylindrical geometry; however, a significant volumetric portion of extraction devices (used in this work) does not participate in the extraction process, whereas Crank's solution considers the whole cylindrical body as the extraction phase. Therefore, we assume that the extraction phase around the support

can be unrolled into a flat sheet that extracts from one side, as expressed by **Equation 3.3.**Error! Reference source not found.

$$\frac{M_t}{M_\infty} = 1 - \sum_{n=1}^{\infty} \frac{2\alpha(\alpha+1)}{1+\alpha+\alpha^2 q_n^2} e^{-\frac{Dq_n^2 t^2}{l}} \quad (3.3.)$$

where $\frac{M_t}{M_\infty}$ represents the ratio of the amounts of extracted analytes, α is the analyte fractional uptake volume, D is the analyte diffusion coefficient [m^2 s^{-1}] in the PDMS of an SPME device, l the PDMS thickness [m], and qn represent solutions to **Equation 3.4.**:

$$\tan(q_n) = -\alpha q_n \quad (3.4.)$$

The first ten non-zero roots of **Equation 3.4.** were determined using Newton's method, a root-finding algorithm of a real-valued function. It should be noted that, in this approach, analyte flux due to radial diffusion is the same for the cylindrical and flat-sheet geometries, and the unwrapped sheet is assumed to be a flat sheet.[36]

3.4. Experimental

3.4.1. Chemicals and Materials

All analyte standards (> 97% purity) were purchased from Sigma-Aldrich (Mississauga, ON, Canada). A list of all compounds used in this research, along with their physicochemical properties and the quantitation ion information used for analysis, is provided in **Table 3.1.** Commercial SPME fibers coated with 100 µm PDMS, 65 µm DVB/PDMS (StableFlex), and 85 µm CAR/PDMS (StableFlex) were obtained from Supelco (Oakville, Canada). Commercial SPME arrows featuring 1.1 mm assemblies of 100 µm PDMS and 120 µm carbon wide range/PDMS (CWR/PDMS) were obtained from PAL CTC Analytics AG (Zwingen, Switzerland).

Table 3.1. Target analytes and their physicochemical properties. [A] accessed from https://pubchem.ncbi.nlm.nih.gov/ on 24. May, 2022. Diffusion coefficient accessed from https://www3.epa.gov/ceampubl/learn2model/part-two/onsite/estdiffusion.html on 24. May, 2022.

Analyte	Molecular mass (g mol^{-1})	log K_{ow}	Diffusion coefficient in air (m^2 s^{-1})	Diffusion coefficient in water (m^2 s^{-1})	Ions monitored	Molecular structure
Benzene	78.11	2.13[A]	8.9 x 10^{-6}	1.03 x 10^{-9}	78	
o-Xylene	106.17	3.12[A]	7.4 x 10^{-6}	8.2 x 10^{-10}	91	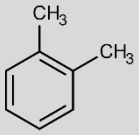

3.4.2. Sample preparation

Extractions were performed using a standard gas generating system (SGGS) that has been described elsewhere.[106] Briefly, the SGGS consisted of a standard gas generator and air sampling chamber. Standard gas generation for benzene and o-xylene was achieved using permeation tubes, which were prepared by placing pure compounds into a polypropylene tube (100 mm long and 1/4 inch) capped with solid Teflon plugs and Swagelok caps. Once the permeation tubes had been prepared, they were placed inside a permeation cylinder swept with the constant flow of dilution air. The permeation cylinder was held inside a permeation oven (100 mm O.D., 45 mm I.D., and 200 mm high), which had been machined from a solid aluminum rod. Two heating rods were placed inside the oven to control the temperature of the permeation cylinder. Extractions with the SPME fibers were performed in Port 1 and Port 3 of the SGGS; both ports had a volumetric flow rate of 4.0 SLPM, but different linear velocities (0.76 m s^{-1} and 0.05 m s^{-1}, respectively). The SPME arrow extractions were performed in Port 2 and Port 3, as it was unable to fit into Port 1 due to its lengthy extraction phase. The linear velocity of Port 2 at 4.0 SLPM is 0.19 m s^{-1}. A schematic of the SGGS air sampling region, along with dimensions of ports and their respective linear

velocities at 4.0 SLPM, is shown in **Figure 3.1.** Before the extraction, the commercial SPME devices were directly inserted into the injection port of the GC at 260 °C for 30 min to clean the fiber and remove any trace impurities. Additionally, a standard gas generating vial was prepared according to the protocol described in our previous work.[107]

3.4.3. Preparation of the Standard Gas Generating Vial

TF-SPME standard gas generating vials were prepared by cutting TF-SPME membrane carbon mesh sheets coated with DVB/PDMS sorbent into 6.2 cm x 5.6 cm rectangles. These membranes were then tightly rolled, inserted, and capped into 20 mL screw top, amber glass autosampler headspace vials (O.D. × H 22.5 mm × 75.5 mm). After membrane insertion, a 10 µL gas-tight syringe was used to deliver 2.3 µL of a pure standard mixture through the vial septa containing respective amounts of 33.3%, 33.3%, and 33.3%, by volume of benzene, ethylbenzene, and o-xylene. After spiking, the vials were placed in a heater block at 55 °C for 24 h to volatilize and evenly distribute the analytes within the sorbent.

3.4.1. Instrumentation

A Hewlett Packard 6890/5973 gas chromatograph/mass spectrometer equipped with a split/splitless injector was used. Chromatographic separations were performed using a SLBTM-5MB (30 m x 0.25 mm x 0.25 µm) fused silica column from Sigma-Aldrich with a helium flow rate of 1.0 mL min^{-1}. The column temperature was initially held at 45 °C for 1.5 min, then gradually increased to 135 °C at a rate of 12 °C min^{-1}, for a total run time of 9.0 min. An injector temperature of 260 °C was used to desorb the fiber. The mass spectrometer working conditions were as follows: electron ionization (EI) 70 eV; mass range 50-350 m/z; ion source temperature 230 °C; quadrupole temperature 150 °C; transfer line temperature 280 °C. For MS detection, the single ion monitoring (SIM) mode was used to detect fragment ions of analytes. The physical-chemical properties and quantitation ions (m/z) ratios of the targeted analytes are listed in Table 3.1. Calibration was performed using liquid injection at a 1:10 split ratio to generate nanograms injected.

The Acme 6100 GC-FID (Young-Lin, South Korea) was used for chromatographic separations. A RTX-WAX (30 m × 0.25 mm × 0.5 µm) fused silica column from Restek with a helium flow rate of 1.2 mL min^{-1} was used. The column temperature was initially held at 42 °C and then raised to 150 °C at a rate of 25 °C min^{-1} and held there for 0.25 min, then raised to 250 °C at a rate of 45 °C min^{-1}, for a total run time of 7.79 min. Desorption of the SPME fibers were carried out for 3 min at a temperature of 260 °C with a split setting of 3:1. The flame ionization detector (FID) was held at a constant temperature of 300 °C with a fuel mixture consisting of 30 mL min^{-1} of hydrogen, 300 mL min^{-1} of air and 30 mL min^{-1} of helium.

3.4.2. Numerical Simulation of the Extraction – COMSOL Multiphysics

In-silico studies used COMSOL Multiphysics software (v.5.6). The model considered a simplified environment of an SPME fiber placed inside the SGGS, shown in **Figure 3.1.**

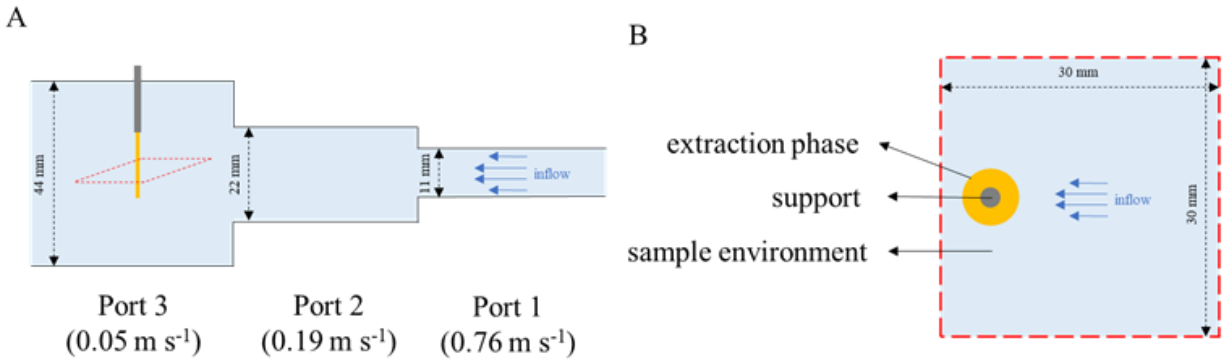

Figure 3.1. (**A**) Schematic view of an SPME device in the SGGS and an overview of the sampling ports (Ports 1, 2, and 3) and their corresponding sample linear velocities (0.76 m s-1, 0.19 m s-1, and 0.05 m s-1, respectively) at a volumetric flow rate of 4.0 SLPM. (**B**) Cross-sectional view used as geometry model in COMSOL Multiphysics.

Briefly, the extraction phase of the SPME device was positioned in the center of the SGGS port at 4.0 SLPM. The dimensions of all SPME devices used in this research are summarized in **Table 3.2.**

Table 3.2. Dimension information of all SPME devices used. The extraction phase length for all SPME fibers is 10 mm and for all SPME arrows is 20 mm.

Extraction Phase	SPME Device	Core	Core Diameter (mm)	Total fiber diameter (mm)	Total phase volume (mm^3)
100 µm PDMS	Fiber	Fused silica	0.110	0.300	0.598
65 µm DVB/PDMS	Fiber	StableFlex	0.130	0.270	0.440
85 µm CAR/PDMS	Fiber	StableFlex	0.130	0.290	0.528
100 µm PDMS	Arrow	Metal	0.500	0.700	3.770
120 µm CWR/PDMS	Arrow	Metal	0.500	0.700	3.770

The extraction process was simulated using a laminar flow profile coupled to the transport of diluted species. In the sample environment, mass transport is governed by diffusion and convection; in the extraction phase, it is governed by diffusion alone. The following equations, which are based on Fick's second law, describe the time-dependent mass transport:

$$\frac{\partial C_S}{\partial t} + \nabla(-D_S \nabla C_S + C_S u) = 0 \tag{3.5.}$$

$$\frac{\partial C_E}{\partial t} + \nabla(-D_E \nabla C_E) = 0 \tag{3.6.}$$

where C_S and C_E represent the compound concentrations in the sample and extraction phase [mol m^{-3}], D_S and D_E represent the compound diffusion coefficients in the sample phase and the extraction phase [m^2 s^{-1}], and u represents the sample velocity field [m s^{-1}]. The initial conditions of the numerical model are summarized below:

$$C_S = C_S^0 \tag{3.7.}$$

$$C_E = 0 \tag{3.8.}$$

where C_S^0 represents the compound concentration in the SGGS. The continuity conditions at the interface between the extraction and sample phases are described with the following flux equations:

$$-D_E \frac{\partial C_E}{\partial x} = M(C_S - K_{ES} C_E) \quad (3.9.)$$

$$-D_S \frac{\partial C_S}{\partial x} = M(C_E K_{ES} - C_S) \quad (3.10.)$$

where M represents an arbitrary parameter [m s^{-1}] intended to ensure sufficient mass exchange between two phases, and K_{ES} represents the partition coefficient, which is the ratio of the concentration of compounds in the extraction phase and sample phase.[107] The flux at the walls of the environment was set to 0 mol m^{-2} s^{-1}, while the concentration inflow was set to C_S^0. The system temperature was set to 25 °C and was maintained at that level by the SGGS heating chamber. Concentrations in the SGGS were calculated by taking frequent measurements of the analyte permeation tubes and system volumetric flow rate at 25 °C and 1 atm. The partition coefficients were calculated using the quantity of extracted analytes (determined by constructing an instrumental calibration curve), the known dimensions of the extraction phase volume (**Table 3.2.**), and the concentration of analytes in the SGGS. Additionally, the same numerical model was used to simulate mass transport from an aqueous matrix, with the compound diffusion coefficient in the sample, the distribution constant, and the model environment material being changed from air to water. **Table 3.3.** summarizes the basic parameters that were used for the numerical model.

Table 3.3. Summarized parameters used for numerical modeling. N/A (not applicable) stands for parameters that were changed depending on the parameters used and other experimental conditions.

Name	Value	Description
D_E	N/A	Analyte diffusion coefficient in the extraction phase
D_S	N/A	Analyte diffusion coefficient in the sample environment
M	1000 [m s^{-1}]	Flux coefficient
K_{ES}	N/A	Analyte partition coefficient between the extraction phase and the sample environment
C_S^0	N/A	Initial analyte concentration
v_{P1}	0.76 [m s^{-1}]	Horizontal component of the flow velocity field at port 1 with 4.0 SLPM

v_{P2}	0.19 [m s^{-1}]	Horizontal component of the flow velocity field at port 1 with 4.0 SLPM
v_{P3}	0.05 [m s^{-1}]	Horizontal component of the flow velocity field at port 1 with 4.0 SLPM

3.5. Results and Discussion

3.5.1. Validation of COMSOL Multiphysics Models

The appropriate benzene (**Figure 3.2.A** and **Figure 3.2.B**) and o-xylene (**Figure 3.2.C** and **Figure 3.2.D**) diffusion coefficients for PDMS coatings were determined by fitting Crank's analytical solution (**Equation 3.3.**) with the experimental extraction time profiles obtained using the standard gas generating vial for SPME-fiber and -arrow format.

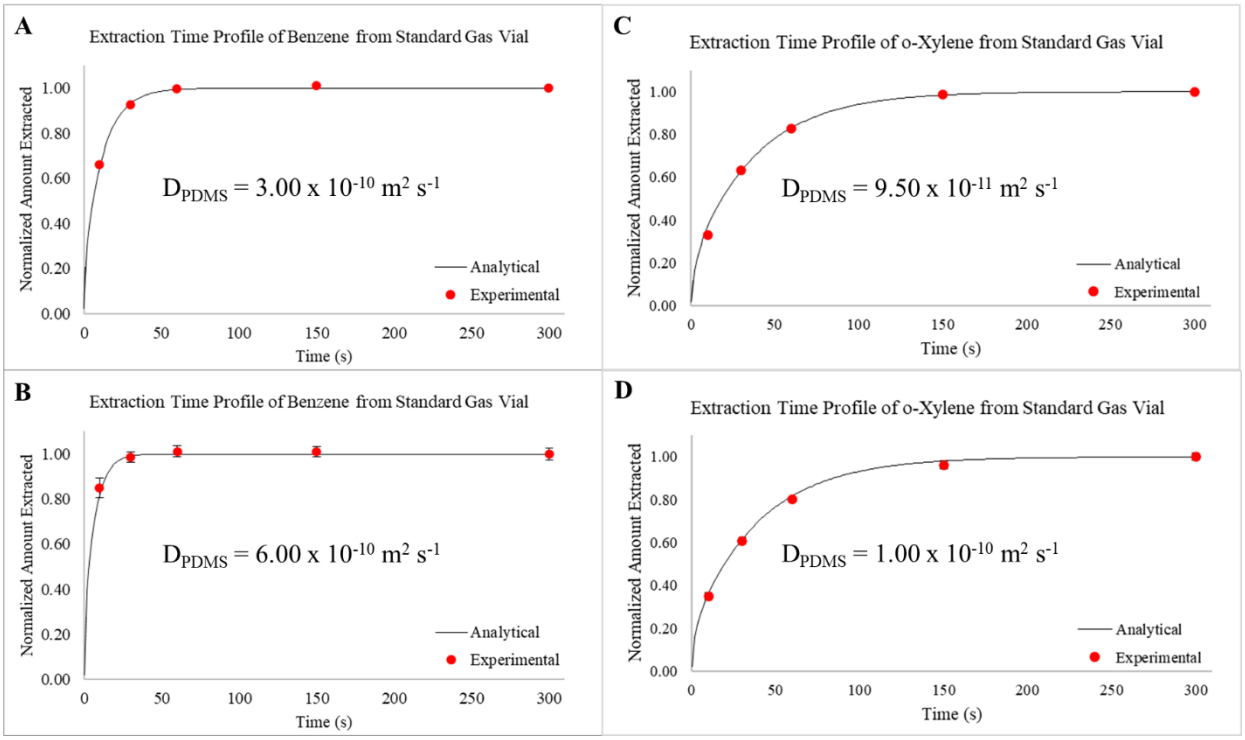

Figure 3.2. Estimation of the diffusion coefficient of benzene (**A**) and o-xylene (**C**) in SPME-PDMS fiber and in SPME-PDMS arrow for benzene (**C**) and o-xylene (**D**) by validating extraction time profile from standard gas generating vial against the analytical solution for sheet geometry.

The diffusion coefficients determined for the PDMS coatings were 3.00 x 10^{-10} m^2 s^{-1} and 9.50 x 10^{-11} m^2 s^{-1} for benzene and o-xylene, respectively, while the diffusion coefficients determined for the PDMS arrow were 6.00 x 10^{-10} m^2 s^{-1} and 1.00 x 10^{-10} m^2 s^{-1} for benzene and o-xylene, respectively. This relatively large

difference in the diffusion coefficients between two compounds has also been documented in the literature by other researchers.[101] Furthermore, we assume that the same composition of PDMS was used in the preparation of the DVB/PDMS, CAR/PDMS, and CWR/PDMS composites. The extraction time profiles for benzene and o-xylene in Port 1 (linear velocity of 0.76 m s^{-1}) and Port 3 (linear velocity of 0.05 m s^{-1}) of the SGGS were compared to the numerical simulation of the extraction process using PDMS coated fibers to validate the model. **Figure 3.3.A** and **Figure 3.3.D** show good agreement.

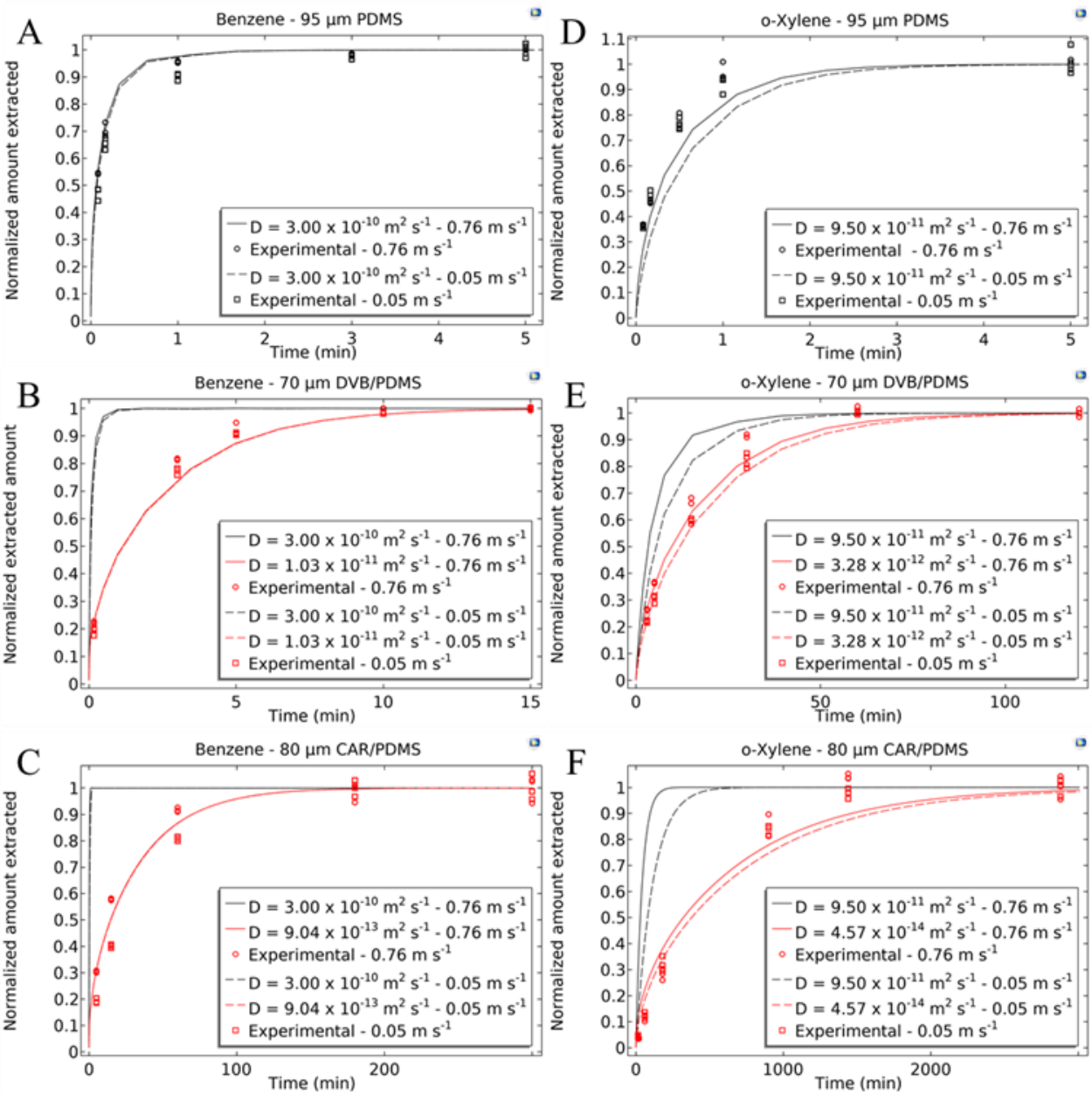

Figure 3.3. Extraction time profile comparison of benzene (**A – C**) and o-xylene (**D – F**) for gaseous linear velocities of 0.76 m s^{-1} and 0.05 m s^{-1} (corresponding to Port 1 and Port 3, respectively) and using 95 µm PDMS, 70 µm DVB/PDMS, and 80 µm CAR/PDMS extraction phases.

Additionally, good agreement was also observed for the extraction time profiles of benzene and o-xylene in Port 2 (linear velocity of 0.19 m s^{-1}) and Port 3 (linear velocity of 0.05 m s^{-1}) from the SGGS system using the SPME arrow, which featured a different PDMS coating thickness and composition (**Figure 3.3.A** and **Figure 3.3.C**). The amounts of benzene and o-xylene captured by each extraction phase are summarized in **Table 3.4.** and **Table 3.5.**

Table 3.4. Amounts extracted of benzene by different SPME fibers and SPME arrows used.

		Amount extracted of benzene (ng)		
		Port 1 (0.76 m s^{-1})	*Port 2 (0.19 m s^{-1})*	*Port 3 (0.05 m s^{-1})*
SPME fiber	PDMS	0.57	-	0.57
	DVB/PDMS	16.72	-	17.32
	CAR/PDMS	219.38	-	188.39
SPME arrow	PDMS	-	0.97	0.76
	CWR/PDMS	-	7.42	7.51

Table 3.5. Amounts extracted of o-xylene by different SPME fibers and SPME arrows used.

		Amount extracted of benzene (ng)		
		Port 1 (0.76 m s^{-1})	*Port 2 (0.19 m s^{-1})*	*Port 3 (0.05 m s^{-1})*
SPME fiber	PDMS	2.34	-	2.17
	DVB/PDMS	111.84	-	68.39
	CAR/PDMS	1191.27	-	1093.98
SPME arrow	PDMS	-	13.46	13.71
	CWR/PDMS	-	217.67	221.19

Moreover, the results also showed good agreement between the equilibration times obtained for the numerically modeled extraction time profile for benzene in an aqueous sample using a PDMS fiber and experimental data published elsewhere (**Figure 3.4.**).[96]

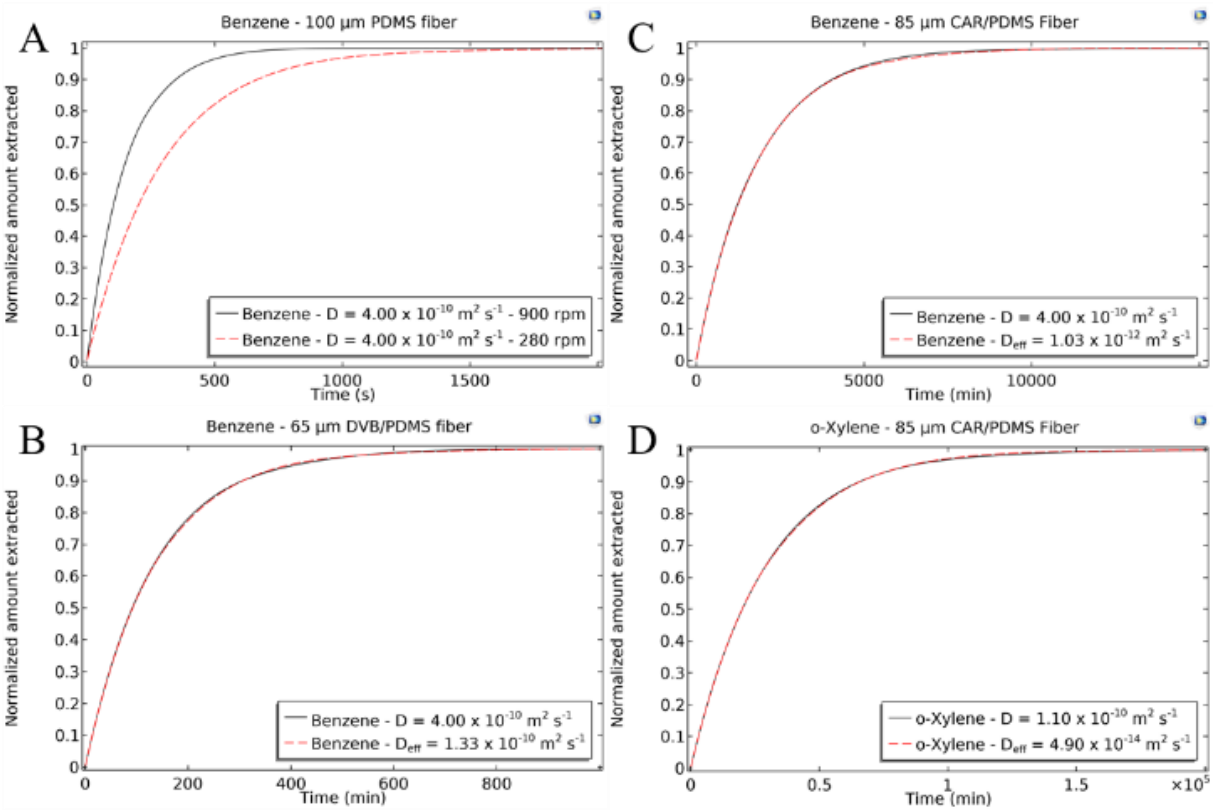

Figure 3.4. Extraction time profiles of benzene for 100 µm PDMS at 900 and 280 rpm from water (A). Extraction time profile of benzene/o-xylene comparing different effective diffusion coefficients at 900 rpm in water: 65 µm DVB/PDMS (B); 85 µm CAR/PDMS (C); 85 µm CAR/PDMS (D).

3.5.2. The Effect of Mass Transfer Resistance Inside the Extraction Phase on Mass Transfer Kinetics in Gaseous Samples

Thus far, little attention has been given to the mass transfer limitation in the extraction phase material. To show that the overall mass transfer resistance is dominated by mass transfer resistance in the extraction phase, it is necessary to compare the extraction time profiles of model compounds at sample linear velocities that create different boundary layer profiles.

Firstly, minor differences in the equilibration times for benzene and relatively larger differences for o-xylene can be observed for the 95 µm PDMS fiber when linear velocity increases from 0.05 to 0.76 m s^{-1} (Port 1 versus Port 3) (**Figure 3.3.A** and **Figure 3.3.D**). This result indicates that, in the case of benzene, mass transfer is mainly controlled by diffusion in the extraction phase. In contrast, for o-xylene the mass

transfer resistance in the boundary layer also impacts the extraction kinetics. Furthermore, both compounds have similar gas-phase diffusion coefficients (Table 3.1.) but significantly different distribution constants (**Table 3.6.**), which provides lower mass transfer resistance in the boundary layer.

Table 3.6. List of all distribution constants of benzene and o-xylene for SPME fiber and SPME arrow extraction phases. Distribution coefficient of the analyte between SPME fiber and water ($K_{fiber/air}$) has been adjusted by air-water ($K_{air/water}$) distribution coefficient ($K_{fiber/air}$ x $K_{air/water}$) whose values have been accessed from www.gsi-net.com (August 8, 2021)

		Extraction/sample phase distribution constant	
		Benzene	*o-Xylene*
SPME Fiber - Air	PDMS	298	2810
	DVB/PDMS	12 265	223 362
	CAR/PDMS	135 000	2 023 440
SPME Fiber – Water*	PDMS	58	618
	DVB/PDMS	2784	47576
	CAR/PDMS	30645	430992
SPME Arrow – Air	PDMS	305	2990
	CWR/PDMS	2 537	44 000

Figure 3.3.B and **Figure 3.3.E.** show how the addition of DVB impacts the extraction time profiles for benzene and o-xylene, while **Figure 3.3.C.** and **Figure 3.3.F.** show how the addition of CAR influences them. The black lines illustrate the diffusion of compounds in pure PDMS, while the red lines show the extraction time profiles as impacted by the retarding force associated with compound adsorption onto the particles. The dashed lines correspond to lower agitation conditions (0.05 m s^{-1}), and the solid lines correspond to higher agitation conditions (0.76 m s^{-1}). As shown in **Figure 3.3.B-C.** and **Figure 3.3.E-F.**, the experimental points align better with the red lines; this result indicates that the mass transfer in the extraction phase can be explained by **Equation 3.1.**, where analyte-sorbent interaction serves as a barrier to the analyte diffusion coefficient in the extraction composite. In addition, agitation conditions had virtually no impact on the extraction time profiles, which indicates that the equilibration time is controlled by the mass transfer in the extraction phase. For benzene, no differences were observed between the

experimental and modeled extraction time profiles for the 70 µm DVB/PDMS and 80 µm CAR/PDMS coatings (**Figure 3.3.B.** and **Figure 3.3.C.**). However, in the case of o-xylene, small differences were observed between the two modeled agitation conditions for the 70 µm DVB/PDMS and 80 µm CAR/PDMS coatings (**Figure 3.3.E.** and **Figure 3.3.F.**). This finding indicates that the mass transfer in the sample matrix has a greater impact on the observed extraction rate, as it increases the analytes' affinities for the coating. Notably, similar results were obtained for thicker extraction phases using different PDMS compositions and CWR/PDMS. **Figure 3.5.A.** and **Figure 3.5.C.** show the extraction time profiles of benzene and o-xylene using a 100 µm PDMS SPME arrow at two different convection conditions (0.19 m s^{-1} for Port 2 and 0.05 m s^{-1} for Port 3), which are represented by the solid and dashed black lines, respectively.

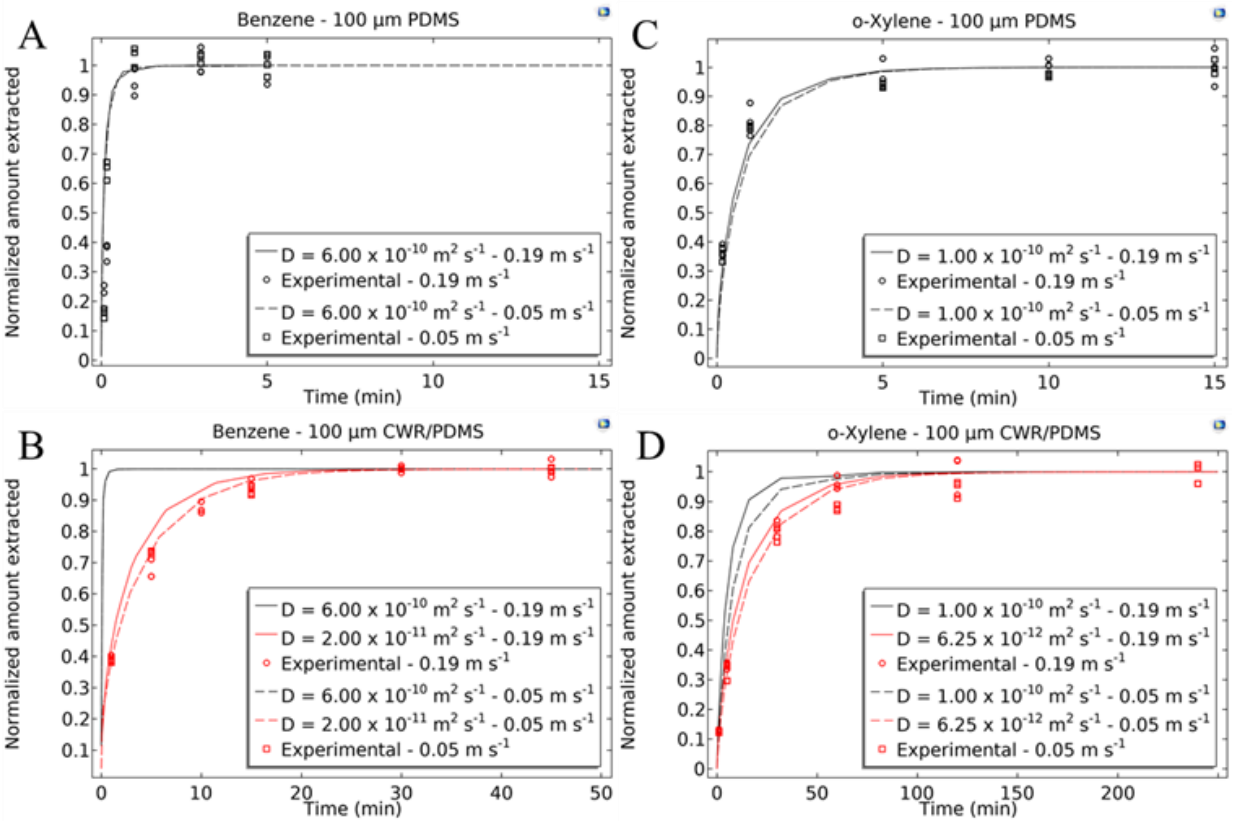

Figure 3.5. Extraction time profile comparison of benzene (A – B) and o-xylene (C – D) for different gaseous linear velocities—0.19 m s-1 and 0.05 m s-1 corresponding to Port 2 and Port 3, respectively using 100 µm PDMS and 100 µm CWR/PDMS extraction phases.

No differences were observed in the extraction time profiles for benzene (low PDMS affinity), which suggests that the extraction is controlled by the mass transfer resistance in the extraction phase. In contrast, some small differences were observed in the extraction time profile for o-xylene (higher affinity for the PDMS), which suggests that, although mass transfer resistance in the extraction phase plays a dominant role, the effects associated with the boundary layers in the sample matrix are also significant. **Figure 3.5.B.** and **Figure 3.5.D.** show the extraction time profiles for benzene and o-xylene using the 100 µm CWR/PDMS coating; as can be seen, the experimental data fit well with modeled lines representing the effective diffusion calculation. A comparison of the equilibration times of benzene and o-xylene in 100 µm PDMS and 100 µm CWR/PDMS revealed that changes in equilibration time were inversely proportional to changes in the diffusion coefficient. For example, the equilibration time for o-xylene increased by approximately 16 (from 5 min to 80 min). At the same time, its diffusion coefficient in the extraction phase dropped by the same factor (**Figure 3.5.C.** and **Figure 3.5.D.**). The same characteristics can be extended to the results for the SPME fibers after adjusting for the differences in their respective thicknesses.

To demonstrate the dramatic effects of D_{eff} on the extraction process, we modeled the concentration profiles for different sampling points inside the extraction phase. The results are depicted in **Figure 3.6.** The red lines represent the concentration profiles in the extraction phases, and the black lines represent the concentration profiles in the sample phase.

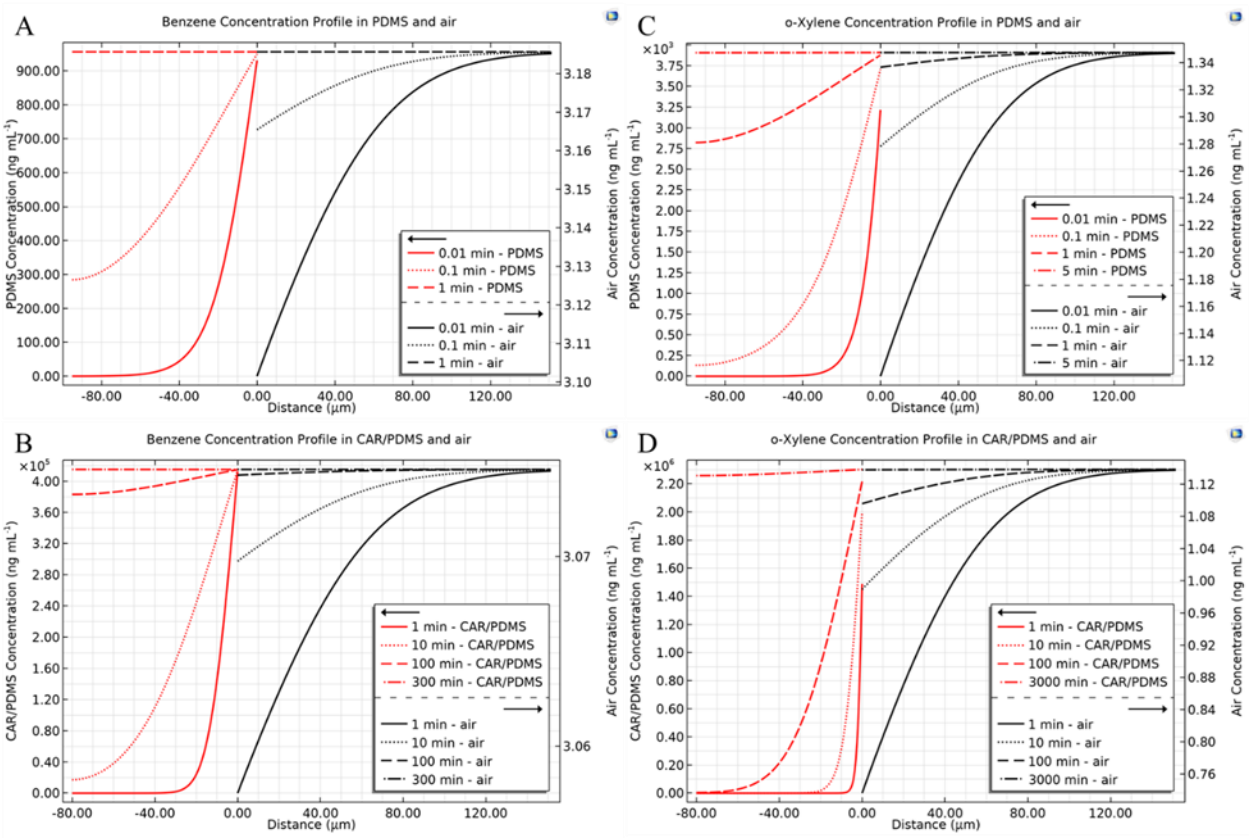

Figure 3.6. Concentration profiles of benzene in PDMS (A) and CAR/PDMS (B) and o-xylene in PDMS (C) and CAR/PDMS (D) SPME fibers for extraction phase and sample phase (air). Sample phase diffusion coefficients are 8.8 x 10-6 m2 s-1 and 8.7 x 10-6 m2 s-1 for benzene and o-xylene, respectively. Distribution constants for benzene are 300 for (A) and 134960 for (B), and distribution coefficients for o-xylene are 2901 for (C) and 202000 for (D). Diffusion coefficients in the extraction phases are 3.00 x 10-10 m2 s-1 (A) and 9.04 x 10-13 m2 s-1 (B) for benzene and 9.50 x 10-11 m2 s-1 (C) and 4.57 x 10-14 m2 s-1 (D) for o-xylene. Sample linear velocity is 0.76 m s-1.

The different time points at which the concentration profiles were calculated in the extraction and sample phases are represented using various lines. The most obvious difference can be seen when comparing the PDMS and CAR/PDMS results in relation to the 1 min concentration profile for benzene. As can be seen, the PDMS case reaches equilibrium (**Figure 3.6.A.**), while the CAR/PDMS case barely penetrates 20 µm of the whole extraction phase (**Figure 3.6.B.**). The same effect can be seen for o-xylene (**Figure 3.6.C.** and **Figure 3.6.D.**), only to a greater extent. In the CAR/PDMS case, the 1 min concentration profile is practically on the surface of the extraction composite, while it is closer to equilibrium in the PDMS case. These results further confirm that the mass transfer resistance at the boundary layer is mainly due to the

difference in distribution constants because both compounds (*i.e.*, benzene and o-xylene) have similar air diffusion coefficients, thus creating similar concentration profiles in the extraction phase. Conversely, differences in the distribution constants result in larger concentration differences at the interface (distance = 0 μm), representing the mass transfer resistance at the boundary. In other words: the higher the concentration profile slope in the boundary layer at the sample phase at the initial sampling point, the higher the mass transfer resistance in the boundary layer. Thus, benzene has a smaller concentration profile slope than o-xylene at 0.01 min (**Figure 3.6.A.** and **Figure 3.6.C.**, it will have less resistance in the gas phase. This explains the lack of differences between the two extraction time profiles in **Figure 3.3.A.** and **Figure 3.5.A**.

3.5.3. The effect of mass transfer resistance inside the extraction phase on the mass transfer kinetics in aqueous samples

The impact of D_{eff} on mass transfer resistance was numerically investigated for extractions from aqueous samples (Figure 3.6.). Four orders of magnitude smaller sample diffusion coefficient (aqueous versus gaseous) results in mass transfer resistance to be dominated by the boundary layer as illustrated in **Figure 3.6.**, where at different convection conditions (900 and 280 rpm) two different equilibration times are obtained for extraction with PDMS fiber. Therefore, forced convection via sample agitation is an important element of extractions from aqueous matrices, as the water's higher viscosity and density create a larger boundary layer.[2] Furthermore, the numerical model was also applied to describe mass transfer in aqueous matrices using DVB/PDMS and CAR/PDMS as extraction phases. The only differences between the aqueous and gaseous models were the changes in the analyte distribution constant, the sample diffusion coefficient, and the sample viscosity and density because of exchanging air with water. The authors of the work[96] wrongly assumed that the mass transfer during extractions from aqueous matrices is controlled by diffusion in the extraction phase, where results show the correlation between agitation conditions and the analyte extraction phase diffusion coefficient. This conclusion is not valid and is the product of an incorrect assumption. In the present work, we used our model to understand how the presence of sorbents influences

extraction time profiles obtained for aqueous samples. The extraction of benzene from water using 70 µm DVB/PDMS and 80 µm CAR/PDMS and o-xylene using 80 µm CAR/PDMS was modeled using the obtained D_{eff}, which are summarized in **Table 3.7.**

Table 3.7. The list of determined effective diffusion coefficients of benzene and o-xylene inside extraction phases of SPME fibers and arrows.

		Effective diffusion coefficient, D_{eff} [m^2 s^{-1}]	
		Benzene	*o-Xylene*
SPME fiber	DVB/PDMS	1.03×10^{-11}	3.28×10^{-12}
	CAR/PDMS	9.04×10^{-13}	4.57×10^{-14}
SPME arrow	CWR/PDMS	2.00×10^{-11}	6.25×10^{-12}

The distribution constants obtained from extractions from air samples were adjusted using the air-water distribution constant of the analytes and are summarized in **Table 3.6.** As shown in **Figure 3.4**., changing the extraction phase diffusion coefficient—even a few magnitudes—resulted in no differences in equilibration times (black solid line for diffusion in PDMS and red dashed line for diffusion retarded by the presence of sorbent), thus showing that the overall mass transfer resistance occurs at the boundary layer. This result is because analyte flux is significantly lower in water samples compared to air samples, mainly due to differences in the sample phase diffusion coefficient and boundary layer dimensions, as aqueous matrices have much higher viscosity and density. As such, one could expect to observe this phenomenon in aqueous matrices provided the applied convection conditions are sufficient to mimic the size of the boundary layer in the gaseous sample; this is possible via vortex agitation.

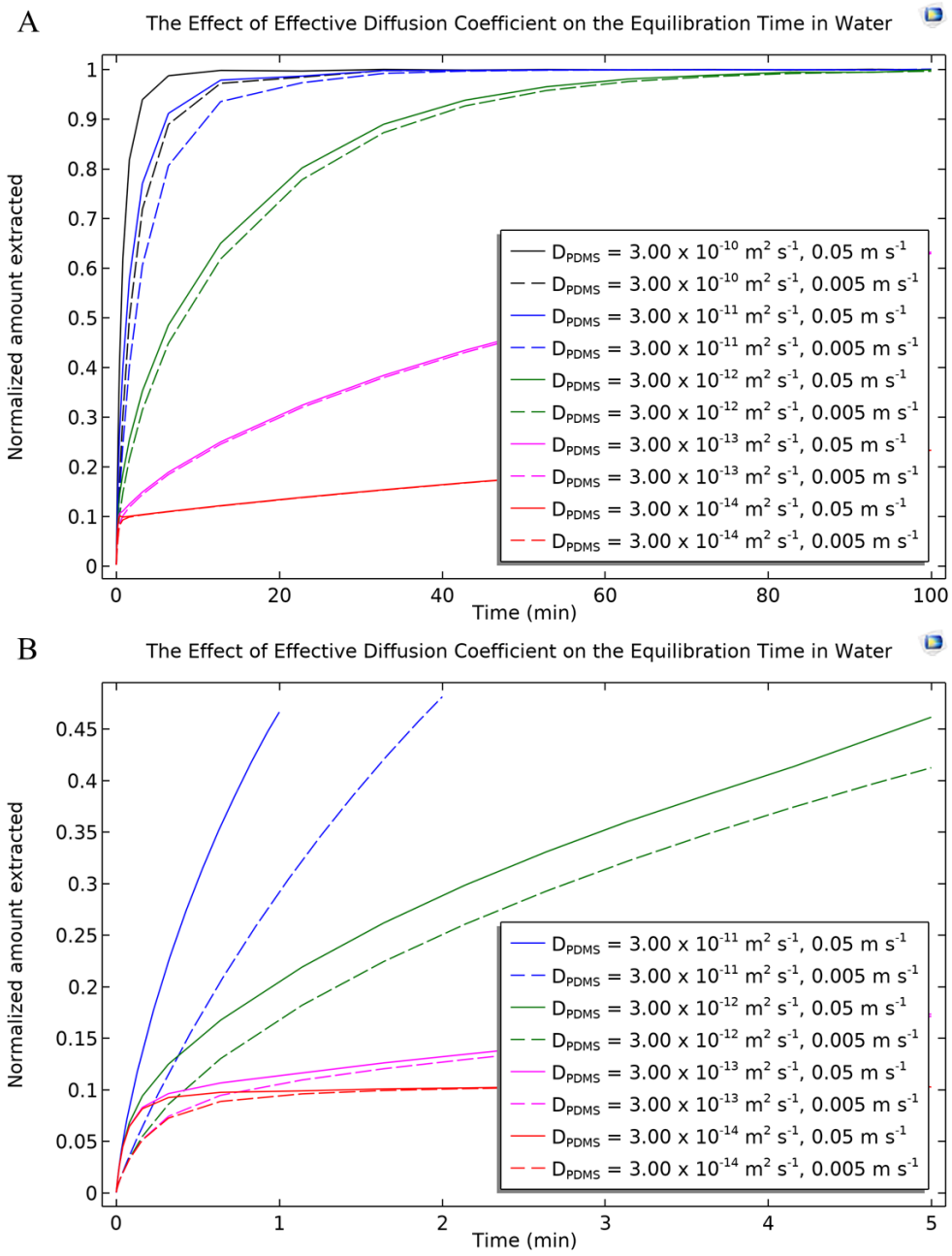

Figure 3.7. The effect of the effective diffusion coefficient on the equilibration time of benzene as the model analyte in water for different convection conditions where K = 58 (theoretical PDMS/water distribution constant for benzene) and diffusion coefficient in water is 9.8 x 10-10 m2 s-1 (A) and zoomed in version of the same graph (B).

Figure 3.7. shows how decreases in the extraction phase diffusion coefficient impact the equilibration times for extractions from aqueous matrices. The main conclusion that can be drawn from **Figure 3.7.** is that, for the same distribution constant, the mass transfer resistance in the extraction phase begins to make an

important contribution when the effective diffusion coefficient is decreased few orders of magnitude, thus resembling the differences in the diffusion coefficient that were observed when changing from an aqueous to a gaseous matrix. If the extraction phase composite has a sorbent that protrudes into the sample phase, the major mass transfer resistance would be at the interface because the distribution constant at this point would be increased. The mass transfer resistance at the extraction phase/sample interface would be lower in cases where the sorbent is fully immersed inside the binder due to a lower binder/water distribution constant, thus making the highest mass transfer resistance located in the extraction phase. It should be noted that the effect is illustrated in **Figure 3.7.** was observed at the initial extraction conditions. Regardless of the magnitude of the effective diffusion coefficient, the extraction phase accumulates a significant portion of analytes at the coating surface. It is important to keep in mind that extraction phases with strong sorbents, which retard the diffusion coefficient, will have very high capacities—even in the thin surface layer—compared to the pure binder. Therefore, there is no need to use thick extraction phases when using strong sorbents, as the equilibrium can be achieved over very short time scales (e.g., around 10% for **Figure 3.7. B.**); indeed, longer extractions do not yield a proportionally greater increase in analytes captured due to the very small slopes of the extraction time profiles, thus making such extraction regimes inefficient. This principle is illustrated in Figure 3.6. where the concentration profile for the initial stages of extraction is focused close to the interface region of the extraction phase, which is consistent with experimental results that have been reported elsewhere.[108]

3.5.4. Considerations for Optimizing the Extraction Phase for Rapid Analysis

Our results demonstrate how effective diffusion, due to the presence of sorbents in the extraction phase, plays an essential role in mass transfer resistance during the extraction process. Therefore, similar mass transfer resistance can be expected for the desorption process, as extraction and desorption are both isotropic processes. This phenomenon would be especially observable in cases wherein significant mass transfer resistance is present in the extraction phase. Such cases would require longer desorption times via gas chromatography (GC), resulting in peak broadening for some analytes. Additionally, the dramatic

temperature increase for GC desorption causes a decrease in the distribution constants of the analytes in the extraction phase and an increase in the analyte diffusion coefficient.

Moreover, constantly sweeping with gas during desorption ensures high analyte flux from the extraction phase into the desorption chamber. However, these approaches will not work for liquid chromatographic (LC) desorption. When solvent meets the extraction composite, it will only decrease the analytes' affinity for the extraction composite without affecting the D_{eff}; thus, using solvents will not speed up desorption. On the other hand, extraction composites containing porous sorbents can be effective, as the solvents can access the pores, increasing D_{eff}. An alternative solution is to use SPME devices with high surface areas and thin extraction phases, such as thin-film microextraction for GC analysis and the dispersive particle format for LC analysis.

For SPME-MS applications intending to achieve rapid analysis, the mass transfer resistance in the extraction phase is a significant issue, as the desorption times used are in the order of seconds (MOI and CBS) or lower (PESI).[83,109,110] When using a thick extraction phase, it is simply not enough to obtain the best possible desorption efficiency. Therefore, the extraction phase must be modified in response to the increase in surface area; specifically, this modification largely entails carefully optimizing the percentage of sorbent in the extraction phase and reducing the extraction phase thickness. In addition to the present work (**Figure 3.6.**), the need to reduce the thickness of the extraction phase has also been demonstrated experimentally elsewhere,[108] with findings showing that analytes require a very long time to reach the deeper parts of the extraction phase during the extraction due to very low free concentrations of the compounds in the binder responsible for facilitating the diffusion. Furthermore, thick extraction phases are not beneficial in surface spectrophotometric applications, as the detection signal will only correspond to analytes on the surface of the extraction phase.[108] Thick extraction phases are also disadvantageous when SPME devices cannot be analyzed immediately following short pre-equilibrium extraction (*e.g.*, in-situ or in-vivo analysis), as the analytes will continue diffusing to the depths of the extraction phase after terminating contact with the sample, which can lead to changes in the analyte concentration profile changes

over time. Such effects will result in imprecise measurements in cases where all the analytes are not desorbed from the coating or when surface spectroscopy is used, as the signal associated with surface concentration will vary according to the time delay between sampling and readout. The delay in readout will result in a weaker signal than a situation wherein the fiber can be analyzed spectrophotometrically immediately after the extraction. The only advantage to using a thicker extraction phase in spectrophotometric determination is if it is followed by other methods (e.g., LC-MS) for comparison, which would require larger amounts of analytes. Moreover, the use of a thicker coating requires longer extraction times to reach equilibrium and, thus, to take full advantage of the increased capacity.

3.6. Conclusions

This work documents the examination of how the addition of sorbent particles to polymeric media impacts the overall diffusion coefficient, which we have termed the effective diffusion coefficient (Deff). The conclusions presented herein will not only impact the design of the coatings used for extraction, but also the composition of the membrane materials used in separation and protective paints/coatings. Our results indicate that, when designing coatings, special attention must be given to kinetics. Optimizing the extraction phase for solid-phase microextraction (or another membrane-based separation technology) should also include the selection of an appropriate binder and extraction particles, as the free concentration of the compound in the binder ultimately governs its diffusion into the composite that contains the sorbent particles. Most prior attempts at optimization have focused on maximizing sorbent strength and increasing its content in the composite to achieve a good, evenly distributed extraction phase that enables high extraction efficiency. However, no prior optimization investigations have considered how sorbent's presence impacts analyte diffusion. As our results show, adding a large quantity of sorbent particles with a strong affinity toward the target analytes will provide higher extraction efficiency and slow the mass transfer of analytes in the extraction phase. Therefore, careful consideration must be given to designing an optimum extraction phase with appropriate sorbent content to ensure that compromise between extraction efficiency and mass transfer resistance can be achieved. Furthermore, this optimization procedure must also

ensure that the analyte has sufficient affinity and an adequate diffusion coefficient for the binder to facilitate high analyte recovery, and thus, an appropriate D_{eff} and satisfactory kinetics of mass transfer through the composite media. In our experiments, we used PDMS, a liquid polymeric binder characterized by its high diffusion coefficient. However, highly porous solid and semisolid polymeric materials can also be used as binders, which has been demonstrated practically in the design of matrix-compatible SPME coatings.[35] Conversely, kinetics that is controlled by the diffusion in the coating is beneficial for passive time-weight average (TWA) sampling[111] or diffusive gradients in thin film[112], as the extraction rate is not dependent on the convection conditions of the sample.

Additionally, thicker coatings create the long equilibration time required in TWA applications. As reported above, this can be conveniently accomplished for gas sampling. Still, achieving these conditions for aqueous matrices is more challenging, as it would require decreasing the effective diffusion coefficient by about four orders of magnitude compared to gas-based TWA sampling. However, it is possible to create such conditions by applying ion-exchange sorbents to a polar binder, as has been shown for extractions of Doxorubicin.[108] The optimization of sorbent-loaded extraction phases should consider homogeneously dispersing the sorbent throughout the extraction phase instead of clumping it together.

Nonetheless, some cases may provide the opportunity to create a well-defined gradient of effective diffusion via non-uniform sorbent distribution or variations in sorbent strength. Another vital approach to consider is using a thin-layer overcoating of sorbent that protrudes into the binder; this approach is effective at minimizing mass transfer resistance at the interface, as the binder's affinity for the target analytes is higher than that of the matrix. The reported results provide a better understanding of how thin films can be designed to facilitate greater selectivity and to produce paints/coatings that provide better protection barriers. Modulating the affinity of sorbents via electrochemical or chemical means could be an interesting opportunity to fine-tune the permeation properties of the separation media.

Chapter 4: Rapid Determination of Tacrolimus and Sirolimus in Whole Human Blood by Direct Coupling of Solid-phase Microextraction via Microfluidic Open Interface

4.1. Preamble

The content of this chapter has been published as a research article: Nazdrajić, E.; Tascon, M.; Rickert, D.A.; Gómez-Ríos, G.A.; Kulasingam, V.; Pawliszyn, J.B. Rapid Determination of Tacrolimus and Sirolimus in Whole Human Blood by Direct Coupling of Solid-phase Microextraction via Microfluidic Open Interface. *Anal. Chim. Acta* **2021**, *1144*, 53-60. (https://doi.org/10.1016/j.aca.2020.11.056) The content of this research article has been reprinted with the permission of Elsevier, and it follows Elsevier and University of Waterloo policies.

The contribution of Marcos Tascon was project design, conduction of the initial experiment, *i.e.*, imprecision of the calibration plot slopes, and assistance in data interpretation. Daniel A. Rickert contributed to the project design and assisted in data interpretation. German A. Gómez-Ríos contributed to the project design and assisted in data interpretation. The contribution of Vathany Kulasingam was project design, assisted in data interpretation, and kindly provided residual whole blood samples of patients undergoing immunosuppression therapy at University Health Network, Toronto, Ontario, Canada. The rest of the experimental work, project design, data processing, data interpretation, and manuscript writing were done by Emir Nazdrajić.

4.2. Introduction

Patients that require suppression of their immune system's activity are usually prescribed immunosuppressive drugs (ISD), especially in cases involving solid organ transplantation, where it is critical to reduce the possibility of organ rejection. Due to the toxicity of ISDs, and to decrease the risk of

organ rejection, the concentration of the prescribed ISDs in the patients' blood must be closely monitored to maintain concentrations within their narrow therapeutic range (5 – 20 ng mL^{-1} for tacrolimus (TAC), 5 – 10 ng mL^{-1} for sirolimus (SIR), 3 – 8 ng mL^{-1} for everolimus (EVE), and 150 – 350 ng mL^{-1} for cyclosporine A (CYC)).[113] Over or under administration of ISDs can lead to severe adverse effects. For instance, over administration can cause infection, malignancy, cardiovascular diseases, and diabetes, whereas under administration can result in graft loss resulting from acute and/or chronic organ rejection.[24] Besides the narrow therapeutic range and the likelihood of ISD misadministration, some additional challenges regarding ISD analysis include highly variable dose/exposure relationships, as well as toxicodynamic effects that cannot be easily differentiated from clinical diseases' symptoms.[114]

In this context, several methods have been developed to monitor the concentration of ISDs in whole blood. Among them, the most widespread and commonly used methods are immunoassay-based.[24,113,114] Some popular immunoassay methods are enzyme-linked immunosorbent assay,[115] quantitative microsphere system,[116] electrochemiluminescence immunoassay,[117,118] microparticle enzyme immunoassay,[119] affinity column-mediated immunoassay,[119] and chemiluminescent microparticle immunoassay.[120] These methods have some important advantages such as fast turnaround time (due to total automation of their workflow) and commercial availability.[116,117,120,121] However, immunoassay methods have major limitations: the possibility of interference and lack of clinical accuracy stemming from cross-reactivity with other drugs or metabolites.[113,114] LC-MS has become the gold standard for the analysis of ISDs since it addresses most of the limitations of immunoassay-based methods without compromising the time of analysis and workflow simplicity.[6,122–124] In general, MS-based methods can monitor multiple analytes simultaneously in a single instrument, a feat otherwise impossible in the case of immunoassays. This feature is especially advantageous when some immunosuppression therapies include the coadministration of ISDs with different modes of action, which is generally carried out to reduce the adverse effects of individual ISDs.[113,125–129] From an economic point of view, even though initial investment costs for an LC-MS system are higher, the lower cost of reagents and consumables offsets the initial investment over time.[124,130] This fact is reflected

in the increased utilization of LC-MS assays in the market in recent years (~ 50 % for CYC and TAC and ~ 70 % for SIR and EVE).[6,114] Because of the growing MS market, various direct-to-MS approaches targeting rapid determination have been developed, such as the Phytronix® Technologies laser diode thermal desorption module[131] and paper spray[132,133], among others. However, despite their practicality, these approaches have several drawbacks, the most detrimental being the higher susceptibility to matrix effects, and instrumental contamination due to the lack of separation and sample preparation, respectively.[46]

It is crucial to emphasize that sample preparation is a critical step in any analytical workflow, given that proper sample preparation can provide sufficient sample cleanup and suitable isolation and enrichment of target analyte(s).[50] In this context, several sample preparation strategies have been employed to determine ISDs in whole blood, generally involving protein precipitation, solid-phase extraction, or liquid-liquid extraction.[113,128] Specifically for direct-to-MS methodologies with online sample preparation, Turboflow[134] and Rapidfire™ have been developed.[33] A methodology worth highlighting for direct-to-MS analysis is the coupling of solid-phase microextraction (SPME). This open-bed extraction methodology has been shown to be an efficient way of introducing a rapid sample preparation step into the analytical workflow.[2,35] SPME-MS provides rapid analyte enrichment onto the matrix-compatible extraction phase with minimal co-extraction of matrix components that cause matrix effects, thus enabling the introduction of clean extracts for quantitative and reproducible results.[22,43,52,135–137] Furthermore, it addresses the drawbacks of the direct-to-MS approaches by offering a more streamlined process since it consolidates a lot of manual steps into a single step while simultaneously eliminating the risk of cartridge/column clogging. Determination of ISDs in whole blood by SPME-MS has been done by blade format[50,109] and fiber format[53] using matrix-compatible hydrophilic-lipophilic balanced coatings.

This work describes developing an SPME-MOI-MS/MS method for the simultaneous determination of four immunosuppressive drugs (tacrolimus, sirolimus, everolimus, and cyclosporine A) from whole human blood via the MOI. The present work serves as an evaluation and further development of the proof-of-concept method that was reported by Tascon et al. in 2018.[53] The MOI system allows analytes on Bio-

SPME devices to be rapidly desorbed in the flow-isolated chamber. At the same time, the desorption solution is continuously supplied to the electrospray source of the instrument. This setup offers excellent sensitivity due to the small volume (< 4 µL) of the flow-isolated region (desorption chamber) and rapid transfer of the concentrated analyte plug toward the electrospray source (**Figure 4.1.**).[52,53,56] In addition, general method development criteria were followed to evaluate the method's inter-day stability, carryover, precision, accuracy, and sensitivity.[114,138] Finally, cross-validation against the routinely used method for ISDs analysis, chemiluminescent microparticle immunoassay (CMIA), was performed, obtaining acceptable values.[120]

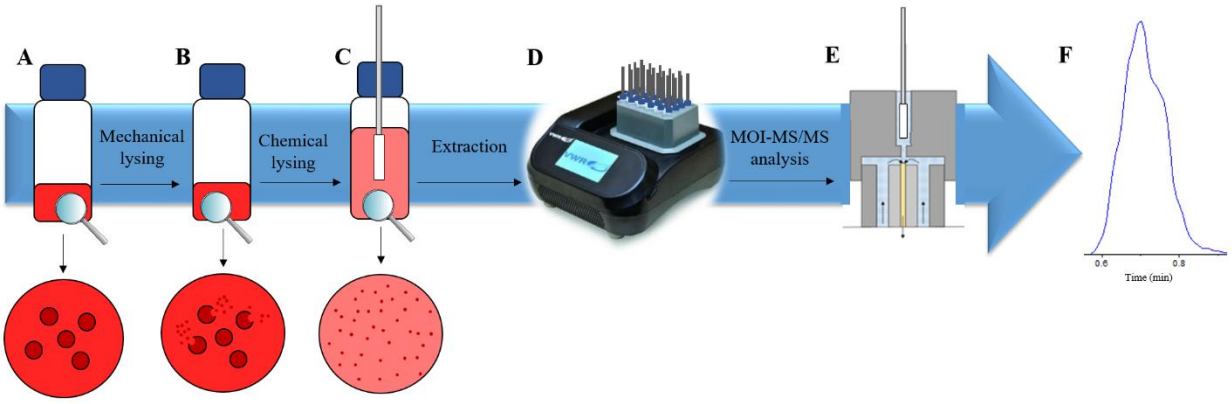

Figure 4.1. General workflow of the proposed method: A. Aliquot whole blood spiked with ISDs, B. Perform mechanical lysing (freeze-thaw cycle, three times), C. Perform chemical lysing (addition of 6:3:1, V:V:V, 0.1 M zinc sulfate:acetonitrile:water mixture containing ISDs' internal standards), D. Extraction using VWR® Thermal Shake Touch at 2200 RPM and 55°C, E. Desorption of 5 seconds in the MOI, F. Instrumental analysis.

4.3. Experimental

4.3.1. Materials and Supplies

LC-MS grade methanol, acetonitrile, isopropanol, and dimethylformamide were purchased from Fisher Scientific (Bartlesville, OK, USA). LC-MS formic acid, polyacrylonitrile, and ammonium acetate were purchased from Sigma-Aldrich (Saint Louis, MO, USA). Tacrolimus (TAC), Sirolimus (SIR), Everolimus (EVE), Cyclosporine A (CYC), TAC ^{13}C d_2, and EVE d_4 were purchased from Cerilliant Corporation

(Round Rock, TX, USA). CYC d_4 was purchased from Toronto Research Chemicals (Toronto, ON, CA). Physicochemical parameters of all analytes can be found in **Table 4.1.**

Table 4.1. Physicochemical properties of immunosuppressive drugs and their therapeutic range.[50]

Compound	log D	Therapeutic range (ng mL^{-1})	Molar mass (g mol^{-1})
Tacrolimus	5.59	3-15	804.0
Tacrolimus, ^{13}C d_2	-	-	807.0
Sirolimus*	7.45	3-20	914.2
Everolimus*	7.40	3-15	958.2
Everolimus d_4	-	-	962.2
Cyclosporine A	3.64	50-350	1202.6
Cyclosporine A d_4	-	-	1206.

Analyte stock solutions were prepared in acetonitrile at 100 µg mL^{-1} and stored at -80 °C. Recipe ClinCal® whole blood immunosuppressant quality control (QC) levels (Blank, Level 1 – 6; LOT#: 1366) were purchased from Recipe (Munich, Germany). Pooled whole human blood containing K_2-EDTA was purchased from BioIVT (Westbury, NY, USA). Whole blood samples were collected from patients receiving immunosuppressant therapy (TAC and SIR) at the University Health Network (Toronto, ON; Canada). Informed consent was obtained prior to sample collection, and ethics approval was waived by the Research Ethics Board at University Health Network for the use of collected samples for evaluation of method performance. Five micrometer Oasis® hydrophilic-lipophilic balance (HLB) particles used to coat the SPME fibers were graciously provided by Waters Corporation (Wilmslow, United Kingdom). Bio-SPME fibers were prepared by dipping nitinol wire (200 µm diameter) with a slurry of in HLB particles suspended in a polyacrylonitrile-dimethylformamide mixture. Polyacrylonitrile (average molecular mass 150 000) has been added to dimethylformamide (7%, m/V) and placed inside the oven at 90 °C for 60 minutes with occasional stirring with a glass rod to make a homogeneous mixture. The lid on the jar has been kept loosely closed to prevent pressure buildup inside the jar. Then the jar has been placed inside the fume hood to cool down. Once cooled down, 5 µm Oasis® HLB particles have been added to the

polyacrylonitrile-dimethylformamide mixture (10 % particles, w/w) to make a suspension. The suspension was left to stir overnight for homogenization. Nitinol wire (60 mm length and 200 μm diameter) was dipped repeatedly for 10 mm inside the suspension until 250 ± 5 μm diameter was reached. Coated nitinol wires (SPME fibers) have been placed inside 300 μL vials and cleaned with methanol:acetonitrile:isopropanol = 2:1:1 (V/V/V) for 30 min at 1500 rpm. Prior to extractions, SPME fibers were conditioned in methanol:water = 1:1 (V/V) for 30 min at 1500 rpm, and were kept in conditioning solution until ready for extraction. All fibers were made for single-use and, as such, were discarded in a biohazard bin following analysis.

4.3.2. Sample preparation

In-house QCs and calibration levels were prepared by spiking pooled whole blood with the ISDs mixture, keeping the organic solvent content in the sample below 1 %. Spiked whole blood samples were incubated overnight at 4°C to allow analytes to bind with the whole blood matrix. Following overnight incubation, spiked samples were pipetted into 200 μL aliquots, and subjected to the following mechanical lysis process: three freeze-thaw cycles (a cycle consisted out of placing the sample for 1 min in liquid nitrogen and then for 1 min in an ice bath). Finally, samples were stored at -80 °C until the moment of the experiment.

Prior to analysis, the samples were subjected to an additional chemical lysis process where 1.3 mL of a lysis solution containing the internal standards 0.1 M zinc sulfate:acetonitrile:water (6:3:1, V/V/V) with 1.1 ng mL^{-1} of TAC ^{13}C d_2, EVE d_4, and 11.2 ng mL^{-1} of CYC d_4; was added to thawed 200 μL aliquot of whole blood. Immediately after, the Bio-SPME fiber was directly immersed in the solution to initiate the extraction. Extractions were performed using a VWR® Thermal Shake Touch set at 2200 rpm and at 55 °C for 60 min.

4.3.3. Analysis via MOI-MS/MS

The analytical workflow consisted of four steps: 1) Extraction of analytes with a Bio-SPME fiber (60 min); 2) Rinsing of fiber in water for 5 seconds so as to remove salt residuals and non-specific matrix components

from blood that could be loosely attached to the coating surface; 3) Placement of the Bio-SPME fiber into the pre-filled MOI chamber; and 4) Introduction of the desorbed analytes into the API 4000 (SCIEX, Concord, ON, Canada) by the self-aspiration of the TurboIon™ electrospray source.[53] More information regarding instrumental parameters for analysis of ISD can be found in Table 4.2. Furthermore, detailed information on the analytical workflow is shown in **Figure 4.1.**

Table 4.2. Multiple reaction monitoring optimized parameters for SCIEX API 4000 mass spectrometer with dwell time of 50 ms.

Compound	Precursor (m/z)	Product (m/z)	Declustering Potential (V)	Entrance Potential (V)	Collision Energy (V)	Cell Exit Potential (V)
Tacrolimus	804.03	821.50	95.22	13.00	28.95	28.70
Tacrolimus, ^{13}C d_2	807.02	824.50	114.41	9.95	28.20	28.22
Sirolimus	914.19	931.60	85.10	9.00	22.31	32.30
Everolimus	958.24	975.60	109.90	5.85	24.10	33.00
Everolimus, d_4	962.25	979.70	100.70	8.40	24.20	32.02
Cyclosporine A	1202.64	1219.80	100.00	9.88	28.80	49.90
Cyclosporine A, d_4	1206.64	1223.80	99.70	11.50	23.91	49.10

A Shimadzu 10AD LC pump was used to supply the desorption solution, which was comprised of 12 mM ammonium acetate and 0.1 % of formic acid (v/v) in methanol, to the MOI setup. The MOI set-up consisted of a Shimadzu LC pump providing the desorption solution through a switch valve to the ESI source and the desorption chamber. Once the desorption chamber was filled and equilibrium was reached between the LC pump supply flow rate and aspiration flow rate (generated by the ESI source), the Bio-SPME fiber was introduced into the desorption chamber. After 5 seconds of fiber immersion for desorption, the Bio-SPME fiber was withdrawn, and the valve was switched to rapidly move the desorbed plug of analytes towards the ESI source.[52,53,56] Once the desorption chamber was emptied, the switch valve was returned to the initial position. At this stage, a higher desorption flow rate was used to fill the desorption chamber. Finally, the

chamber was refilled and drained three consecutive times to prevent any carryover from previous desorption stages. Electrospray ionization parameters for optimum performance of the MOI and for ionization in positive mode were auxiliary gases GS1 = 90 psi, GS2 = 70 psi and, curtain gas = 25 psi, voltage = 5000 V, and temperature = 300 °C. A schematic of the MOI setup and operational features are shown in **Figure 4.2.**

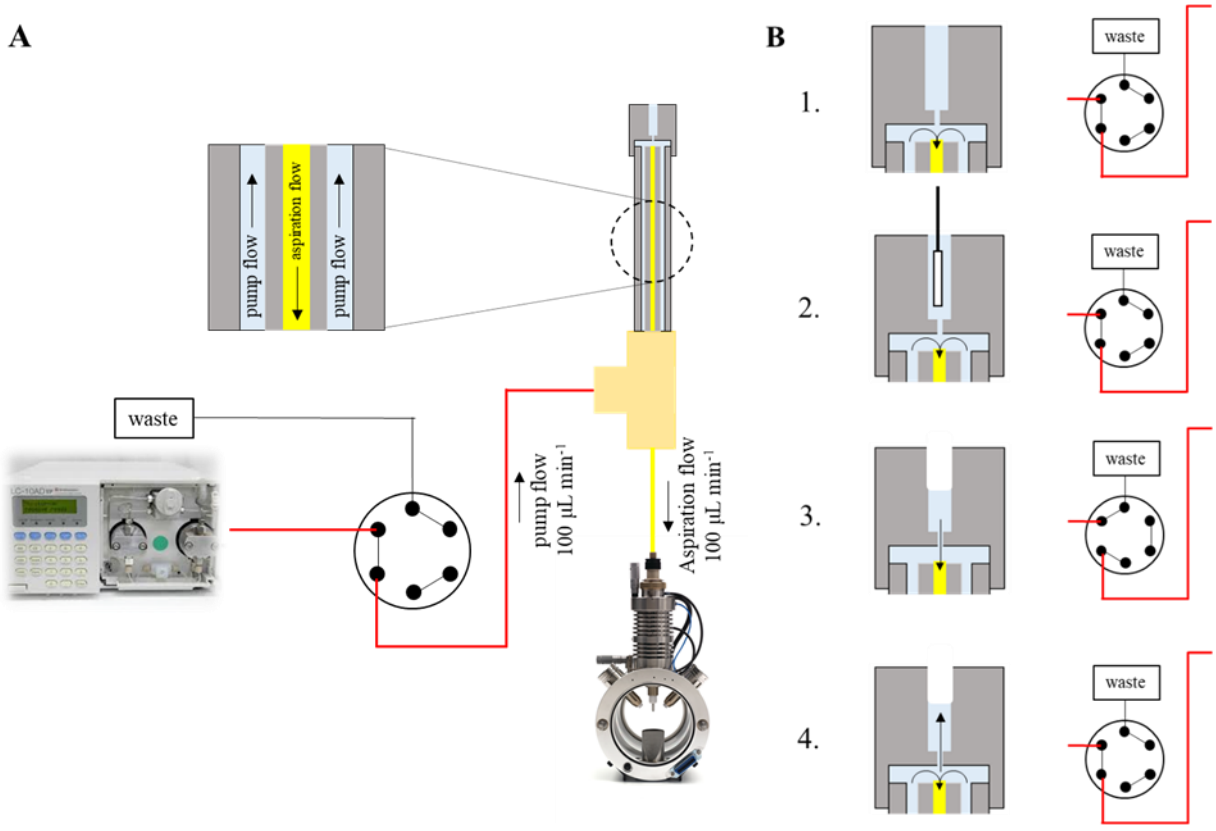

Figure 4.2. Schematic of the MOI setup (A) and operational workflow (B). In the B-1 part, the interface is constantly supplied by the desorption solution (pump flow rate = aspiration flow rate), and the interface is ready for SPME fiber to be introduced (B-2). After 5 seconds of desorption, the SPME fiber is removed and desorption flow is redirected to the waste by the switch valve (B-3), thus aspirating the desorbed analytes. Just before the air gets to be introduced to the aspiration line, the desorption solution flow is redirected back with the switch valve and pump flow is increased to fill the chamber (B-4). Once the desorption chamber is filled, this process is either repeated to deal with the carryover (three times) and then the interface is ready for the next SPME fiber.

4.3.4. Inter-day stability and imprecision evaluation of in-house prepared whole blood QC samples

The inter-day stability was evaluated by performing measurements for ten consecutive days, using four independent replicates per day for three in-house prepared QC levels (*i.e.*, 2.5, 7.5, and 15 ng mL^{-1} for TAC, SIR, and EVE; and 50, 150, and 300 ng mL^{-1} for CYC).

4.3.5. Calibration plots

In order to evaluate the ability of internal standards to correct for experimental and instrumental variances following their addition to lysis solutions, three calibration plots were prepared with three different hematocrit levels in whole blood (20%, 40%, and 70% hematocrits) and analyzed in triplicate, covering the following concentration range: 1.0 – 50.0 ng mL^{-1} for TAC, SIR, and EVE and 10 – 500 ng mL^{-1} for CYC.

The sensitivity of the MOI-MS/MS method was assessed by analyzing seven calibration levels, one blank level, and three in-house prepared QC levels, all in quadruplicate. The calibration solutions were spiked between 1.0 – 50 ng mL^{-1} for TAC, SIR, EVE and 10 – 500 ng mL^{-1} for CYC. In-house QC levels were prepared with different lots of whole blood to meet general method development criteria.[114,138] The limit of quantitation (LOQ) was estimated using the lowest calibration point that met the following requirements: 1) lowest calibration point with the signal to noise ratio ≥ 10, 2) 80 – 120 % back-calculated accuracy using linear regression line, and 3) imprecision of < 20 %.

4.3.6. SPME-MOI-MS/MS cross-validation against CMIA

Experimental information regarding the CMIA method is described elsewhere.[120] Concentrations calculated using the Bio-SPME-MOI-MS/MS assay were compared to those obtained by the Abbot ARCHITECT i2000 CMIA. Two sets of patient samples (n = 95) containing TAC and SIR were analyzed separately for this purpose, using respective immunoassay kits. Each set was analyzed in a single replicate together with a single replicate of calibration levels, in-house QC, and Recipe ClinCal®. Additionally, inter-day imprecision analysis (n = 3) was performed using Recipe ClinCal® QC levels. Previously determined

concentrations with the CMIA assay ranged between 2.5 – 26.3 ng mL^{-1} for TAC and 1.8 – 27.8 ng mL^{-1} for SIR. Statistical analysis comprised slope, intercept, and correlation coefficient determination using Passing-Bablok regression with a 95 % confidence interval. Relative and absolute method bias was determined and visualized using a Bland-Altman plot. The acceptance criteria for method comparison were defined as the slope of 1.00 ± 0.25 and $R2 \geq 0.9$.

All statistical analysis was performed on MedCalc® (v. 14.8.1) and Microsoft® Excel® 2013 (v. 15.0.5059.1000).

4.4. Results and Discussion

4.4.1. SPME-MOI-MS/MS and general method development

The imprecision of the calibration plot slopes prepared with three different lots of blood containing different hematocrit levels was evaluated. Total imprecision was < 6 % for TAC, < 4 % for SIR, < 6 % for EVE, and < 2 % for CYC (**Figure 4.3.**). These results succinctly proved that the spiking of internal standards in the lysis solution was able to accurately correct for hematocrit level variability in whole blood.[94]

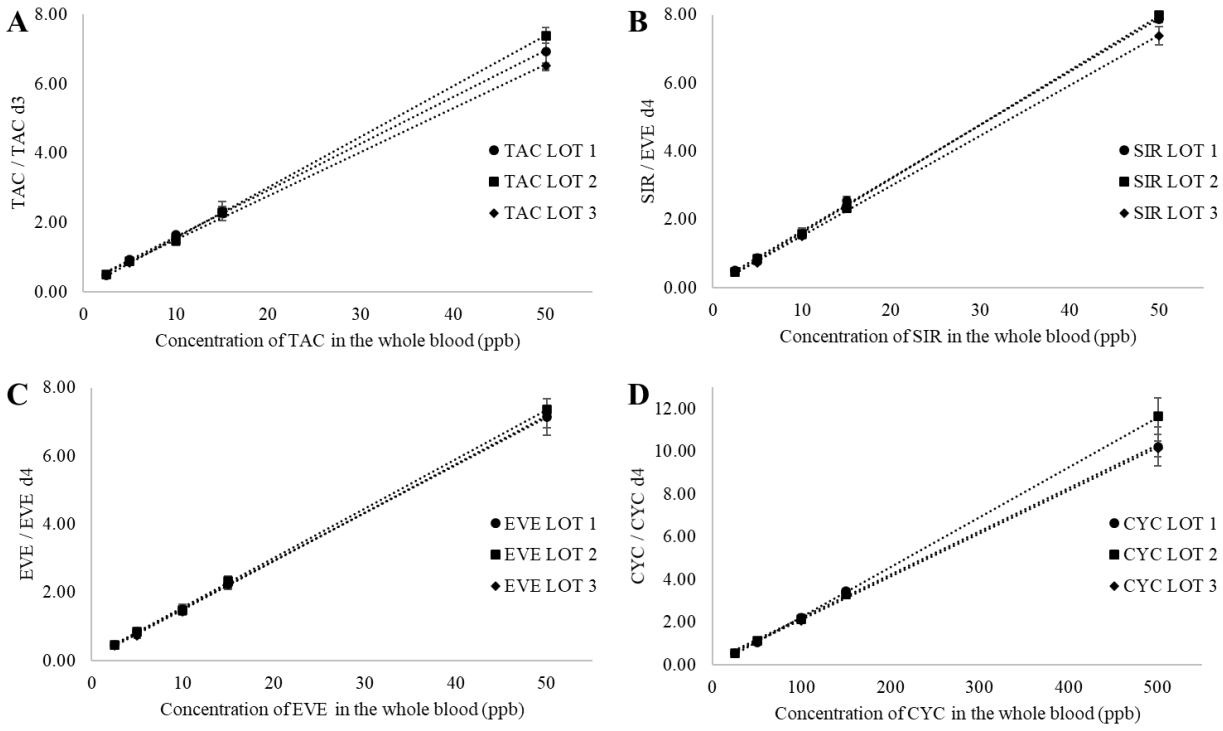

Figure 4.3. Evaluation of the ability of internal standard to correct for various lots with different hematocrit levels (LOT 1 = 40 %, LOT 2 = 20 %, LOT 3 = 60 %) for tacrolimus (A), sirolimus (B), everolimus (C), and cyclosporine A (D); (n = 4).

The inter-day imprecision of the proposed methodology was evaluated by analyzing the in-house prepared QCs in quadruplicate. Additionally, an inter-day evaluation of Recipe® ClinCal QCs in a single replicate was carried out in three days as an alternative imprecision evaluation of the MOI-MS/MS method. Imprecision values for all QCs are summarized in Table 4.3. For the three different levels of in-house prepared QCs, imprecision was determined to be ≤ 4 % for TAC, ≤ 10 % for SIR, ≤ 6 % for EVE, and ≤ 6 % for CYC. Recipe® ClinCal QC imprecision values were ≤ 9 % for TAC, ≤ 10 % for SIR, ≤ 7 % for EVE, and ≤ 9 % for CYC.

Table 4.3. Total inter-day imprecision of method for TAC, SIR, EVE, and CYC from Recipe ClinCal® and in-house prepared QCs.

		Imprecision, %, (n=10)				**Concentration (ng mL^{-1})**			
		TAC	*SIR*	*EVE*	*CYC*	*TAC*	*SIR*	*EVE*	*CYC*
In-house QC	Level 1	4	8	6	2	2.5	2.5	2.5	50.0
	Level 2	3	4	5	6	7.5	7.5	7.5	150.0
	Level 3	3	10	6	3	15.0	15.0	15.0	300.0
Recipe ClinCal®	Level 1	9	10	7	1	1.3	1.5	1.5	26.3
	Level 2	3	3	4	9	2.5	2.9	2.9	48.9
	Level 3	1	9	3	7	5.3	5.7	5.3	93.0
	Level 4	4	3	5	4	10.9	11.9	11.7	180.0
	Level 5	5	4	3	9	21.6	23.5	23.2	440.0
	Level 6	1	1	6	N/A	44.1	49.8	48	1287.0

Since the desorption solution does not continuously flow through the desorption chamber during analysis, there is a chance that carryover may occur between the introduction of the isolated volume for the analysis. The desorbed plug of analytes is carried to the detector surrounded by a pure desorption solution.[139] To further prevent carryover from affecting results, three additional 'dummy' desorption steps (fill the desorption chamber, hold for 5 seconds, drain the desorption chamber to the MS) were carried out prior to

the introduction of each Bio-SPME fiber. This set of measures was able to clean the desorption chamber prior to subsequent analysis and prevent carryover, **Figure 4.4.** and **Figure 4.5.**

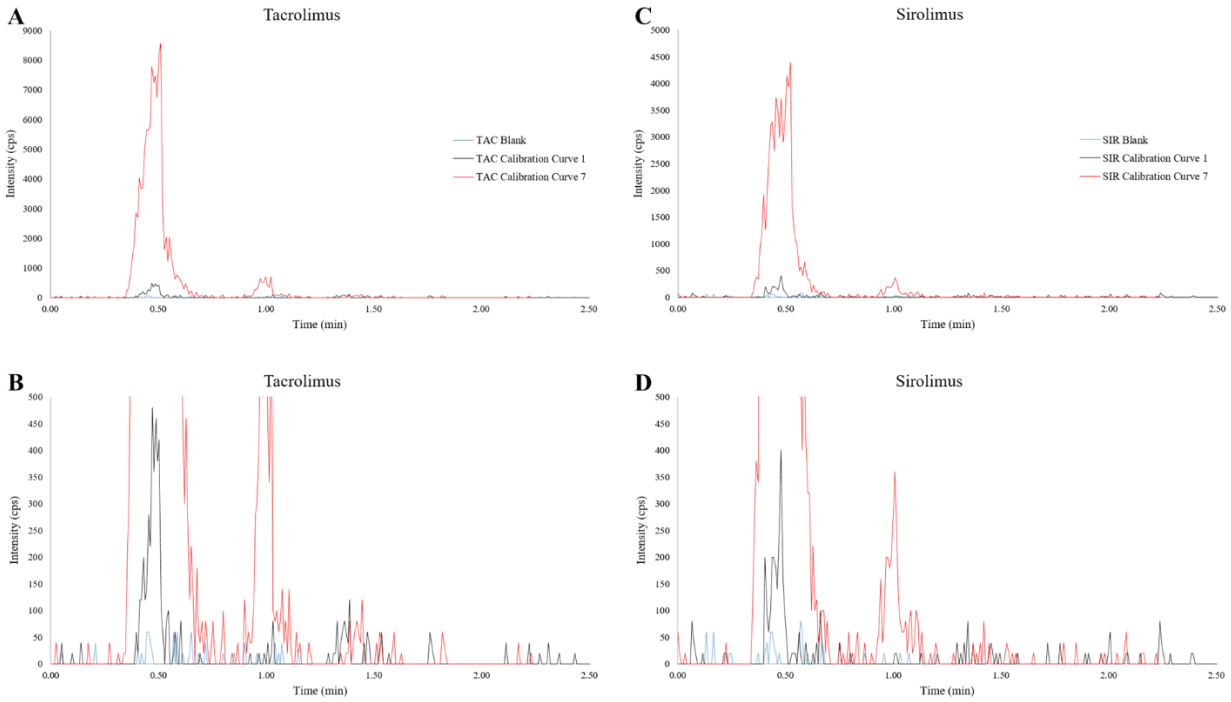

Figure 4.4. Carryover evaluation for TAC (A and B) and SIR (C and D) using extraction from whole blood blank sample, calibration point 1 (1.0 ppb), and calibration point 7 (50.0 ppb). Analyte elution is done manually and is approximately at 0.5 min for the peak used for quantitation, and three additional elutions (dummy desorptions) are approximately at 1.0 min, 1.5 min, and 2.0 min. A and C represent full sized comparison while B and D represent zoomed-in comparison.

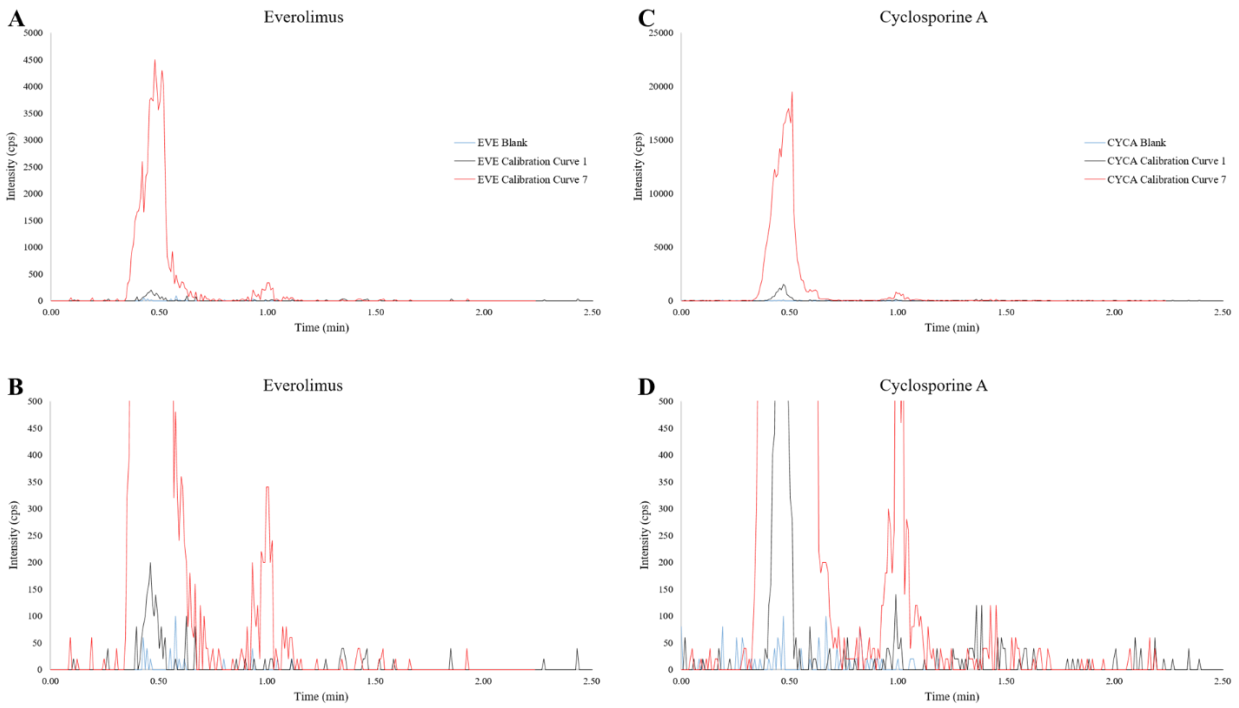

Figure 4.5. Carryover evaluation for EVE (A and B) and CYC (C and D) using extraction from whole blood blank sample, calibration point 1 (1.0 ppb for TAC and 10.0 ppb for CYC), and calibration point 7 (50.0 ppb for TAC and 500 ppb for CYC). Analyte elution is done manually and is approximately at 0.5 min for the peak used for quantitation, and three additional elutions (dummy desorptions) are approximately at 1.0 min, 1.5 min, and 2.0 min. A and C represent full sized comparison while B and D represent zoomed-in comparison.

4.4.2. Limit of quantitation, limit of detection, and linearity evaluation

The method´s LOQ achieved for a given ISD should be at least one-third to one-half of the lower limit of its target concentration window.[114] LOQs and linearity of the MOI-MS/MS method were determined for each ISD analyte using matrix-matched calibration plots (**Table 4.4.** and **Figure 4.6.**). The LOQs were determined to be 0.8 ng mL^{-1} for TAC, 0.7 ng mL^{-1} for SIR, 1.0 ng mL^{-1} for EVE, and 0.8 ng mL^{-1} for CYC. These were determined using the lowest calibration point and detection limits we have taken as one-third of the limit of quantitation. In this manner, the therapeutic range of all ISD is wholly covered with a determined linear dynamic range.[50,114]

Table 4.4. Figures of merit for determination of tacrolimus (TAC), sirolimus (SIR), everolimus (EVE), and cyclosporine A (CYC) in whole human blood. TAC, SIR, and EVE in-house quality control (QC) concentrations were 2.5 ng mL^{-1}, 7.5 ng mL^{-1}, and 15 ng mL^{-1} for QC Level 1, QC Level 2, and QC Level

3, respectively; while CYC concentrations were 50 ng mL^{-1}, 150 ng mL^{-1}, and 300 ng mL^{-1} for QC Level 1, QC Level 2, and QC Level 3, respectively.

				Accuracy, %, (n=4)		
Analyte	*LDR (ng mL^{-1})*	*LOQ (ng mL^{-1})*	*LOD (ng mL^{-1})*	*QC Level 1*	*QC Level 2*	*QC Level 3*
TAC	1.0 – 50.0	0.8	0.3	86	115	101
SIR	1.0 – 50.0	0.7	0.2	112	107	93
EVE	1.0 – 50.0	1.0	0.3	81	87	83
CYC	2.5 – 500.0	0.8	0.3	96	91	89

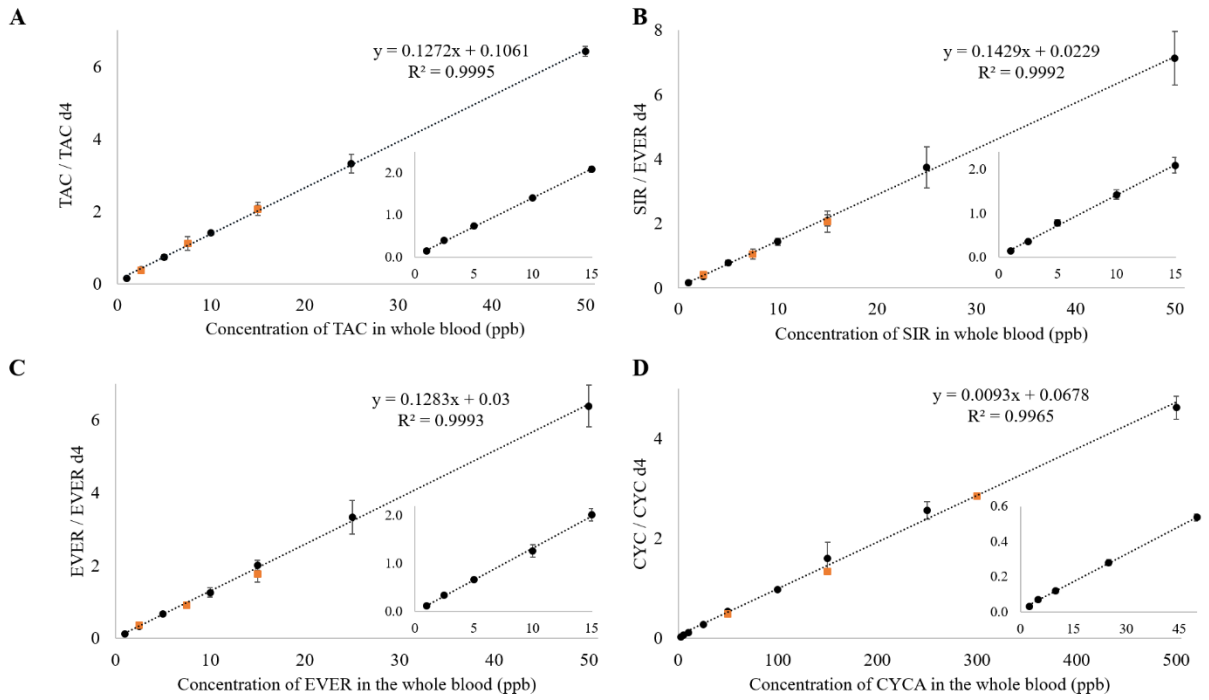

Figure 4.6. Linear regression analysis of tacrolimus (TAC), sirolimus (SIR), everolimus (EVE), and cyclosporine A (CYC) in whole human blood. Black circles correspond to the calibration points, orange squares correspond to the internal quality control levels, and small insert on the right-bottom side of each graph is enlarged calibration plot at the limit of quantification levels for each analyte.

4.4.3. SPME-MOI-MS/MS vs CMIA for TAC and SIR

Anonymized residual whole blood samples from patients undergoing immunosuppressive therapy were quantified with the developed MOI-MS/MS method and statistically compared to an already validated

CMIA assay (**Figure 4.7.** and **Figure 4.8.**). The acceptance criteria were defined as a slope of 1.00 ± 0.25 and R2 ≥ 0.9 for Passing and Bablok regression analysis.

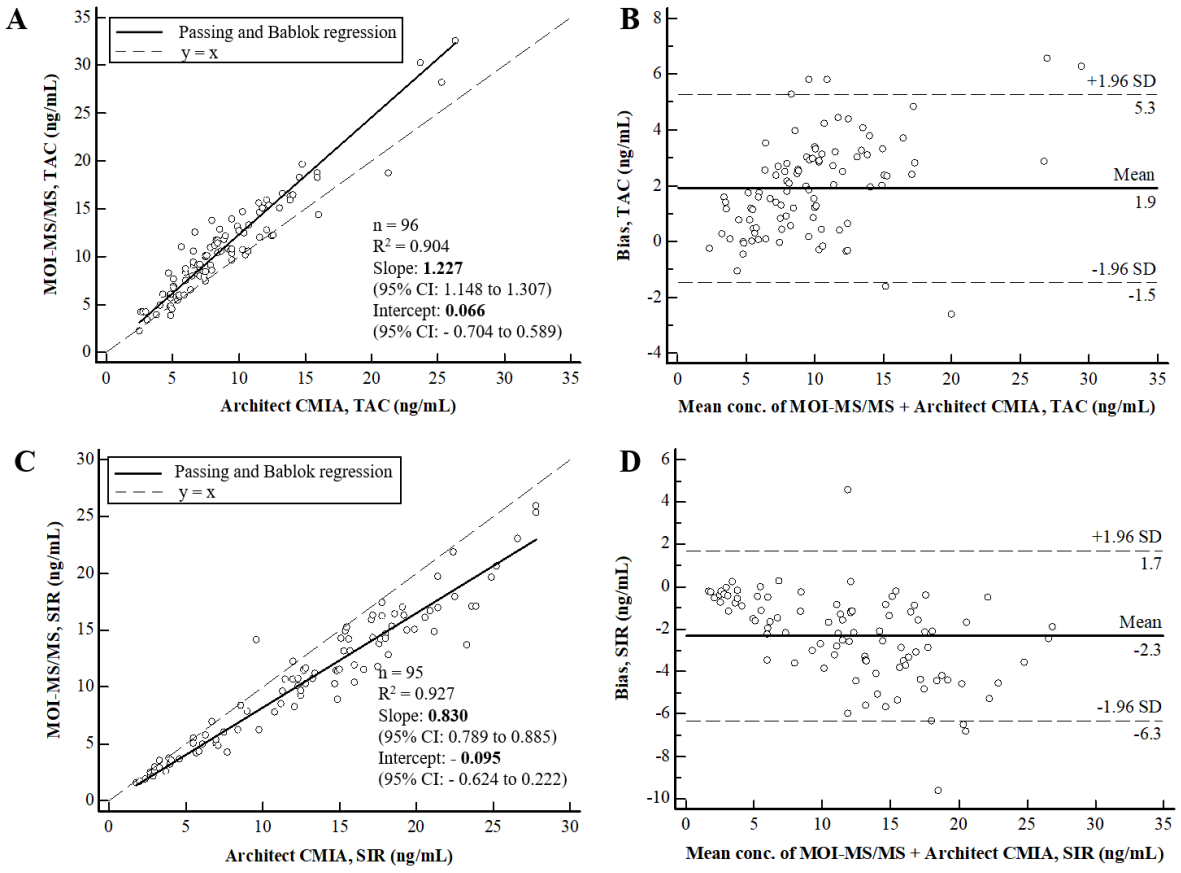

Figure 4.7. Passing and Bablok regression comparisons and Bland-Altman plots for TAC (A and B) and SIR (C and D) between MOI-MS/MS and Architect CMIA.

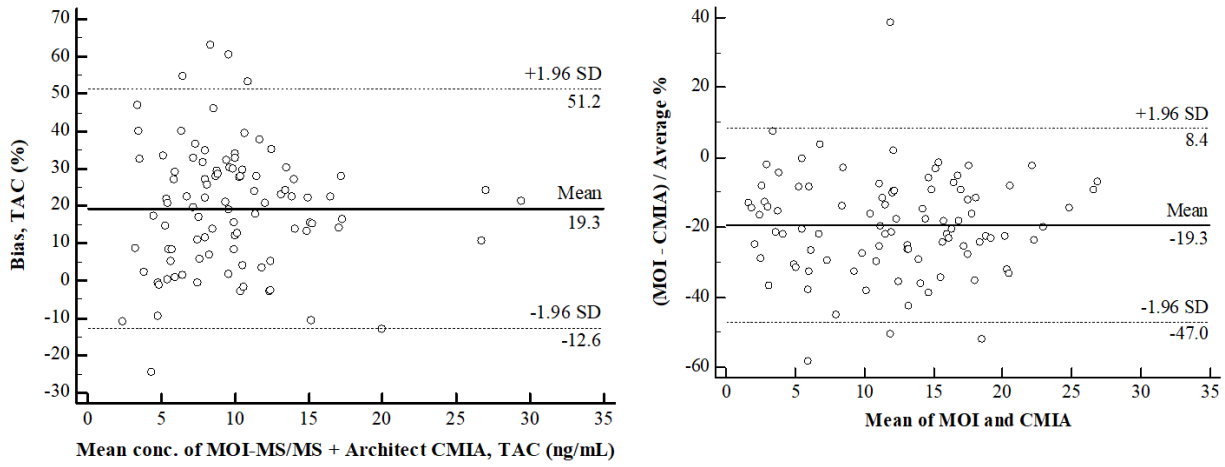

Figure 4.8. Passing and Bablok regression comparisons and Bland-Altman plots for TAC (left) and SIR (right) between MOI-MS/MS and Architect CMIA.

For the set of TAC samples, MOI-MS/MS showed acceptable agreement with CMIA with a slope of 1.227 (95 % confidence interval: 1.148 to 1.307), an intercept of 0.066 (95 % confidence interval: - 0.704 to 0.589), and R^2 of 0.904. The lack of a slope value of 1 in the 95 % confidence interval explains the proportional differences between the two methods. Additionally, no systematic differences could be studied given that the 95 % confidence interval contains an intercept value of 0. A Bland-Altman plot identified 93.75 % (90/95) of samples within a 95 % confidence interval. The average bias was determined to be + 1.9 ng mL^{-1} or 19.3 %.

Regarding the set of samples containing SIR, the method showed good agreement with CMIA, providing a slope of 0.830 (95 % confidence interval: 0.789 to 0.885) and an intercept of - 0.095 (95 % confidence interval: - 0.624 to 0.222). Similarly, TAC and SIR samples showed some proportional and no systematic bias. Additionally, the Bland-Altman plot identified 95.8 % (91/95) of samples within a 95 % confidence interval. The average bias was determined to be – 2.3 ng mL^{-1} or approximately – 19.3 %.

Several studies have shown the positive bias of immunoassay-based methods compared to LC-MS/MS-based methods. These differences have been primarily attributed to the cross-reactivity of ISD metabolites. Proportional differences are mainly observed for SIR, but it also must be kept in mind that proportional and systematic differences depend on the type of commercial immunoassay kit and external calibrator reference

materials used.[119,120,140,141] Moreover, similar results have been achieved herein as compared to another recent publication based on the SPME.[109]

4.4.4. Comparison of SPME-MOI-MS/MS vs. other technologies

Reports in the literature suggest that a total turnaround time of 3 – 6 hours is desirable for clinical applications to allow for daily dose adjustments.[114] Therefore, in this case, aiming to achieve total turnaround times that meet the requirements demanded in clinical environments, the IS's are added to the lysis solution instead of being spiked to the whole blood. As a result, a single sample can be analyzed entirely in less than 62 minutes, an appropriate timeframe for clinical environments. Additionally, considering the high throughput capabilities of the method (reduction by a factor of 24, number of vials VWR® Thermal Shake Touch can accept at once), a total time of 4.5 minutes per single sample can be achieved. By doing this, the IS mixture can still be accurately correct for subsequent experimental and/or instrumental variations. This is evidenced in **Figure 4.3.** where an imprecision ≤ 10 % was achieved for method evaluation by using different whole blood lots with varying hematocrit levels.

Even though the proposed method met the desired turnaround time for daily dose adjustments in clinical environments,111 the SPME-MOI-MS/MS method is at a disadvantage compared to other methods in terms of single sample turnaround time.[33,133,134,142] However, the method turnaround time is comparable to other reported assays when samples are run in a high-throughput fashion. Most traditional sample methodologies involve manual steps that reduce their high throughput capability (*e.g.*, centrifugation of samples[33,120,131,134,142] or drying of samples[132,133]). In contrast, SPME fibers can be arranged to be operated on liquid handlers previously used for other SPME devices in high-throughput applications.[4,65,136] Thus, simplifying the overall workflow to minimize manual work. Additionally, SPME-MOI-MS/MS does not require a pressurized system for analysis, an advantage that reduces overall system cost and contributes to design simplicity compared to existing methodologies.[33,124,134]

Additionally, the developed method uses a combination of mechanical and chemical lysing of the matrix (freeze-thaw cycles and addition of zinc sulfate:acetonitrile composition) to ensure that all analytes are

released from the matrix before the extraction process. The complete lysis is desirable for a non-exhaustive technique like SPME, which extracts exclusively via the free concentration of analytes. Furthermore, it allows our method to obtain comparable LOQs with other methodologies[33,109,134,142,143] for determining ISDs in whole human blood, with different methods capable of reaching the recommended requirement of ≤ 1.0 ng mL^{-1} for tested analytes (except for paper spray[133]).

The developed method's uniqueness lies in performing extraction with matrix-compatible devices (SPME fibers) that are then placed into a very low microliter volume desorption chamber. In this way, the Bio-SPME fiber enriches analytes of interest with minimal coextraction of matrix components, which is a very important factor in analyses of complex matrices such as whole blood. Hence, a simple and elegant design provides a distinct advantage over analytical methods that require packed devices (LC columns or SPE cartridges), as such methods must incorporate a centrifugation step during the sample preparation step to prevent clogging. Thus, SPME fiber introduces clean and concentrated extracts directly to the mass spectrometer.[144]

4.5.Conclusions

This manuscript presents a method for the simultaneous analysis of four ISDs from whole human blood using SPME-MOI-MS/MS technology. The technique contributed to a single turnaround time of 62 min, surpassing the total turnaround time desirable in clinical environments (3 – 6 hours) without compromising the assay's sensitivity, precision and/or accuracy. Additionally, it is essential to mention that when experiments are carried out in a high-throughput fashion, the total turnaround time decreases by a factor of 24, yielding a total turnaround time of 4.5 min per single sample. The imprecision of the assay was determined to be ≤ 10 % for in-house prepared QCs of each ISD over a 10-day period, while commercial QCs ((Recipe ClinCal®). also yielded an imprecision of ≤ 10 %. LOQs of less than one-third of the lowest concentration level for TAC, SIR, EVER, and CYC were achieved. Results of cross-validation against a well-established CMIA assay for TAC and SIR did not show any systematic differences (TAC: Passing and Bablok intercept of 0.066 with the interval of -0.704 – 0.589 and SIR: -0.905 with the interval of -0.624 –

0.222), but it has evidenced some proportional differences for both TAC and SIR (TAC: Passing and Bablok slope of 1.227 with an interval of 1.148 – 1.307 and SIR: Passing and Bablok slope of 0.830 with an interval of 0.789 – 0.885). The latter is inherent in comparisons between any MS-based method and immunoassay-based methods. To make a more appropriate method comparison, future work will involve comparing the SPME-MOI-MS/MS to validated LC-MS methods instead of knowingly biased immunoassay-based methods. In conclusion, this method offers a fast option for ISDs determination from whole blood matrixes while meeting general method development criteria.

Chapter 5: The Analysis of Fentanyl and Several Analogues from the Whole Blood using Solid-phase Microextraction Coupled Directly to Mass Spectrometry via Newely Improved Microfluidic Open Interface

5.1. Preamble

The content of this Chapter has not been published yet. The work is being prepared for submission to an academic journal. Daniel Rickert has assisted Emir Nazdrajić with experimental design, preparation for the experiments, performing experiments, and analysis using the microfluidic open interface. Daniel Rickert and Janusz Pawliszyn assisted Emir Nazdrajić in data interpretation. Janusz Pawliszyn supervised the whole project.

5.2. Introduction

Fentanyl is a synthetic opioid that was first introduced in the 1960s, and it is 50 – 100 times more potent than morphine.[145,146] Soon after, other fentanyl analogs were created, mainly for medicinal and veterinary use, aiming to modify their potency compared to fentanyl.[145] There is a concerning trend of fentanyl use and the use of its analogs across the world. This use contributes to overdose deaths reported in North America[147,148], Europe[149,150], and other parts of the world.[151] One of the most potent analogs is carfentanil which is 10 000 times more potent than morphine.[148] Determining the LD_{50} (lethal dose to half of the population studied) in animal studies of carfentanil is very difficult due to limitations in limits of detections. Thus, the number of carfentanil human exposures is probably underestimated due to these limitations in routine detections.[152] Therefore, it is essential to have very sensitive and rapid methods at disposal for monitoring the overdose cases and potentially methods capable of identifying new illicitly manufactured fentanyl analogs.

The most common biofluids used to analyze fentanyl, and its analogs are whole blood, urine, and hair.[153–156] These samples are mainly analyzed using LC-MS/MS because tandem mass spectrometry provides high selectivity and sensitivity. SPE or LLE are typically used to enrich fentanyl and its analogs before LC-MS/MS analysis. For LLE, typical steps include mixing a blood aliquot with an internal standard and a buffer (pH = 9-11) and then using ethyl acetate to perform the extraction. Samples are then shaken, centrifuged, and the organic layer is transferred to another vial where the solution is evaporated and reconstituted with a solvent compatible with the LC-MS/MS system.[157–159] For SPE, typical steps comprise diluting the whole blood aliquot with a phosphate buffer (pH = 6.0), then combining the resulting solution with calibrants and internal standards before mixing and centrifugation. Then, the SPE cartridge is preconditioned, washed, and conditioned before the sample is introduced, followed by a few washing steps and the elution step.[146,153,154,160–162] These methods have many manual steps and are considered the limiting step in the analytical protocol. A step toward automation of the extraction process has been taken to minimize the number of manual steps by implementing a flow-through desorption system coupled with online SPE-MS.[155] However, the disadvantage of such a method is using a separation system that can take a considerable amount of time to perform the overall analysis.

Some forensic/toxicological laboratories prefer to use (semi) automated immunoassays for routine detection of fentanyl and its analogs.[145,163] This may be preferred due to the fast turnaround and easy-to-follow protocols. However, the main drawback of this approach is the lack of assay selectivity towards the target analyte, which results in these methods mainly being used for screening.[145,164,165] After a positive hit with an immunoassay method, the sample is flagged for confirmation analysis, mostly done by LC-MS/MS.[163] In both cases, LC-MS/MS is required for quantification, so researchers have explored alternative methods such as direct-to-MS approaches.[163] One of the examples of a direct-to-MS approach that analyzes fentanyl in a very short time is using the OPI coupled to MS, where authors have used mail/packages to screen for opioids and have been able to detect as low as 31 ng of fentanyl.[166] Another example of the direct-to-MS approach is PS, a technique that offers limited sample preparation and no chromatographic

separation, so the total analysis time is relatively short.[167–169] Typically, paper spray analysis involves spotting the matrix sample on the paper substrate followed by a drying step and then adding a low volume of a desorption solution. The major disadvantage of this approach is introducing the complex matrix into the instrument, thus exposing the analysis to matrix effects and the instrument to contamination.

An appropriate sample preparation method is required to prevent instrument contamination and reduce the matrix effects. The main goal of any sample preparation step in the analytical protocol is to provide analyte enrichment.[2] SPE and LLE methods are exhaustive and often coextract sample components that cause matrix effects and instrument contamination. An alternative sample preparation method capable of addressing such disadvantages of exhaustive sample preparation methods is SPME. SPME is a sample preparation method that enriches a small portion of analytes that equilibrate with the extraction phase (non-exhaustive approach).[35] This results in the minimal introduction of analytes and coextracted interferences that offer lower matrix effects and instrument contamination compared to exhaustive methods while maintaining good method sensitivity. Additionally, matrix effects are mainly lowered using matrix-compatible extraction phases that contain a particle embedded in the binder (mainly polyacrylonitrile) that can eliminate the coextraction of macromolecules from complex samples, such as blood, while extracting small molecules.[170]

This work describes the development of an ultrasensitive SPME method coupled directly to tandem mass spectrometry via MOI for the rapid analysis of a set of opioids (acetylfentanyl, alfentanil, carfentanil, fentanyl, sufentanil) and a common fentanyl analog precursor (4-ANPP). MOI is a complete system for coupling SPME devices (e.g., *fibers*) directly to the MS. Analytes extracted onto SPME fiber are desorbed in a low volume flow isolated region (i.e., *desorption chamber*) and later introduced to the MS as a concentrated analyte plug that provides great analytical sensitivity.[52,53,56,110,171]

5.3. Experimental

5.3.1. Materials and Supplies

LC-MS grade methanol was purchased from Thermo Fisher Scientific (Bartlesville, OK, USA). LC-MS formic acid, methanol, acetonitrile, and isopropanol were purchased from Millipore Sigma (Bellefonte, PA, USA). Acetylfentanyl, acetylfentanyl-$^{13}C_6$, alfentanil, carfentanil, carfentanil-d_5, fentanyl, fentanyl-d_5, sufentanil, sufentanil-d_5, and 4-ANPP were purchased from Cerilliant (Round Rock, TX, USA). A table with analyte physicochemical parameters can be found in **Table 5.1.**

Table 5.1. Physicochemical properties of analytes. LogP, pKa, and molar mass obtained from Chemicalize, Last accessed = 2022-04-18, https://chemicalize.com/app/calculation.

Analyte	Strongest Basic pKa	LogP	Molar mass (g mol^{-1})	Structure
Acetylfentanyl	8.8	3.1	322.4	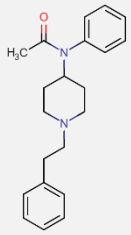
Alfentanil	7.5	2.8	416.5	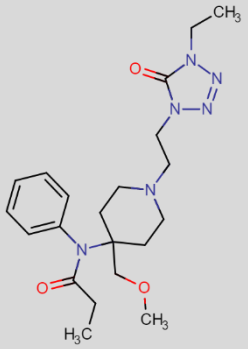
Carfentanil	8.0	3.7	394.5	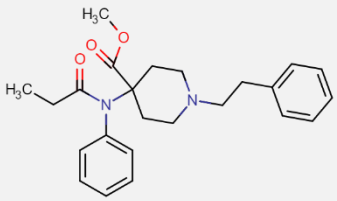

Fentanyl	8.8	3.8	336.5	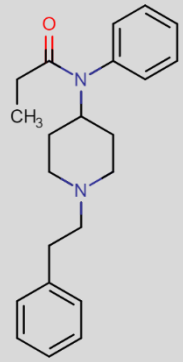
Sufentanil	8.9	3.6	386.6	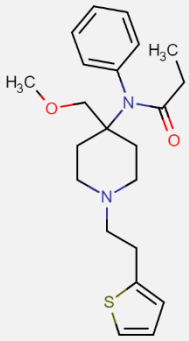
4-ANPP	9.2	3.5	280.4	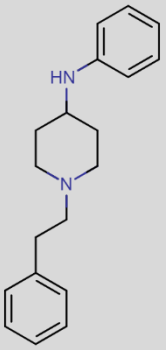

Analyte stock solutions were prepared in methanol at 10 µg mL^{-1} and were stored at -80 °C. Human whole blood K_2EDTA (gender pooled) was purchased from BioIVT (Hicksville, NY). 1 mL wellplates were purchased from Thermo Fisher Scientific (Bartlesville, OK, USA). Mixed-mode (strong cation exchange – C_8) SPME fibers were kindly donated by Millipore Sigma (Bellefonte, PA, USA). Potassium phosphate dibasic and potassium phosphate monobasic were purchased from Millipore Sigma (Bellefonte, PA, USA). The water used in this work is produced by a Milli-Q water purification system (Millipore Sigma, Bellefonte, PA, USA).

5.3.2. Whole blood preparation

Pooled human K_2-EDTA whole blood purchased from BioIVT was aliquoted in 5 mL aliquots and then frozen at -80 °C. Two days before using whole blood spiked with analytes, required whole blood aliquots were taken outside the freezer and placed in a +4 °C fridge overnight for blood to thaw. The next day thawed whole blood was additionally pooled (if more than 5 mL was needed) and then spiked with analytes, followed by being placed at +4 °C overnight to allow analyte-matrix binding to occur. During the optimization process, analytes were spiked at 20 ng mL^{-1}.

5.3.3. Optimization process

All sample preparation steps were run in the high-throughput format using Concept96 (PAS Technologies, Magdala, Germany) using 1 mL wellplates. All stages of the analytical protocol (cleaning, conditioning, extraction, and washing) were performed at 1200 rpm.

5.3.4. Conditioning solution optimization

Typically, in SPE-based protocols, before the introduction of the sample solution to the cartridge, the cartridge is preconditioned and activated with methanol, washed with water, and then conditioned with PBS (pH = 6.0). In this case, the particles used in the SPE cartridge are cation-exchange because at the pH of the PBS, fentanyl and its analogs will be mainly positively charged.[146] In this work, mixed-mode fibers contain particles capable of performing cation exchange and a polyacrylonitrile binder. The role of a binder in the SPME has not been studied deeply,[172] but the purpose of this optimization step is to see whether extraction efficiency is bigger after conditioning and activating SPME fibers with PBS (pH = 6.0) or methanol:water = 1:1 (V:V) solution would work better. PBS solution (pH = 6.0) was prepared by mixing 2.405 g of dipotassium phosphate and 11.728 g of monopotassium phosphate with 1 L of MiliQ water resulting in a 0.1 M PBS solution. The performance of SPME fibers in different solutions (methanol:water = 1:1 and PBS, pH = 6.0) was evaluated after being conditioned for 15 min. Prior to conditioning step, fibers were cleaned in methanol:acetonitrile:isopropanol = 1:1:1 (V:V:V) solution for 15 min. The extraction step consisted of placing SPME fibers in a 1 mL solution for 60 min (200 uL of whole blood

diluted with 800 uL of PBS, pH = 6.0). The washing step consisted of placing SPME fibers in the MilliQ water for 5 seconds. This was done to remove any residual salt and/or nonspecific attachment from the extraction phase surface. Extracted analytes were desorbed for 10 s with methanol:acetonitrile:water = 7:2:1 (V:V:V) spiked with 0.1 % formic acid (V:V).

5.3.5. Extraction dilution optimization

The next step in the optimization procedure was to evaluate the solution with which a 200 uL blood aliquot was diluted. Based on our previous experience, we have found that for a set of analytes that show a very high affinity for the red blood cells, a 0.1M zinc sulfate:acetonitrile:water = 6:3:1 (V:V:V) solution was needed for lysis process.[109,110] This solution was evaluated against 0.1 M PBS (pH = 6.0):acetonitrile:water = 6:3:1 (V:V:V) and PBS (pH = 6.0). Prior to extraction, SPME fibers were cleaned in methanol:acetonitrile:isopropanol = 1:1:1 (V:V:V) solution for 15 min, conditioned in methanol:water = 1:1 (V:V). After 60 min extraction step, SPME fibers were washed in MilliQ water for 5 s. Extracted analytes were desorbed for 10 s with methanol:acetonitrile:water = 7:2:1 (V:V:V) spiked with 0.1 % formic acid (V:V).

5.3.6. Extraction time optimization

Since SPME is a non-exhaustive method, analytes in the sample equilibrate with the extraction phase. A time profile must be studied to show when the maximum amount of analytes is enriched. SPME fibers were cleaned in methanol:acetonitrile:isopropanol = 1:1:1 (V:V:V) solution for 15 min, conditioned in methanol:water = 1:1 (V:V), then for the extraction step a 200 uL whole blood aliquot was diluted with 800 uL of PBS (pH = 6.0). A blank whole blood aliquot was analyzed with each extraction time point to check if the signal-to-noise ratio changed during the extraction time. After extraction, SPME fibers were washed with MilliQ water for 5 s and then desorbed for 10 s with methanol:acetonitrile:water = 7:2:1 (V:V:V) spiked with 0.1 % formic acid (V:V).

5.3.7. Desorption additive optimization

SPE-based protocols in the elution solution contain some small amounts of ammonium hydroxide, approximately 2 % (10.1021/acsomega.7b01536). The reason for adding ammonium hydroxide is to release extracted analytes from the ion exchange medium. Hence, methanol:acetonitrile:water = 7:2:1 (V:V:V) spiked with 0.1% formic acid (V:V) was evaluated at two levels of ammonium formate: 0.5 mM and 2 mM. Prior to extraction, SPME fibers were cleaned in methanol:acetonitrile:isopropanol = 1:1:1 (V:V:V) and conditioned in methanol:water = 1:1 (V:V). Extraction was performed for 60 min in 1 mL of diluted whole blood (200 uL whole blood diluted with PBS, pH = 6.0) followed by washing step in MilliQ water for 5 sec and desorption for 10 s.

5.3.8. Desorption time profile

The desorption time profile was studied to evaluate the time that provides the best desorption efficiency while maintaining the rapid-analysis attributes. Prior to extraction, SPME fibers were cleaned in methanol:acetonitrile:isopropanol = 1:1:1 (V:V:V) and conditioned in methanol:water = 1:1 (V:V). Extraction was performed for 60 min in 1 mL of diluted whole blood (200 uL whole blood diluted with PBS, pH = 6.0) followed by a washing step in MilliQ water for 5 sec, and desorption for 10 s in 2 mM ammonium formate in methanol:acetonitrile:water = 7:2:1 (V:V:V) spiked with 0.1 % formic acid (V:V).

5.3.9. Optimized Analytical Workflow

The SPME fibers prior to extraction were cleaned in methanol:acetonitrile:isopropanol = 1:1:1 (V:V:V) solution for 15 min and conditioned in methanol:water = 1:1, for 15 min. The conditioned SPME fiber was placed in a 1 mL sample solution (200 uL whole blood aliquot diluted with 800 uL of PBS, pH = 6.0) for 60 min for the extraction step. After extraction, SPME fibers were placed in MilliQ water for 5 s to remove any residual salt or nonspecific attachment. The analytes on the SPME fiber were desorbed for 10 s in 2.0 mM ammonium formate in methanol:acetonitrile:water = 7:2:1 spiked with 0.1 % formic acid using MOI.

5.3.10. Calibration plot, quality control, limit of quantification, and limit of detection

Whole blood aliquots were spiked from 0.010 – 25 ng $mL^{-1}$with analytes, while validation points (VP) were spiked at 2.0 ng mL^{-1} and 20 ng mL^{-1}, which is the concentration range typically found in the whole blood of fentanyl abusers.[160,162] Both aliquots were spiked with the internal standard at 5.0 ng mL^{-1}. The LOQ was estimated by extrapolating a signal-to-noise ratio to 10 using the lowest calibrator (at least 20 % precision, at least 80 % accuracy, and at least a signal-to-noise ratio of 10). The limit of detection (LOD) was estimated as one-third of the LOQ.

5.3.11. Description of the Microfluidic Open Interface and Instrumental Analysis

A schematic of the MOI system is shown in **Figure 5.1.** A programmable syringe pump (Harvard Apparatus, Holliston, MA, USA) was equipped with an SGE 10 mL gas-tight syringe (Millipore Sigma, Bellefonte, PA, USA) to provide inflow to the MOI system via a green PEEK tubing (ID: 0.75 mm, OD: 1/16 in). It is connected to a metal union that serves the role of the upstream electrospray ground. The metal union is connected to a PEEK three-way chromatographic tee, being held by a stainless-steel holder machined at the University of Waterloo Science Technical Services. Another three-way connection leads toward the desorption chamber designed out of two tubes. An outer FEP tubing (OD: 1/16 in, ID: 1/32 in) and a 2 cm shorter inner yellow PEEK tubing (OD: 1/32 in, ID: 0.007 in) concentrically placed make a desorption chamber.

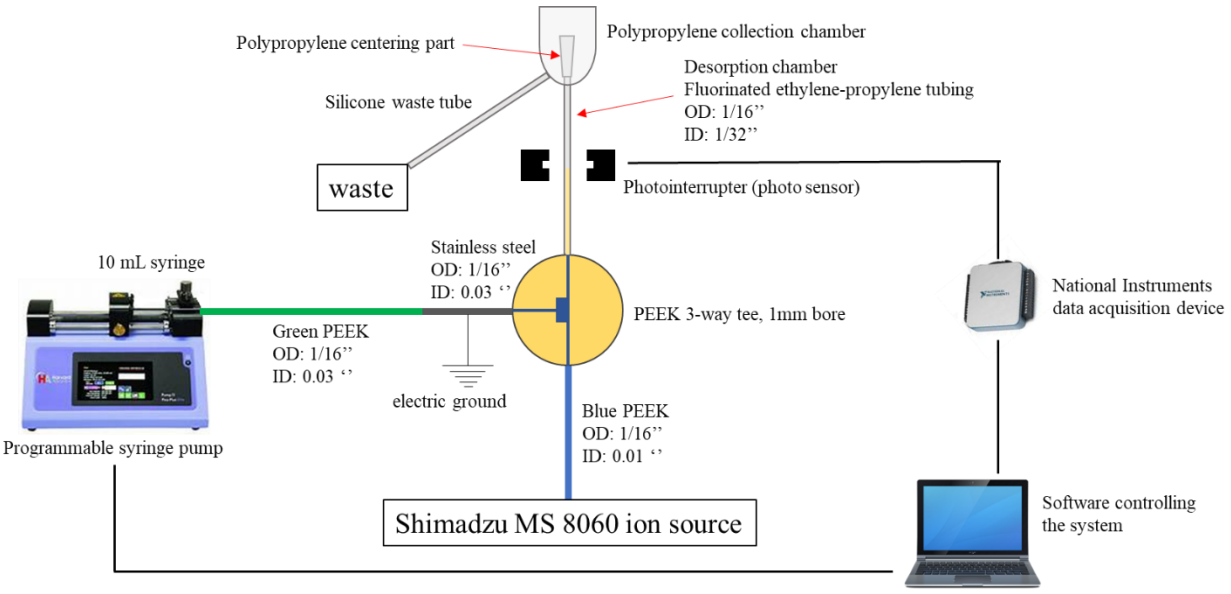

Figure 5.1. Schematic design of the MOI.

The desorption chamber is placed in the optical path of a photo interrupter supporting the stainless-steel holder. The photo interrupter monitors the change in the air-water interface at the bottom of the desorption chamber. Finally, the last three-way connection leads towards the electrospray source of the Shimadzu 8060 mass spectrometer via a blue PEEK tubing (OD: 1/16 in, ID: 0.010 in).

The Shimadzu ion source interface conditions are summarized in **Table 5.2.**

Table 5.2. Shimadzu MS 8060 ion source interface conditions.

Nebulizing gas flow (L min^{-1})	3.0
Drying gas flow (L min^{-1})	Off
Heating gas flow (L min^{-1})	Off
Interface voltage (V)	4000
Interface temperature (°C)	Off
DL Temperature (°C)	250
Heat block temperature (°C)	400

Briefly, the heating gas, the drying gas, and the interface temperature have been turned off because heating the electrospray stainless steel capillary beyond the boiling point of the desorption solution creates bubbles

that can appear inside the capillary. The appearance of these bubbles causes the suction flow rate to be inconsistent. The instrumental parameters of analytes and isotopically labeled compounds can be found in **Table 5.3.**

Table 5.3. Instrumental conditions. Dwell time was 10 ms.

Compound	Precursor ion (m/z)	Product ion (m/z)	Q1 Pre-rod bias (V)	Collision Energy (V)	Q3 Pre-rod bias (V)
Acetylfentanyl	323.1	188.1	-15.0	-23.0	-19.0
Acetylfentanyl	323.1	105.1	-16.0	-38.0	-22.0
Acetylfentanyl-$^{13}C_6$	329.1	188.1	-16.0	-24.0	-19.0
Alfentanil	417.2	268.2	-11.0	-32.0	-21.0
Alfentanil	417.2	197.2	-11.0	-32.0	-21.0
Carfentanil	395.2	335.2	-11.0	-20.0	-23.0
Carfentanil	395.2	113.2	-11.0	-32.0	-21.0
Carfentanil-d_5	400.2	340.3	-18.0	-20.0	-16.0
Fentanyl	337.2	188.2	-10.0	-24.0	-19.0
Fentanyl	337.2	105.1	-10.0	-38.0	-20.0
Fentanyl-d_5	342.1	188.2	-16.0	-24.0	-20.0
Sufentanil	387.2	238.2	-11.0	-20.0	-16.0
Sufentanil	387.2	111.1	-11.0	-38.0	-11.0
Sufentanil-d_5	392.2	238.2	-18.0	-21.0	-16.0
4-ANPP	281.3	188.2	-10.0	-18.0	-19.0
4-ANPP	281.3	105.1	-10.0	-32.0	-19.0

5.4. Results and Discussion

5.4.1. Extraction Optimization Results: Conditioning, Dilution, and Extraction Time Profile

To fully maximize the analytical utility of our assay, we went through the SPME workflow optimization. This includes optimizing the preconditioning solution, evaluating the best dilution solvent and volume, and an extraction time profile. The SPME fibers show much better extraction efficiency when conditioned with methanol:water = 1:1 (V:V) solution rather than with PBS (pH = 6.0), unlike SPE particles in the cartridge. We assume that methanol:water = 1:1 (V:V) solution penetrates and solvates the pores of polyacrylonitrile binder of the SPME devices better (and eventually the particles) rather than water and phosphate ions. Conditioning with PBS (pH = 6.0) solution decreases the extraction efficiency by a considerable amount (14 – 70 %) for the set of analytes, shown in **Figure 5.2.**

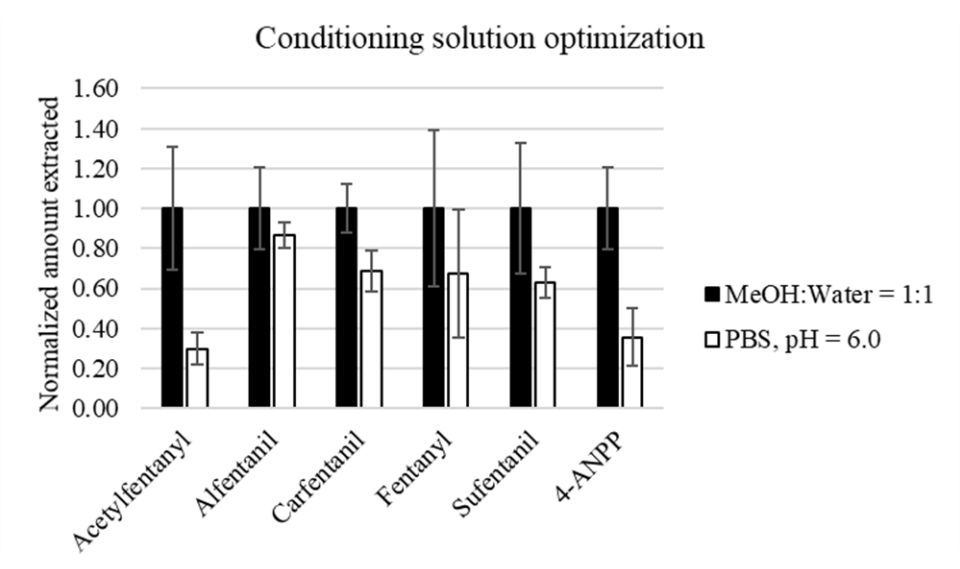

Figure 5.2. Conditioning solution optimization for the extraction of acetylfentanyl, alfentanil, carfentanil, fentanyl, sufentanil, and 4-ANPP from whole blood.

Diluting the 200 uL of whole blood with 800 uL of PBS (pH = 6.0) provides the best extraction efficiency for the SPME fiber when compared with other solutions. Analytes have the strongest basic pKa values ranging from 7.5 to 8.8 (Table 5.1), meaning that when diluted, they will be mainly positively charged in

the solution because the pH is almost two units below the pKa values. Since the SPME fiber is composed of PAN-C_8-SCX, the analyte must be positively charged because then analytes can equilibrate with the SCX portion of the extraction phase, in addition to C_8. The other two solutions did not perform as well, even though slightly acidic solutions have been mixed with acetonitrile to protein crash the matrix, as shown in **Figure 5.3.**

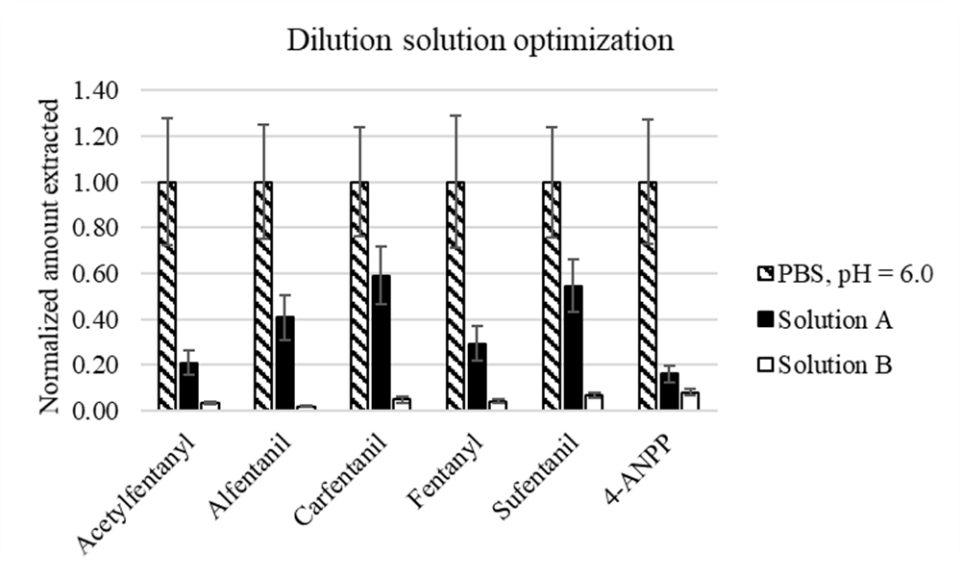

Figure 5.3. Dilution solution composition optimization of different solutions for extraction of acetylfentanyl, alfentanil, carfentanil, fentanyl, sufentanil, and 4-ANPP from whole blood. Solution A is 0.1 M zinc sulfate:acetonitrile:water = 6:3:1 and solution B is PBS:acetonitrile:water = 6:3:1.

The final optimization was an extraction time profile to evaluate at what time point do the analytes equilibrate with the extraction phase. Considering some previous publications,[108,172] the analytes most likely do not equilibrate with the whole coating, instead only with the surface since the primary interaction is the ion exchange. Since the effective diffusion coefficients of analytes are extremely low, to maintain a rapid aspect of this work, the optimum extraction time is selected to be 60 min because the extraction rate rapidly slows down around that time, as shown in **Figure 5.4.**

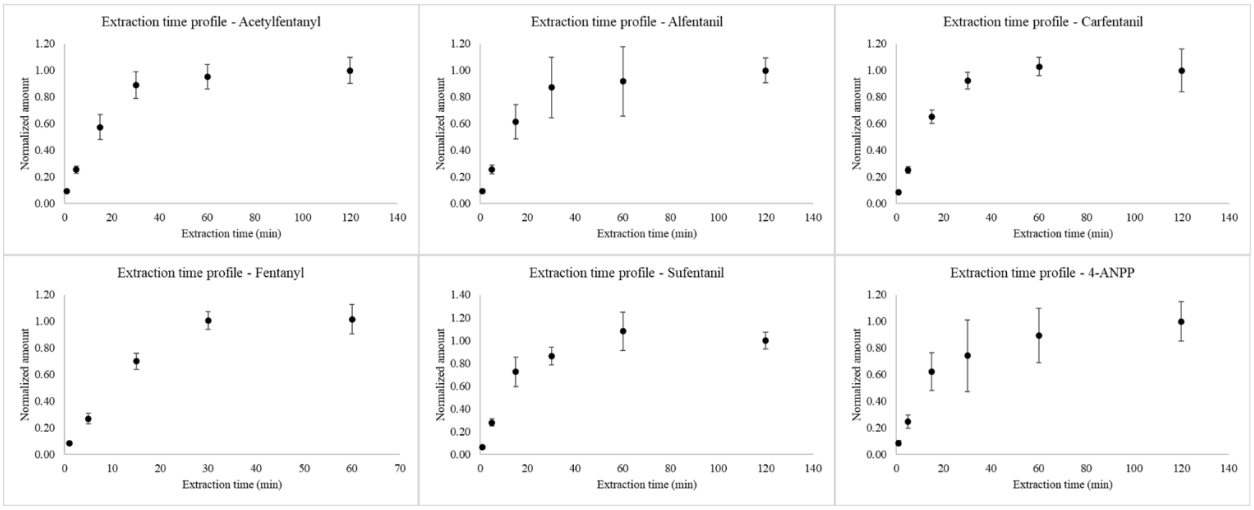

Figure 5.4. Extraction time profiles of acetylfentanyl, alfentanil, carfentanil, fentanyl, sufentanil, and 4-ANPP from whole blood.

From the point of view of this application, this method achieved excellent sensitivity (discussed more below) regardless of not completely reaching full equilibration during the extraction or desorption.

5.4.2. Desorption optimization results: Solvent Composition, Additive Concentration, and Desorption Time Profile

After optimizing the extraction conditions, we investigated the ideal desorption additive to enhance the desorption efficiency. SPE-based protocols use approximately 2 % of ammonium hydroxide to perform ion exchange and release the extracted analytes.[146,162,173] Since SPME fibers contain less extraction material and desorption solution is also used for ionization, we compared the desorption efficiency of 0.1 % formic acid versus 0.1 % formic acid with 0.5 mM or 2.0 mM ammonium formate. Higher concentrations of ammonium formate increase the solution conductivity, leading to corona discharge and instability of the electrospray in the ion source. The results show (**Figure 5.5.**) that the best desorption efficiency was obtained with 2.0 mM ammonium formate with 0.1 % in formic acid.

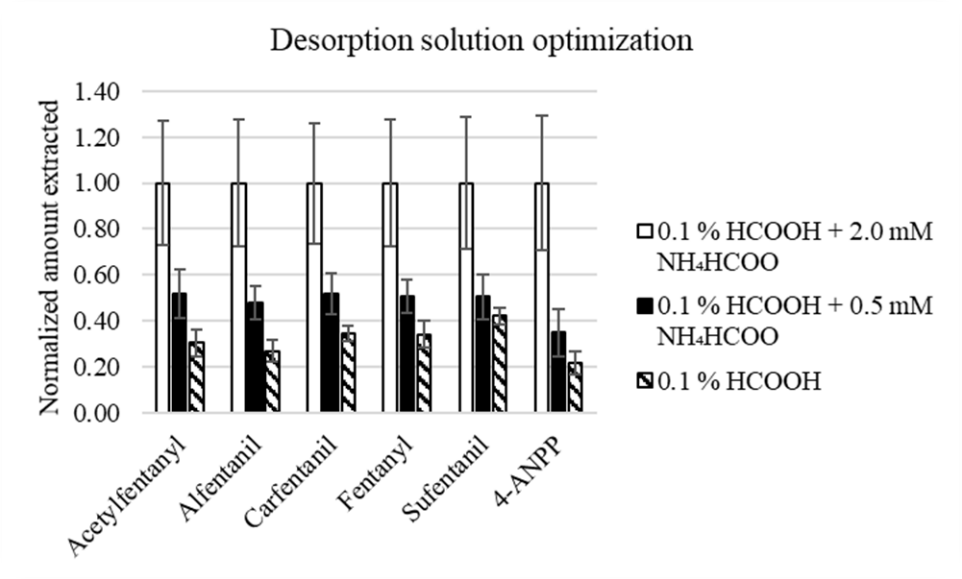

Figure 5.5. Desorption solution optimization for desorbing acetylfentanyl, alfentanil, carfentanil, fentanyl, sufentanil, and 4-ANPP from PAN-C_8-SCX SPME fiber.

Therefore, this desorption solution has been selected to be used for the desorption time profile. The desorption time profiles (**Figure 5.6.**) show that the optimum desorption time for all analytes is 10 s.

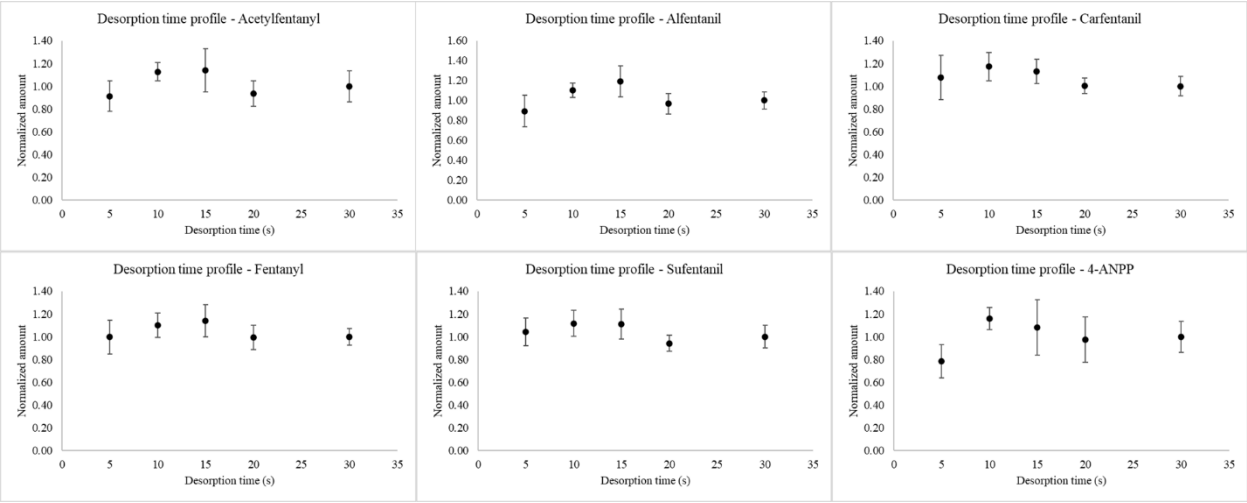

Figure 5.6. Desorption time profiles of acetylfentanyl, alfentanil, carfentanil, fentanyl, sufentanil, and 4-ANPP from SPME PAN-C8-SCX SPME fiber.

5.4.3. Figures of Merit: Limit of Quantification, Limit of Detection, Linearity, and Calibration Plot

Estimated limits of quantifications for analytes range 0.002 – 0.031 ng mL^{-1}, while limits of detections for analytes range 0.0007 – 0.010 ng mL^{-1}. The linearity ranges from 0.010 – 25 ng mL^{-1} for all analytes except acetylfentanyl where the linearity ranges from 0.050 – 25 ng mL^{-1} because of the relatively higher limit of quantification. Figure 5.7. shows the comparison of the lowest calibrator with a signal-to-noise ratio of 10 with the blank signal.

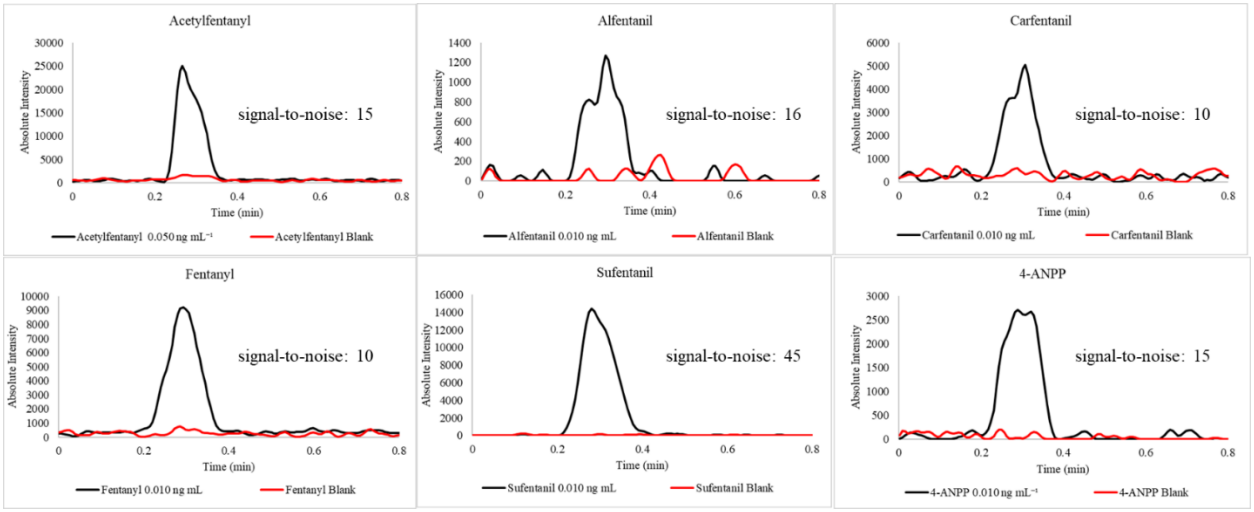

Figure 5.7. Lowest calibrator comparison (0.010 ng mL^{-1} for alfentanil, carfentanil, fentanyl, sufentanil, and 4-ANPP; 0.050 ng mL^{-1} for acetylfentanyl) to blank (whole blood, unspiked) signal.

Figures of merit are summarized in **Table 5.4.**

Table 5.4. List of limits of quantifications (LOQ), limits of detections (LOD), and linear dynamic range (LDR) of analytes for extraction from whole blood.

Analyte	LOQ (ng mL^{-1})	LOD (ng mL^{-1})	LDR (ng mL^{-1})
Acetylfentanyl	0.031	0.010	0.050 – 25.0
Alfentanil	0.010	0.003	0.010 – 25.0
Carfentanil	0.010	0.003	0.010 – 25.0
Fentanyl	0.010	0.003	0.010 – 25.0
Sufentanil	0.002	0.0007	0.010 – 25.0
4-ANPP	0.007	0.002	0.010 – 25.0

Figure 5.8. shows weighted calibration plots of analytes using a weighting factor inversely proportional to the variance of the corrected responses with inserts for the lowest five calibrators.

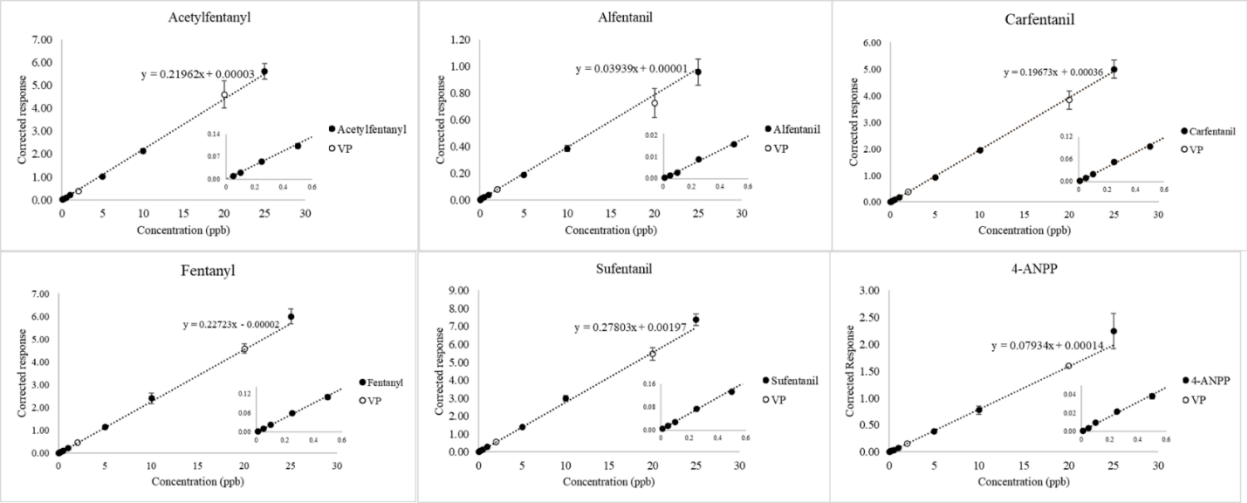

Figure 5.8. Weighted calibration plots with a weighting factor of inverse variance for acetylfentanyl, alfentanil, carfentanil, fentanyl, sufentanil, and 4-ANPP extraction from whole blood.

The accuracy of calibration points ranges from 81 – 100 %, and the relative precision ranges from 1 – 17 % for all analytes. On the other hand, the accuracy of validation points ranges from 89 – 99 %, and the relative precision ranges from 4 – 15 % for all analytes. The four-day inter-day reproducibility varies from 6 – 15 % for all analytes, as shown in **Table 5.5.** and **Figure 5.9.**

Table 5.5. The precision of uncorrected extracted amount for inter-day validation.

Analyte	Acetylfentanyl	Alfentanil	Carfentanil	Fentanyl	Sufentanil	4-ANPP
Precision (%)	8	15	6	12	8	10

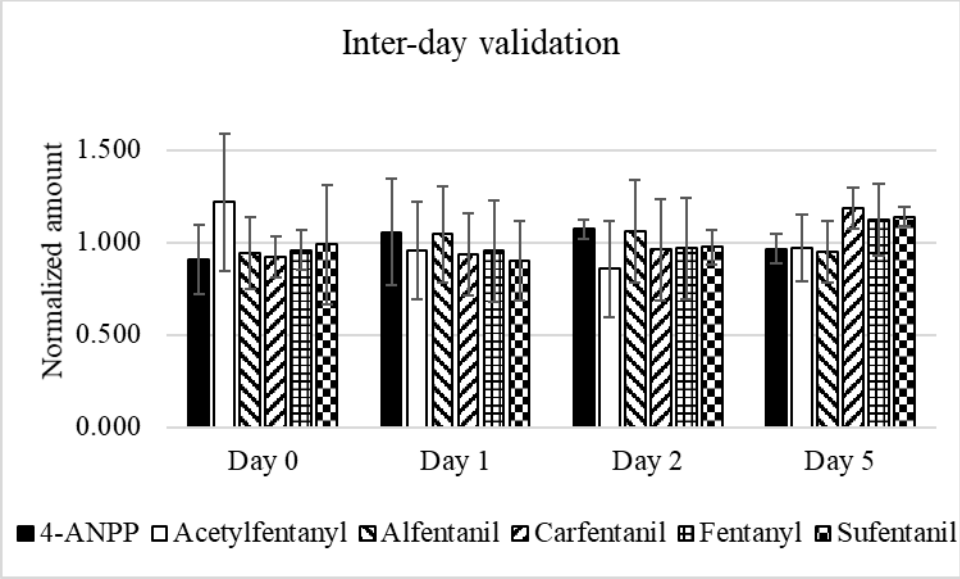

Figure 5.9. Inter-day validation showing uncorrected normalized amount injected using MOI.

Table 5.6. Method comparison of literature methods and this work. * Liquid chromatography method runtime. ‡Instrumental analysis time per sample. †Total method analysis time (including high-throughput sample preparation). WB – whole blood, WB[1] - whole blood dried blood spot, U – urine, DU – diluted urine, LC – liquid chromatography coupled to tandem mass spectrometry, UHPLC – ultra-high-performance liquid chromatography coupled to tandem mass spectrometry, PS – paper spray tandem mass spectrometry, Online SPE – online solid-phase extraction coupled to tandem mass spectrometry, SPE – solid-phase extraction, LLE – liquid-liquid extraction, SPME – solid-phase microextraction, LOQ – limit of quantitation.

Method	**Matrix**	**Sample prep.**	**Acetylfentanyl**	**Alfentanil**	**Carfentanil**	**Fentanyl**	**Sufentanil**	**4-ANPP**	**Time**	**Ref.**
			LOQ	*LOQ*	*LOQ*	*LOQ*	*LOQ*	*LOQ*		
LC	WB	SPE	0.100	NA	0.100	1.0	N/A	N/A	5 min*	[162]
LC	WB	SPE	0.100	0.100	0.100	0.100	0.250	0.100	10 min*	[146]
LC	WB	LLE	N/A	NA	N/A	N/A	N/A	N/A	13 min*	[157]
LC	WB	LLE	NA	0.100	0.200	0.100	0.400	0.200	13 min*	[174]
UHPLC	WB	LLE	0.050	0.050	0.050	0.200	0.050	0.050	8 min*	[158]
UHPLC	WB	LLE	0.003	0.004	0.005	0.003	0.003	0.003	8 min*	[154]
UHPLC	WB	LLE	0.004	0.004	0.004	0.008	0.004	0.004	9 min*	[175]
PS	U	NA	0.089	NA	0.060	0.135	0.075	NA	< 1 min‡	[169]
MOI	WB	SPME	0.031	0.010	0.010	0.010	0.002	0.007	2.4 min†	This work

5.4.4. Method Comparisons

The figures of merit obtained for our work are compared to other reported methods in **Table 5.6.** When compared to LC-MS, for which SPE has been used as the sample preparation from whole blood samples, LOQ are on average ten times higher (worse) for LC-MS methods compared to MOI-MS/MS herein. On the other hand, when our method is compared to LC-MS (or UHPLC-MS) methods that use LLE for the sample preparation from the whole blood, similar LOQs are obtained. However, the critical distinction is that those methods require a lot of manual steps to achieve similar LOQ. Remember that LOQ in mentioned literature has been calculated slightly differently across all publications.

With this said, we believe a direct-to-MS method reported here can be explored in the future as an alternative to chromatography coupled to MS for the analysis of fentanyl and its analogs from whole blood. The most significant advantages of our method over general LC-MS/MS methods are the circumvention of the quite manual sample preparation steps and lengthy instrument analysis times. However, our sample preparation can be considered long. When run in a high-throughput fashion for a set of 96 samples (a single 96 wellplate), our method requires approximately 2.4 min per sample (accounting for 15 min cleaning,15 min conditioning, 60 min extraction, and 1.5 min per sample of instrumental analysis). When MOI-MS/MS is compared to UHPLC-MS/MS methods with excellent LOQs, MOI-MS/MS is superior when accounting for 96 samples because of chromatographic runtime is 8 – 9 min (without accounting for the sample preparation).[154,158,175] MOI-MS/MS can finish sample preparation and the analysis in about 2.4 min per sample, while UHPLC-MS/MS methods need 8 – 9 min per sample. When put into this context, the MOI-MS/MS method here can be considered a rapid analysis method.

There aren't many methods describing a direct coupling to mass spectrometry for fentanyl and its analogs from the whole blood. Since our method described in this work is a direct-to-MS method, our LOQ are significantly lower when comparing it to PS. An essential thing to differentiate is that the matrix used for paper spray analysis was urine, a much simpler matrix than whole blood. Nevertheless, the main reason PS has worse LOQ compared to this work is limited sample preparation. Appropriate sample preparation is

mandatory for obtaining sensitivity comparable to LC-MS/MS because when chromatography is circumvented, analytes together with coextracted matrix constituents are also introduced that offer a risk of matrix effects.

MOI-MS/MS method is suitable for monitoring fentanyl and its analog concentrations in blood samples of suspected opioid users. Selected literature reports show that the concentrations of fentanyl range 0.01 – 107 ng mL^{-1}, carfentanil 0.01 – 120 ng mL^{-1}, acetylfentanyl 0.31 ng mL^{-1}, and 4-ANPP 0.1 – 410 ng mL^{-1}.[160–162,176]

5.5. Conclusions

This manuscript reports a direct-to-mass spectrometry method for simultaneous analysis of fentanyl, several fentanyl analogs, and a common fentanyl analog precursor from whole blood. Matrix-compatible solid-phase microextraction fibers have been used as enrichment devices in a high-throughput fashion and later coupled directly to mass spectrometry using MOI. This method can perform sample preparation and instrumental analysis for 96 samples in 2.4 min per sample. This is very short compared to liquid chromatography methods in the literature in which instrumental analysis alone consists of 5 – 13 min (without considering manual sample preparation steps). The calibration and validation points have precision (1 – 18 %) and accuracy (81 – 100 %). The four-day inter-day reproducibility ranges 6 – 15 %. The linearity of the weighted calibration curve ranges 0.010 – 25 ng mL^{-1} for 4-ANPP, fentanyl, carfentanil, sufentanil, and alfentanil, while for acetylfentanyl ranges 0.050 – 25 ng mL^{-1}. These results result from using matrix-compatible SPME devices that limit the coextraction of macromolecules responsible for ionization matrix effects and desorption of enriched analytes into very low volume (desorption chamber of MOI) for extremely sensitive analysis. The method reported here looks promising in the fields where rapid opioid analysis is required.

Chapter 6: Coupling Microfluidic Open Interface to Ultraviolet-visible Detection

6.1. Preamble

The content of this chapter is not published yet; however, the goal is to publish it soon with a few additional experiments. The University of Waterloo Science Technical Services constructed the homemade electronic circuits. Victor Galievsky assisted in incorporating photointerrupters into the MOI design, assembling the electronic circuit around NI-DAQ, and fitting the optical fibers into standardized nuts for a four-way chromatographic tee. The rest, SPME fiber coating, prototype software development, experimental procedure, analysis, and data processing, have been done by Emir Nazdrajić. Janusz Pawliszyn assisted Emir Nazdrajić in data interpretation. Janusz Pawliszyn supervised the whole project.

6.2. Introduction

Microfluidic devices have been researched for many years so far. Development of soft lithography allowed for easier manufacturing of microfluidic devices.[177] Additionally, with the rapid growth of many fields such as environmental,[178] food,[179] medical,[180] and biochemical[181] among others, there is increased demand for the development of rapid and straightforward methods that would serve to maintain safety regulations and/or to monitor toxic or other compounds of interest. Microfluidic systems are an excellent solution for new social demands. These systems require low sample and reagent consumption, low waste production, and high portability for on-site analysis relative to the conventional macroscale methods.[182] In the medical field, these devices can be used as point-of-care analysis for rapid screening to take some weight out of the shoulders of instrumental laboratories overloaded with the number of samples to be processed daily.[183–185]

Many microfluidic devices are based on colorimetric sensors where analytes exhibit UV-visible absorption,[186] fluorescence,[187] bioluminescence,[188] or chemiluminescence.[189] The analysis of colorimetric response can be performed simply by visual comparison.[190] Conversely, quantitative analysis of colorimetric response requires more sophisticated, bulky, and expensive equipment.[190] Although

absorbance is very popular in conventional macroscale light-sensing systems, it can be applied in microfluidic systems but suffers significantly due to short path lengths. In some applications, there have been attempts to extend the detector cell's length in “Z”-shape to increase the path length directly proportional to the absorbance.[191,192] On the other hand, fluorescence and chemiluminescence possess great sensitivity and selectivity, but disadvantages can be seen in relatively limited analyte coverage and the limited number of luminescent reagents.[193,194] The analyte coverage can be expanded by derivatization reactions, but the additional step in the sample preparation can be the limiting factor if the derivatization is slow.[195]

There is extensive research in lab-on-chip microfluidic designs that use light sensing as a detection mechanism.[183,196–200] Some of the advantages of on-chip designs include low manufacturing cost, ease of use and compactness, and very low sample volumes. In contrast, some of the disadvantages can consist of a low signal-to-noise ratio relative to the conventional macroscale methods, the necessity of having highly trained personnel to make such devices, complicated fluid transport systems, and can at the moment be used for screening purposes only.[192,201] These devices are often coupled with smartphone-based detection because of rapid and simple analysis, which are pretty available today.[202,203]

The aim of **Chapter 6** is to describe the MOI coupled to ultraviolet-visible light (UV-Vis) absorbance detection. The work herein aims to create a microfluidic system with colorimetric detection that has a reasonable compromise between system complexity and sensitivity. One part of the system resembles MOI described in **Chapter 2**, and the other part contains the construction of detector cells by using a cross through which a glass capillary guiding sample passes.[139,204,205] In sets of experiments described below, two azo dyes present in the liquid water enhancing solution are used as model analytes to establish some ground of MOI-UV/Vis system for rapid screening purposes.

6.3. Experimental

6.3.1. Chemicals and materials

The MiO liquid water enhancer was purchased at the local store. Ultrapure water was produced by a Milli-Q® system (Millipore, 0.22 m filtered, 18.2 MΩ cm at 25 °C). Gastight glass-plastic syringes were purchased from Hamilton (5 mL) and from SGE (10 mL). The 11 Elite syringe pumps (two of them) were purchased from Harvard Apparatus. PEEK tee and PEEK cross (1 mm bore) were purchased from VICI Valco Instruments Canada Corporation. Female Luer adapters were purchased from Scientific Products and Equipment. Yellow PEEK tubing (OD: 1/32 in, ID: 0.007 in) was purchased from IDEX Health & Science, and glass capillaries (1.5 mm OD and 0.8 mm ID) have been purchased from Warner Instruments. Matrix-compatible SPME fibers containing HLB coating chemistry were made according to the procedure reported elsewhere.[136] The data acquisition device (NI USB-6002) was purchased from National Instruments (Austin, TX, USA). Single-mode fiber-coupled laser diode QFLD-405-10SAX (QPhotonics, Ann Arbor, MI, USA) had an optical power of 10 mW at 403.3 nm. The spectral width of the laser line was one nm. The laser fiber with a core diameter of three µm and an external diameter of 245 µm was glued into a homemade stainless stainless steel ferrule with a diameter of OD 1/16 in and a length of 15 mm. The ferrule end was polished and inspected using CK01termination tool kit (Thorlabs, Newton, NJ, USA). The blue laser diode controller IP250-BV was purchased from Thorlabs, Newton, NJ, USA. Si photodiode FD11A used as a photodetector was glued with a polished end of multimode fiber FT400UMT using the UV-curing optical adhesive NOA68 (all from Thorlabs, Newton, NJ, USA). The other end of the FT400UMT fiber was glued into OD 1/16 in stainless steel ferrule and polished. The photodiode was operated in a photoconductive mode with the 5V bias. The homemade electronic circuit based on the 5th-order low-pass filter LTC1062 (Linear Technology, Milpitas, CA, USA) was utilized to suppress the high-frequency noise with a cutoff frequency of 100 Hz.

6.3.2. MOI-UV/Vis Setup

This system consists of two programmable syringe pumps, with one pump providing the inflow and the other providing the constant suction flow. The syringe pump providing the inflow is equipped with the 5 mL Hamilton gastight glass-plastic syringe that is connected to the fluorinated ethylene propylene (FEP) tubing (OD: 1/16 in and ID: 1/32 in) via a female luer adapter. The tubing is then connected to the PEEK tee. One of the tee openings contains the microfluidic open port composed of two concentric tubes. The outer tubing used is FEP tubing, and the inner tubing used is 0.007 in ID Yellow PEEK tubing. The inner tubing serves as the flow restrictor and as the guide for the matrix-compatible SPME fibers by allowing only 1 cm of the matrix-compatible SPME fiber to be placed in the MOI port, which is the length of the coating on the matrix-compatible SPME fiber. With this, the volume of the desorption chamber of the microfluidic open port is approximately 5 μL. The other opening of the PEEK tee leads to the borosilicate glass capillary (OD: 15 mm, ID: 0.8 mm) that passes through the PEEK cross, previously drilled with a 1/16 in drill to allow the borosilicate glass capillary to pass through. The glass capillary is further connected to the plastic tubing and the 10 mL SGE gastight glass-plastic syringe placed on the second 11 Elite syringe pump. The PEEK cross mentioned above serves as the detector since the other two openings are connected to the laser fiber and optical fiber leading to the photodiode. The analog signal from the photodiode is converted to the digital signal by a digital to analog converter (NI DAQ), which is connected to a laptop via a USB-type connection. The schematic of the described setup is shown in **Figure 6.1.** The system in real-life is shown in **Figure 6.2.**

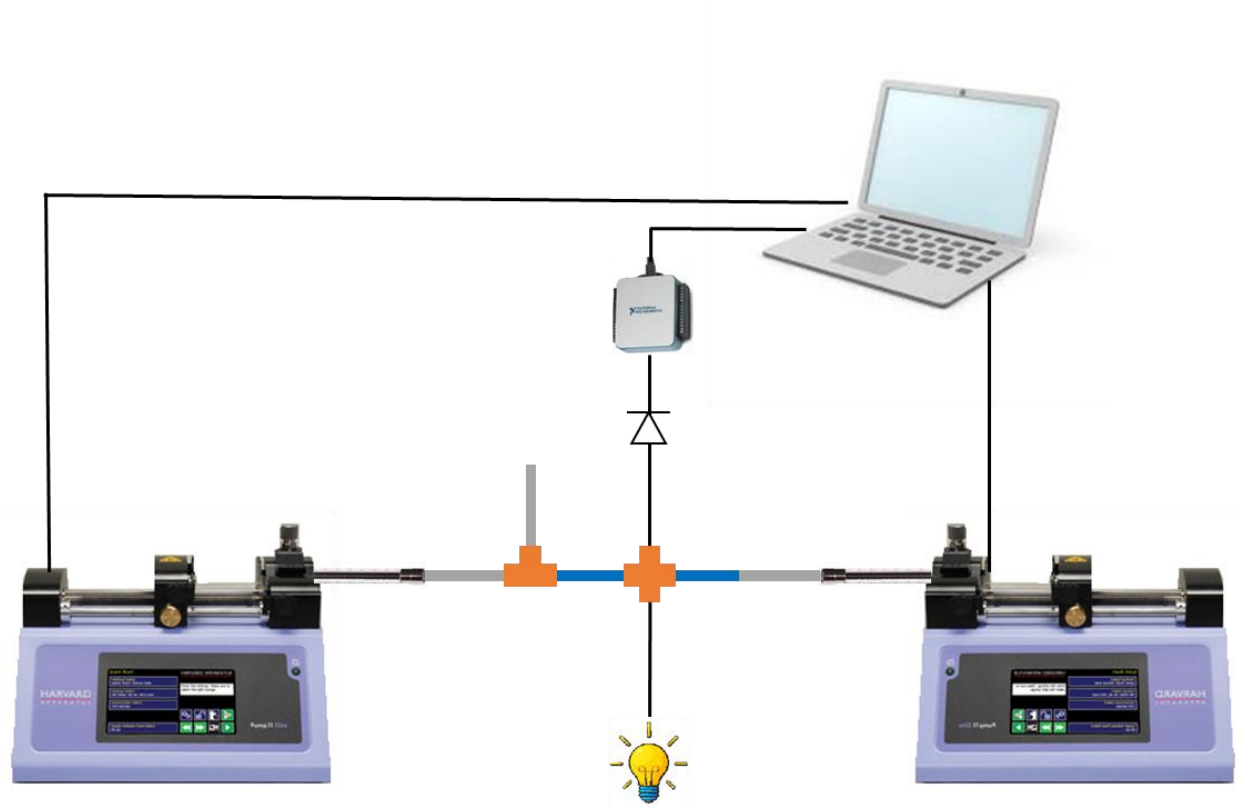

Figure 6.1. MOI-UV/Vis system schematic. It is composed out of two programmable syringe pumps, laser diode, photodiode, NI data acquisition device, computer, and a software that controls two syringe pumps.

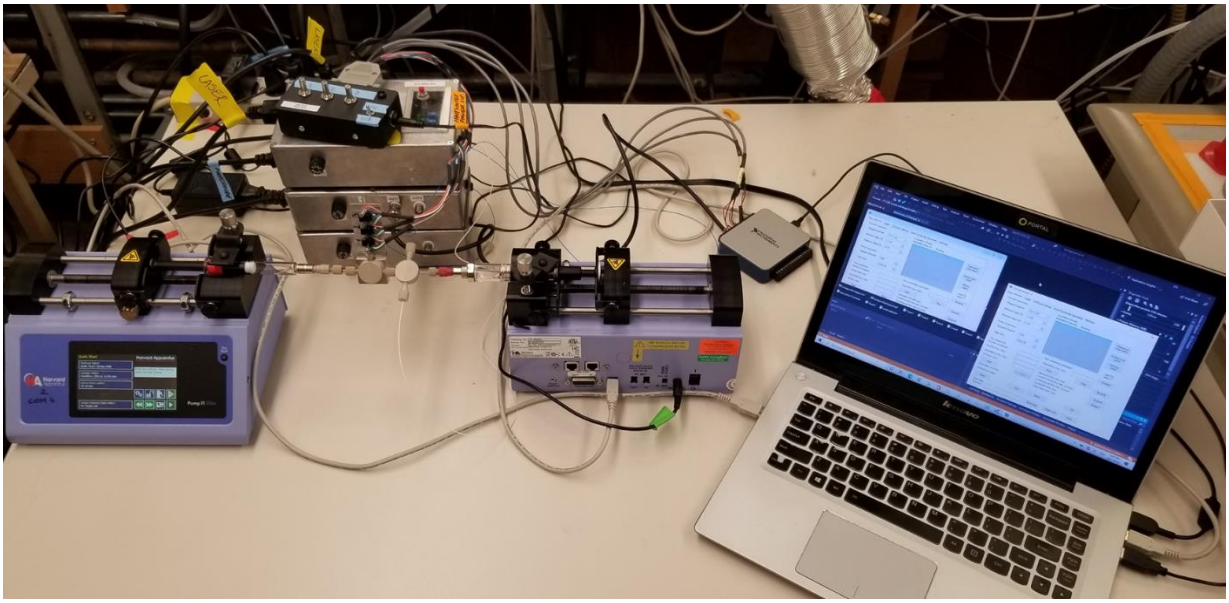

Figure 6.2. The real-life picture of the MOI-UV/Vis setup.

6.3.3. Software

The Microsoft Visual Studio Express 2013 v. 12.0.21005.1 REL application was used to control 11 Elite syringe pumps and acquire data from the NI DAQ. The software is similar to the version described in **Section 2.3.5.** The only differences are the graph of live acquisition, saving collected data as a .txt file, sending commands to each 11 Elite syringe pump separately, and having a tab capable of syringe pump method management.

The collected data in the .txt file was transferred to the Microsoft® Excel® 2013, v. 15.0.5059.1000, where further data processing has been done.

6.3.4. Experimental procedure

The MiO liquid enhancer solution was bought at the local store. Before the extraction, matrix-compatible SPME fibers were immersed in the 2:1:1 (V:V:V) of methanol:acetonitrile:isopropanol solution for cleaning process (30 minutes), followed by immersion in methanol:water = 1:1 (V:V) for the coating conditioning (30 minutes).

For the extraction procedure, the matrix-compatible SPME fibers were agitated on the benchtop mixer in 1 mL of water enhancer solutions for 10 s. After that, the matrix-compatible SPME fibers were introduced to the MOI-UV/Vis system, according to the workflow described in **Section 6.3.4.**

6.3.5. SPME-MOI-UV/Vis System Workflow

The void volume of the whole system is filled with desorption solution (methanol) manually by running each pump at inflow conditions until the water expels all air from the system. Then, the syringe pump method was chosen such that the inflow flow rate was programmed with the following flow rates: 100 μL min^{-1} for 30 s, 0 μL min^{-1} for 3 s, and 500 μL min^{-1} for 1 s, while the suction flow rate is kept constant at 100 μL min^{-1} throughout the whole operational process of the system. This process is put into a loop until the 5 mL gastight glass-plastic syringe is emptied.

The SPME fiber is placed for 10 s for analyte desorption. Then the user presses “Start” to start collecting the data that is displayed on a graph in another tab. When the draining step is started, the user removes the SPME fiber. The workflow of the SPME-MOI-UV/Vis is shown in the schematics in **Figure 6.3.**

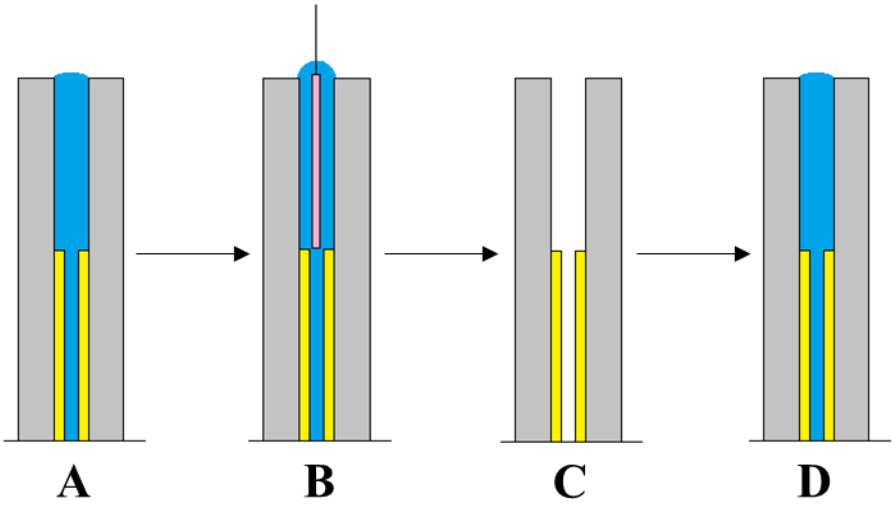

Figure 6.3. SPME-MOI-UV/Vis workflow schematic. (A) The desorption chamber is filled with the desorption solution. (B) The SPME fiber is placed for 10 s desorption. (C) After desorption, the SPME fiber is removed, and the MOI chamber is drained. (D) The system is refilled/drained three times to remove carryover.

6.4. Results and Discussion

6.4.1. Raw signal and processing

The overlay of the raw signal obtained from the extraction of the dye analytes from the MiO liquid enhancer solution and a blank extraction is shown in Figure 6.4. Since the UV/Vis detector baseline is not at zero (*i.e.*, 0 V), it was adjusted by subtracting the obtained response from the average blank signal (first 10 seconds of each measurement). The area under the curve was calculated using the Rieman sum. The average sum of *upper* and *lower* rectangles is taken as the area under the curve. The area under the curve approaches the actual value as the rectangle width is smaller. The rectangle width was selected to be the interval at which data is plotted (10 ms). This data processing is done using Microsoft Excel.

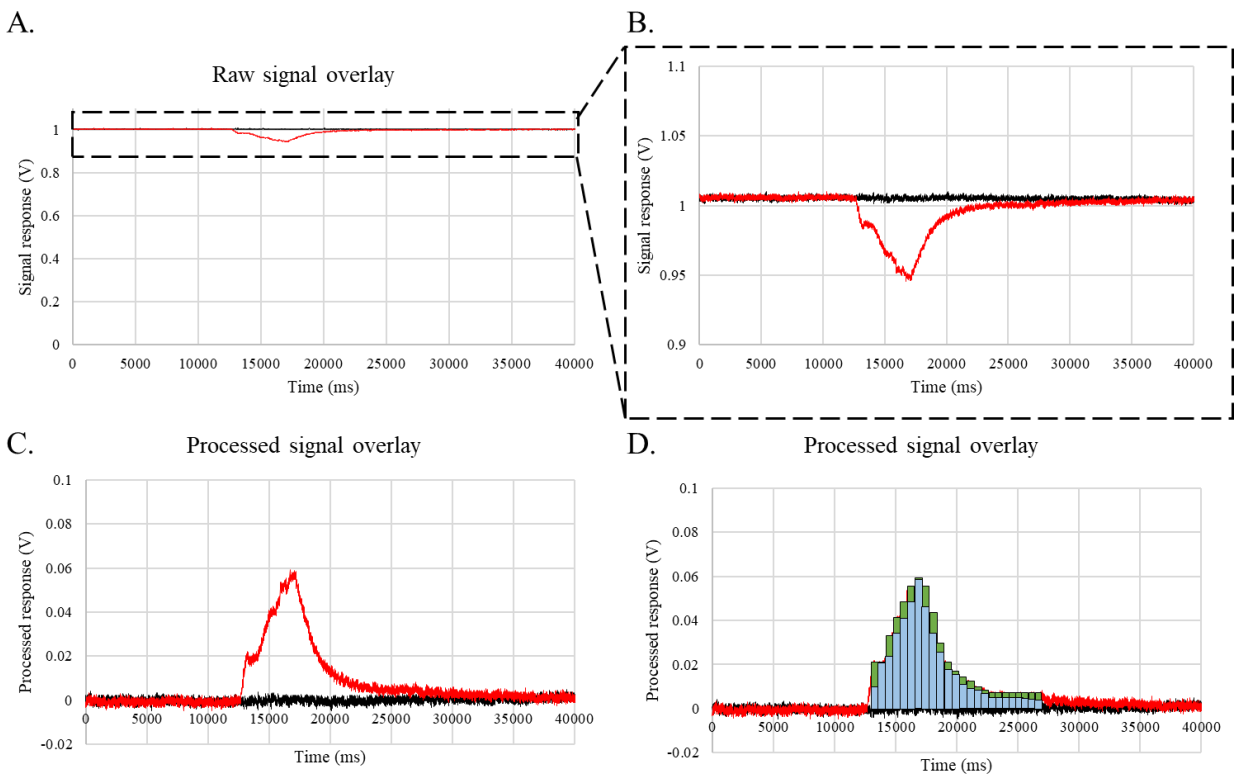

Figure 6.4. Absorbance measurement of the extracted allure red dye. (A) Raw signal overlay of blank extraction and 10 s extraction from water enhancer solution. (B) Zoomed-in insert of the raw signal overlay. (C) Processed (inverted) signal overlay. (D) Schematic application of Rieman sum for the calculation of the area under the produced curve.

6.4.2. Discussion

The results are obtained in **Section 6.4.1.** show that the MOI-UV/Vis system can be used for the screening analysis of dyes. The laser used in this setup has a wavelength of 403.3 nm with a spectral width of 1 nm. Therefore, this system, as is, is suitable for the analysis of analytes that have suitable absorbance at this wavelength range. However, expanding on this concept is difficult because there is no separation before analysis. Therefore, if the sample contains at least two dyes, the concentration determination becomes much more convoluted. On the other hand, this system would be useful for screening the application of UV/Vis sensitive analytes in various matrices. Another disadvantage of this part of the software is that it uses the Timer function of Microsoft Visual Studio 2019, which starts deviating after prolonged time measurements; however, it has been minimized by implementing a stopwatch function.[206]

6.5. Conclusions and Future Perspective

This chapter summarizes a simple concept of coupling MOI systems to UV/Vis detection. The idea is that expensive and sophisticated instrumentation is not necessarily required to use the SPME with MOI. Herein, it is an application of 10 s extraction of a dye from MiO liquid enhancer solution using PAN-HLB SPME fiber. The difficulties this technology faces forward are the need for selective extraction or lack of separation prior to detection. Nevertheless, the software code requires slight modification to remove the delay as the Microsoft Visual Studio 2019 timer keeps ticking. One of the ways this can be fixed is to tap into a computer's real-time clock and only measure the time elapsed from a certain point. Additionally, the advantage of the system is that a laser diode with any wavelength range can easily be adjusted onto the system (simply by unscrewing the fitting and placing a new one into a four-way chromatographic tee). An additional goal in improving the system is to integrate an autosampler that the software will control, so that the whole system can be integrated and made portable for in-situ analysis and benchtop analysis.

Chapter 7: Summary and Future Directions

7.1. Summary

The main goal of this thesis was to redesign the MOI system to make it more appealing and practical than the existing system. This was achieved using (mostly) standard commercial materials for its manufacturing and system (semi) automation. The redesigned system maintained the status for rapid analysis while the overall design simplification offers fewer know-hows so that it can more easily be adapted to laboratories worldwide. **Chapter 2** summarizes how different tubing types and other materials have been put together to create a new design that has been adopted to different instrumentation manufacturers. Practical aspects and theoretical microfluidic considerations support the tubing dimension and materials choice. **Chapter 2** describes a home-written software prototype design to control the overall MOI system.

Nevertheless, in **Chapter 2,** different matrix-compatible SPME coatings have been used to study the MOI interface, where some interaction between matrix-compatible binder and sorbent particle in the coating seems to exist. This idea is closely investigated in **Chapter 3** using well-studied SPME coatings. Briefly, the matrix-compatible SPME coating behaves similarly to the separation media (*e.g.*, a chromatographic column), so studying the effective diffusion coefficient in the coating is crucial for the MOI and rapid analysis. Even though MOI has not been used directly for the study, the work describes the effective diffusion in the coating quantitatively; therefore, it can be easily translated to other SPME applications, including with MOI. Standard SPME applications use relatively long desorption times (*e.g.*, 20 minutes), while for the MOI, it is a few seconds. In order to achieve the best desorption efficiency, the sorbent and binder need to be carefully selected to allow minimal mass transfer resistance in the coating during the desorption step.

Furthermore, the next two chapters offer applications of coupling SPME directly to MS via MOI. Firstly, **Chapter 4** describes the study of simultaneous analysis of ISDs from whole human blood for therapeutic

drug monitoring. The single turnaround time of the method is 62 minutes, while the total turnaround time, with the assistance of high throughput sample preparation, is only 4.5 minutes per sample. These times are very rapid and promising for implementing MOI-MS in clinical laboratories because the desirable total turnaround time in clinical environments is 3 – 6 hours. Additionally, the developed MOI-MS/MS method has been compared to CMIA (immunoassay) method yielding similar systematic and proportional differences as already reported in the literature between MS-based and immunoassay-based detection. While these results have been obtained for the previous design of the MOI, **Chapter 5** describes the SPME-MOI-MS/MS method applied for determining fentanyl, several fentanyl analogs, and a common fentanyl precursor from whole blood using the improved MOI design. The developed method had a turnaround time of 2.4 min per single sample (using high-throughput sample preparation and an automated MOI analysis system).

In comparison, LC-MS based method has a total turnaround time of 5 – 13 min per sample without considering manual and multi-step sample preparation. More importantly, the reduction in the total turnaround time did not affect the SPME-MOI-MS/MS method sensitivity, as LOQs obtained are comparable to the most sensitive LC-MS/MS method in the literature. Lastly, **Chapter 6** describes a proof-of-concept coupling MOI to a UV/Vis detection system. The idea of this chapter is to show that the MOI does not necessarily need an expensive and sophisticated MS detector because a simple UV/Vis detector cell is sufficient to make a system capable of portability and automation. Additionally, the overall system has a less complicated microfluidic setup than lab-on-chips, thus offering a reasonable compromise between sensitivity and simplicity compared to MS-based and colorimetric microfluidic detectors.

7.2. Future Perspective

The applicability and potential of the SPME-MOI-MS or SPME-MOI-UV/Vis have been demonstrated herein. However, there is a lot of room for the overall system improvement. These improvements are required for the MOI to gain more appeal to be incorporated into different laboratories worldwide.

One improvement aspect can be seen in the improvement of the SPME coatings. Additional research is required to fully understand the mass transfer limitations to and out of the coating. Traditional SPME applications might be comfortable with relatively lengthy extraction or desorption times. Still, this mass transfer limitation needs to be decreased to increase the desorption efficiency for MOI and maintain the rapid status. One of the ways to improve the desorption throughput is to implement a desorption chamber for SPME devices with higher surface areas (*e.g.*, thin-film or dispersive format). This implementation provides higher surface-to-volume ratios without sacrificing sensitivity by using smaller amounts of particles in the coating. In terms of coupling thin-film format, the challenge in this area is to couple rectangular desorption chamber with standardized tubing. When attempting the dispersive format, the obvious avenue is to use magnetic particles because this idea has already been demonstrated with the previous MOI design.[56] The desorption time can be improved by implementing a vibrational mechanism in the SPME device. The desorption takes place in a static environment, while adding vibrational mechanisms will provide the necessary agitation to reduce the boundary layer. Nevertheless, the desorption efficiency can be improved by implementing a thermal mechanism to increase the diffusion coefficients of analytes; thus, analytes leaving the coating can *exit* faster.

In addition, there are several possible future improvements regarding MOI design and its coupling to MS. One obstacle in standardizing the MOI design for coupling with MS is that different MS manufacturers make slightly different ionization sources and front-end of the MS. Therefore, the overall design needs slight modifications before being easily transferred from one instrument to another. Additionally, there is no doubt that MOI is capable of having similar sensitivity as LC-MS, but laboratories worldwide would first require MOI design simplification through automation. There is already an automated high-throughput SPME system (i.e., Concept96), but the MOI will succeed with the automation of the analysis part. With this, the know-how is almost entirely removed, and it will be easier to convince laboratories worldwide to use it because personnel training is typically seen as one of the downsides to procedures that lack automation.[24] The ideal protocol would be to transfer the 96-device used for Concept96 to another

autosampler that will introduce the SPME devices to the desorption chamber of the MOI. Therefore, the complete MOI integration to the MS system is a key to its success.

Although the focus is to use MOI for coupling SPME devices directly to MS, the MOI can be coupled to other detection mechanisms. **Chapter 6** portrayed the successful implementation of a homemade MOI-UV/Vis system. The limitation of the system, and some areas where the system needs further improvement, are software and finding the appropriate application. The laser diode used has a very narrow wavelength range where many compounds do not have good molar absorptivity. Nevertheless, this is one of the most significant limitations of UV/Vis applications, and sometimes a derivatization step is required.

Additionally, this system lacks some separation steps capable of separating UV/Vis visible compounds; otherwise, the quantitation step becomes very convoluted. However, the design can still be used for qualitative/screening analysis of systems where identity and specific information about the amount is not out of the outermost interest. Nevertheless, some online separation systems that could be attempted are in-tube SPME or capillary electrophoresis, which will separate analytes after desorption and before the UV/Vis detection cell. However, the separation step can be achieved by coupling MOI to the IMS system, which performs gas-phase separation in a fraction of seconds. This IMS system can be standalone with a simple ion detector or be coupled to the mass spectrometer for additional selectivity.

Letters of Copyright Permissions

Copyright permission for the Chapter 3 content

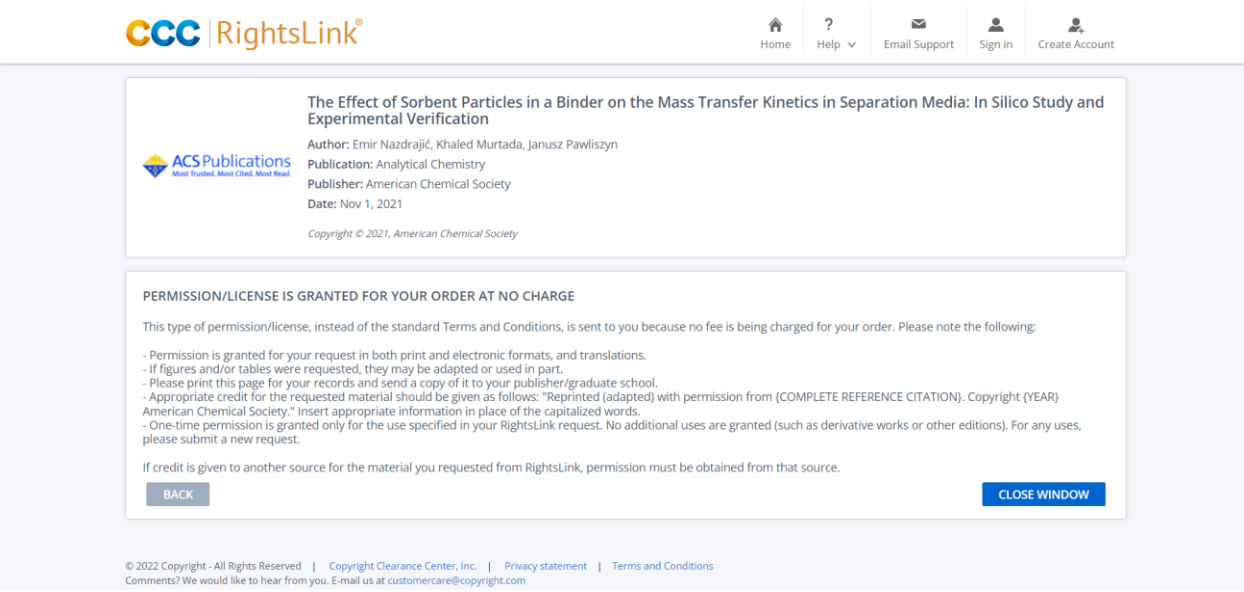

CCC RightsLink®

Home | Help | Email Support | Sign in | Create Account

The Effect of Sorbent Particles in a Binder on the Mass Transfer Kinetics in Separation Media: In Silico Study and Experimental Verification

Author: Emir Nazdrajić, Khaled Murtada, Janusz Pawliszyn

Publication: Analytical Chemistry

Publisher: American Chemical Society

Date: Nov 1, 2021

Copyright © 2021, American Chemical Society

PERMISSION/LICENSE IS GRANTED FOR YOUR ORDER AT NO CHARGE

This type of permission/license, instead of the standard Terms and Conditions, is sent to you because no fee is being charged for your order. Please note the following:

- Permission is granted for your request in both print and electronic formats, and translations.
- If figures and/or tables were requested, they may be adapted or used in part.
- Please print this page for your records and send a copy of it to your publisher/graduate school.
- Appropriate credit for the requested material should be given as follows: "Reprinted (adapted) with permission from {COMPLETE REFERENCE CITATION}. Copyright {YEAR} American Chemical Society." Insert appropriate information in place of the capitalized words.
- One-time permission is granted only for the use specified in your RightsLink request. No additional uses are granted (such as derivative works or other editions). For any uses, please submit a new request.

If credit is given to another source for the material you requested from RightsLink, permission must be obtained from that source.

BACK CLOSE WINDOW

Copyright permission for the Chapter 4 content.

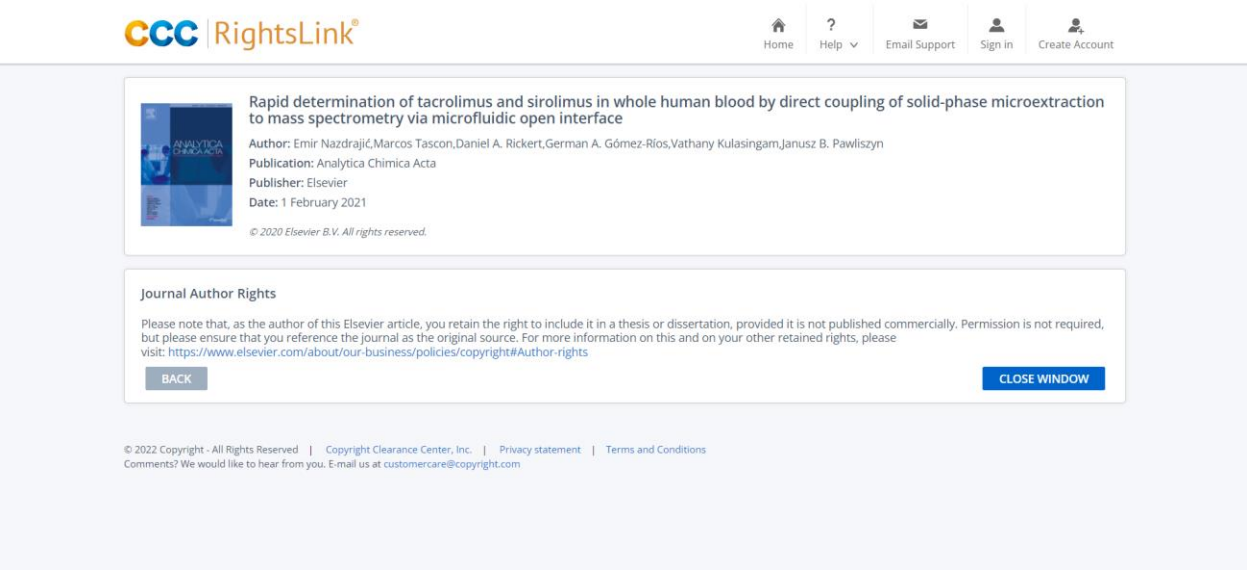

CCC RightsLink

Home | Help | Email Support | Sign in | Create Account

Rapid determination of tacrolimus and sirolimus in whole human blood by direct coupling of solid-phase microextraction to mass spectrometry via microfluidic open interface

Author: Emir Nazdrajić,Marcos Tascon,Daniel A. Rickert,German A. Gómez-Ríos,Vathany Kulasingam,Janusz B. Pawliszyn

Publication: Analytica Chimica Acta

Publisher: Elsevier

Date: 1 February 2021

© 2020 Elsevier B.V. All rights reserved.

Journal Author Rights

Please note that, as the author of this Elsevier article, you retain the right to include it in a thesis or dissertation, provided it is not published commercially. Permission is not required, but please ensure that you reference the journal as the original source. For more information on this and on your other retained rights, please visit: https://www.elsevier.com/about/our-business/policies/copyright#Author-rights

BACK CLOSE WINDOW

© 2022 Copyright - All Rights Reserved | Copyright Clearance Center, Inc. | Privacy statement | Terms and Conditions

Comments? We would like to hear from you. E-mail us at customercare@copyright.com

References

(1) Skoog, D. A. .; West, D. M. .; Holler, J. F. .; Crouch, S. R. . *Fundamentals of Analytical Chemistry*, 9th Editio.; Mary Finch, 201AD.

(2) Pawliszyn, J. *Handbook of Solid Phase Microextraction*; Chemical Industry Press of China: Beijing, 2009. https://doi.org/10.1016/C2011-0-04297-7.

(3) Hoffman, E.; Stroobant, V. *Mass Spectrometry Principles and Applications*, 3rd Editio.; John Wiley & Sons, Inc., 2007.

(4) Boyaci, E.; Gorynski, K.; Rodriguez-Lafuente, A.; Bojko, B.; Pawliszyn, J. Introduction of Solid-Phase Microextraction as a High-Throughput Sample Preparation Tool in Laboratory Analysis of Prohibited Substances. *Anal. Chim. Acta* **2014**, *809*, 69–81. https://doi.org/10.1016/j.aca.2013.11.056.

(5) Zawatzky, K.; Barhate, C. L.; Regalado, E. L.; Mann, B. F.; Marshall, N.; Moore, J. C.; Welch, C. J. Overcoming “Speed Limits” in High Throughput Chromatographic Analysis. *J. Chromatogr. A* **2017**, *1499*, 211–216. https://doi.org/10.1016/j.chroma.2017.04.002.

(6) Shipkova, M.; Valbuena, H. Liquid Chromatography Tandem Mass Spectrometry for Therapeutic Drug Monitoring of Immunosuppressive Drugs: Achievements, Lessons and Open Issues. *Trends in Anal. Chem.* **2016**, *84*, 23–33. https://doi.org/10.1016/j.trac.2016.01.031.

(7) Regalado, E. L.; Welch, C. J. Pushing the Speed Limit in Enantioselective Supercritical Fluid Chromatography. *J. Sep. Sci.* **2015**, *38* (16), 2826–2832. https://doi.org/10.1002/jssc.201500270.

(8) Pingale, S. G.; Nerurkar, K. K.; Padgaonkar, A. M.; Pawar, U. D.; Mangaonkar, K. V. Alternative LC-MS-MS Method for Simultaneous Determination of Proguanil, Its Active Metabolite in Human Plasma and Application to a Bioequivalence Study. *Chromatographia* **2009**, *70* (7–8), 1095–1102. https://doi.org/10.1365/s10337-009-1259-9.

(9) Bianchi, F.; Caffarri, E.; Cavalli, S.; Lagrasta, C.; Musci, M.; Quaini, F.; Savi, M. Development and Validation of an High Performance Liquid Chromatography-Tandem Mass Spectrometry Method for the Determination of Imatinib in Rat Tissues. *J. Pharm. Biomed. Anal.* **2013**, *73*, 103–107. https://doi.org/10.1016/j.jpba.2012.05.034.

(10) Takyi-williams, J.; Liu, C.; Tang, K. Ambient Ionization MS for Bioanalysis : Recent Developments and Challenges. *Bioanalysis* **2015**, *7*, 1901–1923. https://doi.org/10.4155/BIO.15.116.

(11) Reiter, A.; Herbst, L.; Wiechert, W.; Oldiges, M. Need for Speed: Evaluation of Dilute and Shoot-Mass Spectrometry for Accelerated Metabolic Phenotyping in Bioprocess Development. *Anal. Bioanal. Chem.* **2021**, *413* (12), 3253–3268. https://doi.org/10.1007/s00216-021-03261-3.

(12) Fernández, F. M.; Garcia-Reyes, J. F. Ambient Mass Spectrometry. *Science (80-.).* **2006**, *311*, 1566–1570. https://doi.org/10.1039/c7ay90107k.

(13) Feider, C. L.; Krieger, A.; Dehoog, R. J.; Eberlin, L. S. Ambient Ionization Mass Spectrometry: Recent Developments and Applications. *Anal. Chem.* **2019**, *91* (7), 4266–4290. https://doi.org/10.1021/acs.analchem.9b00807.

(14) Monge, M. E.; Fernández, F. M. An Introduction to Ambient Ionization Mass Spectrometry. *New Dev. Mass Spectrom.* **2015**, *2015-Janua* (2), 1–22.

(15) Takáts, Z.; Wiseman, J. M.; Gologan, B.; Cooks, R. G. Mass Spectrometry Sampling under Ambient Conditions with Desorption Electrospray Ionization. *Science (80-.).* **2004**, *306* (5695), 471–473. https://doi.org/10.1126/science.1104404.

(16) Wu, C.; Ifa, D. R.; Manicke, N. E.; Cooks, R. G. Molecular Imaging of Adrenal Gland by Desorption Electrospray Ionization Mass Spectrometry. *Analyst* **2010**, *135* (1), 28–32. https://doi.org/10.1039/b919816d.

(17) Wang, H.; Liu, J.; Cooks, R. G.; Ouyang, Z. Paper Spray for Direct Analysis of Complex Mixtures Using Mass Spectrometry. *Angew. Chemie* **2010**, *122* (5), 889–892. https://doi.org/10.1002/ange.200906314.

(18) Cody, R. B.; Laramée, J. A.; Durst, H. D. Versatile New Ion Source for the Analysis of Materials in Open Air under Ambient Conditions. *Anal. Chem.* **2005**, *77* (8), 2297–2302. https://doi.org/10.1021/ac050162j.

(19) Harper, J. D.; Charipar, N. A.; Mulligan, C. C.; Zhang, X.; Cooks, R. G.; Ouyang, Z. Low-Temperature Plasma Probe for Ambient Desorption Ionization. *Anal. Chem.* **2008**, *80* (23), 9097–9104. https://doi.org/10.1021/ac801641a.

(20) Wen, X.; Liu, C.; Ghislain, L.; Tovar, K.; Shah, V.; Stout, S. J.; Cifelli, S.; Satapati, S.; O'Donnell, G.; Sheth, P. R.; Wildey, M. J.; Datwani, S. S.; Covey, T. R.; Bateman, K. P.; McLaren, D. G. Direct Analysis from Phase-Separated Liquid Samples Using ADE-OPI-MS: Applicability to High-Throughput Screening for Inhibitors of Diacylglycerol Acyltransferase 2. *Anal. Chem.* **2021**, *93* (15), 6071–6079. https://doi.org/10.1021/acs.analchem.0c04312.

(21) Häbe, T. T.; Liu, C.; Covey, T. R.; Simon, R. P.; Reindl, W.; Büttner, F. H.; Winter, M.; Bischoff, D.; Luippold, A. H.; Runge, F. Ultrahigh-Throughput ESI-MS: Sampling Pushed to Six Samples per Second by Acoustic Ejection Mass Spectrometry. *Anal. Chem.* **2020**, *92* (18), 12242–12249. https://doi.org/10.1021/acs.analchem.0c01632.

(22) Liu, C.; Gómez-Ríos, G. A.; Schneider, B. B.; Le Blanc, J. C. Y.; Reyes-Garcés, N.; Arnold, D. W.; Covey, T. R.; Pawliszyn, J. Fast Quantitation of Opioid Isomers in Human Plasma by Differential Mobility Spectrometry/Mass Spectrometry via SPME/Open-Port Probe Sampling Interface. *Anal. Chim. Acta* **2017**, *991*, 89–94. https://doi.org/10.1016/j.aca.2017.08.023.

(23) Manicke, N. E.; Belford, M. Separation of Opiate Isomers Using Electrospray Ionization and Paper Spray Coupled to High-Field Asymmetric Waveform Ion Mobility Spectrometry. *J. Am. Soc. Mass Spectrom.* **2015**, *26* (5), 701–705. https://doi.org/10.1007/s13361-015-1096-z.

(24) Christians, U.; Vinks, A. A.; Langman, L. J.; Clarke, W.; Wallemacq, P.; Van Gelder, T.; Renjen, V.; Marquet, P.; Meyer, E. J. Impact of Laboratory Practices on Interlaboratory Variability in Therapeutic Drug Monitoring of Immunosuppressive Drugs. *Ther. Drug Monit.* **2015**, *37* (6), 718–724. https://doi.org/10.1097/FTD.0000000000000205.

(25) Daniel C. Harris; Lucy A. Charles. *Quantitative Chemical Analysis*, 9th Editio.; W.H. Freeman and Co.: New York, 2016.

(26) Dénes, J.; Katona, M.; Hosszú, Á.; Czuczy, N.; Takáts, Z. Analysis of Biological Fluids by Direct Combination of Solid Phase Extraction and Desorption Electrospray Ionization Mass Spectrometry. *Anal. Chem.* **2009**, *81* (4), 1669–1675. https://doi.org/10.1021/ac8024812.

(27) Li, X.; Ma, W.; Li, H.; Ai, W.; Bai, Y.; Liu, H. Sampling and Analyte Enrichment Strategies for Ambient Mass Spectrometry. *Anal. Bioanal. Chem.* **2018**, *410* (3), 715–724. https://doi.org/10.1007/s00216-017-0658-2.

(28) Fang, L.; Deng, J.; Yu, Y.; Yang, Y.; Wang, X.; Liu, H.; Luan, T. Coupling Liquid-Phase Microextraction with Paper Spray for Rapid Analysis of Malachite Green, Crystal Violet and Their Metabolites in Complex Samples Using Mass Spectrometry. *Anal. Methods* **2016**, *8* (36), 6651–6656. https://doi.org/10.1039/c6ay01466f.

(29) Zhou, Z.; Zhang, J.; Zhang, W.; Bai, Y.; Liu, H. Rapid Screening for Synthetic Antidiabetic Drug Adulteration in Herbal Dietary Supplements Using Direct Analysis in Real Time Mass Spectrometry. *Analyst* **2011**, *136* (12), 2613–2618. https://doi.org/10.1039/c0an01047b.

(30) Haunschmidt, M.; Klampfl, C. W.; Buchberger, W.; Hertsens, R. Determination of Organic UV Filters in Water by Stir Bar Sorptive Extraction and Direct Analysis in Real-Time Mass Spectrometry. *Anal. Bioanal. Chem.* **2010**, *397* (1), 269–275. https://doi.org/10.1007/s00216-009-3438-9.

(31) Loftin, K. Development Of Novel Dart Tofms Analytical Techniques For The Identification Of Organic Contamination On Spaceflight-Related Substrates And Aqueous Media, University of Central Florida, 2009.

(32) Martins, R. O.; de Araújo, G. L.; de Freitas, C. S.; Silva, A. R.; Simas, R. C.; Vaz, B. G.; Chaves, A. R. Miniaturized Sample Preparation Techniques and Ambient Mass Spectrometry as Approaches for Food Residue Analysis. *J. Chromatogr. A* **2021**, *1640*, 461949. https://doi.org/10.1016/j.chroma.2021.461949.

(33) Grote-koska, D.; Czajkowski, S.; Brand, K. Performance of the New RapidFire System for Therapeutic Monitoring of Immunosuppressants. *Ther Drug Monit* **2015**, *37* (3), 400–404. https://doi.org/10.1097/FTD.0000000000000139.

(34) Arthur, C. L.; Pawliszyn, J. Solid Phase Microextraction with Thermal Desorption Using Fused Silica Optical Fibers. *Anal. Chem.* **1990**, *62* (19), 2145–2148. https://doi.org/10.1021/ac00218a019.

(35) Reyes-Garcés, N.; Gionfriddo, E.; Gómez-Ríos, G. A.; Alam, M. N.; Boyacl, E.; Bojko, B.; Singh, V.; Grandy, J.; Pawliszyn, J. Advances in Solid Phase Microextraction and Perspective on Future Directions. *Anal. Chem.* **2018**, *90* (1), 302–360. https://doi.org/10.1021/acs.analchem.7b04502.

(36) Alam, M. N.; Nazdrajić, E.; Singh, V.; Tascon, M.; Pawliszyn, J. Effect of Transport Parameters and Device Geometry on Extraction Kinetics and Efficiency in Direct Immersion Solid-Phase Microextraction. *Anal. Chem.* **2018**, *90* (19), 11548–11555. https://doi.org/10.1021/acs.analchem.8b02855.

(37) Lord, H.; Pawliszyn, J. *Evolution of Solid-Phase Microextraction Technology*; 2000; Vol. 885. https://doi.org/10.1016/S0021-9673(00)00535-5.

(38) Piri-Moghadam, H.; Alam, M. N.; Pawliszyn, J. Review of Geometries and Coating Materials in Solid Phase Microextraction: Opportunities, Limitations, and Future Perspectives. *Anal. Chim. Acta* **2017**, *984*, 42–65. https://doi.org/10.1016/j.aca.2017.05.035.

(39) Rosales-Solano, H.; Galievsky, V.; Murtada, K.; Radovanovic, P. V.; Pawliszyn, J. Profiling of Unsaturated Lipids by Raman Spectroscopy Directly on Solid-Phase Microextraction Probes. *Anal. Chem.* **2022**, *94* (2), 606–611. https://doi.org/10.1021/acs.analchem.1c04054.

(40) Musteata, M. L.; Musteata, F. M.; Pawliszyn, J. Biocompatible Solid-Phase Microextraction Coatings Based on Polyacrylonitrile and Solid-Phase Extraction Phases. *Anal. Chem.* **2007**, *79* (18), 6903–6911. https://doi.org/10.1021/ac070296s.

(41) Alam, M. N.; Pawliszyn, J. Effect of Binding Components in Complex Sample Matrices on

Recovery in Direct Immersion Solid-Phase Microextraction: Friends or Foe? *Anal. Chem.* **2018**, *90*, 2430–2433. https://doi.org/10.1021/acs.analchem.7b05436.

(42) Mirabelli, M. F.; Wolf, J. C.; Zenobi, R. Direct Coupling of Solid-Phase Microextraction with Mass Spectrometry: Sub-Pg/g Sensitivity Achieved Using a Dielectric Barrier Discharge Ionization Source. *Anal. Chem.* **2016**, *88* (14), 7252–7258. https://doi.org/10.1021/acs.analchem.6b01507.

(43) Gómez-Ríos, G. A.; Tascon, M.; Reyes-Garcés, N.; Boyacl, E.; Poole, J.; Pawliszyn, J. Quantitative Analysis of Biofluid Spots by Coated Blade Spray Mass Spectrometry, a New Approach to Rapid Screening. *Sci. Rep.* **2017**, *7* (1), 1–7. https://doi.org/10.1038/s41598-017-16494-z.

(44) Kasperkiewicz, A.; Gómez-Ríos, G. A.; Hein, D.; Pawliszyn, J. Breaching the 10 Second Barrier of Total Analysis Time for Complex Matrices via Automated Coated Blade Spray. *Anal. Chem.* **2019**, *91* (20), 13039–13046. https://doi.org/10.1021/acs.analchem.9b03225.

(45) Deng, J.; Yang, Y.; Xu, M.; Wang, X.; Lin, L.; Yao, Z. P.; Luan, T. Surface-Coated Probe Nanoelectrospray Ionization Mass Spectrometry for Analysis of Target Compounds in Individual Small Organisms. *Anal. Chem.* **2015**, *87* (19), 9923–9930. https://doi.org/10.1021/acs.analchem.5b03110.

(46) Gómez-Ríos, G. A.; Mirabelli, M. F. Solid Phase Microextraction-Mass Spectrometry: Metanoia. *TrAC - Trends Anal. Chem.* **2019**, *112*, 201–211. https://doi.org/10.1016/j.trac.2018.12.030.

(47) D'Agostino, P. A.; Chenier, C. L.; Hancock, J. R.; Jackson Lepage, C. R. Desorption Electrospray Ionisation Mass Spectrometric Analysis of Chemical Warfare Agents from Solid-Phase Microextraction Fibers. *Rapid Commun. Mass Spectrom.* **2007**, *21* (4), 543–549. https://doi.org/10.1002/rcm.2867.

(48) Kennedy, J. H.; Aurand, C.; Shirey, R.; Laughlin, B. C.; Wiseman, J. M. Coupling Desorption Electrospray Ionization with Solid-Phase Microextraction for Screening and Quantitative Analysis of Drugs in Urine. *Anal. Chem.* **2010**, *82* (17), 7502–7508. https://doi.org/10.1021/ac101295g.

(49) Lendor, S.; Gómez-ríos, G. A.; Boyaci, E.; Heide, H. Vander; Pawliszyn, J. Space-Resolved Tissue Analysis by Solid Phase Microextraction Coupled to High Resolution Mass Spectrometry via Desorption Electrospray Ionization Space-Resolved Tissue Analysis by Solid Phase Microextraction Coupled to High Resolution Mass Spectrometry Vi. *Anal. Chem.* **2019**, *91* (15), 10141–10148. https://doi.org/10.1021/acs.analchem.9b02157.

(50) Gómez-Ríos, G. A.; Tascon, M.; Reyes-Garcés, N.; Boyacı, E.; Poole, J. J.; Pawliszyn, J. Rapid Determination of Immunosuppressive Drug Concentrations in Whole Blood by Coated Blade Spray-Tandem Mass Spectrometry (CBS-MS/MS). *Anal. Chim. Acta* **2018**, *999*, 69–75. https://doi.org/10.1016/j.aca.2017.10.016.

(51) Newsome, G. A.; Kavich, G.; Alvarez-Martin, A. Interface for Reproducible, Multishot Direct Analysis of Solid-Phase Microextraction Samples. *Anal. Chem.* **2020**, *92* (6), 4182–4186. https://doi.org/10.1021/acs.analchem.9b05691.

(52) Looby, N. T. .; Tascon, M.; Acquaro, V.; Reyes-Garcés, N.; Vasiljevic, T.; Wasowicz, M.; Pawliszyn, J. Solid Phase Microextraction Coupled to Mass Spectrometry via Microfluidic Interface for Rapid Therapeutic Drug Monitoring. *Analyst* **2019**, *144*, 3721–3728. https://doi.org/10.1039/C9AN00041K.

(53) Tascon, M.; Alam, M. N.; Gómez-Ríos, G. A.; Pawliszyn, J. Development of a Microfluidic Open

Interface with Flow Isolated Desorption Volume for the Direct Coupling of SPME Devices to Mass Spectrometry. *Anal. Chem.* **2018**, *90* (4), 2631–2638. https://doi.org/10.1021/acs.analchem.7b04295.

(54) Gómez-Ríos, G. A.; Liu, C.; Tascon, M.; Reyes-Garcés, N.; Arnold, D. W.; Covey, T. R.; Pawliszyn, J. Open Port Probe Sampling Interface for the Direct Coupling of Biocompatible Solid-Phase Microextraction to Atmospheric Pressure Ionization Mass Spectrometry. *Anal. Chem.* **2017**, *89* (7), 3805–3809. https://doi.org/10.1021/acs.analchem.6b04737.

(55) Berkel, G. J. Van; Kertesz, V. An Open Port Sampling Interface for Liquid Introduction Atmospheric Pressure Ionization Mass Spectrometry. *Rapid Commun. Mass Spectrom.* **2015**, No. 29, 1749–1756. https://doi.org/10.1002/rcm.7274.

(56) Tascon, M.; Singh, V.; Huq, M.; Pawliszyn, J. Direct Coupling of Dispersive Extractions with Magnetic Particles to Mass Spectrometry via Microfluidic Open Interface. *Anal. Chem* **2019**, *91* (7), 4762–4770. https://doi.org/10.1021/acs.analchem.9b00308.

(57) Lendor, S.; Olkowicz, M.; Boyaci, E.; Yu, M.; Diwan, M.; Hamani, C.; Palmer, M.; Reyes-Garcés, N.; Gómez-Ríos, G. A.; Pawliszyn, J. Investigation of Early Death-Induced Changes in Rat Brain by Solid Phase Microextraction via Untargeted High Resolution Mass Spectrometry: In Vivo versus Postmortem Comparative Study . *ACS Chem. Neurosci.* **2020**. https://doi.org/10.1021/acschemneuro.0c00270.

(58) Ouyang, G.; Pawliszyn, J. A Critical Review in Calibration Methods for Solid-Phase Microextraction. *Anal. Chim. Acta* **2008**, *627* (2), 184–197. https://doi.org/10.1016/j.aca.2008.08.015.

(59) Alam, M. N.; Ricardez-Sandoval, L.; Pawliszyn, J. Calibrant Free Sampling and Enrichment with Solid-Phase Microextraction: Computational Simulation and Experimental Verification. *Ind. Eng. Chem. Res.* **2017**, *56* (13), 3679–3686. https://doi.org/10.1021/acs.iecr.7b00131.

(60) Kenessov, B.; Derbissalin, M.; Koziel, J. A.; Kosyakov, D. S. Modeling Solid-Phase Microextraction of Volatile Organic Compounds by Porous Coatings Using Fi Nite Element Analysis. *Anal. Chim. Acta* **2019**, *1076*, 73–81. https://doi.org/10.1016/j.aca.2019.05.042.

(61) Motlagh, S.; Pawliszyn, J. On-Line Monitoring of Flowing Samples Using Solid Phase Microextraction-Gas Chromatography. *Anal. Chim. Acta* **1993**, *284* (2), 265–273. https://doi.org/10.1016/0003-2670(93)85310-G.

(62) Goryński, K. A Critical Review of Solid-Phase Microextraction Applied in Drugs of Abuse Determinations and Potential Applications for Targeted Doping Analysis. *Trends Anal. Chem.* **2018**. https://doi.org/10.1016/j.trac.2018.12.029.

(63) Arya, Y.; Tascon, M.; Eroglu, A. E.; Boyac, E. Trends in Analytical Chemistry Thin Fi Lm Microextraction : Towards Faster and More Sensitive Microextraction. **2019**, *113*, 93–101. https://doi.org/10.1016/j.trac.2019.01.022.

(64) Khaled, A.; Singh, V.; Pawliszyn, J. Comparison of Solid-Phase Microextraction to Solvent Extraction and QuEChERS for Quantitative Analysis of Veterinary Drug Residues in Chicken and Beef Matrices. *J. Agric. Food Chem.* **2019**, *67* (46), 12663–12669. https://doi.org/10.1021/acs.jafc.9b01570.

(65) Reyes-Garcés, N.; Bojko, B.; Pawliszyn, J. High Throughput Quantification of Prohibited Substances in Plasma Using Thin Film Solid Phase Microextraction. *J. Chromatogr. A* **2014**, *1374*, 40–49. https://doi.org/10.1016/j.chroma.2014.11.047.

(66) Boyacl, E.; Bojko, B.; Reyes-Garcés, N.; Poole, J. J.; Gómez-Ríos, G. A.; Teixeira, A.; Nicol, B.; Pawliszyn, J. High-Throughput Analysis Using Non-Depletive SPME: Challenges and Applications to the Determination of Free and Total Concentrations in Small Sample Volumes. *Sci. Rep.* **2018**, *8* (1), 1–10. https://doi.org/10.1038/s41598-018-19313-1.

(67) Mirnaghi, F. S.; Pawliszyn, J. Development of Coatings for Automated 96-Blade Solid Phase Microextraction-Liquid Chromatography-Tandem Mass Spectrometry System, Capable of Extracting a Wide Polarity Range of Analytes from Biological Fluids. *J. Chromatogr. A* **2012**, *1261*, 91–98. https://doi.org/10.1016/j.chroma.2012.07.012.

(68) Khaled, A.; Gómez-Ríos, G. A.; Pawliszyn, J. Optimization of Coated Blade Spray for Rapid Screening and Quantitation of 105 Veterinary Drugs in Biological Tissue Samples. *Anal. Chem.* **2020**, *92* (8), 5937–5943. https://doi.org/10.1021/acs.analchem.0c00093.

(69) Huq, M.; Tascon, M.; Nazdrajić, E.; Roszkowska, A.; Pawliszyn, J. Measurement of Free Drug Concentration from Biological Tissue by Solid-Phase Microextraction: In Silico and Experimental Study. *Anal. Chem.* **2019**, *91*, 7719–7728. https://doi.org/10.1021/acs.analchem.9b00983.

(70) Xu, J.; Hu, Q.; Liu, X.; Wei, S.; Zheng, J.; Lin, W.; Ye, Y.; Zhu, F.; Ouyang, G. Determination of the Mass Transfer Coefficients in Direct Immersion Solid-phase Microextraction. *J. Sep. Sci.* **2020**, No. February, 1–7. https://doi.org/10.1002/jssc.201901345.

(71) Alam, M. N.; Ricardez-Sandoval, L.; Pawliszyn, J. Numerical Modeling of Solid-Phase Microextraction: Binding Matrix Effect on Equilibrium Time. *Anal. Chem.* **2015**, *87* (19), 9846–9854. https://doi.org/10.1021/acs.analchem.5b02239.

(72) Rapp, B. E. *Microfluidics: Modeling, Mechanics and Mathematics*; William Andrew, 2016. https://doi.org/10.1016/c2012-0-02230-2.

(73) Pritchard, P. J. *Fox and McDonald's Introduction to Fluid Mechanics*, 8th Editio.; John Wiley & Sons, Inc.: Danvers, MA, 2011.

(74) Fang, L.; Deng, J.; Yang, Y.; Wang, X.; Chen, B.; Liu, H.; Zhou, H.; Ouyang, G.; Luan, T. Coupling Solid-Phase Microextraction with Ambient Mass Spectrometry: Strategies and Applications. *TrAC - Trends Anal. Chem.* **2016**, *85*, 61–72. https://doi.org/10.1016/j.trac.2016.05.025.

(75) Pu, F.; Chiang, S.; Zhang, W.; Ouyang, Z. Direct Sampling Mass Spectrometry for Clinical Analysis. *Analyst* **2019**, *144* (4), 1034–1051. https://doi.org/10.1039/c8an01722k.

(76) Zaitsu, K.; Hayashi, Y.; Murata, T.; Ohara, T.; Nakagiri, K.; Kusano, M.; Nakajima, H.; Nakajima, T.; Ishikawa, T.; Tsuchihashi, H.; Ishii, A. Intact Endogenous Metabolite Analysis of Mice Liver by Probe Electrospray Ionization/Triple Quadrupole Tandem Mass Spectrometry and Its Preliminary Application to in Vivo Real-Time Analysis. *Anal. Chem.* **2016**, *88* (7), 3556–3561. https://doi.org/10.1021/acs.analchem.5b04046.

(77) Frey, B. S.; Heiss, D. R.; Badu-Tawiah, A. K. Embossed Paper Platform for Whole Blood Collection, Room Temperature Storage, and Direct Analysis by Pinhole Paper Spray Mass Spectrometry. *Anal. Chem.* **2022**, *94* (10), 4417–4425. https://doi.org/10.1021/acs.analchem.1c05340.

(78) Chen, H.; Talaty, N. N.; Takáts, Z.; Cooks, R. G. Desorption Electrospray Ionization Mass Spectrometry for High-Throughput Analysis of Pharmaceutical Samples in the Ambient Environment. *Anal. Chem.* **2005**, *77* (21), 6915–6927. https://doi.org/10.1021/ac050989d.

(79) Guo, T.; Yong, W.; Jin, Y.; Zhang, L.; Liu, J.; Wang, S.; Chen, Q.; Dong, Y.; Su, H.; Tan, T.

Applications of DART-MS for Food Quality and Safety Assurance in Food Supply Chain. *Mass Spectrom. Rev.* **2017**, *36* (2), 161–187. https://doi.org/10.1002/mas.21466.

(80) Khaled, A.; Gionfriddo, E.; Acquaro, V.; Singh, V.; Pawliszyn, J. Development and Validation of a Fully Automated Solid Phase Microextraction High Throughput Method for Quantitative Analysis of Multiresidue Veterinary Drugs in Chicken Tissue. *Anal. Chim. Acta* **2019**, *1056*, 34–46. https://doi.org/10.1016/j.aca.2018.12.044.

(81) Looby, N.; Vasiljevic, T.; Reyes-Garcés, N.; Roszkowska, A.; Bojko, B.; Wąsowicz, M.; Jerath, A.; Pawliszyn, J. Therapeutic Drug Monitoring of Tranexamic Acid in Plasma and Urine of Renally Impaired Patients Using Solid Phase Microextraction. *Talanta* **2021**, *225* (August 2020). https://doi.org/10.1016/j.talanta.2020.121945.

(82) Vasiljevic, T.; Gómez-Ríos, G. A.; Li, F.; Liang, P.; Pawliszyn, J. High-Throughput Quantification of Drugs of Abuse in Biofluids via 96-Solid-Phase Microextraction–Transmission Mode and Direct Analysis in Real Time Mass Spectrometry. *Rapid Commun. Mass Spectrom.* **2019**, *33* (18), 1423–1433. https://doi.org/10.1002/rcm.8477.

(83) Thirukumaran, M.; Singh, V.; Arao, Y.; Fujito, Y.; Nishimura, M.; Ogura, T.; Pawliszyn, J. Solid-Phase Microextraction- Probe Electrospray Ionization Devices for Screening and Quantitating Drugs of Abuse in Small Amounts of Biofluids. *Talanta* **2021**, *231* (March), 122317. https://doi.org/10.1016/j.talanta.2021.122317.

(84) Hu, B.; Zheng, B.; Rickert, D.; Gómez-Ríos, G. A.; Bojko, B.; Pawliszyn, J.; Yao, Z. P. Direct Coupling of Solid Phase Microextraction with Electrospray Ionization Mass Spectrometry: A Case Study for Detection of Ketamine in Urine. *Anal. Chim. Acta* **2019**, *1075*, 112–119. https://doi.org/10.1016/j.aca.2019.05.044.

(85) Vasiljevic, T.; Gómez-Ríos, G. A.; Pawliszyn, J. Single-Use Poly(Etheretherketone) Solid-Phase Microextraction-Transmission Mode Devices for Rapid Screening and Quantitation of Drugs of Abuse in Oral Fluid and Urine via Direct Analysis in Real-Time Tandem Mass Spectrometry. *Anal. Chem.* **2018**, *90* (1), 952–960. https://doi.org/10.1021/acs.analchem.7b04005.

(86) Ahmad, S.; Tucker, M.; Spooner, N.; Murnane, D.; Gerhard, U. Direct Ionization of Solid-Phase Microextraction Fibers for Quantitative Drug Bioanalysis: From Peripheral Circulation to Mass Spectrometry Detection. *Anal. Chem.* **2015**, *87* (1), 754–759. https://doi.org/10.1021/ac503706n.

(87) Gómez-Ríos, G. A.; Pawliszyn, J. Development of Coated Blade Spray Ionization Mass Spectrometry for the Quantitation of Target Analytes Present in Complex Matrices. *Angew. Chemie - Int. Ed.* **2014**, *53* (52), 14503–14507. https://doi.org/10.1002/anie.201407057.

(88) Grandy, J. J.; Singh, V.; Lashgari, M.; Gauthier, M.; Pawliszyn, J. Development of a Hydrophilic Lipophilic Balanced Thin Film Solid Phase Microextraction Device for Balanced Determination of Volatile Organic Compounds. *Anal. Chem.* **2018**, *90* (23), 14072–14080. https://doi.org/10.1021/acs.analchem.8b04544.

(89) Lendor, S.; Hassani, S. A.; Boyaci, E.; Singh, V.; Womelsdorf, T.; Pawliszyn, J. Solid Phase Microextraction-Based Miniaturized Probe and Protocol for Extraction of Neurotransmitters from Brains in Vivo. *Anal. Chem.* **2019**, *91* (7), 4896–4905. https://doi.org/10.1021/acs.analchem.9b00995.

(90) Risticevic, S.; Pawliszyn, J. Solid-Phase Microextraction in Targeted and Nontargeted Analysis: Displacement and Desorption Effects. *Anal. Chem.* **2013**, *85* (19), 8987–8995. https://doi.org/10.1021/ac4003112.

(91) Souza Silva, E. A.; Risticevic, S.; Pawliszyn, J. Recent Trends in SPME Concerning Sorbent Materials, Configurations and in Vivo Applications. *TrAC - Trends Anal. Chem.* **2013**, *43*, 24–36. https://doi.org/10.1016/j.trac.2012.10.006.

(92) Semenov, S. N.; Koziel, J. A.; Pawliszyn, J. Kinetics of Solid-Phase Extraction and Solid-Phase Microextraction in Thin Adsorbent Layer with Saturation Sorption Isotherm. *J. Chrom. A.* **2000**, *873*, 39–51. https://doi.org/10.1016/S0021-9673(99)01338-2.

(93) Pawllszyn, J. *Solid Phase Microextraction: Theory and Practice*; Wiley-VCH Publishers, Inc.: New York, 1997.

(94) Reyes-Garcés, N.; Alam, M. N.; Pawliszyn, J. The Effect of Hematocrit on Solid-Phase Microextraction. *Anal. Chim. Acta* **2018**, *1001*, 40–50. https://doi.org/10.1016/j.aca.2017.11.014.

(95) Xu, J.; Huang, S.; Wei, S.; Yang, M.; Cao, C.; Jiang, R.; Zhu, F.; Ouyang, G. Study on the Diffusion-Dominated Solid-Phase Microextraction Kinetics in Semisolid Sample Matrix. *Anal. Chem.* **2016**, *88* (18), 8921–8925. https://doi.org/10.1021/acs.analchem.6b02673.

(96) Chao, K.; Wang, V.; Yang, H.; Wang, C. Estimation of Effective Diffusion Coef Fi Cients for Benzene and Toluene in PDMS for Direct Solid Phase Microextraction. *Polym. Test.* **2011**, *30* (5), 501–508. https://doi.org/10.1016/j.polymertesting.2011.04.004.

(97) Zhang, Z.; Pawliszyn, J. Studying Activity Coefficients of Probe Solutes in Selected Liquid Polymer Coatings Using Solid Phase Microextraction. *J. Phys. Chem.* **1996**, *100* (44), 17648–17654. https://doi.org/10.1021/jp962317k.

(98) Kenessov, B.; Koziel, J. A.; Baimatova, N.; Demyanenko, O. P.; Derbissalin, M. Optimization of Time-Weighted Average Air Sampling by Solid-Phase Microextraction Fibers Using Finite Element Analysis Software. *Molecules* **2018**, *23* (11), 2736. https://doi.org/10.3390/molecules23112736.

(99) Souza-Silva, É. A.; Gionfriddo, E.; Alam, M. N.; Pawliszyn, J. Insights into the Effect of the PDMS-Layer on the Kinetics and Thermodynamics of Analyte Sorption onto the Matrix-Compatible Solid Phase Microextraction Coating. *Anal. Chem.* **2017**, *89* (5), 2978–2985. https://doi.org/10.1021/acs.analchem.6b04442.

(100) Knox, J. H.; Scott, H. P. B and C Terms in the van Deemter Equation for Liquid Chromatography. *J. Chrom. A.* **1983**, *282*, 297–313. https://doi.org/10.1016/S0021-9673(00)91609-1.

(101) Boscaini, E.; Alexander, M. L.; Prazeller, P.; Märk, T. D. Investigation of Fundamental Physical Properties of a Polydimethylsiloxane (PDMS) Membrane Using a Proton Transfer Reaction Mass Spectrometer (PTRMS). *Int. J. Mass Spectrom.* **2004**, *239* (2–3), 179–186. https://doi.org/10.1016/j.ijms.2004.08.011.

(102) Oh, K.; Koo, Y.; Jung, K. Characterization of a Sheet Membrane Interface for Sample Introduction into a Time-of-Flight Mass Spectrometer. *Int. J. Mass Spectrom.* **2006**, *253*, 65–70. https://doi.org/10.1016/j.ijms.2006.02.017.

(103) Belles, A.; Franke, C.; Alary, C.; Aminot, Y.; Readman, J. W. Understanding and Predicting the Diffusivity of Organic Compounds in Polydimethylsiloxane Material for Passive Sampler Applications Using a Simple Quantitative Structure–Property Relationship Model. *Environ. Toxicol. Chem.* **2018**, *37* (5), 1291–1300. https://doi.org/10.1002/etc.4101.

(104) Lue, S. J.; Chen, W. W.; Wang, S. F. Vapor Permeation of Toluene, m-Xylene, and Methanol Vapors on Poly(Dimethylsiloxane) Membranes. *Sep. Sci. Technol.* **2014**, *44* (14), 3412–3434. https://doi.org/10.1080/01496390903212615.

(105) Crank, J. *The Mathematics of Diffusion*; Oxford University Press, 1979. https://doi.org/10.1016/0306-4549(77)90072-X.

(106) Koziel, J. A.; Martos, P. A.; Pawliszyn, J. System for the Generation of Standard Gas Mixtures of Volatile and Semi-Volatile Organic Compounds for Calibrations of Solid-Phase Microextraction and Other Sampling Devices. *J. Chromatogr. A* **2004**, *1025* (1), 3–9. https://doi.org/10.1016/j.chroma.2003.10.079.

(107) Grandy, J. J.; Murtada, K.; Belinato, J. R.; Suárez, P. A. O.; Pawliszyn, J. Development and Validation of an Improved, Thin Film Solid Phase Microextraction Based, Standard Gas Generating Vial for the Repeatable Generation of Gaseous Standards. *J. Chromatogr. A* **2020**, *1632*, 461541. https://doi.org/10.1016/j.chroma.2020.461541.

(108) Galievsky, V. A.; Pawliszyn, J. Fluorometer for Screening of Doxorubicin in Perfusate Solution and Tissue with Solid-Phase Microextraction Chemical Biopsy Sampling Fluorometer for Screening of Doxorubicin in Perfusate Solution and Tissue with Solid-Phase Microextraction. *Anal. Chem.* **2020**, *92* (19), 13025–13033. https://doi.org/10.1021/acs.analchem.0c01905.

(109) Rickert, D. A.; Gómez-Ríos, G. A.; Nazdrajić, E.; Tascon, M.; Kulasingam, V.; Pawliszyn, J. B. Evaluation of a Coated Blade Spray-Tandem Mass Spectrometry Assay as a New Tool for the Determination of Immunosuppressive Drugs in Whole Blood. *Anal. Bioanal. Chem.* **2020**, *412* (21), 5067–5076. https://doi.org/10.1007/s00216-019-02367-z.

(110) Nazdrajić, E.; Tascon, M.; Rickert, D. A.; German, A. G.; Kulasingam, V.; Pawliszyn, J. B. Rapid Determination of Tacrolimus and Sirolimus in Whole Human Blood by Direct Coupling of Solid-Phase Microextraction to Mass Spectrometry via Microfluidic Open Interface. *Anal. Chim. Acta* **2021**, *1144*, 53–60. https://doi.org/10.1016/j.aca.2020.11.056.

(111) Koziel, J. A.; Nguyen, L. T.; Glanville, T. D.; Ahn, H.; Frana, T. S.; (Hans) van Leeuwen, J. Method for Sampling and Analysis of Volatile Biomarkers in Process Gas from Aerobic Digestion of Poultry Carcasses Using Time-Weighted Average SPME and GC–MS. *Food Chem.* **2017**, *232*, 799–807. https://doi.org/10.1016/j.foodchem.2017.04.062.

(112) Zheng, J. L.; Guan, D. X.; Luo, J.; Zhang, H.; Davison, W.; Cui, X. Y.; Wang, L. H.; Ma, L. Q. Activated Charcoal Based Diffusive Gradients in Thin Films for in Situ Monitoring of Bisphenols in Waters. *Anal. Chem.* **2015**, *87* (1), 801–807. https://doi.org/10.1021/ac503814j.

(113) Zhang, Y.; Zhang, R. Recent Advances in Analytical Methods for the Therapeutic Drug Monitoring of Immunosuppressive Drugs. *Drug Test. Anal.* **2018**, *10* (1), 81–94. https://doi.org/10.1002/dta.2290.

(114) Seger, C.; Shipkova, M.; Christians, U.; Billaud, E. M.; Wang, P.; Holt, D. W.; Brunet, M.; Kunicki, P. K.; Pawinski, T.; Langman, L. J.; Marquet, P.; Oellerich, M.; Wieland, E.; Wallemacq, P. Assuring the Proper Analytical Performance of Measurement Procedures for Immunosuppressive Drug Concentrations in Clinical Practice: Recommendations of the International Association of Therapeutic Drug Monitoring and Clinical Toxicology Immunosuppressive . *Ther. Drug Monit.* **2016**, *38* (2), 170–189. https://doi.org/10.1097/FTD.0000000000000269.

(115) Wei, T. Q.; Zheng, Y. F.; Dubowy, M.; Sharma, M. Sandwich Assay for Tacrolimus Using 2 Antitacrolimus Antibodies. *Clin. Chem.* **2014**, *60* (4), 621–630. https://doi.org/10.1373/clinchem.2013.214023.

(116) Dasgupta, A.; Davis, B.; Chow, L. Evaluation of QMS Everolimus Assay Using Hitachi 917 Analyzer: Comparison with Liquid Chromatography/Mass Spectrometry. *Ther. Drug Monit.* **2011**,

33 (2), 149–154. https://doi.org/10.1097/FTD.0b013e31820afc97.

(117) Shipkova, M.; Vogeser, M.; Ramos, P. A.; Verstraete, A. G.; Orth, M.; Schneider, C.; Wallemacq, P. Multi-Center Analytical Evaluation of a Novel Automated Tacrolimus Immunoassay. *Clin. Biochem.* **2014**, *47* (12), 1069–1077. https://doi.org/10.1016/j.clinbiochem.2014.03.023.

(118) Vogeser, M.; Shipkova, M.; Rigo-Bonnin, R.; Wallemacq, P.; Orth, M.; Widmann, M.; Verstraete, A. G. Multicenter Analytical Evaluation of the Automated Electrochemiluminescence Immunoassay for Cyclosporine. *Ther. Drug Monit.* **2014**, *36* (5), 640–650. https://doi.org/10.1097/FTD.0000000000000068.

(119) Hashi, S.; Masuda, S.; Kikuchi, M.; Uesugi, M.; Yano, I.; Omura, T.; Yonezawa, A.; Fujimoto, Y.; Ogawa, K.; Kaido, T.; Uemoto, S.; Matsubara, K. Assessment of Four Methodologies (Microparticle Enzyme Immunoassay, Chemiluminescent Enzyme Immunoassay, Affinity Column-Mediated Immunoassay, and Flow Injection Assay-Tandem Mass Spectrometry) for Measuring Tacrolimus Blood Concentration in Japanese Live. *Transplant. Proc.* **2014**, *46* (3), 758–760. https://doi.org/10.1016/j.transproceed.2013.11.060.

(120) Fung, A. W. S.; Knauer, M. J.; Blasutig, I. M.; Colantonio, D. A.; Kulasingam, V. Evaluation of Electrochemiluminescence Immunoassays for Immunosuppressive Drugs on the Roche Cobas E411 Analyzer. *F1000Research* **2017**, *6* (0), 1832–1843. https://doi.org/10.12688/f1000research.12775.1.

(121) Johnson-Davis, K. L.; De, S.; Jimenez, E.; McMillin, G. A.; De, B. K. Evaluation of the Abbott ARCHITECT I2000 Sirolimus Assay and Comparison with the Abbott IMx Sirolimus Assay and an Established Liquid Chromatography-Tandem Mass Spectrometry Method. *Ther. Drug Monit.* **2011**, *33*, 453–459. https://doi.org/10.1097/FTD.0b013e3182263981.

(122) Shipkova, M.; Svinarov, D. LC–MS/MS as a Tool for TDM Services: Where Are We? *Clin. Biochem.* **2016**, *49* (13–14), 1009–1023. https://doi.org/10.1016/j.clinbiochem.2016.05.001.

(123) Dubbelboer, I. R.; Pohanka, A.; Said, R.; Rosenborg, S.; Beck, O. Quantification of Tacrolimus and Three Demethylated Metabolites in Human Whole Blood Using LC – ESI – MS / MS. *Ther Drug Monit* **2012**, *34*, 134–142. https://doi.org/10.1097/FTD.0b013e31824b0bfb.

(124) Marinova, M.; Artusi, C.; Brugnolo, L.; Antonelli, G.; Zaninotto, M.; Plebani, M. Immunosuppressant Therapeutic Drug Monitoring by LC-MS / MS : Workflow Optimization through Automated Processing of Whole Blood Samples. *Clin. Biochem.* **2013**, *46* (16–17), 1723–1727. https://doi.org/10.1016/j.clinbiochem.2013.08.013.

(125) Peddi, V. R.; Wiseman, A.; Chavin, K.; Slakey, D. Review of Combination Therapy with MTOR Inhibitors and Tacrolimus Minimization after Transplantation. *Transplant. Rev.* **2013**, *27* (4), 97–107. https://doi.org/10.1016/j.trre.2013.06.001.

(126) Webster, A. C.; Woodroffe, R. C.; Taylor, R. S.; Chapman, J. R.; Craig, J. C. Tacrolimus versus Ciclosporin as Primary Immunosuppression for Kidney Transplant Recipients: Meta-Analysis and Meta-Regression of Randomised Trial Data. *Br. Med. J.* **2005**, *331* (7520), 810–814. https://doi.org/10.1136/bmj.38569.471007.AE.

(127) Ekberg, H.; Tedesco-Silva, H.; Demirbas, A.; Vítko, Š.; Nashan, B.; Gürkan, A.; Margreiter, R.; Hugo, C.; Grinyó, J. M.; Frei, U.; Vanrenterghem, Y.; Daloze, P.; Halloran, P. F. Reduced Exposure to Calcineurin Inhibitors in Renal Transplantation. *N. Engl. J. Med.* **2007**, *357* (25), 2562–2575. https://doi.org/10.1056/NEJMoa067411.

(128) Freudenberger, K.; Hilbig, U.; Gauglitz, G. Recent Advances in Therapeutic Drug Monitoring of

Immunosuppressive Drugs. *Trends Anal. Chem.* **2016**, *79*, 257–268. https://doi.org/10.1016/j.trac.2015.11.016.

(129) Jacob, S.; Nair, A. B. A Review on Therapeutic Drug Monitoring of the MTOR Class of Immunosuppressants: Everolimus and Sirolimus. *Drugs Ther. Perspect.* **2017**, *33*, 290–301. https://doi.org/10.1007/s40267-017-0403-0.

(130) Hétu, P. O.; Robitaille, R.; Vinet, B. Successful and Cost-Efficient Replacement of Immunoassays by Tandem Mass Spectrometry for the Quantification of Immunosuppressants in the Clinical Laboratory. *J. Chromatogr. B Anal. Technol. Biomed. Life Sci.* **2012**, *883–884*, 95–101. https://doi.org/10.1016/j.jchromb.2011.10.034.

(131) Jourdil, J. F.; Picard, P.; Meunier, C.; Auger, S.; Stanke-Labesque, F. Ultra-Fast Cyclosporin A Quantitation in Whole Blood by Laser Diode Thermal Desorption - Tandem Mass Spectrometry; Comparison with High Performance Liquid Chromatography-Tandem Mass Spectrometry. *Anal. Chim. Acta* **2013**, *805*, 80–86. https://doi.org/10.1016/j.aca.2013.10.051.

(132) Shi, R. Z.; El Gierari, E. T. M.; Manicke, N. E.; Faix, J. D. Rapid Measurement of Tacrolimus in Whole Blood by Paper Spray-Tandem Mass Spectrometry (PS-MS/MS). *Clin. Chim. Acta* **2015**, *441*, 99–104. https://doi.org/10.1016/j.cca.2014.12.022.

(133) Shi, R.-Z.; El Gierari, E. T. M.; Faix, J. D.; Manicke, N. E. Rapid Measurement of Cyclosporine and Sirolimus in Whole Blood by PS MS MS. *Clin. Chem.* **2016**, *62* (1), 295–299. https://doi.org/10.1097/gme.0b013e3181967b88.

(134) Mueller, D. M.; Rentsch, K. M. Sensitive Quantification of Sirolimus and Everolimus by LC – MS / MS with Online Sample Cleanup. *J. Chromatogr. B* **2010**, *878* (13–14), 1007–1012. https://doi.org/10.1016/j.jchromb.2010.02.029.

(135) Tascon, M.; Gómez-Ríos, G. A.; Reyes-Garcés, N.; Poole, J.; Boyacı, E.; Pawliszyn, J. Ultra-Fast Quantitation of Voriconazole in Human Plasma by Coated Blade Spray Mass Spectrometry. *J. Pharm. Biomed. Anal.* **2017**, *144*, 106–111. https://doi.org/10.1016/j.jpba.2017.03.009.

(136) Tascon, M.; Gómez-Ríos, G. A.; Reyes-Garcés, N.; Poole, J.; Boyacl, E.; Pawliszyn, J. High-Throughput Screening and Quantitation of Target Compounds in Biofluids by Coated Blade Spray-Mass Spectrometry. *Anal. Chem.* **2017**, *89* (16), 8421–8428. https://doi.org/10.1021/acs.analchem.7b01877.

(137) Gómez-Ríos, G. A.; Reyes-Garcés, N.; Bojko, B.; Pawliszyn, J. Biocompatible Solid-Phase Microextraction Nanoelectrospray Ionization: An Unexploited Tool in Bioanalysis. *Anal. Chem.* **2016**, *88* (2), 1259–1265. https://doi.org/10.1021/acs.analchem.5b03668.

(138) CLSI. C62-A. **2014**, No. October.

(139) Pawliszyn, J. Properties and Applications of the Concentration Gradient Sensor to Detection of Flowing Samples. *Anal. Chem* **1986**, *58* (7), 3207–3215.

(140) Polledri, E.; Mercadante, R.; Ferraris Fusarini, C.; Maiavacca, R.; Fustinoni, S. Immunosuppressive Drugs in Whole Blood: Validation of a Commercially Available Liquid Chromatography/Tandem Mass Spectrometry Kit and Comparison with Immunochemical Assays. *Rapid Commun. Mass Spectrom.* **2017**, *31* (13), 1111–1120. https://doi.org/10.1002/rcm.7887.

(141) Bazin, C.; Guinedor, A.; Barau, C.; Gozalo, C.; Grimbert, P.; Duvoux, C.; Furlan, V.; Massias, L.; Hulin, A. Evaluation of the Architect ® Tacrolimus Assay in Kidney , Liver , and Heart Transplant Recipients. *J. Pharm. Biomed. Anal.* **2010**, *53* (4), 997–1002. https://doi.org/10.1016/j.jpba.2010.06.022.

(142) Seger, C.; Tentschert, K.; Stöggl, W.; Griesmacher, A.; Ramsay, S. L. A Rapid HPLC-MS/MS Method for the Simultaneous Quantification of Cyclosporine A, Tacrolimus, Sirolimus and Everolimus in Human Blood Samples. *Nat. Protoc.* **2009**, *4* (4), 526–534. https://doi.org/10.1038/nprot.2009.25.

(143) Rigo, R.; Ariadna, B.; Roca, A. Simultaneous Measurement of Cyclosporine A , Everolimus , Sirolimus and Tacrolimus Concentrations in Human Blood by UPLC – MS / MS. *Chromatographia* **2015**, *78* (23), 1459–1474. https://doi.org/10.1007/s10337-015-2981-0.

(144) Piri-Moghadam, H.; Ahmadi, F.; Gómez-Ríos, G. A.; Boyacı, E.; Reyes-Garcés, N.; Aghakhani, A.; Bojko, B.; Pawliszyn, J. Fast Quantitation of Target Analytes in Small Volumes of Complex Samples by Matrix-Compatible Solid-Phase Microextraction Devices. *Angew. Chemie - Int. Ed.* **2016**, *55* (26), 7510–7514. https://doi.org/10.1002/anie.201601476.

(145) Armenian, P.; Vo, K. T.; Barr-Walker, J.; Lynch, K. L. Fentanyl, Fentanyl Analogs and Novel Synthetic Opioids: A Comprehensive Review. *Neuropharmacology* **2018**, *134*, 121–132. https://doi.org/10.1016/j.neuropharm.2017.10.016.

(146) Strayer, K. E.; Antonides, H. M.; Juhascik, M. P.; Daniulaityte, R.; Sizemore, I. E. LC-MS/MS-Based Method for the Multiplex Detection of 24 Fentanyl Analogues and Metabolites in Whole Blood at Sub Ng ML−1 Concentrations. *ACS Omega* **2018**, *3* (1), 514–523. https://doi.org/10.1021/acsomega.7b01536.

(147) Scholl, L.; Seth, P.; Kariisa, M.; Wilson, N.; Baldwin, G. Drug and Opioid-Involved Overdose Deaths — United States, 2013–2017. *MMWR. Morb. Mortal. Wkly. Rep.* **2018**, *67* (5152), 2013–2017. https://doi.org/10.15585/mmwr.mm675152e1.

(148) Jalal, H.; Burke, D. S. Carfentanil and the Rise and Fall of Overdose Deaths in the United States. *Addiction* **2020**, 1–7. https://doi.org/10.1111/add.15260.

(149) Mounteney, J.; Giraudon, I.; Denissov, G.; Griffiths, P. Fentanyls: Are We Missing the Signs? Highly Potent and on the Rise in Europe. *Int. J. Drug Policy* **2015**, *26* (7), 626–631. https://doi.org/10.1016/j.drugpo.2015.04.003.

(150) Uusküla, A.; Talu, A.; Vorobjov, S.; Salekešin, M.; Rannap, J.; Lemsalu, L.; Des, D. International Journal of Drug Policy The Fentanyl Epidemic in Estonia : Factors in Its Evolution and Opportunities for a Comprehensive Public Health Response , a Scoping Review. *Int. J. Drug Policy* **2020**, *81*, 102757. https://doi.org/10.1016/j.drugpo.2020.102757.

(151) Taylor, J.; Pardo, B.; Hulme, S.; Bouey, J.; Greenfield, V.; Zhang, S.; Kilmer, B. Illicit Synthetic Opioid Consumption in Asia and the Pacific: Assessing the Risks of a Potential Outbreak. *Drug Alcohol Depend.* **2021**, *220* (December 2020), 108500. https://doi.org/10.1016/j.drugalcdep.2020.108500.

(152) Leen, J. L. S.; Juurlink, D. N. Carfentanil: A Narrative Review of Its Pharmacology and Public Health Concerns. *Can. J. Anesth.* **2019**, *66* (4), 414–421. https://doi.org/10.1007/s12630-019-01294-y.

(153) Freni, F.; Moretti, M.; Radaelli, D.; Carelli, C.; Osculati, A. M. M.; Tronconi, L.; Vignali, C.; Morini, L. Determination of Fentanyl and 19 Derivatives in Hair: Application to an Italian Population. *J. Pharm. Biomed. Anal.* **2020**, *189*, 113476. https://doi.org/10.1016/j.jpba.2020.113476.

(154) Busardò, F. P.; Carlier, J.; Giorgetti, R.; Tagliabracci, A.; Pacifici, R.; Gottardi, M.; Pichini, S. Ultra-High-Performance Liquid Chromatography-Tandem Mass Spectrometry Assay for

Quantifying Fentanyl and 22 Analogs and Metabolites in Whole Blood, Urine, and Hair. *Front. Chem.* **2019**, *7* (APR), 1–13. https://doi.org/10.3389/fchem.2019.00184.

(155) Shaner, R. L.; Kaplan, P.; Hamelin, E. I.; Bragg, W. A.; Johnson, R. C. Comparison of Two Automated Solid Phase Extractions for the Detection of Ten Fentanyl Analogs and Metabolites in Human Urine Using Liquid Chromatography Tandem Mass Spectrometry. *J. Chromatogr. B Anal. Technol. Biomed. Life Sci.* **2014**, *962*, 52–58. https://doi.org/10.1016/j.jchromb.2014.05.025.

(156) Mochizuki, A.; Nakazawa, H.; Adachi, N.; Takekawa, K. Identification and Quantification of Mepirapim and Acetyl Fentanyl in Authentic Human Whole Blood and Urine Samples by GC – MS / MS and LC – MS / MS. *Forensic Toxicol.* **2018**, *36* (1), 81–87. https://doi.org/10.1007/s11419-017-0384-7.

(157) Adamowicz, P.; Bakhmut, Z.; Mikolajczyk, A. Screening Procedure for 38 Fentanyl Analogues and Five Other New Opioids in Whole Blood by Liquid Chromatography-Tandem Mass Spectrometry. *J. Appl. Toxicol.* **2020**, *40* (8), 1033–1046. https://doi.org/10.1002/jat.3962.

(158) Nan, Q.; Ping, X.; Baohua, S.; Xianyi, Z.; Yan, S.; Fenyun, S. Application of a Validated UHPLC-MS / MS Method for 28 Fentanyl-Analogue and Novel Synthetic Opioids in Whole Blood in Authentic Forensic Cases. *J. Chromatogr. B* **2019**, *1124* (January), 82–99. https://doi.org/10.1016/j.jchromb.2019.05.025.

(159) Mahlke, N. S.; Ziesenitz, V.; Mikus, G.; Skopp, G. Quantitative Low-Volume Assay for Simultaneous Determination of Fentanyl, Norfentanyl, and Minor Metabolites in Human Plasma and Urine by Liquid Chromatography - Tandem Mass Spectrometry (LC-MS/MS). *Int. J. Legal Med.* **2014**, *128* (5), 771–778. https://doi.org/10.1007/s00414-014-1040-y.

(160) Fogarty, M. F.; Papsun, D. M.; Logan, B. K. Analysis of Fentanyl and 18 Novel Fentanyl Analogs and Metabolites by LC-MS-MS, and Report of Fatalities Associated with Methoxyacetylfentanyl and Cyclopropylfentanyl. *J. Anal. Toxicol.* **2018**, *42* (9), 592–604. https://doi.org/10.1093/jat/bky035.

(161) Moody, M. T.; Diaz, S.; Shah, P.; Papsun, D.; Logan, B. K. Analysis of Fentanyl Analogs and Novel Synthetic Opioids in Blood, Serum/Plasma, and Urine in Forensic Casework. *Drug Test. Anal.* **2018**, *10* (9), 1358–1367. https://doi.org/10.1002/dta.2393.

(162) Sofalvi, S.; Schueler, H. E.; Lavins, E. S.; Kaspar, C. K.; Brooker, I. T.; Mazzola, C. D.; Dolinak, D.; Gilson, T. P.; Perch, S. An LC-MS-MS Method for the Analysis of Carfentanil, 3-Methylfentanyl, 2-Furanyl Fentanyl, Acetyl Fentanyl, Fentanyl and Norfentanyl in Postmortem and Impaired-Driving Cases. *J. Anal. Toxicol.* **2017**, *41* (6), 473–483. https://doi.org/10.1093/jat/bkx052.

(163) Krug, S. A.; Scott, K. S. A Toxicological Exploration of the Opioid Crisis. *WIREs Forensic Sci.* **2020**, *2* (6), 1–23. https://doi.org/10.1002/wfs2.1386.

(164) Schackmuth, M.; Kerrigan, S. Immunoassay-Based Detection of Fentanyl Analogs in Forensic Toxicology. *Forensic Toxicol.* **2019**, *37* (1), 231–237. https://doi.org/10.1007/s11419-018-0445-6.

(165) Tiscione, N. B.; Wegner, K.; Unit, T.; Beach, P.; Sheriff, C.; Road, G. C.; Beach, W. P. Validation of the Neogen ® Fentanyl ELISA Kit for Blood and Urine. **2017**, No. January, 313–317. https://doi.org/10.1093/jat/bkx005.

(166) Metwally, H.; Agrawal, P.; Smith, R.; Liu, C.; LeBlanc, Y.; Covey, T. R.; Oleschuk, R. Detection of Opioids on Mail/Packages Using Open Port Interface Mass Spectrometry (OPI-MS). *J. Am. Soc. Mass Spectrom.* **2020**. https://doi.org/10.1021/jasms.0c00295.

(167) Vandergrift, G. W.; Hessels, A. J.; Palaty, J.; Krogh, E. T.; Gill, C. G. Paper Spray Mass Spectrometry for the Direct, Semi-Quantitative Measurement of Fentanyl and Norfentanyl in Complex Matrices. *Clin. Biochem.* **2018**, *54* (February), 106–111. https://doi.org/10.1016/j.clinbiochem.2018.02.005.

(168) W. De Silva, I.; Couch, A. N.; Verbeck, G. F. Paper Spray Mass Spectrometry Utilized with a Synthetic Microporous Polyolefin Silica Matrix Substrate in the Rapid Detection and Identification of More than 190 Synthetic Fentanyl Analogs. *J. Am. Soc. Mass Spectrom.* **2021**, *32* (2), 420–428. https://doi.org/10.1021/jasms.0c00250.

(169) Kennedy, J. H.; Palaty, J.; Gill, C. G.; Wiseman, J. M. Rapid Analysis of Fentanyls and Other Novel Psychoactive Substances in Substance Use Disorder Patient Urine Using Paper Spray Mass Spectrometry. *Rapid Commun. Mass Spectrom.* **2018**, *32* (15), 1280–1286. https://doi.org/10.1002/rcm.8164.

(170) Roy, K. S.; Nazdrajić, E.; Shimelis, O. I.; Ross, M. J.; Chen, Y.; Cramer, H.; Pawliszyn, J. Optimizing a High-Throughput Solid-Phase Microextraction System to Determine the Plasma Protein Binding of Drugs in Human Plasma. *Anal. Chem.* **2021**, *93* (32), 11061–11065. https://doi.org/10.1021/acs.analchem.1c01986.

(171) Rocío-Bautista, P.; Famiglini, G.; Termopoli, V.; Palma, P.; Nazdrajić, E.; Pawliszyn, J.; Cappiello, A. Direct Coupling of Bio-SPME to Liquid Electron Ionization-MS/MS via a Modified Microfluidic Open Interface. *J. Am. Soc. Mass Spectrom.* **2020**, *32*, 262–269. https://doi.org/10.1021/jasms.0c00303.

(172) Nazdrajić, E.; Murtada, K.; Pawliszyn, J. The Effect of Sorbent Particles in a Binder on the Mass Transfer Kinetics in Separation Media:In Silico Study and Experimental Verification. *Anal. Chem.* **2021**, *93* (44), 14764–14772. https://doi.org/10.1021/acs.analchem.1c03373.

(173) Shaner, R. L.; Schulze, N. D.; Seymour, C.; Hamelin, E. I.; Thomas, J. D.; Johnson, R. C. Quantitation of Fentanyl Analogs in Dried Blood Spots by Flow-through Desorption Coupled to Online Solid Phase Extraction Tandem Mass Spectrometry. *Anal. Methods* **2017**, *9* (25), 3876–3883. https://doi.org/10.1039/c7ay00532f.

(174) Jung, J.; Kolodziej, A.; Pape, E.; Bisch, M.; Javot, L.; Gibaja, V.; Jouzeau, J. Y.; Scala-Bertola, J.; Gambier, N. Multiplex Detection of 14 Fentanyl Analogues and U-47700 in Biological Samples: Application to a Panel of French Hospitalized Patients. *Forensic Sci. Int.* **2020**, *317*. https://doi.org/10.1016/j.forsciint.2020.110437.

(175) Bergh, M. S. S.; Bogen, I. L.; Wilson, S. R.; Øiestad, Å. M. L. Addressing the Fentanyl Analogue Epidemic by Multiplex UHPLC-MS/MS Analysis of Whole Blood. *Ther. Drug Monit.* **2018**, *40* (6), 738–748. https://doi.org/10.1097/FTD.0000000000000564.

(176) Rab, E.; Flanagan, R. J.; Hudson, S. Detection of Fentanyl and Fentanyl Analogues in Biological Samples Using Liquid Chromatography–High Resolution Mass Spectrometry. *Forensic Sci. Int.* **2019**, *300*, 13–18. https://doi.org/10.1016/j.forsciint.2019.04.008.

(177) Xia, Y.; Whitesides, G. M. Soft Lithography. *Annu. Rev. Mater. Sci.* **1998**, *28* (1), 153–184. https://doi.org/10.1146/annurev.matsci.28.1.153.

(178) Dogru, S.; Yilmaz, E.; Soylak, S. B. G. M. An Easy and Green Amine - Based Microextraction Strategy Combined UV – Vis Spectrophotometric Detection for Mercury in Natural Water Samples. *J. Iran. Chem. Soc.* **2021**, No. 0123456789. https://doi.org/10.1007/s13738-021-02256-2.

(179) Ray, R.; Prabhu, A.; Prasad, D.; Aminabhavi, M.; Kumar, N.; Simal-gandara, J. Paper-Based Microfluidic Devices for Food Adulterants : Cost-Effective Technological Monitoring Systems. *Food Chem.* **2022**, *390* (January), 133173. https://doi.org/10.1016/j.foodchem.2022.133173.

(180) Ghafary, Z.; Hallaj, R.; salimi, A.; Mafakheri, S. Ultrasensitive Fluorescence Immunosensor Based on Mesoporous Silica and Magnetic Nanoparticles: Capture and Release Strategy. *Spectrochim. Acta - Part A Mol. Biomol. Spectrosc.* **2021**, *257*, 119749. https://doi.org/10.1016/j.saa.2021.119749.

(181) Okwundu, C. I.; Saini, S. S. Noninvasive Methods for Bilirubin Measurements in Newborns: A Report. *Semin. Perinatol.* **2020**, *2*, 151355. https://doi.org/10.1016/j.semperi.2020.151355.

(182) Pena-Pereira, F.; Costas-Mora, I.; Romero, V.; Lavilla, I.; Bendicho, C. Advances in Miniaturized UV-Vis Spectrometric Systems. *TrAC - Trends Anal. Chem.* **2011**, *30* (10), 1637–1648. https://doi.org/10.1016/j.trac.2011.04.018.

(183) Tan, W.; Zhang, L.; Doery, J. C. G. .; Shen, W. Three-Dimensional Microfluidic Tape-Paper-Based Sensing Device for Blood Total Bilirubin Measurement in Jaundiced Neonates. **2014**, 2539–2547. https://doi.org/10.1039/c4lc00188e.

(184) Li, H. F.; Lin, J. M. Applications of Microfluidic Systems in Environmental Analysis. *Anal. Bioanal. Chem.* **2009**, *393* (2), 555–567. https://doi.org/10.1007/s00216-008-2439-4.

(185) Zou, Y.; Zhang, Y.; Xu, Y.; Chen, Y.; Huang, S.; Lyu, Y.; Duan, H.; Chen, Z.; Tan, W. Portable and Label-Free Detection of Blood Bilirubin with Graphene-Isolated-Au-Nanocrystals Paper Strip. *Anal. Chem.* **2018**, *90* (22), 13687–13694. https://doi.org/10.1021/acs.analchem.8b04058.

(186) Lee SK, Sheridan M, M. A. (2005) T. Novel UV-Activated Colorimetric Oxygen Indicator. Chem Mater 17(10):2744–2751. *Chem. Mater.* **2005**, *2* (7), 2744–2751. https://doi.org/10.1021/cm0403863.

(187) Hu, J.; Li, C.; Cui, Y.; Liu, S. Highly Selective Colorimetric and Fluorometric Probes for Fluoride Ions Based on Nitrobenzofurazan-Containing Polymers. *Macromol. Rapid Commun.* **2011**, *32* (7), 610–615. https://doi.org/10.1002/marc.201100024.

(188) Haggart, R.; Thorpe, G. H.; Moseley, S. B.; Kricka, L. J.; Whitehead, T. P. An Enhanced Chemiluminescent Enzyme Immunoassay for Serum Carcinoembryonic Antigen Based on a Modification of a Commercial Kit. *J. Biolumin. Chemilumin.* **1986**, *1* (1), 29–34. https://doi.org/10.1002/bio.1170010106.

(189) Melucci, D.; Roda, B.; Zattoni, A.; Casolari, S.; Reschiglian, P.; Roda, A. Field-Flow Fractionation of Cells with Chemiluminescence Detection. *J. Chromatogr. A* **2004**, *1056* (1-2 SPEC.ISS.), 229–236. https://doi.org/10.1016/j.chroma.2004.08.084.

(190) Zhang, Y.; Tseng, T.; Schlichtmann, U. HardwareX ColoriSens : An Open-Source and Low-Cost Portable Color Sensor Board for Microfluidic Integration with Wireless Communication and Fluorescence Detection. *HardwareX* **2022**, *11*, e00312. https://doi.org/10.1016/j.ohx.2022.e00312.

(191) Ro, K. W.; Lim, K.; Shim, B. C.; Hahn, J. H. Integrated Light Collimating System for Extended Optical-Path-Length Absorbance Detection in Microchip-Based Capillary Electrophoresis. *Anal. Chem.* **2005**, *77* (16), 5160–5166. https://doi.org/10.1021/ac050420c.

(192) Kuswandi, B.; Nuriman; Huskens, J.; Verboom, W. Optical Sensing Systems for Microfluidic Devices: A Review. *Anal. Chim. Acta* **2007**, *601* (2), 141–155. https://doi.org/10.1016/j.aca.2007.08.046.

(193) Reyes, D. R.; Iossifidis, D.; Auroux, P. A.; Manz, A. Micro Total Analysis Systems. 1. Introduction, Theory, and Technology. *Anal. Chem.* **2002**, *74* (12), 2623–2636. https://doi.org/10.1021/ac0202435.

(194) Hata, K.; Kichise, Y.; Kaneta, T.; Imasaka, T. Hadamard Transform Microchip Electrophoresis Combined with Diode Laser Fluorometry. *Anal. Chem.* **2003**, *75* (7), 1765–1768. https://doi.org/10.1021/ac026330e.

(195) Peng, G.; He, Q.; Lu, Y.; Huang, J.; Lin, J. M. Flow Injection Microfluidic Device with On-Line Fluorescent Derivatization for the Determination of Cr(III) and Cr(VI) in Water Samples after Solid Phase Extraction. *Anal. Chim. Acta* **2017**, *955*, 58–66. https://doi.org/10.1016/j.aca.2016.11.057.

(196) Minas, G.; Martins, J. S.; Ribeiro, J. C.; Wolffenbuttel, R. F.; Correia, J. H. Biological Microsystem for Measuring Uric Acid in Biological Fluids. *Sensors Actuators, A Phys.* **2004**, *110* (1–3), 33–38. https://doi.org/10.1016/j.sna.2003.10.049.

(197) Hofmann, O.; Voirin, G.; Niedermann, P.; Manz, A. Three-Dimensional Microfluidic Confinement for Efficient Sample Delivery to Biosensor Surfaces. Application to Immunoassays on Planar Optical Waveguides. *Anal. Chem.* **2002**, *74* (20), 5243–5250. https://doi.org/10.1021/ac025777k.

(198) Jorgensen, A. M.; Mogensen, K. B.; Kutter, J. P.; Geschke, O. A Biochemical Microdevice with an Integrated Chemiluminescence Detector. *Sensors Actuators, B Chem.* **2003**, *90* (1–3), 15–21. https://doi.org/10.1016/S0925-4005(03)00016-9.

(199) Hong, J.; Choi, J. S.; Han, G.; Kang, J. K.; Kim, C. M.; Kim, T. S.; Yoon, D. S. A Mach-Zehnder Interferometer Based on Silicon Oxides for Biosensor Applications. *Anal. Chim. Acta* **2006**, *573–574*, 97–103. https://doi.org/10.1016/j.aca.2006.04.045.

(200) Sengupta, J.; Hussain, C. M. Graphene and Its Derivatives for Analytical Lab on Chip Platforms. *TrAC - Trends Anal. Chem.* **2019**, *114*, 326–337. https://doi.org/10.1016/j.trac.2019.03.015.

(201) Abgrall, P.; Gué, A. M. Lab-on-Chip Technologies: Making a Microfluidic Network and Coupling It into a Complete Microsystem - A Review. *J. Micromechanics Microengineering* **2007**, *17* (5). https://doi.org/10.1088/0960-1317/17/5/R01.

(202) Chen, Y.; Fu, Q.; Li, D.; Xie, J.; Ke, D.; Song, Q.; Tang, Y.; Wang, H. A Smartphone Colorimetric Reader Integrated with an Ambient Light Sensor and a 3D Printed Attachment for On-Site Detection of Zearalenone. *Anal. Bioanal. Chem.* **2017**, *409* (28), 6567–6574. https://doi.org/10.1007/s00216-017-0605-2.

(203) Mutlu, A. Y.; Kiliç, V.; Özdemir, G. K.; Bayram, A.; Horzum, N.; Solmaz, M. E. Smartphone-Based Colorimetric Detection: Via Machine Learning. *Analyst* **2017**, *142* (13), 2434–2441. https://doi.org/10.1039/c7an00741h.

(204) Pawliszyn, J. Chemical Sensing Using Concentration Gradient Transients Produced during Diffusive Transport of Analytes. *Anal. Chem.* **1992**, *64* (14), 1552–1555. https://doi.org/10.1021/ac00038a010.

(205) Pawliszyn, J. Concentration Gradient Detection Based on Schlieren Optics. *Spectrochimica acta reviews*. 1990, pp 311–354.

(206) Wei, F.; Huaxue, J.; Yin, W.; Yuchen, F. The Influence of Software Timing Error on Measurement Accuracy of Data Acquisition. *Meas. Control (United Kingdom)* **2019**, *52* (7–8), 1008–1016. https://doi.org/10.1177/0020294019858093.

Appendix A: Code written in Visual Basic, Visual Studio 2019

This Appendix contains compressed code (without comments and de-formatted) used to make the prototype software (Software development).

```
1. Imports NationalInstruments.DAQmx
2. Imports System
3. Imports System.Threading
4. Imports System.IO.Ports
5. Imports System.ComponentModel
6. Imports System.IO
7. Imports System.Collections.Generic
8. Imports System.Text
9. Imports System.Runtime.InteropServices
10. Public Class MainForm
11. Inherits System.Windows.Forms.Form
12. <DllImport("winmm.dll")> Private Shared Function mmtimer(ByVal command As String, ByVal buffer As
    StringBuilder, ByVal bufferSize As Integer, ByVal hwndCallback As IntPtr) As Integer
13. End Function
14. Dim file As System.IO.StreamWriter
15. Dim myPort As Array
16. Delegate Sub SetTextCallBack(ByVal [text] As String)
17. Private myTask As Task  'Main Task which is Assigned when the Start Button is Clicked
18. Private runningTask As Task
19. Private data As AnalogWaveform(Of Double)()
20. Private analogInReader As AnalogMultiChannelReader
21. Private analogCallback As AsyncCallback
22. Private dataColumn As DataColumn()
23. Private myTaskPI2 As Task 'Task for photointerrupter2'
24. Private runningTaskPI2 As Task
25. Private dataPI2 As AnalogWaveform(Of Double)()
26. Private analogInReaderPI2 As AnalogMultiChannelReader
27. Private analogCallbackPI2 As AsyncCallback
28. Private dataColumnPI2 As DataColumn()
29. Private myTaskPI3 As Task 'Task for photointerrupter2'
30. Private runningTaskPI3 As Task
31. Private dataPI3 As AnalogWaveform(Of Double)()
32. Private analogInReaderPI3 As AnalogMultiChannelReader
33. Private analogCallbackPI3 As AsyncCallback
34. Private dataColumnPI3 As DataColumn()
35. Friend WithEvents TabControl1 As System.Windows.Forms.TabControl
36. Friend WithEvents TabPage1 As System.Windows.Forms.TabPage
37. Friend WithEvents TabPage2 As System.Windows.Forms.TabPage
38. Friend WithEvents TabPage3 As System.Windows.Forms.TabPage
39. Friend WithEvents TabPage4 As System.Windows.Forms.TabPage
40. Friend WithEvents channelParametersGroupBoxPI1 As System.Windows.Forms.GroupBox
41. Friend WithEvents minimumValueNumericPI1 As System.Windows.Forms.NumericUpDown
42. Friend WithEvents maximumValueNumericPI1 As System.Windows.Forms.NumericUpDown
43. Friend WithEvents maximumLabel As System.Windows.Forms.Label
44. Friend WithEvents minimumLabel As System.Windows.Forms.Label
45. Friend WithEvents physicalChannelLabel As System.Windows.Forms.Label
46. Friend WithEvents acquisitionResultGroupBox As System.Windows.Forms.GroupBox
47. Friend WithEvents resultLabel As System.Windows.Forms.Label
48. Friend WithEvents acquisitionDataGrid As System.Windows.Forms.DataGrid
49. Friend WithEvents timingParametersGroupBoxPI1 As System.Windows.Forms.GroupBox
```

50. Friend WithEvents samplesPerChannelNumericPI1 As System.Windows.Forms.NumericUpDown
51. Friend WithEvents rateNumericPI1 As System.Windows.Forms.NumericUpDown
52. Friend WithEvents rateLabel As System.Windows.Forms.Label
53. Friend WithEvents samplesLabel As System.Windows.Forms.Label
54. Friend WithEvents physicalChannelComboBoxPI1 As System.Windows.Forms.ComboBox
55. Friend WithEvents btnNexttab0 As System.Windows.Forms.Button
56. Friend WithEvents TabPage5 As System.Windows.Forms.TabPage
57. Friend WithEvents btnNexttab1 As System.Windows.Forms.Button
58. Friend WithEvents btnPrevioustab1 As System.Windows.Forms.Button
59. Friend WithEvents grpboxSyringepump1 As System.Windows.Forms.GroupBox
60. Friend WithEvents cmbboxBaudratepump1 As System.Windows.Forms.ComboBox
61. Friend WithEvents btnConnect1 As System.Windows.Forms.Button
62. Friend WithEvents cmbboxSyringepump1 As System.Windows.Forms.ComboBox
63. Friend WithEvents lbllistparameterspump1 As System.Windows.Forms.Label
64. Friend WithEvents btnDisconnect1 As System.Windows.Forms.Button
65. Friend WithEvents lblparameterspump1 As System.Windows.Forms.Label
66. Friend WithEvents lblCOMPort1 As System.Windows.Forms.Label
67. Friend WithEvents lblBaudrate1 As System.Windows.Forms.Label
68. Friend WithEvents btnclearallports As System.Windows.Forms.Button
69. Friend WithEvents btnscanforports As System.Windows.Forms.Button
70. Friend WithEvents btnNexttab2 As System.Windows.Forms.Button
71. Friend WithEvents btnPrevioustab2 As System.Windows.Forms.Button
72. Friend WithEvents btnNexttab3 As System.Windows.Forms.Button
73. Friend WithEvents btnPrevioustab3 As System.Windows.Forms.Button
74. Friend WithEvents serialportSyringepump1 As System.IO.Ports.SerialPort
75. Friend WithEvents serialportSyringepump2 As System.IO.Ports.SerialPort
76. Friend WithEvents chartPI1 As System.Windows.Forms.DataVisualization.Charting.Chart
77. Friend WithEvents ChartingtimerPI1 As System.Windows.Forms.Timer
78. Friend WithEvents btnStopcollectionchart As System.Windows.Forms.Button
79. Friend WithEvents GroupBox2 As System.Windows.Forms.GroupBox
80. Friend WithEvents btnSend1sendcommands As System.Windows.Forms.Button
81. Friend WithEvents txtboxInput1sendcommands As System.Windows.Forms.TextBox
82. Friend WithEvents lblOutput1sendcommands As System.Windows.Forms.Label
83. Friend WithEvents Label7 As System.Windows.Forms.Label
84. Friend WithEvents Label6 As System.Windows.Forms.Label
85. Friend WithEvents btnPreviousMethods As System.Windows.Forms.Button
86. Friend WithEvents watchPI1timer As System.Windows.Forms.Timer
87. Private dataTable As DataTable = New DataTable
88. Private dataTablePI2 As DataTable = New DataTable
89. Private dataTablePI3 As DataTable = New DataTable
90. Dim counter1 As Integer = 0
91. Dim counter2 As Integer = 0
92. Dim counter3 As Integer = 0
93. Dim counter4 As Integer = 0
94. Dim counter5 As Integer = 0
95. Dim counter6 As Integer = 0
96. Dim counter7 As Integer = 0
97. Dim counter8 As Integer = 0
98. Dim counterDesorption As Integer = 0
99. Dim counterauto1 As Decimal = 0
100. Dim counterautosuctiontime As Integer = 0
101. Dim n As Integer = 0
102. Dim suctiontimecutoff As Integer = 0
103. Dim suctiontimecutoffdatacollection As Integer = 0
104. Dim timeleft As Integer = 0
105. Dim setflowrate As Integer = 0
106. Dim fillingflowrate As Integer = 0
107. Dim filluptime As Decimal = 0
108. Dim washwaitcounter As Integer = 0
109. Dim timefullchamber As Decimal = 0
110. Dim suctionflowrate As Integer = 0
111. Dim currentpumpflowrate As Integer = 0

```
112. Dim washtime As Integer = 0
113. Dim desorptiontimestopwatch As New Stopwatch
114. Dim filluptimestopwatch As New Stopwatch
115. Dim suctiontimestopwatch As New Stopwatch
116. Dim washwaitstopwatch As New Stopwatch
117. Dim photointerrupterstopwatchPI1 As New Stopwatch
118. Dim photointerrupterstopwatchPI2 As New Stopwatch
119. Dim photointerrupterstopwatchPI3 As New Stopwatch
120. Dim suctiontimestopwatchPI1 As New Stopwatch
121. Dim washing200ulminstopwatch As New Stopwatch
122. Dim elapseddesorptiontime As Integer
123. Dim elapsedsuctiontime As Integer
124. Dim elapsedfilluptime As Integer
125. Dim elapsedwashswait As Integer
126. Dim suctiontimePI1 As Integer
127. Dim washing200ulmintime As Integer
128. Dim washingulmin As Integer
129. Dim newpumpflowrate As Integer = 0
130. Dim elapsedtimePI1 As Integer
131. Dim elapsedtimePI2 As Integer
132. Dim elapsedtimePI3 As Integer
133. Friend WithEvents adjustmentpi2timer As System.Windows.Forms.Timer
134.         Friend WithEvents grpboxSyringepump1parametersforrunning As System.Windows.Forms.GroupBox
135. Friend WithEvents cmbboxInfusewithdraw1 As System.Windows.Forms.ComboBox
136. Friend WithEvents lblForce1 As System.Windows.Forms.Label
137. Friend WithEvents cmbboxForce1 As System.Windows.Forms.ComboBox
138. Friend WithEvents txtboxTargetvolume1 As System.Windows.Forms.TextBox
139. Friend WithEvents cmbboxTargetvolume1 As System.Windows.Forms.ComboBox
140. Friend WithEvents txtboxRate1 As System.Windows.Forms.TextBox
141. Friend WithEvents lblTargetVolume1 As System.Windows.Forms.Label
142. Friend WithEvents cmbboxSyringeselect1 As System.Windows.Forms.ComboBox
143. Friend WithEvents cmbboxRate1 As System.Windows.Forms.ComboBox
144. Friend WithEvents lblRate1 As System.Windows.Forms.Label
145. Friend WithEvents lblInfusewithdraw1 As System.Windows.Forms.Label
146. Friend WithEvents lblSyringeselect1 As System.Windows.Forms.Label
147. Friend WithEvents lblListcurrentpump1parameters As System.Windows.Forms.Label
148. Friend WithEvents lblCurrentpump1parameters As System.Windows.Forms.Label
149. Friend WithEvents btnCheckcurrent1 As System.Windows.Forms.Button
150. Friend WithEvents grpboxRunpumpstogether As System.Windows.Forms.GroupBox
151. Friend WithEvents btnLoadMethod As System.Windows.Forms.Button
152. Friend WithEvents btnSavemethod As System.Windows.Forms.Button
153. Friend WithEvents btnClearall As System.Windows.Forms.Button
154. Friend WithEvents btnSubmit1 As System.Windows.Forms.Button
155. Friend WithEvents DesorptionTimer As System.Windows.Forms.Timer
156. Friend WithEvents lblDesorptiontimer As System.Windows.Forms.Label
157. Friend WithEvents btnStartauto As System.Windows.Forms.Button
158. Friend WithEvents DesorptionTimerauto As System.Windows.Forms.Timer
159. Friend WithEvents lblbroken As System.Windows.Forms.Label
160. Friend WithEvents grpboxRunparametersauto As System.Windows.Forms.GroupBox
161. Friend WithEvents Label3 As System.Windows.Forms.Label
162. Friend WithEvents Label1 As System.Windows.Forms.Label
163. Friend WithEvents lblcurrentsuctiontime As System.Windows.Forms.Label
164. Friend WithEvents Label4 As System.Windows.Forms.Label
165. Friend WithEvents washingtimer200ulmin As System.Windows.Forms.Timer
166. Friend WithEvents washwaittimer As System.Windows.Forms.Timer
167. Friend WithEvents lblwash200ulmintimer As System.Windows.Forms.Label
168. Friend WithEvents Label5 As System.Windows.Forms.Label
169. Friend WithEvents btnStopauto As System.Windows.Forms.Button
170. Friend WithEvents lblcurrentpumpflowrate As System.Windows.Forms.Label
171. Friend WithEvents Label14 As System.Windows.Forms.Label
172. Friend WithEvents txtboxDesorptiontimeauto As System.Windows.Forms.TextBox
173. Friend WithEvents Label16 As System.Windows.Forms.Label
```

```
Friend WithEvents GroupBox4 As GroupBox
Friend WithEvents channelParametersGroupBoxPI2 As GroupBox
Friend WithEvents physicalChannelComboBoxPI2 As ComboBox
Friend WithEvents minimumValueNumericPI2 As NumericUpDown
Friend WithEvents maximumValueNumericPI2 As NumericUpDown
Friend WithEvents Label17 As Label
Friend WithEvents lbltest2 As Label
Friend WithEvents Label18 As Label
Friend WithEvents Label19 As Label
Friend WithEvents timingParametersGroupBoxPI2 As GroupBox
Friend WithEvents samplesPerChannelNumericPI2 As NumericUpDown
Friend WithEvents rateNumericPI2 As NumericUpDown
Friend WithEvents Label20 As Label
Friend WithEvents Label21 As Label
Friend WithEvents GroupBox8 As GroupBox
Friend WithEvents Label22 As Label
Friend WithEvents acquisitionDataGridPI2 As DataGrid
Friend WithEvents GroupBox1 As GroupBox
Friend WithEvents btnStopPI2 As Button
Friend WithEvents btnStartPI2 As Button
Friend WithEvents btnStopPI1 As Button
Friend WithEvents btnStartPI1 As Button
Friend WithEvents lblreadingPI1 As Label
Friend WithEvents lblreadingPI2 As Label
Friend WithEvents lblreadingPI1_1 As Label
Friend WithEvents lblreadingPI2_1 As Label
Friend WithEvents photointerruptertimerPI1 As Windows.Forms.Timer
Friend WithEvents photointerruptertimerPI2 As Windows.Forms.Timer
Friend WithEvents photointerruptertimerPI3 As Windows.Forms.Timer
Friend WithEvents chartPI2 As DataVisualization.Charting.Chart
Friend WithEvents ChartingtimerPI2 As Windows.Forms.Timer
Friend WithEvents ChartingtimerPI3 As Windows.Forms.Timer
Friend WithEvents txtboxdesorptionvolume As TextBox
Friend WithEvents Label2 As Label
Friend WithEvents btnDrainauto As Button
Friend WithEvents txtboxWashflowrate As TextBox
Friend WithEvents Label13 As Label
Friend WithEvents lblgraphreadingPI2 As Label
Friend WithEvents Label15 As Label
Friend WithEvents lblgraphreadingPI1 As Label
Friend WithEvents Label10 As Label
Friend WithEvents txtboxWashtime As TextBox
Friend WithEvents grpboxSaveloadmethodMS As GroupBox
Friend WithEvents btnLoadMS As Button
Friend WithEvents btnSaveMS As Button
Friend WithEvents Label11 As Label
Public Sub New()
MyBase.New()
Application.EnableVisualStyles()
InitializeComponent()
analogCallback = New AsyncCallback(AddressOf AnalogInCallback)
        physicalChannelComboBoxPI1.Items.AddRange(DaqSystem.Local.GetPhysicalChannels(PhysicalChannelTy
        pes.AI, PhysicalChannelAccess.External))
If (physicalChannelComboBoxPI1.Items.Count > 0) Then
physicalChannelComboBoxPI1.SelectedIndex = 1
        End If
        physicalChannelComboBoxPI2.Items.AddRange(DaqSystem.Local.GetPhysicalChannels(PhysicalChannelTy
        pes.AI, PhysicalChannelAccess.External))
If (physicalChannelComboBoxPI2.Items.Count > 0) Then
physicalChannelComboBoxPI2.SelectedIndex = 2
End If
End Sub
```

```
233. Protected Overloads Overrides Sub Dispose(ByVal disposing As Boolean)
234. If disposing Then
235. If Not (components Is Nothing) Then
236. components.Dispose()
237. End If
238. If Not (myTask Is Nothing) Then
239. runningTask = Nothing
240. myTask.Dispose()
241. End If
242. End If
243. MyBase.Dispose(disposing)
244. End Sub
245. Private components As System.ComponentModel.IContainer
246. <System.Diagnostics.DebuggerStepThrough()> Private Sub InitializeComponent()
247. Me.components = New System.ComponentModel.Container()
248. Dim ChartArea1 As System.Windows.Forms.DataVisualization.Charting.ChartArea = New
     System.Windows.Forms.DataVisualization.Charting.ChartArea()
249. Dim Legend1 As System.Windows.Forms.DataVisualization.Charting.Legend = New
     System.Windows.Forms.DataVisualization.Charting.Legend()
250. Dim Series1 As System.Windows.Forms.DataVisualization.Charting.Series = New
     System.Windows.Forms.DataVisualization.Charting.Series()
251. Dim ChartArea2 As System.Windows.Forms.DataVisualization.Charting.ChartArea = New
     System.Windows.Forms.DataVisualization.Charting.ChartArea()
252. Dim Legend2 As System.Windows.Forms.DataVisualization.Charting.Legend = New
     System.Windows.Forms.DataVisualization.Charting.Legend()
253. Dim Series2 As System.Windows.Forms.DataVisualization.Charting.Series = New
     System.Windows.Forms.DataVisualization.Charting.Series()
254. Dim resources As System.ComponentModel.ComponentResourceManager = New
     System.ComponentModel.ComponentResourceManager(GetType(MainForm))
255. Me.TabControl1 = New System.Windows.Forms.TabControl()
256. Me.TabPage1 = New System.Windows.Forms.TabPage()
257. Me.grpboxSaveloadmethodMS = New System.Windows.Forms.GroupBox()
258. Me.btnLoadMS = New System.Windows.Forms.Button()
259. Me.btnSaveMS = New System.Windows.Forms.Button()
260. Me.GroupBox4 = New System.Windows.Forms.GroupBox()
261. Me.channelParametersGroupBoxPI2 = New System.Windows.Forms.GroupBox()
262. Me.physicalChannelComboBoxPI2 = New System.Windows.Forms.ComboBox()
263. Me.minimumValueNumericPI2 = New System.Windows.Forms.NumericUpDown()
264. Me.maximumValueNumericPI2 = New System.Windows.Forms.NumericUpDown()
265. Me.Label17 = New System.Windows.Forms.Label()
266. Me.Label18 = New System.Windows.Forms.Label()
267. Me.Label19 = New System.Windows.Forms.Label()
268. Me.timingParametersGroupBoxPI2 = New System.Windows.Forms.GroupBox()
269. Me.samplesPerChannelNumericPI2 = New System.Windows.Forms.NumericUpDown()
270. Me.rateNumericPI2 = New System.Windows.Forms.NumericUpDown()
271. Me.Label20 = New System.Windows.Forms.Label()
272. Me.Label21 = New System.Windows.Forms.Label()
273. Me.GroupBox8 = New System.Windows.Forms.GroupBox()
274. Me.lblreadingPI2_1 = New System.Windows.Forms.Label()
275. Me.Label22 = New System.Windows.Forms.Label()
276. Me.acquisitionDataGridPI2 = New System.Windows.Forms.DataGrid()
277. Me.lblreadingPI2 = New System.Windows.Forms.Label()
278. Me.btnStopPI2 = New System.Windows.Forms.Button()
279. Me.btnStartPI2 = New System.Windows.Forms.Button()
280. Me.GroupBox1 = New System.Windows.Forms.GroupBox()
281. Me.channelParametersGroupBoxPI1 = New System.Windows.Forms.GroupBox()
282. Me.physicalChannelComboBoxPI1 = New System.Windows.Forms.ComboBox()
283. Me.minimumValueNumericPI1 = New System.Windows.Forms.NumericUpDown()
284. Me.maximumValueNumericPI1 = New System.Windows.Forms.NumericUpDown()
285. Me.maximumLabel = New System.Windows.Forms.Label()
286. Me.minimumLabel = New System.Windows.Forms.Label()
287. Me.physicalChannelLabel = New System.Windows.Forms.Label()
```

```
288. Me.timingParametersGroupBoxPI1 = New System.Windows.Forms.GroupBox()
289. Me.samplesPerChannelNumericPI1 = New System.Windows.Forms.NumericUpDown()
290. Me.rateNumericPI1 = New System.Windows.Forms.NumericUpDown()
291. Me.rateLabel = New System.Windows.Forms.Label()
292. Me.samplesLabel = New System.Windows.Forms.Label()
293. Me.acquisitionResultGroupBox = New System.Windows.Forms.GroupBox()
294. Me.lblreadingPI1_1 = New System.Windows.Forms.Label()
295. Me.resultLabel = New System.Windows.Forms.Label()
296. Me.acquisitionDataGrid = New System.Windows.Forms.DataGrid()
297. Me.lblreadingPI1 = New System.Windows.Forms.Label()
298. Me.btnStopPI1 = New System.Windows.Forms.Button()
299. Me.btnStartPI1 = New System.Windows.Forms.Button()
300. Me.grpboxRunparametersauto = New System.Windows.Forms.GroupBox()
301. Me.txtboxWashtime = New System.Windows.Forms.TextBox()
302. Me.Label11 = New System.Windows.Forms.Label()
303. Me.txtboxWashflowrate = New System.Windows.Forms.TextBox()
304. Me.Label13 = New System.Windows.Forms.Label()
305. Me.btnDrainauto = New System.Windows.Forms.Button()
306. Me.txtboxdesorptionvolume = New System.Windows.Forms.TextBox()
307. Me.Label2 = New System.Windows.Forms.Label()
308. Me.txtboxDesorptiontimeauto = New System.Windows.Forms.TextBox()
309. Me.lblDesorptiontimer = New System.Windows.Forms.Label()
310. Me.Label1 = New System.Windows.Forms.Label()
311. Me.Label16 = New System.Windows.Forms.Label()
312. Me.btnStopauto = New System.Windows.Forms.Button()
313. Me.lblcurrentpumpflowrate = New System.Windows.Forms.Label()
314. Me.Label14 = New System.Windows.Forms.Label()
315. Me.lblwash200ulmintimer = New System.Windows.Forms.Label()
316. Me.Label5 = New System.Windows.Forms.Label()
317. Me.lblcurrentsuctiontime = New System.Windows.Forms.Label()
318. Me.Label4 = New System.Windows.Forms.Label()
319. Me.Label3 = New System.Windows.Forms.Label()
320. Me.btnStartauto = New System.Windows.Forms.Button()
321. Me.lblbroken = New System.Windows.Forms.Label()
322. Me.btnNexttab0 = New System.Windows.Forms.Button()
323. Me.TabPage2 = New System.Windows.Forms.TabPage()
324. Me.lblgraphreadingPI2 = New System.Windows.Forms.Label()
325. Me.Label15 = New System.Windows.Forms.Label()
326. Me.lblgraphreadingPI1 = New System.Windows.Forms.Label()
327. Me.Label10 = New System.Windows.Forms.Label()
328. Me.chartPI2 = New System.Windows.Forms.DataVisualization.Charting.Chart()
329. Me.btnStopcollectionchart = New System.Windows.Forms.Button()
330. Me.chartPI1 = New System.Windows.Forms.DataVisualization.Charting.Chart()
331. Me.btnNexttab1 = New System.Windows.Forms.Button()
332. Me.btnPrevioustab1 = New System.Windows.Forms.Button()
333. Me.TabPage3 = New System.Windows.Forms.TabPage()
334. Me.grpboxSyringepump1 = New System.Windows.Forms.GroupBox()
335. Me.cmbboxBaudratepump1 = New System.Windows.Forms.ComboBox()
336. Me.btnConnect1 = New System.Windows.Forms.Button()
337. Me.cmbboxSyringepump1 = New System.Windows.Forms.ComboBox()
338. Me.lbllistparameterspump1 = New System.Windows.Forms.Label()
339. Me.btnDisconnect1 = New System.Windows.Forms.Button()
340. Me.lblparameterspump1 = New System.Windows.Forms.Label()
341. Me.lblCOMPort1 = New System.Windows.Forms.Label()
342. Me.lblBaudrate1 = New System.Windows.Forms.Label()
343. Me.btnclearallports = New System.Windows.Forms.Button()
344. Me.btnscanforports = New System.Windows.Forms.Button()
345. Me.btnNexttab2 = New System.Windows.Forms.Button()
346. Me.btnPrevioustab2 = New System.Windows.Forms.Button()
347. Me.TabPage4 = New System.Windows.Forms.TabPage()
348. Me.GroupBox2 = New System.Windows.Forms.GroupBox()
349. Me.btnSend1sendcommands = New System.Windows.Forms.Button()
```

```
350. Me.txtboxInput1sendcommands = New System.Windows.Forms.TextBox()
351. Me.lblOutput1sendcommands = New System.Windows.Forms.Label()
352. Me.Label7 = New System.Windows.Forms.Label()
353. Me.Label6 = New System.Windows.Forms.Label()
354. Me.btnNexttab3 = New System.Windows.Forms.Button()
355. Me.btnPrevioustab3 = New System.Windows.Forms.Button()
356. Me.TabPage5 = New System.Windows.Forms.TabPage()
357. Me.grpboxRunpumpstogether = New System.Windows.Forms.GroupBox()
358. Me.btnLoadMethod = New System.Windows.Forms.Button()
359. Me.btnSavemethod = New System.Windows.Forms.Button()
360. Me.btnClearall = New System.Windows.Forms.Button()
361.         Me.grpboxSyringepump1parametersforrunning = New System.Windows.Forms.GroupBox()
362. Me.btnSubmit1 = New System.Windows.Forms.Button()
363. Me.lblListcurrentpump1parameters = New System.Windows.Forms.Label()
364. Me.lblCurrentpump1parameters = New System.Windows.Forms.Label()
365. Me.btnCheckcurrent1 = New System.Windows.Forms.Button()
366. Me.lblForce1 = New System.Windows.Forms.Label()
367. Me.txtboxTargetvolume1 = New System.Windows.Forms.TextBox()
368. Me.cmbboxTargetvolume1 = New System.Windows.Forms.ComboBox()
369. Me.txtboxRate1 = New System.Windows.Forms.TextBox()
370. Me.cmbboxForce1 = New System.Windows.Forms.ComboBox()
371. Me.lblTargetVolume1 = New System.Windows.Forms.Label()
372. Me.cmbboxSyringeselect1 = New System.Windows.Forms.ComboBox()
373. Me.cmbboxRate1 = New System.Windows.Forms.ComboBox()
374. Me.lblRate1 = New System.Windows.Forms.Label()
375. Me.lblInfusewithdraw1 = New System.Windows.Forms.Label()
376. Me.lblSyringeselect1 = New System.Windows.Forms.Label()
377. Me.cmbboxInfusewithdraw1 = New System.Windows.Forms.ComboBox()
378. Me.btnPreviousMethods = New System.Windows.Forms.Button()
379. Me.serialportSyringepump1 = New System.IO.Ports.SerialPort(Me.components)
380. Me.serialportSyringepump2 = New System.IO.Ports.SerialPort(Me.components)
381. Me.ChartingtimerPI1 = New System.Windows.Forms.Timer(Me.components)
382. Me.watchPI1timer = New System.Windows.Forms.Timer(Me.components)
383. Me.adjustmentpi2timer = New System.Windows.Forms.Timer(Me.components)
384. Me.DesorptionTimer = New System.Windows.Forms.Timer(Me.components)
385. Me.DesorptionTimerauto = New System.Windows.Forms.Timer(Me.components)
386. Me.washingtimer200ulmin = New System.Windows.Forms.Timer(Me.components)
387. Me.washwaittimer = New System.Windows.Forms.Timer(Me.components)
388. Me.photointerruptertimerPI1 = New System.Windows.Forms.Timer(Me.components)
389. Me.photointerruptertimerPI2 = New System.Windows.Forms.Timer(Me.components)
390. Me.photointerruptertimerPI3 = New System.Windows.Forms.Timer(Me.components)
391. Me.ChartingtimerPI2 = New System.Windows.Forms.Timer(Me.components)
392. Me.ChartingtimerPI3 = New System.Windows.Forms.Timer(Me.components)
393. Me.TabControl1.SuspendLayout()
394. Me.TabPage1.SuspendLayout()
395. Me.grpboxSaveloadmethodMS.SuspendLayout()
396. Me.GroupBox4.SuspendLayout()
397. Me.channelParametersGroupBoxPI2.SuspendLayout()
398.         CType(Me.minimumValueNumericPI2, System.ComponentModel.ISupportInitialize).BeginInit()
399.         CType(Me.maximumValueNumericPI2, System.ComponentModel.ISupportInitialize).BeginInit()
400. Me.timingParametersGroupBoxPI2.SuspendLayout()
401.         CType(Me.samplesPerChannelNumericPI2, System.ComponentModel.ISupportInitialize).BeginInit()
402. CType(Me.rateNumericPI2, System.ComponentModel.ISupportInitialize).BeginInit()
403. Me.GroupBox8.SuspendLayout()
404.         CType(Me.acquisitionDataGridPI2, System.ComponentModel.ISupportInitialize).BeginInit()
405. Me.GroupBox1.SuspendLayout()
406. Me.channelParametersGroupBoxPI1.SuspendLayout()
407.         CType(Me.minimumValueNumericPI1, System.ComponentModel.ISupportInitialize).BeginInit()
408.         CType(Me.maximumValueNumericPI1, System.ComponentModel.ISupportInitialize).BeginInit()
409. Me.timingParametersGroupBoxPI1.SuspendLayout()
410.         CType(Me.samplesPerChannelNumericPI1, System.ComponentModel.ISupportInitialize).BeginInit()
411. CType(Me.rateNumericPI1, System.ComponentModel.ISupportInitialize).BeginInit()
```

412. Me.acquisitionResultGroupBox.SuspendLayout()
413. CType(Me.acquisitionDataGrid, System.ComponentModel.ISupportInitialize).BeginInit()
414. Me.grpboxRunparametersauto.SuspendLayout()
415. Me.TabPage2.SuspendLayout()
416. CType(Me.chartPI2, System.ComponentModel.ISupportInitialize).BeginInit()
417. CType(Me.chartPI1, System.ComponentModel.ISupportInitialize).BeginInit()
418. Me.TabPage3.SuspendLayout()
419. Me.grpboxSyringepump1.SuspendLayout()
420. Me.TabPage4.SuspendLayout()
421. Me.GroupBox2.SuspendLayout()
422. Me.TabPage5.SuspendLayout()
423. Me.grpboxRunpumpstogether.SuspendLayout()
424. Me.grpboxSyringepump1parametersforrunning.SuspendLayout()
425. Me.SuspendLayout()
426. Me.TabControl1.Controls.Add(Me.TabPage1)
427. Me.TabControl1.Controls.Add(Me.TabPage2)
428. Me.TabControl1.Controls.Add(Me.TabPage3)
429. Me.TabControl1.Controls.Add(Me.TabPage4)
430. Me.TabControl1.Controls.Add(Me.TabPage5)
431. Me.TabControl1.Location = New System.Drawing.Point(1, 1)
432. Me.TabControl1.Name = "TabControl1"
433. Me.TabControl1.SelectedIndex = 0
434. Me.TabControl1.Size = New System.Drawing.Size(1111, 692)
435. Me.TabControl1.TabIndex = 6
436. Me.TabPage1.Controls.Add(Me.grpboxSaveloadmethodMS)
437. Me.TabPage1.Controls.Add(Me.GroupBox4)
438. Me.TabPage1.Controls.Add(Me.GroupBox1)
439. Me.TabPage1.Controls.Add(Me.grpboxRunparametersauto)
440. Me.TabPage1.Controls.Add(Me.btnNexttab0)
441. Me.TabPage1.Location = New System.Drawing.Point(4, 25)
442. Me.TabPage1.Name = "TabPage1"
443. Me.TabPage1.Padding = New System.Windows.Forms.Padding(3)
444. Me.TabPage1.Size = New System.Drawing.Size(1103, 663)
445. Me.TabPage1.TabIndex = 0
446. Me.TabPage1.Text = "MS Flow Control"
447. Me.TabPage1.UseVisualStyleBackColor = True
448. Me.grpboxSaveloadmethodMS.Controls.Add(Me.btnLoadMS)
449. Me.grpboxSaveloadmethodMS.Controls.Add(Me.btnSaveMS)
450. Me.grpboxSaveloadmethodMS.Location = New System.Drawing.Point(630, 366)
451. Me.grpboxSaveloadmethodMS.Name = "grpboxSaveloadmethodMS"
452. Me.grpboxSaveloadmethodMS.Size = New System.Drawing.Size(209, 59)
453. Me.grpboxSaveloadmethodMS.TabIndex = 33
454. Me.grpboxSaveloadmethodMS.TabStop = False
455. Me.grpboxSaveloadmethodMS.Text = "Save/Load Method"
456. Me.btnLoadMS.Location = New System.Drawing.Point(117, 23)
457. Me.btnLoadMS.Name = "btnLoadMS"
458. Me.btnLoadMS.Size = New System.Drawing.Size(75, 23)
459. Me.btnLoadMS.TabIndex = 1
460. Me.btnLoadMS.Text = "Load"
461. Me.btnLoadMS.UseVisualStyleBackColor = True
462. Me.btnSaveMS.Location = New System.Drawing.Point(21, 23)
463. Me.btnSaveMS.Name = "btnSaveMS"
464. Me.btnSaveMS.Size = New System.Drawing.Size(75, 23)
465. Me.btnSaveMS.TabIndex = 0
466. Me.btnSaveMS.Text = "Save"
467. Me.btnSaveMS.UseVisualStyleBackColor = True
468. Me.GroupBox4.Controls.Add(Me.channelParametersGroupBoxPI2)
469. Me.GroupBox4.Controls.Add(Me.timingParametersGroupBoxPI2)
470. Me.GroupBox4.Controls.Add(Me.GroupBox8)
471. Me.GroupBox4.Controls.Add(Me.btnStopPI2)
472. Me.GroupBox4.Controls.Add(Me.btnStartPI2)
473. Me.GroupBox4.Location = New System.Drawing.Point(6, 217)

```
Me.GroupBox4.Name = "GroupBox4"
Me.GroupBox4.Size = New System.Drawing.Size(618, 209)
Me.GroupBox4.TabIndex = 32
Me.GroupBox4.TabStop = False
Me.GroupBox4.Text = "Photointerrupter 2"
Me.channelParametersGroupBoxPI2.Controls.Add(Me.physicalChannelComboBoxPI2)
Me.channelParametersGroupBoxPI2.Controls.Add(Me.minimumValueNumericPI2)
Me.channelParametersGroupBoxPI2.Controls.Add(Me.maximumValueNumericPI2)
Me.channelParametersGroupBoxPI2.Controls.Add(Me.Label17)
Me.channelParametersGroupBoxPI2.Controls.Add(Me.Label18)
Me.channelParametersGroupBoxPI2.Controls.Add(Me.Label19)
        Me.channelParametersGroupBoxPI2.FlatStyle = System.Windows.Forms.FlatStyle.System
Me.channelParametersGroupBoxPI2.Location = New System.Drawing.Point(6, 17)
Me.channelParametersGroupBoxPI2.Name = "channelParametersGroupBoxPI2"
Me.channelParametersGroupBoxPI2.Size = New System.Drawing.Size(279, 90)
Me.channelParametersGroupBoxPI2.TabIndex = 2
Me.channelParametersGroupBoxPI2.TabStop = False
Me.channelParametersGroupBoxPI2.Text = "Channel Parameters"
Me.physicalChannelComboBoxPI2.Location = New System.Drawing.Point(144, 15)
Me.physicalChannelComboBoxPI2.Name = "physicalChannelComboBoxPI2"
Me.physicalChannelComboBoxPI2.Size = New System.Drawing.Size(115, 24)
Me.physicalChannelComboBoxPI2.TabIndex = 1
Me.physicalChannelComboBoxPI2.Text = "Dev1/ai0"
Me.minimumValueNumericPI2.DecimalPlaces = 2
Me.minimumValueNumericPI2.Location = New System.Drawing.Point(144, 40)
Me.minimumValueNumericPI2.Maximum = New Decimal(New Integer() {10, 0, 0, 0})
        Me.minimumValueNumericPI2.Minimum = New Decimal(New Integer() {10, 0, 0, -2147483648})
Me.minimumValueNumericPI2.Name = "minimumValueNumericPI2"
Me.minimumValueNumericPI2.Size = New System.Drawing.Size(115, 22)
Me.minimumValueNumericPI2.TabIndex = 3
        Me.minimumValueNumericPI2.Value = New Decimal(New Integer() {100, 0, 0, -2147418112})
Me.maximumValueNumericPI2.DecimalPlaces = 2
Me.maximumValueNumericPI2.Location = New System.Drawing.Point(144, 63)
Me.maximumValueNumericPI2.Maximum = New Decimal(New Integer() {10, 0, 0, 0})
        Me.maximumValueNumericPI2.Minimum = New Decimal(New Integer() {10, 0, 0, -2147483648})
Me.maximumValueNumericPI2.Name = "maximumValueNumericPI2"
Me.maximumValueNumericPI2.Size = New System.Drawing.Size(115, 22)
Me.maximumValueNumericPI2.TabIndex = 5
Me.maximumValueNumericPI2.Value = New Decimal(New Integer() {100, 0, 0, 65536})
Me.Label17.FlatStyle = System.Windows.Forms.FlatStyle.System
Me.Label17.Location = New System.Drawing.Point(19, 65)
Me.Label17.Name = "Label17"
Me.Label17.Size = New System.Drawing.Size(135, 18)
Me.Label17.TabIndex = 4
Me.Label17.Text = "Maximum Value (V):"
Me.Label18.FlatStyle = System.Windows.Forms.FlatStyle.System
Me.Label18.Location = New System.Drawing.Point(19, 42)
Me.Label18.Name = "Label18"
Me.Label18.Size = New System.Drawing.Size(125, 18)
Me.Label18.TabIndex = 2
Me.Label18.Text = "Minimum Value (V):"
Me.Label19.FlatStyle = System.Windows.Forms.FlatStyle.System
Me.Label19.Location = New System.Drawing.Point(19, 18)
Me.Label19.Name = "Label19"
Me.Label19.Size = New System.Drawing.Size(115, 18)
Me.Label19.TabIndex = 0
Me.Label19.Text = "Physical Channel:"
Me.timingParametersGroupBoxPI2.Controls.Add(Me.samplesPerChannelNumericPI2)
Me.timingParametersGroupBoxPI2.Controls.Add(Me.rateNumericPI2)
Me.timingParametersGroupBoxPI2.Controls.Add(Me.Label20)
Me.timingParametersGroupBoxPI2.Controls.Add(Me.Label21)
Me.timingParametersGroupBoxPI2.FlatStyle = System.Windows.Forms.FlatStyle.System
```

```
536. Me.timingParametersGroupBoxPI2.Location = New System.Drawing.Point(6, 109)
537. Me.timingParametersGroupBoxPI2.Name = "timingParametersGroupBoxPI2"
538. Me.timingParametersGroupBoxPI2.Size = New System.Drawing.Size(279, 67)
539. Me.timingParametersGroupBoxPI2.TabIndex = 3
540. Me.timingParametersGroupBoxPI2.TabStop = False
541. Me.timingParametersGroupBoxPI2.Text = "Timing Parameters"
542. Me.samplesPerChannelNumericPI2.Location = New System.Drawing.Point(144, 17)
543.             Me.samplesPerChannelNumericPI2.Maximum = New Decimal(New Integer() {100000, 0, 0, 0})
544. Me.samplesPerChannelNumericPI2.Name = "samplesPerChannelNumericPI2"
545. Me.samplesPerChannelNumericPI2.Size = New System.Drawing.Size(115, 22)
546. Me.samplesPerChannelNumericPI2.TabIndex = 1
547. Me.samplesPerChannelNumericPI2.Value = New Decimal(New Integer() {1000, 0, 0, 0})
548. Me.rateNumericPI2.DecimalPlaces = 2
549. Me.rateNumericPI2.Location = New System.Drawing.Point(144, 40)
550. Me.rateNumericPI2.Maximum = New Decimal(New Integer() {100000, 0, 0, 0})
551. Me.rateNumericPI2.Name = "rateNumericPI2"
552. Me.rateNumericPI2.Size = New System.Drawing.Size(115, 22)
553. Me.rateNumericPI2.TabIndex = 3
554. Me.rateNumericPI2.Value = New Decimal(New Integer() {10000, 0, 0, 0})
555. Me.Label20.FlatStyle = System.Windows.Forms.FlatStyle.System
556. Me.Label20.Location = New System.Drawing.Point(19, 42)
557. Me.Label20.Name = "Label20"
558. Me.Label20.Size = New System.Drawing.Size(67, 18)
559. Me.Label20.TabIndex = 2
560. Me.Label20.Text = "Rate (Hz):"
561. Me.Label21.FlatStyle = System.Windows.Forms.FlatStyle.System
562. Me.Label21.Location = New System.Drawing.Point(19, 17)
563. Me.Label21.Name = "Label21"
564. Me.Label21.Size = New System.Drawing.Size(125, 16)
565. Me.Label21.TabIndex = 0
566. Me.Label21.Text = "Samples/Channel:"
567. Me.GroupBox8.Controls.Add(Me.lblreadingPI2_1)
568. Me.GroupBox8.Controls.Add(Me.Label22)
569. Me.GroupBox8.Controls.Add(Me.acquisitionDataGridPI2)
570. Me.GroupBox8.Controls.Add(Me.lblreadingPI2)
571. Me.GroupBox8.FlatStyle = System.Windows.Forms.FlatStyle.System
572. Me.GroupBox8.Location = New System.Drawing.Point(286, 17)
573. Me.GroupBox8.Name = "GroupBox8"
574. Me.GroupBox8.Size = New System.Drawing.Size(332, 159)
575. Me.GroupBox8.TabIndex = 4
576. Me.GroupBox8.TabStop = False
577. Me.GroupBox8.Text = "Acquisition Results"
578. Me.lblreadingPI2_1.AutoSize = True
579. Me.lblreadingPI2_1.Location = New System.Drawing.Point(170, 18)
580. Me.lblreadingPI2_1.Name = "lblreadingPI2_1"
581. Me.lblreadingPI2_1.Size = New System.Drawing.Size(59, 17)
582. Me.lblreadingPI2_1.TabIndex = 42
583. Me.lblreadingPI2_1.Text = "Label31"
584. Me.Label22.FlatStyle = System.Windows.Forms.FlatStyle.System
585. Me.Label22.Location = New System.Drawing.Point(10, 18)
586. Me.Label22.Name = "Label22"
587. Me.Label22.Size = New System.Drawing.Size(134, 19)
588. Me.Label22.TabIndex = 0
589. Me.Label22.Text = "Acquisition Data (V):"
590. Me.acquisitionDataGridPI2.AllowSorting = False
591. Me.acquisitionDataGridPI2.DataMember = ""
592.             Me.acquisitionDataGridPI2.HeaderForeColor = System.Drawing.SystemColors.ControlText
593. Me.acquisitionDataGridPI2.Location = New System.Drawing.Point(12, 40)
594. Me.acquisitionDataGridPI2.Name = "acquisitionDataGridPI2"
595. Me.acquisitionDataGridPI2.ParentRowsVisible = False
596. Me.acquisitionDataGridPI2.ReadOnly = True
597. Me.acquisitionDataGridPI2.Size = New System.Drawing.Size(313, 112)
```

```
598. Me.acquisitionDataGridPI2.TabIndex = 5
599. Me.acquisitionDataGridPI2.TabStop = False
600. Me.lblreadingPI2.AutoSize = True
601. Me.lblreadingPI2.Location = New System.Drawing.Point(131, 18)
602. Me.lblreadingPI2.Name = "lblreadingPI2"
603. Me.lblreadingPI2.Size = New System.Drawing.Size(59, 17)
604. Me.lblreadingPI2.TabIndex = 42
605. Me.lblreadingPI2.Text = "Label32"
606. Me.btnStopPI2.Location = New System.Drawing.Point(86, 180)
607. Me.btnStopPI2.Name = "btnStopPI2"
608. Me.btnStopPI2.Size = New System.Drawing.Size(75, 23)
609. Me.btnStopPI2.TabIndex = 37
610. Me.btnStopPI2.Text = "Stop PI 2"
611. Me.btnStopPI2.UseVisualStyleBackColor = True
612. Me.btnStartPI2.Location = New System.Drawing.Point(5, 180)
613. Me.btnStartPI2.Name = "btnStartPI2"
614. Me.btnStartPI2.Size = New System.Drawing.Size(75, 23)
615. Me.btnStartPI2.TabIndex = 36
616. Me.btnStartPI2.Text = "Start PI 2"
617. Me.btnStartPI2.UseVisualStyleBackColor = True
618. Me.GroupBox1.Controls.Add(Me.channelParametersGroupBoxPI1)
619. Me.GroupBox1.Controls.Add(Me.timingParametersGroupBoxPI1)
620. Me.GroupBox1.Controls.Add(Me.acquisitionResultGroupBox)
621. Me.GroupBox1.Controls.Add(Me.btnStopPI1)
622. Me.GroupBox1.Controls.Add(Me.btnStartPI1)
623. Me.GroupBox1.Location = New System.Drawing.Point(6, 6)
624. Me.GroupBox1.Name = "GroupBox1"
625. Me.GroupBox1.Size = New System.Drawing.Size(618, 209)
626. Me.GroupBox1.TabIndex = 31
627. Me.GroupBox1.TabStop = False
628. Me.GroupBox1.Text = "Photointerrupter 1"
629. Me.channelParametersGroupBoxPI1.Controls.Add(Me.physicalChannelComboBoxPI1)
630. Me.channelParametersGroupBoxPI1.Controls.Add(Me.minimumValueNumericPI1)
631. Me.channelParametersGroupBoxPI1.Controls.Add(Me.maximumValueNumericPI1)
632. Me.channelParametersGroupBoxPI1.Controls.Add(Me.maximumLabel)
633. Me.channelParametersGroupBoxPI1.Controls.Add(Me.minimumLabel)
634. Me.channelParametersGroupBoxPI1.Controls.Add(Me.physicalChannelLabel)
635.         Me.channelParametersGroupBoxPI1.FlatStyle = System.Windows.Forms.FlatStyle.System
636. Me.channelParametersGroupBoxPI1.Location = New System.Drawing.Point(6, 17)
637. Me.channelParametersGroupBoxPI1.Name = "channelParametersGroupBoxPI1"
638. Me.channelParametersGroupBoxPI1.Size = New System.Drawing.Size(279, 90)
639. Me.channelParametersGroupBoxPI1.TabIndex = 2
640. Me.channelParametersGroupBoxPI1.TabStop = False
641. Me.channelParametersGroupBoxPI1.Text = "Channel Parameters"
642. Me.physicalChannelComboBoxPI1.Location = New System.Drawing.Point(144, 15)
643. Me.physicalChannelComboBoxPI1.Name = "physicalChannelComboBoxPI1"
644. Me.physicalChannelComboBoxPI1.Size = New System.Drawing.Size(115, 24)
645. Me.physicalChannelComboBoxPI1.TabIndex = 1
646. Me.physicalChannelComboBoxPI1.Text = "Dev1/ai0"
647. Me.minimumValueNumericPI1.DecimalPlaces = 2
648. Me.minimumValueNumericPI1.Location = New System.Drawing.Point(144, 40)
649. Me.minimumValueNumericPI1.Maximum = New Decimal(New Integer() {10, 0, 0, 0})
650.         Me.minimumValueNumericPI1.Minimum = New Decimal(New Integer() {10, 0, 0, -2147483648})
651. Me.minimumValueNumericPI1.Name = "minimumValueNumericPI1"
652. Me.minimumValueNumericPI1.Size = New System.Drawing.Size(115, 22)
653. Me.minimumValueNumericPI1.TabIndex = 3
654.         Me.minimumValueNumericPI1.Value = New Decimal(New Integer() {100, 0, 0, -2147418112})
655. Me.maximumValueNumericPI1.DecimalPlaces = 2
656. Me.maximumValueNumericPI1.Location = New System.Drawing.Point(144, 63)
657. Me.maximumValueNumericPI1.Maximum = New Decimal(New Integer() {10, 0, 0, 0})
658.         Me.maximumValueNumericPI1.Minimum = New Decimal(New Integer() {10, 0, 0, -2147483648})
659. Me.maximumValueNumericPI1.Name = "maximumValueNumericPI1"
```

```
660. Me.maximumValueNumericPI1.Size = New System.Drawing.Size(115, 22)
661. Me.maximumValueNumericPI1.TabIndex = 5
662. Me.maximumValueNumericPI1.Value = New Decimal(New Integer() {100, 0, 0, 65536})
663. Me.maximumLabel.FlatStyle = System.Windows.Forms.FlatStyle.System
664. Me.maximumLabel.Location = New System.Drawing.Point(19, 65)
665. Me.maximumLabel.Name = "maximumLabel"
666. Me.maximumLabel.Size = New System.Drawing.Size(135, 18)
667. Me.maximumLabel.TabIndex = 4
668. Me.maximumLabel.Text = "Maximum Value (V):"
669. Me.minimumLabel.FlatStyle = System.Windows.Forms.FlatStyle.System
670. Me.minimumLabel.Location = New System.Drawing.Point(19, 42)
671. Me.minimumLabel.Name = "minimumLabel"
672. Me.minimumLabel.Size = New System.Drawing.Size(125, 18)
673. Me.minimumLabel.TabIndex = 2
674. Me.minimumLabel.Text = "Minimum Value (V):"
675. Me.physicalChannelLabel.FlatStyle = System.Windows.Forms.FlatStyle.System
676. Me.physicalChannelLabel.Location = New System.Drawing.Point(19, 18)
677. Me.physicalChannelLabel.Name = "physicalChannelLabel"
678. Me.physicalChannelLabel.Size = New System.Drawing.Size(115, 18)
679. Me.physicalChannelLabel.TabIndex = 0
680. Me.physicalChannelLabel.Text = "Physical Channel:"
681. Me.timingParametersGroupBoxPI1.Controls.Add(Me.samplesPerChannelNumericPI1)
682. Me.timingParametersGroupBoxPI1.Controls.Add(Me.rateNumericPI1)
683. Me.timingParametersGroupBoxPI1.Controls.Add(Me.rateLabel)
684. Me.timingParametersGroupBoxPI1.Controls.Add(Me.samplesLabel)
685. Me.timingParametersGroupBoxPI1.FlatStyle = System.Windows.Forms.FlatStyle.System
686. Me.timingParametersGroupBoxPI1.Location = New System.Drawing.Point(6, 109)
687. Me.timingParametersGroupBoxPI1.Name = "timingParametersGroupBoxPI1"
688. Me.timingParametersGroupBoxPI1.Size = New System.Drawing.Size(279, 67)
689. Me.timingParametersGroupBoxPI1.TabIndex = 3
690. Me.timingParametersGroupBoxPI1.TabStop = False
691. Me.timingParametersGroupBoxPI1.Text = "Timing Parameters"
692. Me.samplesPerChannelNumericPI1.Location = New System.Drawing.Point(144, 17)
693.             Me.samplesPerChannelNumericPI1.Maximum = New Decimal(New Integer() {100000, 0, 0, 0})
694. Me.samplesPerChannelNumericPI1.Name = "samplesPerChannelNumericPI1"
695. Me.samplesPerChannelNumericPI1.Size = New System.Drawing.Size(115, 22)
696. Me.samplesPerChannelNumericPI1.TabIndex = 1
697. Me.samplesPerChannelNumericPI1.Value = New Decimal(New Integer() {1000, 0, 0, 0})
698. Me.rateNumericPI1.DecimalPlaces = 2
699. Me.rateNumericPI1.Location = New System.Drawing.Point(144, 40)
700. Me.rateNumericPI1.Maximum = New Decimal(New Integer() {100000, 0, 0, 0})
701. Me.rateNumericPI1.Name = "rateNumericPI1"
702. Me.rateNumericPI1.Size = New System.Drawing.Size(115, 22)
703. Me.rateNumericPI1.TabIndex = 3
704. Me.rateNumericPI1.Value = New Decimal(New Integer() {10000, 0, 0, 0})
705. Me.rateLabel.FlatStyle = System.Windows.Forms.FlatStyle.System
706. Me.rateLabel.Location = New System.Drawing.Point(19, 42)
707. Me.rateLabel.Name = "rateLabel"
708. Me.rateLabel.Size = New System.Drawing.Size(67, 18)
709. Me.rateLabel.TabIndex = 2
710. Me.rateLabel.Text = "Rate (Hz):"
711. Me.samplesLabel.FlatStyle = System.Windows.Forms.FlatStyle.System
712. Me.samplesLabel.Location = New System.Drawing.Point(19, 17)
713. Me.samplesLabel.Name = "samplesLabel"
714. Me.samplesLabel.Size = New System.Drawing.Size(125, 16)
715. Me.samplesLabel.TabIndex = 0
716. Me.samplesLabel.Text = "Samples/Channel:"
717. Me.acquisitionResultGroupBox.Controls.Add(Me.lblreadingPI1_1)
718. Me.acquisitionResultGroupBox.Controls.Add(Me.resultLabel)
719. Me.acquisitionResultGroupBox.Controls.Add(Me.acquisitionDataGrid)
720. Me.acquisitionResultGroupBox.Controls.Add(Me.lblreadingPI1)
721. Me.acquisitionResultGroupBox.FlatStyle = System.Windows.Forms.FlatStyle.System
```

```
722. Me.acquisitionResultGroupBox.Location = New System.Drawing.Point(286, 17)
723. Me.acquisitionResultGroupBox.Name = "acquisitionResultGroupBox"
724. Me.acquisitionResultGroupBox.Size = New System.Drawing.Size(332, 159)
725. Me.acquisitionResultGroupBox.TabIndex = 4
726. Me.acquisitionResultGroupBox.TabStop = False
727. Me.acquisitionResultGroupBox.Text = "Acquisition Results"
728. Me.lblreadingPI1_1.AutoSize = True
729. Me.lblreadingPI1_1.Location = New System.Drawing.Point(170, 18)
730. Me.lblreadingPI1_1.Name = "lblreadingPI1_1"
731. Me.lblreadingPI1_1.Size = New System.Drawing.Size(59, 17)
732. Me.lblreadingPI1_1.TabIndex = 40
733. Me.lblreadingPI1_1.Text = "Label23"
734. Me.resultLabel.FlatStyle = System.Windows.Forms.FlatStyle.System
735. Me.resultLabel.Location = New System.Drawing.Point(10, 18)
736. Me.resultLabel.Name = "resultLabel"
737. Me.resultLabel.Size = New System.Drawing.Size(134, 19)
738. Me.resultLabel.TabIndex = 0
739. Me.resultLabel.Text = "Acquisition Data (V):"
740. Me.acquisitionDataGrid.AllowSorting = False
741. Me.acquisitionDataGrid.DataMember = ""
742. Me.acquisitionDataGrid.HeaderForeColor = System.Drawing.SystemColors.ControlText
743. Me.acquisitionDataGrid.Location = New System.Drawing.Point(12, 40)
744. Me.acquisitionDataGrid.Name = "acquisitionDataGrid"
745. Me.acquisitionDataGrid.ParentRowsVisible = False
746. Me.acquisitionDataGrid.ReadOnly = True
747. Me.acquisitionDataGrid.Size = New System.Drawing.Size(313, 112)
748. Me.acquisitionDataGrid.TabIndex = 5
749. Me.acquisitionDataGrid.TabStop = False
750. Me.lblreadingPI1.AutoSize = True
751. Me.lblreadingPI1.Location = New System.Drawing.Point(131, 18)
752. Me.lblreadingPI1.Name = "lblreadingPI1"
753. Me.lblreadingPI1.Size = New System.Drawing.Size(63, 17)
754. Me.lblreadingPI1.TabIndex = 40
755. Me.lblreadingPI1.Text = "Label 31"
756. Me.btnStopPI1.Location = New System.Drawing.Point(86, 180)
757. Me.btnStopPI1.Name = "btnStopPI1"
758. Me.btnStopPI1.Size = New System.Drawing.Size(75, 23)
759. Me.btnStopPI1.TabIndex = 35
760. Me.btnStopPI1.Text = "Stop PI 1"
761. Me.btnStopPI1.UseVisualStyleBackColor = True
762. Me.btnStartPI1.Location = New System.Drawing.Point(5, 180)
763. Me.btnStartPI1.Name = "btnStartPI1"
764. Me.btnStartPI1.Size = New System.Drawing.Size(75, 23)
765. Me.btnStartPI1.TabIndex = 34
766. Me.btnStartPI1.Text = "Start PI 1"
767. Me.btnStartPI1.UseVisualStyleBackColor = True
768. Me.grpboxRunparametersauto.Controls.Add(Me.txtboxWashtime)
769. Me.grpboxRunparametersauto.Controls.Add(Me.Label11)
770. Me.grpboxRunparametersauto.Controls.Add(Me.txtboxWashflowrate)
771. Me.grpboxRunparametersauto.Controls.Add(Me.Label13)
772. Me.grpboxRunparametersauto.Controls.Add(Me.btnDrainauto)
773. Me.grpboxRunparametersauto.Controls.Add(Me.txtboxdesorptionvolume)
774. Me.grpboxRunparametersauto.Controls.Add(Me.Label2)
775. Me.grpboxRunparametersauto.Controls.Add(Me.txtboxDesorptiontimeauto)
776. Me.grpboxRunparametersauto.Controls.Add(Me.lblDesorptiontimer)
777. Me.grpboxRunparametersauto.Controls.Add(Me.Label1)
778. Me.grpboxRunparametersauto.Controls.Add(Me.Label16)
779. Me.grpboxRunparametersauto.Controls.Add(Me.btnStopauto)
780. Me.grpboxRunparametersauto.Controls.Add(Me.lblcurrentpumpflowrate)
781. Me.grpboxRunparametersauto.Controls.Add(Me.Label14)
782. Me.grpboxRunparametersauto.Controls.Add(Me.lblwash200ulmintimer)
783. Me.grpboxRunparametersauto.Controls.Add(Me.Label5)
```

```
784. Me.grpboxRunparametersauto.Controls.Add(Me.lblcurrentsuctiontime)
785. Me.grpboxRunparametersauto.Controls.Add(Me.Label4)
786. Me.grpboxRunparametersauto.Controls.Add(Me.Label3)
787. Me.grpboxRunparametersauto.Controls.Add(Me.btnStartauto)
788. Me.grpboxRunparametersauto.Controls.Add(Me.lblbroken)
789. Me.grpboxRunparametersauto.Location = New System.Drawing.Point(630, 11)
790. Me.grpboxRunparametersauto.Name = "grpboxRunparametersauto"
791. Me.grpboxRunparametersauto.Size = New System.Drawing.Size(305, 354)
792. Me.grpboxRunparametersauto.TabIndex = 30
793. Me.grpboxRunparametersauto.TabStop = False
794. Me.grpboxRunparametersauto.Text = "Run parameters (automatic)"
795. Me.txtboxWashtime.Location = New System.Drawing.Point(177, 121)
796. Me.txtboxWashtime.Name = "txtboxWashtime"
797. Me.txtboxWashtime.Size = New System.Drawing.Size(119, 22)
798. Me.txtboxWashtime.TabIndex = 46
799. Me.Label11.AutoSize = True
800. Me.Label11.Location = New System.Drawing.Point(11, 124)
801. Me.Label11.Name = "Label11"
802. Me.Label11.Size = New System.Drawing.Size(110, 17)
803. Me.Label11.TabIndex = 45
804. Me.Label11.Text = "Wash time: (ms)"
805. Me.txtboxWashflowrate.Location = New System.Drawing.Point(177, 87)
806. Me.txtboxWashflowrate.Name = "txtboxWashflowrate"
807. Me.txtboxWashflowrate.Size = New System.Drawing.Size(119, 22)
808. Me.txtboxWashflowrate.TabIndex = 44
809. Me.Label13.AutoSize = True
810. Me.Label13.Location = New System.Drawing.Point(10, 90)
811. Me.Label13.Name = "Label13"
812. Me.Label13.Size = New System.Drawing.Size(161, 17)
813. Me.Label13.TabIndex = 43
814. Me.Label13.Text = "Wash flow rate: (uL/min)"
815. Me.btnDrainauto.Location = New System.Drawing.Point(45, 297)
816. Me.btnDrainauto.Name = "btnDrainauto"
817. Me.btnDrainauto.Size = New System.Drawing.Size(75, 23)
818. Me.btnDrainauto.TabIndex = 42
819. Me.btnDrainauto.Text = "Drain"
820. Me.btnDrainauto.UseVisualStyleBackColor = True
821. Me.txtboxdesorptionvolume.Location = New System.Drawing.Point(176, 54)
822. Me.txtboxdesorptionvolume.Name = "txtboxdesorptionvolume"
823. Me.txtboxdesorptionvolume.Size = New System.Drawing.Size(120, 22)
824. Me.txtboxdesorptionvolume.TabIndex = 41
825. Me.Label2.AutoSize = True
826. Me.Label2.Location = New System.Drawing.Point(10, 57)
827. Me.Label2.Name = "Label2"
828. Me.Label2.Size = New System.Drawing.Size(160, 17)
829. Me.Label2.TabIndex = 40
830. Me.Label2.Text = "Desorption volume: (uL)"
831. Me.txtboxDesorptiontimeauto.Location = New System.Drawing.Point(176, 22)
832. Me.txtboxDesorptiontimeauto.Name = "txtboxDesorptiontimeauto"
833. Me.txtboxDesorptiontimeauto.Size = New System.Drawing.Size(120, 22)
834. Me.txtboxDesorptiontimeauto.TabIndex = 39
835. Me.lblDesorptiontimer.AutoSize = True
836. Me.lblDesorptiontimer.Location = New System.Drawing.Point(241, 184)
837. Me.lblDesorptiontimer.Name = "lblDesorptiontimer"
838. Me.lblDesorptiontimer.Size = New System.Drawing.Size(20, 17)
839. Me.lblDesorptiontimer.TabIndex = 7
840. Me.lblDesorptiontimer.Text = "..."
841. Me.Label1.AutoSize = True
842. Me.Label1.Location = New System.Drawing.Point(10, 184)
843. Me.Label1.Name = "Label1"
844. Me.Label1.Size = New System.Drawing.Size(143, 17)
845. Me.Label1.TabIndex = 28
```

```
846. Me.Label1.Text = "Desorption time: (ms)"
847. Me.Label16.AutoSize = True
848. Me.Label16.Location = New System.Drawing.Point(10, 29)
849. Me.Label16.Name = "Label16"
850. Me.Label16.Size = New System.Drawing.Size(143, 17)
851. Me.Label16.TabIndex = 38
852. Me.Label16.Text = "Desorption time: (ms)"
853. Me.btnStopauto.Location = New System.Drawing.Point(206, 152)
854. Me.btnStopauto.Name = "btnStopauto"
855. Me.btnStopauto.Size = New System.Drawing.Size(90, 27)
856. Me.btnStopauto.TabIndex = 37
857. Me.btnStopauto.Text = "Stop"
858. Me.btnStopauto.UseVisualStyleBackColor = True
859. Me.lblcurrentpumpflowrate.AutoSize = True
860. Me.lblcurrentpumpflowrate.Location = New System.Drawing.Point(241, 224)
861. Me.lblcurrentpumpflowrate.Name = "lblcurrentpumpflowrate"
862. Me.lblcurrentpumpflowrate.Size = New System.Drawing.Size(20, 17)
863. Me.lblcurrentpumpflowrate.TabIndex = 36
864. Me.lblcurrentpumpflowrate.Text = "..."
865. Me.Label14.AutoSize = True
866. Me.Label14.Location = New System.Drawing.Point(10, 224)
867. Me.Label14.Name = "Label14"
868. Me.Label14.Size = New System.Drawing.Size(211, 17)
869. Me.Label14.TabIndex = 35
870. Me.Label14.Text = "Current pump flow rate: (uL/min)"
871. Me.lblwash200ulmintimer.AutoSize = True
872. Me.lblwash200ulmintimer.Location = New System.Drawing.Point(241, 266)
873. Me.lblwash200ulmintimer.Name = "lblwash200ulmintimer"
874. Me.lblwash200ulmintimer.Size = New System.Drawing.Size(20, 17)
875. Me.lblwash200ulmintimer.TabIndex = 34
876. Me.lblwash200ulmintimer.Text = "..."
877. Me.Label5.AutoSize = True
878. Me.Label5.Location = New System.Drawing.Point(10, 266)
879. Me.Label5.Name = "Label5"
880. Me.Label5.Size = New System.Drawing.Size(110, 17)
881. Me.Label5.TabIndex = 33
882. Me.Label5.Text = "Wash time: (ms)"
883. Me.lblcurrentsuctiontime.AutoSize = True
884. Me.lblcurrentsuctiontime.Location = New System.Drawing.Point(241, 244)
885. Me.lblcurrentsuctiontime.Name = "lblcurrentsuctiontime"
886. Me.lblcurrentsuctiontime.Size = New System.Drawing.Size(20, 17)
887. Me.lblcurrentsuctiontime.TabIndex = 31
888. Me.lblcurrentsuctiontime.Text = "..."
889. Me.Label4.AutoSize = True
890. Me.Label4.Location = New System.Drawing.Point(10, 245)
891. Me.Label4.Name = "Label4"
892. Me.Label4.Size = New System.Drawing.Size(170, 17)
893. Me.Label4.TabIndex = 30
894. Me.Label4.Text = "Current suction time: (ms)"
895. Me.Label3.AutoSize = True
896. Me.Label3.Location = New System.Drawing.Point(10, 203)
897. Me.Label3.Name = "Label3"
898. Me.Label3.Size = New System.Drawing.Size(221, 17)
899. Me.Label3.TabIndex = 29
900. Me.Label3.Text = "Current suction flow rate: (uL/min)"
901. Me.btnStartauto.Location = New System.Drawing.Point(13, 152)
902. Me.btnStartauto.Name = "btnStartauto"
903. Me.btnStartauto.Size = New System.Drawing.Size(108, 27)
904. Me.btnStartauto.TabIndex = 21
905. Me.btnStartauto.Text = "Start"
906. Me.btnStartauto.UseVisualStyleBackColor = True
907. Me.lblbroken.AutoSize = True
```

```
908. Me.lblbroken.Location = New System.Drawing.Point(241, 203)
909. Me.lblbroken.Name = "lblbroken"
910. Me.lblbroken.Size = New System.Drawing.Size(20, 17)
911. Me.lblbroken.TabIndex = 27
912. Me.lblbroken.Text = "..."
913. Me.btnNexttab0.Location = New System.Drawing.Point(845, 387)
914. Me.btnNexttab0.Name = "btnNexttab0"
915. Me.btnNexttab0.Size = New System.Drawing.Size(90, 27)
916. Me.btnNexttab0.TabIndex = 7
917. Me.btnNexttab0.Text = "Next"
918. Me.btnNexttab0.UseVisualStyleBackColor = True
919. Me.TabPage2.Controls.Add(Me.lblgraphreadingPI2)
920. Me.TabPage2.Controls.Add(Me.Label15)
921. Me.TabPage2.Controls.Add(Me.lblgraphreadingPI1)
922. Me.TabPage2.Controls.Add(Me.Label10)
923. Me.TabPage2.Controls.Add(Me.chartPI2)
924. Me.TabPage2.Controls.Add(Me.btnStopcollectionchart)
925. Me.TabPage2.Controls.Add(Me.chartPI1)
926. Me.TabPage2.Controls.Add(Me.btnNexttab1)
927. Me.TabPage2.Controls.Add(Me.btnPrevioustab1)
928. Me.TabPage2.Location = New System.Drawing.Point(4, 25)
929. Me.TabPage2.Name = "TabPage2"
930. Me.TabPage2.Padding = New System.Windows.Forms.Padding(3)
931. Me.TabPage2.Size = New System.Drawing.Size(1103, 663)
932. Me.TabPage2.TabIndex = 1
933. Me.TabPage2.Text = "Graph"
934. Me.TabPage2.UseVisualStyleBackColor = True
935. Me.lblgraphreadingPI2.AutoSize = True
936. Me.lblgraphreadingPI2.Location = New System.Drawing.Point(534, 209)
937. Me.lblgraphreadingPI2.Name = "lblgraphreadingPI2"
938. Me.lblgraphreadingPI2.Size = New System.Drawing.Size(20, 17)
939. Me.lblgraphreadingPI2.TabIndex = 18
940. Me.lblgraphreadingPI2.Text = "..."
941. Me.Label15.AutoSize = True
942. Me.Label15.Location = New System.Drawing.Point(416, 209)
943. Me.Label15.Name = "Label15"
944. Me.Label15.Size = New System.Drawing.Size(112, 17)
945. Me.Label15.TabIndex = 16
946. Me.Label15.Text = "PI2 Reading (V):"
947. Me.lblgraphreadingPI1.AutoSize = True
948. Me.lblgraphreadingPI1.Location = New System.Drawing.Point(534, 7)
949. Me.lblgraphreadingPI1.Name = "lblgraphreadingPI1"
950. Me.lblgraphreadingPI1.Size = New System.Drawing.Size(20, 17)
951. Me.lblgraphreadingPI1.TabIndex = 15
952. Me.lblgraphreadingPI1.Text = "..."
953. Me.Label10.AutoSize = True
954. Me.Label10.Location = New System.Drawing.Point(416, 7)
955. Me.Label10.Name = "Label10"
956. Me.Label10.Size = New System.Drawing.Size(112, 17)
957. Me.Label10.TabIndex = 14
958. Me.Label10.Text = "PI1 Reading (V):"
959. ChartArea1.AxisX.Title = "Time (ms)"
960. ChartArea1.AxisY.Title = "Voltage (V)"
961. ChartArea1.Name = "ChartArea1"
962. Me.chartPI2.ChartAreas.Add(ChartArea1)
963. Legend1.Name = "Legend1"
964. Me.chartPI2.Legends.Add(Legend1)
965. Me.chartPI2.Location = New System.Drawing.Point(8, 209)
966. Me.chartPI2.Name = "chartPI2"
967. Series1.ChartArea = "ChartArea1"
968.             Series1.ChartType = System.Windows.Forms.DataVisualization.Charting.SeriesChartType.Line
969. Series1.Legend = "Legend1"
```

```
970. Series1.Name = "Series1"
971. Me.chartPI2.Series.Add(Series1)
972. Me.chartPI2.Size = New System.Drawing.Size(431, 218)
973. Me.chartPI2.TabIndex = 13
974. Me.chartPI2.Text = "chartPI2"
975. Me.btnStopcollectionchart.Location = New System.Drawing.Point(526, 291)
976. Me.btnStopcollectionchart.Name = "btnStopcollectionchart"
977. Me.btnStopcollectionchart.Size = New System.Drawing.Size(112, 26)
978. Me.btnStopcollectionchart.TabIndex = 11
979. Me.btnStopcollectionchart.Text = "Stop PI"
980. Me.btnStopcollectionchart.UseVisualStyleBackColor = True
981. ChartArea2.AxisX.Title = "Time (ms)"
982. ChartArea2.AxisY.Title = "Voltage (V)"
983. ChartArea2.Name = "ChartArea1"
984. Me.chartPI1.ChartAreas.Add(ChartArea2)
985. Legend2.Name = "Legend1"
986. Me.chartPI1.Legends.Add(Legend2)
987. Me.chartPI1.Location = New System.Drawing.Point(8, 7)
988. Me.chartPI1.Name = "chartPI1"
989. Series2.ChartArea = "ChartArea1"
990.             Series2.ChartType = System.Windows.Forms.DataVisualization.Charting.SeriesChartType.Line
991. Series2.Legend = "Legend1"
992. Series2.Name = "Series1"
993. Me.chartPI1.Series.Add(Series2)
994. Me.chartPI1.Size = New System.Drawing.Size(431, 196)
995. Me.chartPI1.TabIndex = 10
996. Me.chartPI1.Text = "chartPI1"
997. Me.btnNexttab1.Location = New System.Drawing.Point(593, 353)
998. Me.btnNexttab1.Name = "btnNexttab1"
999. Me.btnNexttab1.Size = New System.Drawing.Size(90, 27)
1000.         Me.btnNexttab1.TabIndex = 9
1001.         Me.btnNexttab1.Text = "Next"
1002.         Me.btnNexttab1.UseVisualStyleBackColor = True
1003.         Me.btnPrevioustab1.Location = New System.Drawing.Point(466, 354)
1004.         Me.btnPrevioustab1.Name = "btnPrevioustab1"
1005.         Me.btnPrevioustab1.Size = New System.Drawing.Size(90, 26)
1006.         Me.btnPrevioustab1.TabIndex = 8
1007.         Me.btnPrevioustab1.Text = "Previous"
1008.         Me.btnPrevioustab1.UseVisualStyleBackColor = True
1009.         Me.TabPage3.Controls.Add(Me.grpboxSyringepump1)
1010.         Me.TabPage3.Controls.Add(Me.btnclearallports)
1011.         Me.TabPage3.Controls.Add(Me.btnscanforports)
1012.         Me.TabPage3.Controls.Add(Me.btnNexttab2)
1013.         Me.TabPage3.Controls.Add(Me.btnPrevioustab2)
1014.         Me.TabPage3.Location = New System.Drawing.Point(4, 25)
1015.         Me.TabPage3.Name = "TabPage3"
1016.         Me.TabPage3.Size = New System.Drawing.Size(1103, 663)
1017.         Me.TabPage3.TabIndex = 2
1018.         Me.TabPage3.Text = "COM port settings"
1019.         Me.TabPage3.UseVisualStyleBackColor = True
1020.         Me.grpboxSyringepump1.Controls.Add(Me.cmbboxBaudratepump1)
1021.         Me.grpboxSyringepump1.Controls.Add(Me.btnConnect1)
1022.         Me.grpboxSyringepump1.Controls.Add(Me.cmbboxSyringepump1)
1023.         Me.grpboxSyringepump1.Controls.Add(Me.lbllistparameterspump1)
1024.         Me.grpboxSyringepump1.Controls.Add(Me.btnDisconnect1)
1025.         Me.grpboxSyringepump1.Controls.Add(Me.lblparameterspump1)
1026.         Me.grpboxSyringepump1.Controls.Add(Me.lblCOMPort1)
1027.         Me.grpboxSyringepump1.Controls.Add(Me.lblBaudrate1)
1028.         Me.grpboxSyringepump1.Location = New System.Drawing.Point(6, 3)
1029.         Me.grpboxSyringepump1.Name = "grpboxSyringepump1"
1030.         Me.grpboxSyringepump1.Size = New System.Drawing.Size(646, 130)
1031.         Me.grpboxSyringepump1.TabIndex = 43
```

```
1032.         Me.grpboxSyringepump1.TabStop = False
1033.         Me.grpboxSyringepump1.Text = "Syringe pump 1"
1034.         Me.cmbboxBaudratepump1.DropDownStyle = System.Windows.Forms.ComboBoxStyle.DropDownList
1035.         Me.cmbboxBaudratepump1.FormattingEnabled = True
1036.         Me.cmbboxBaudratepump1.Items.AddRange(New Object() {"9600", "115200"})
1037.         Me.cmbboxBaudratepump1.Location = New System.Drawing.Point(78, 60)
1038.         Me.cmbboxBaudratepump1.Name = "cmbboxBaudratepump1"
1039.         Me.cmbboxBaudratepump1.Size = New System.Drawing.Size(145, 24)
1040.         Me.cmbboxBaudratepump1.TabIndex = 26
1041.         Me.btnConnect1.Location = New System.Drawing.Point(268, 20)
1042.         Me.btnConnect1.Name = "btnConnect1"
1043.         Me.btnConnect1.Size = New System.Drawing.Size(99, 26)
1044.         Me.btnConnect1.TabIndex = 29
1045.         Me.btnConnect1.Text = "Connect 1"
1046.         Me.btnConnect1.UseVisualStyleBackColor = True
1047.         Me.cmbboxSyringepump1.DropDownStyle = System.Windows.Forms.ComboBoxStyle.DropDownList
1048.         Me.cmbboxSyringepump1.FormattingEnabled = True
1049.         Me.cmbboxSyringepump1.Location = New System.Drawing.Point(78, 22)
1050.         Me.cmbboxSyringepump1.Name = "cmbboxSyringepump1"
1051.         Me.cmbboxSyringepump1.Size = New System.Drawing.Size(145, 24)
1052.         Me.cmbboxSyringepump1.TabIndex = 24
1053.         Me.lbllistparameterspump1.AutoSize = True
1054.         Me.lbllistparameterspump1.Location = New System.Drawing.Point(402, 37)
1055.         Me.lbllistparameterspump1.Name = "lbllistparameterspump1"
1056.         Me.lbllistparameterspump1.Size = New System.Drawing.Size(46, 17)
1057.         Me.lbllistparameterspump1.TabIndex = 39
1058.         Me.lbllistparameterspump1.Text = "List ..."
1059.         Me.btnDisconnect1.Location = New System.Drawing.Point(268, 58)
1060.         Me.btnDisconnect1.Name = "btnDisconnect1"
1061.         Me.btnDisconnect1.Size = New System.Drawing.Size(99, 26)
1062.         Me.btnDisconnect1.TabIndex = 32
1063.         Me.btnDisconnect1.Text = "Disconnect 1"
1064.         Me.btnDisconnect1.UseVisualStyleBackColor = True
1065.         Me.lblparameterspump1.AutoSize = True
1066.         Me.lblparameterspump1.Location = New System.Drawing.Point(402, 20)
1067.         Me.lblparameterspump1.Name = "lblparameterspump1"
1068.         Me.lblparameterspump1.Size = New System.Drawing.Size(222, 17)
1069.         Me.lblparameterspump1.TabIndex = 37
1070.         Me.lblparameterspump1.Text = "List of current pump 1 parameters"
1071.         Me.lblCOMPort1.AutoSize = True
1072.         Me.lblCOMPort1.Location = New System.Drawing.Point(1, 25)
1073.         Me.lblCOMPort1.Name = "lblCOMPort1"
1074.         Me.lblCOMPort1.Size = New System.Drawing.Size(69, 17)
1075.         Me.lblCOMPort1.TabIndex = 28
1076.         Me.lblCOMPort1.Text = "COM Port"
1077.         Me.lblBaudrate1.AutoSize = True
1078.         Me.lblBaudrate1.Location = New System.Drawing.Point(1, 63)
1079.         Me.lblBaudrate1.Name = "lblBaudrate1"
1080.         Me.lblBaudrate1.Size = New System.Drawing.Size(75, 17)
1081.         Me.lblBaudrate1.TabIndex = 30
1082.         Me.lblBaudrate1.Text = "Baud Rate"
1083.         Me.btnclearallports.Location = New System.Drawing.Point(322, 327)
1084.         Me.btnclearallports.Name = "btnclearallports"
1085.         Me.btnclearallports.Size = New System.Drawing.Size(103, 26)
1086.         Me.btnclearallports.TabIndex = 42
1087.         Me.btnclearallports.Text = "Clear all ports"
1088.         Me.btnclearallports.UseVisualStyleBackColor = True
1089.         Me.btnscanforports.Location = New System.Drawing.Point(212, 327)
1090.         Me.btnscanforports.Name = "btnscanforports"
1091.         Me.btnscanforports.Size = New System.Drawing.Size(102, 26)
1092.         Me.btnscanforports.TabIndex = 41
1093.         Me.btnscanforports.Text = "Scan for ports"
```

```
1094.         Me.btnscanforports.UseVisualStyleBackColor = True
1095.         Me.btnNexttab2.Location = New System.Drawing.Point(562, 327)
1096.         Me.btnNexttab2.Name = "btnNexttab2"
1097.         Me.btnNexttab2.Size = New System.Drawing.Size(90, 26)
1098.         Me.btnNexttab2.TabIndex = 11
1099.         Me.btnNexttab2.Text = "Next"
1100.         Me.btnNexttab2.UseVisualStyleBackColor = True
1101.         Me.btnPrevioustab2.Location = New System.Drawing.Point(6, 327)
1102.         Me.btnPrevioustab2.Name = "btnPrevioustab2"
1103.         Me.btnPrevioustab2.Size = New System.Drawing.Size(90, 26)
1104.         Me.btnPrevioustab2.TabIndex = 10
1105.         Me.btnPrevioustab2.Text = "Previous"
1106.         Me.btnPrevioustab2.UseVisualStyleBackColor = True
1107.         Me.TabPage4.Controls.Add(Me.GroupBox2)
1108.         Me.TabPage4.Controls.Add(Me.btnNexttab3)
1109.         Me.TabPage4.Controls.Add(Me.btnPrevioustab3)
1110.         Me.TabPage4.Location = New System.Drawing.Point(4, 25)
1111.         Me.TabPage4.Name = "TabPage4"
1112.         Me.TabPage4.Size = New System.Drawing.Size(1103, 663)
1113.         Me.TabPage4.TabIndex = 3
1114.         Me.TabPage4.Text = "Send Commands Separately"
1115.         Me.TabPage4.UseVisualStyleBackColor = True
1116.         Me.GroupBox2.Controls.Add(Me.btnSend1sendcommands)
1117.         Me.GroupBox2.Controls.Add(Me.txtboxInput1sendcommands)
1118.         Me.GroupBox2.Controls.Add(Me.lblOutput1sendcommands)
1119.         Me.GroupBox2.Controls.Add(Me.Label7)
1120.         Me.GroupBox2.Controls.Add(Me.Label6)
1121.         Me.GroupBox2.Location = New System.Drawing.Point(8, 16)
1122.         Me.GroupBox2.Name = "GroupBox2"
1123.         Me.GroupBox2.Size = New System.Drawing.Size(610, 163)
1124.         Me.GroupBox2.TabIndex = 14
1125.         Me.GroupBox2.TabStop = False
1126.         Me.GroupBox2.Text = "Communicate to Syringe pump 1"
1127.         Me.btnSend1sendcommands.Location = New System.Drawing.Point(298, 23)
1128.         Me.btnSend1sendcommands.Name = "btnSend1sendcommands"
1129.         Me.btnSend1sendcommands.Size = New System.Drawing.Size(90, 27)
1130.         Me.btnSend1sendcommands.TabIndex = 4
1131.         Me.btnSend1sendcommands.Text = "Send"
1132.         Me.btnSend1sendcommands.UseVisualStyleBackColor = True
1133.         Me.txtboxInput1sendcommands.Location = New System.Drawing.Point(131, 25)
1134.         Me.txtboxInput1sendcommands.Name = "txtboxInput1sendcommands"
1135.         Me.txtboxInput1sendcommands.Size = New System.Drawing.Size(120, 22)
1136.         Me.txtboxInput1sendcommands.TabIndex = 3
1137.         Me.lblOutput1sendcommands.AutoSize = True
1138.         Me.lblOutput1sendcommands.Location = New System.Drawing.Point(472, 29)
1139.         Me.lblOutput1sendcommands.Name = "lblOutput1sendcommands"
1140.         Me.lblOutput1sendcommands.Size = New System.Drawing.Size(118, 17)
1141.         Me.lblOutput1sendcommands.TabIndex = 2
1142.         Me.lblOutput1sendcommands.Text = "Output pump 1 ..."
1143.         Me.Label7.AutoSize = True
1144.         Me.Label7.Location = New System.Drawing.Point(409, 29)
1145.         Me.Label7.Name = "Label7"
1146.         Me.Label7.Size = New System.Drawing.Size(59, 17)
1147.         Me.Label7.TabIndex = 1
1148.         Me.Label7.Text = "Output: "
1149.         Me.Label6.AutoSize = True
1150.         Me.Label6.Location = New System.Drawing.Point(6, 29)
1151.         Me.Label6.Name = "Label6"
1152.         Me.Label6.Size = New System.Drawing.Size(47, 17)
1153.         Me.Label6.TabIndex = 0
1154.         Me.Label6.Text = "Input: "
1155.         Me.btnNexttab3.Location = New System.Drawing.Point(559, 320)
```

```
1156.          Me.btnNexttab3.Name = "btnNexttab3"
1157.          Me.btnNexttab3.Size = New System.Drawing.Size(90, 26)
1158.          Me.btnNexttab3.TabIndex = 13
1159.          Me.btnNexttab3.Text = "Next"
1160.          Me.btnNexttab3.UseVisualStyleBackColor = True
1161.          Me.btnPrevioustab3.Location = New System.Drawing.Point(8, 323)
1162.          Me.btnPrevioustab3.Name = "btnPrevioustab3"
1163.          Me.btnPrevioustab3.Size = New System.Drawing.Size(90, 27)
1164.          Me.btnPrevioustab3.TabIndex = 12
1165.          Me.btnPrevioustab3.Text = "Previous"
1166.          Me.btnPrevioustab3.UseVisualStyleBackColor = True
1167.          Me.TabPage5.Controls.Add(Me.grpboxRunpumpstogether)
1168.          Me.TabPage5.Controls.Add(Me.grpboxSyringepump1parametersforrunning)
1169.          Me.TabPage5.Controls.Add(Me.btnPreviousMethods)
1170.          Me.TabPage5.Location = New System.Drawing.Point(4, 25)
1171.          Me.TabPage5.Name = "TabPage5"
1172.          Me.TabPage5.Size = New System.Drawing.Size(1103, 663)
1173.          Me.TabPage5.TabIndex = 4
1174.          Me.TabPage5.Text = "Methods"
1175.          Me.TabPage5.UseVisualStyleBackColor = True
1176.          Me.grpboxRunpumpstogether.Controls.Add(Me.btnLoadMethod)
1177.          Me.grpboxRunpumpstogether.Controls.Add(Me.btnSavemethod)
1178.          Me.grpboxRunpumpstogether.Controls.Add(Me.btnClearall)
1179.          Me.grpboxRunpumpstogether.Location = New System.Drawing.Point(8, 176)
1180.          Me.grpboxRunpumpstogether.Name = "grpboxRunpumpstogether"
1181.          Me.grpboxRunpumpstogether.Size = New System.Drawing.Size(639, 62)
1182.          Me.grpboxRunpumpstogether.TabIndex = 9
1183.          Me.grpboxRunpumpstogether.TabStop = False
1184.          Me.grpboxRunpumpstogether.Text = "Save/Load Method"
1185.          Me.btnLoadMethod.Location = New System.Drawing.Point(227, 22)
1186.          Me.btnLoadMethod.Name = "btnLoadMethod"
1187.          Me.btnLoadMethod.Size = New System.Drawing.Size(99, 26)
1188.          Me.btnLoadMethod.TabIndex = 2
1189.          Me.btnLoadMethod.Text = "Load Method"
1190.          Me.btnLoadMethod.UseVisualStyleBackColor = True
1191.          Me.btnSavemethod.Location = New System.Drawing.Point(120, 22)
1192.          Me.btnSavemethod.Name = "btnSavemethod"
1193.          Me.btnSavemethod.Size = New System.Drawing.Size(100, 26)
1194.          Me.btnSavemethod.TabIndex = 1
1195.          Me.btnSavemethod.Text = "Save Method"
1196.          Me.btnSavemethod.UseVisualStyleBackColor = True
1197.          Me.btnClearall.Location = New System.Drawing.Point(13, 22)
1198.          Me.btnClearall.Name = "btnClearall"
1199.          Me.btnClearall.Size = New System.Drawing.Size(100, 26)
1200.          Me.btnClearall.TabIndex = 0
1201.          Me.btnClearall.Text = "Clear all"
1202.          Me.btnClearall.UseVisualStyleBackColor = True
1203.          Me.grpboxSyringepump1parametersforrunning.Controls.Add(Me.btnSubmit1)
1204.          Me.grpboxSyringepump1parametersforrunning.Controls.Add(Me.lblListcurrentpump1parameters)
1205.          Me.grpboxSyringepump1parametersforrunning.Controls.Add(Me.lblCurrentpump1parameters)
1206.          Me.grpboxSyringepump1parametersforrunning.Controls.Add(Me.btnCheckcurrent1)
1207.          Me.grpboxSyringepump1parametersforrunning.Controls.Add(Me.lblForce1)
1208.          Me.grpboxSyringepump1parametersforrunning.Controls.Add(Me.txtboxTargetvolume1)
1209.          Me.grpboxSyringepump1parametersforrunning.Controls.Add(Me.cmbboxTargetvolume1)
1210.          Me.grpboxSyringepump1parametersforrunning.Controls.Add(Me.txtboxRate1)
1211.          Me.grpboxSyringepump1parametersforrunning.Controls.Add(Me.cmbboxForce1)
1212.          Me.grpboxSyringepump1parametersforrunning.Controls.Add(Me.lblTargetVolume1)
1213.            Me.grpboxSyringepump1parametersforrunning.Controls.Add(Me.cmbboxSyringeselect1)
1214.          Me.grpboxSyringepump1parametersforrunning.Controls.Add(Me.cmbboxRate1)
1215.          Me.grpboxSyringepump1parametersforrunning.Controls.Add(Me.lblRate1)
1216.          Me.grpboxSyringepump1parametersforrunning.Controls.Add(Me.lblInfusewithdraw1)
1217.          Me.grpboxSyringepump1parametersforrunning.Controls.Add(Me.lblSyringeselect1)
```

```
1218.         Me.grpboxSyringepump1parametersforrunning.Controls.Add(Me.cmbboxInfusewithdraw1)
1219.         Me.grpboxSyringepump1parametersforrunning.Location = New System.Drawing.Point(8, 3)
1220.         Me.grpboxSyringepump1parametersforrunning.Name = "grpboxSyringepump1parametersforrunning"
1221.         Me.grpboxSyringepump1parametersforrunning.Size = New System.Drawing.Size(639, 157)
1222.         Me.grpboxSyringepump1parametersforrunning.TabIndex = 7
1223.         Me.grpboxSyringepump1parametersforrunning.TabStop = False
1224.         Me.grpboxSyringepump1parametersforrunning.Text = "Syringe Pump 1 Parameters for Running"
1225.         Me.btnSubmit1.Location = New System.Drawing.Point(294, 90)
1226.         Me.btnSubmit1.Name = "btnSubmit1"
1227.         Me.btnSubmit1.Size = New System.Drawing.Size(121, 27)
1228.         Me.btnSubmit1.TabIndex = 13
1229.         Me.btnSubmit1.Text = "Submit"
1230.         Me.btnSubmit1.UseVisualStyleBackColor = True
1231.         Me.lblListcurrentpump1parameters.AutoSize = True
1232.         Me.lblListcurrentpump1parameters.Location = New System.Drawing.Point(430, 74)
1233.         Me.lblListcurrentpump1parameters.Name = "lblListcurrentpump1parameters"
1234.         Me.lblListcurrentpump1parameters.Size = New System.Drawing.Size(51, 17)
1235.         Me.lblListcurrentpump1parameters.TabIndex = 12
1236.         Me.lblListcurrentpump1parameters.Text = "Label1"
1237.         Me.lblCurrentpump1parameters.AutoSize = True
1238.         Me.lblCurrentpump1parameters.Location = New System.Drawing.Point(430, 46)
1239.         Me.lblCurrentpump1parameters.Name = "lblCurrentpump1parameters"
1240.         Me.lblCurrentpump1parameters.Size = New System.Drawing.Size(186, 17)
1241.         Me.lblCurrentpump1parameters.TabIndex = 11
1242.         Me.lblCurrentpump1parameters.Text = "Current pump 1 parameters:"
1243.         Me.btnCheckcurrent1.Location = New System.Drawing.Point(294, 120)
1244.         Me.btnCheckcurrent1.Name = "btnCheckcurrent1"
1245.         Me.btnCheckcurrent1.Size = New System.Drawing.Size(121, 27)
1246.         Me.btnCheckcurrent1.TabIndex = 10
1247.         Me.btnCheckcurrent1.Text = "Check current"
1248.         Me.btnCheckcurrent1.UseVisualStyleBackColor = True
1249.         Me.lblForce1.AutoSize = True
1250.         Me.lblForce1.Location = New System.Drawing.Point(290, 23)
1251.         Me.lblForce1.Name = "lblForce1"
1252.         Me.lblForce1.Size = New System.Drawing.Size(44, 17)
1253.         Me.lblForce1.TabIndex = 5
1254.         Me.lblForce1.Text = "Force"
1255.         Me.txtboxTargetvolume1.Location = New System.Drawing.Point(154, 92)
1256.         Me.txtboxTargetvolume1.Name = "txtboxTargetvolume1"
1257.         Me.txtboxTargetvolume1.Size = New System.Drawing.Size(120, 22)
1258.         Me.txtboxTargetvolume1.TabIndex = 7
1259.         Me.cmbboxTargetvolume1.DropDownStyle = System.Windows.Forms.ComboBoxStyle.DropDownList
1260.         Me.cmbboxTargetvolume1.FormattingEnabled = True
1261.         Me.cmbboxTargetvolume1.Location = New System.Drawing.Point(154, 122)
1262.         Me.cmbboxTargetvolume1.Name = "cmbboxTargetvolume1"
1263.         Me.cmbboxTargetvolume1.Size = New System.Drawing.Size(121, 24)
1264.         Me.cmbboxTargetvolume1.TabIndex = 3
1265.         Me.txtboxRate1.Location = New System.Drawing.Point(14, 92)
1266.         Me.txtboxRate1.Name = "txtboxRate1"
1267.         Me.txtboxRate1.Size = New System.Drawing.Size(120, 22)
1268.         Me.txtboxRate1.TabIndex = 6
1269.         Me.cmbboxForce1.DropDownStyle = System.Windows.Forms.ComboBoxStyle.DropDownList
1270.         Me.cmbboxForce1.FormattingEnabled = True
1271.         Me.cmbboxForce1.Location = New System.Drawing.Point(294, 44)
1272.         Me.cmbboxForce1.Name = "cmbboxForce1"
1273.         Me.cmbboxForce1.Size = New System.Drawing.Size(121, 24)
1274.         Me.cmbboxForce1.TabIndex = 2
1275.         Me.lblTargetVolume1.AutoSize = True
1276.         Me.lblTargetVolume1.Location = New System.Drawing.Point(149, 74)
1277.         Me.lblTargetVolume1.Name = "lblTargetVolume1"
1278.         Me.lblTargetVolume1.Size = New System.Drawing.Size(101, 17)
1279.         Me.lblTargetVolume1.TabIndex = 3
```

```
1280.          Me.lblTargetVolume1.Text = "Target Volume"
1281.          Me.cmbboxSyringeselect1.DropDownStyle = System.Windows.Forms.ComboBoxStyle.DropDownList
1282.          Me.cmbboxSyringeselect1.FormattingEnabled = True
1283.          Me.cmbboxSyringeselect1.Items.AddRange(New Object() {"Hamilton 1750", "Hamilton 1005"})
1284.          Me.cmbboxSyringeselect1.Location = New System.Drawing.Point(154, 44)
1285.          Me.cmbboxSyringeselect1.Name = "cmbboxSyringeselect1"
1286.          Me.cmbboxSyringeselect1.Size = New System.Drawing.Size(121, 24)
1287.          Me.cmbboxSyringeselect1.TabIndex = 5
1288.          Me.cmbboxRate1.DropDownStyle = System.Windows.Forms.ComboBoxStyle.DropDownList
1289.          Me.cmbboxRate1.FormattingEnabled = True
1290.          Me.cmbboxRate1.Location = New System.Drawing.Point(13, 122)
1291.          Me.cmbboxRate1.Name = "cmbboxRate1"
1292.          Me.cmbboxRate1.Size = New System.Drawing.Size(121, 24)
1293.          Me.cmbboxRate1.TabIndex = 4
1294.          Me.lblRate1.AutoSize = True
1295.          Me.lblRate1.Location = New System.Drawing.Point(11, 74)
1296.          Me.lblRate1.Name = "lblRate1"
1297.          Me.lblRate1.Size = New System.Drawing.Size(38, 17)
1298.          Me.lblRate1.TabIndex = 4
1299.          Me.lblRate1.Text = "Rate"
1300.          Me.lblInfusewithdraw1.AutoSize = True
1301.          Me.lblInfusewithdraw1.Location = New System.Drawing.Point(10, 24)
1302.          Me.lblInfusewithdraw1.Name = "lblInfusewithdraw1"
1303.          Me.lblInfusewithdraw1.Size = New System.Drawing.Size(108, 17)
1304.          Me.lblInfusewithdraw1.TabIndex = 1
1305.          Me.lblInfusewithdraw1.Text = "Infuse/Withdraw"
1306.          Me.lblSyringeselect1.AutoSize = True
1307.          Me.lblSyringeselect1.Location = New System.Drawing.Point(150, 24)
1308.          Me.lblSyringeselect1.Name = "lblSyringeselect1"
1309.          Me.lblSyringeselect1.Size = New System.Drawing.Size(97, 17)
1310.          Me.lblSyringeselect1.TabIndex = 0
1311.          Me.lblSyringeselect1.Text = "Syringe select"
1312.          Me.cmbboxInfusewithdraw1.DropDownStyle = System.Windows.Forms.ComboBoxStyle.DropDownList
1313.          Me.cmbboxInfusewithdraw1.FormattingEnabled = True
1314.          Me.cmbboxInfusewithdraw1.Items.AddRange(New Object() {"Infuse", "Withdraw"})
1315.          Me.cmbboxInfusewithdraw1.Location = New System.Drawing.Point(13, 44)
1316.          Me.cmbboxInfusewithdraw1.Name = "cmbboxInfusewithdraw1"
1317.          Me.cmbboxInfusewithdraw1.Size = New System.Drawing.Size(121, 24)
1318.          Me.cmbboxInfusewithdraw1.TabIndex = 0
1319.          Me.btnPreviousMethods.Location = New System.Drawing.Point(8, 256)
1320.          Me.btnPreviousMethods.Name = "btnPreviousMethods"
1321.          Me.btnPreviousMethods.Size = New System.Drawing.Size(90, 27)
1322.          Me.btnPreviousMethods.TabIndex = 6
1323.          Me.btnPreviousMethods.Text = "Previous"
1324.          Me.btnPreviousMethods.UseVisualStyleBackColor = True
1325.          Me.serialportSyringepump1.PortName = "COM5"
1326.          Me.serialportSyringepump1.ReadTimeout = 500
1327.          Me.serialportSyringepump2.PortName = "COM4"
1328.          Me.serialportSyringepump2.ReadTimeout = 500
1329.          Me.ChartingtimerPI1.Interval = 1000
1330.          Me.DesorptionTimerauto.Interval = 25
1331.          Me.photointerruptertimerPI1.Interval = 10
1332.          Me.photointerruptertimerPI2.Interval = 10
1333.          Me.photointerruptertimerPI3.Interval = 10
1334.          Me.ChartingtimerPI2.Interval = 1000
1335.          Me.ChartingtimerPI3.Interval = 1000
1336.          Me.AutoScaleBaseSize = New System.Drawing.Size(6, 15)
1337.          Me.ClientSize = New System.Drawing.Size(947, 459)
1338.          Me.Controls.Add(Me.TabControl1)
1339.          Me.FormBorderStyle = System.Windows.Forms.FormBorderStyle.FixedDialog
1340.          Me.Icon = CType(resources.GetObject("$this.Icon"), System.Drawing.Icon)
1341.          Me.MaximizeBox = False
```

```
1342.         Me.MaximumSize = New System.Drawing.Size(1200, 808)
1343.         Me.Name = "MainForm"
1344.         Me.StartPosition = System.Windows.Forms.FormStartPosition.CenterScreen
1345.         Me.Text = "Syringe pump v4"
1346.         Me.TabControl1.ResumeLayout(False)
1347.         Me.TabPage1.ResumeLayout(False)
1348.         Me.grpboxSaveloadmethodMS.ResumeLayout(False)
1349.         Me.GroupBox4.ResumeLayout(False)
1350.         Me.channelParametersGroupBoxPI2.ResumeLayout(False)
1351.         CType(Me.minimumValueNumericPI2, System.ComponentModel.ISupportInitialize).EndInit()
1352.         CType(Me.maximumValueNumericPI2, System.ComponentModel.ISupportInitialize).EndInit()
1353.         Me.timingParametersGroupBoxPI2.ResumeLayout(False)
1354.         CType(Me.samplesPerChannelNumericPI2, System.ComponentModel.ISupportInitialize).EndInit()
1355.         CType(Me.rateNumericPI2, System.ComponentModel.ISupportInitialize).EndInit()
1356.         Me.GroupBox8.ResumeLayout(False)
1357.         Me.GroupBox8.PerformLayout()
1358.         CType(Me.acquisitionDataGridPI2, System.ComponentModel.ISupportInitialize).EndInit()
1359.         Me.GroupBox1.ResumeLayout(False)
1360.         Me.channelParametersGroupBoxPI1.ResumeLayout(False)
1361.         CType(Me.minimumValueNumericPI1, System.ComponentModel.ISupportInitialize).EndInit()
1362.         CType(Me.maximumValueNumericPI1, System.ComponentModel.ISupportInitialize).EndInit()
1363.         Me.timingParametersGroupBoxPI1.ResumeLayout(False)
1364.         CType(Me.samplesPerChannelNumericPI1, System.ComponentModel.ISupportInitialize).EndInit()
1365.         CType(Me.rateNumericPI1, System.ComponentModel.ISupportInitialize).EndInit()
1366.         Me.acquisitionResultGroupBox.ResumeLayout(False)
1367.         Me.acquisitionResultGroupBox.PerformLayout()
1368.         CType(Me.acquisitionDataGrid, System.ComponentModel.ISupportInitialize).EndInit()
1369.         Me.grpboxRunparametersauto.ResumeLayout(False)
1370.         Me.grpboxRunparametersauto.PerformLayout()
1371.         Me.TabPage2.ResumeLayout(False)
1372.         Me.TabPage2.PerformLayout()
1373.         CType(Me.chartPI2, System.ComponentModel.ISupportInitialize).EndInit()
1374.         CType(Me.chartPI1, System.ComponentModel.ISupportInitialize).EndInit()
1375.         Me.TabPage3.ResumeLayout(False)
1376.         Me.grpboxSyringepump1.ResumeLayout(False)
1377.         Me.grpboxSyringepump1.PerformLayout()
1378.         Me.TabPage4.ResumeLayout(False)
1379.         Me.GroupBox2.ResumeLayout(False)
1380.         Me.GroupBox2.PerformLayout()
1381.         Me.TabPage5.ResumeLayout(False)
1382.         Me.grpboxRunpumpstogether.ResumeLayout(False)
1383.         Me.grpboxSyringepump1parametersforrunning.ResumeLayout(False)
1384.         Me.grpboxSyringepump1parametersforrunning.PerformLayout()
1385.         Me.ResumeLayout(False)
1386.         End Sub
1387.         Private Sub stopButton_Click(ByVal sender As System.Object, ByVal e As System.EventArgs)
1388.         timingParametersGroupBoxPI1.Enabled = True
1389.         ChartingtimerPI1.Stop()
1390.         watchPI1timer.Stop()
1391.         adjustmentpi2timer.Stop()
1392.         If Not (runningTask Is Nothing) Then
1393.         runningTask = Nothing
1394.         myTask.Dispose()
1395.         TabControl1.TabPages(2).Enabled = True
1396.         TabControl1.TabPages(3).Enabled = True
1397.         TabControl1.TabPages(4).Enabled = True
1398.         channelParametersGroupBoxPI1.Enabled = True
1399.         DesorptionTimer.Stop()
1400.         End If
1401.         End Sub
1402.         Private Sub MainForm_Load(sender As Object, e As EventArgs) Handles MyBase.Load
1403.         Me.TabControl1.SelectedIndex = 2
```

```
1404.  cmbboxInfusewithdraw1.SelectedIndex = 0
1405.  cmbboxSyringeselect1.SelectedIndex = 0
1406.  cmbboxForce1.SelectedIndex = 0
1407.  txtboxRate1.Text = "30"
1408.  cmbboxRate1.SelectedIndex = 2
1409.  txtboxTargetvolume1.Text = "500"
1410.  cmbboxTargetvolume1.SelectedIndex = 0
1411.  btnCheckcurrent1.Enabled = False
1412.  lblreadingPI1.Text = ""
1413.  lblreadingPI2.Text = ""
1414.  lblreadingPI1_1.Text = "0"
1415.  lblreadingPI2_1.Text = "0"
1416.  txtboxDesorptiontimeauto.Text = "10000"
1417.  txtboxdesorptionvolume.Text = "5"
1418.  txtboxWashflowrate.Text = "500"
1419.  txtboxWashtime.Text = "10000"
1420.  btnDrainauto.Hide()
1421.  End Sub
1422.  Private Sub btnNexttab0_Click(sender As Object, e As EventArgs) Handles btnNexttab0.Click
1423.  TabControl1.SelectTab(1)
1424.  End Sub
1425.  Private Sub btnPrevioustab1_Click(sender As Object, e As EventArgs) Handles btnPrevioustab1.Click
1426.  TabControl1.SelectTab(0)
1427.  End Sub
1428.  Private Sub btnNexttab1_Click(sender As Object, e As EventArgs) Handles btnNexttab1.Click
1429.  TabControl1.SelectTab(2)
1430.  End Sub
1431.  Private Sub btnPrevioustab2_Click(sender As Object, e As EventArgs) Handles btnPrevioustab2.Click
1432.  TabControl1.SelectTab(1)
1433.  End Sub
1434.  Private Sub btnNexttab2_Click(sender As Object, e As EventArgs) Handles btnNexttab2.Click
1435.  TabControl1.SelectTab(3)
1436.  End Sub
1437.  Private Sub btnPrevioustab3_Click(sender As Object, e As EventArgs) Handles btnPrevioustab3.Click
1438.  TabControl1.SelectTab(2)
1439.  End Sub
1440.  Private Sub btnNexttab3_Click(sender As Object, e As EventArgs) Handles btnNexttab3.Click
1441.  TabControl1.SelectTab(4)
1442.  End Sub
1443.  Private Sub btnConnect1_Click(sender As Object, e As EventArgs) Handles btnConnect1.Click
1444.  serialportSyringepump1.PortName = cmbboxSyringepump1.Text
1445.  If serialportSyringepump1.PortName = serialportSyringepump2.PortName Then
1446.  MsgBox("Pump1 = Pump2. Program doesnt like that. Different ports for different pumps! Pump 2 = COM 4,
      Pump 1 = COM 5, Clear - scan and try again!")
1447.  Else
1448.  serialportSyringepump1.BaudRate = cmbboxBaudratepump1.Text
1449.  serialportSyringepump1.Open()
1450.  btnConnect1.Enabled = False
1451.  btnDisconnect1.Enabled = True
1452.  btnscanforports.Enabled = False
1453.  btnclearallports.Enabled = True
1454.  lblparameterspump1.Show()
1455.  lbllistparameterspump1.Show()
1456.  lbllistparameterspump1.Text = "Baud rate: " & serialportSyringepump1.BaudRate.ToString + vbCrLf &
      "Stop bits: " & serialportSyringepump1.StopBits.ToString +
1457.  vbCrLf & "Data bits: " & serialportSyringepump1.DataBits.ToString + vbCrLf & "Parity: " &
      serialportSyringepump1.Parity.ToString + vbCrLf & "Handshake: " +
1458.  serialportSyringepump1.Handshake.ToString() + vbCrLf & "Read timeout: " +
      serialportSyringepump1.ReadTimeout.ToString + " ms"
1459.  btnNexttab2.Enabled = True
1460.  btnPrevioustab2.Enabled = True
1461.  TabControl1.TabPages(0).Enabled = True
```

```
1462.          TabControl1.TabPages(1).Enabled = True
1463.          TabControl1.TabPages(3).Enabled = True
1464.          TabControl1.TabPages(4).Enabled = True
1465.          cmbboxBaudratepump1.Enabled = False
1466.          cmbboxSyringepump1.Enabled = False
1467.          End If
1468.          End Sub
1469.          Private Sub btnscanforports_Click(sender As Object, e As EventArgs) Handles btnscanforports.Click
1470.          myPort = IO.Ports.SerialPort.GetPortNames()
1471.          cmbboxSyringepump1.Items.AddRange(myPort)
1472.          If cmbboxSyringepump1.Items.Count = 0 Then
1473.          MsgBox("No COM ports detected for syringe pump 1.")
1474.          ElseIf cmbboxSyringepump1.Items.Count > 0 Then
1475.          MsgBox("Syringe pump 1 COM port connected successfully.")
1476.          Else
1477.          MsgBox("You fucked up something!")
1478.          End If
1479.          cmbboxBaudratepump1.SelectedIndex = 0
1480.          cmbboxSyringepump1.SelectedIndex = 0
1481.          btnDisconnect1.Enabled = False
1482.          btnConnect1.Enabled = True
1483.          TabControl1.TabPages(0).Enabled = True
1484.          TabControl1.TabPages(1).Enabled = True
1485.          TabControl1.TabPages(3).Enabled = True
1486.          btnclearallports.Enabled = False
1487.          End Sub
1488.          Private Sub btnclearallports_Click(sender As Object, e As EventArgs) Handles btnclearallports.Click
1489.          serialportSyringepump1.Close()
1490.          serialportSyringepump2.Close()
1491.          cmbboxSyringepump1.Enabled = True
1492.          cmbboxBaudratepump1.Enabled = True
1493.          cmbboxSyringepump1.Items.Clear()
1494.          btnscanforports.Enabled = True
1495.          btnDisconnect1.Enabled = False
1496.          btnConnect1.Enabled = False
1497.          btnclearallports.Enabled = False
1498.          TabControl1.TabPages(0).Enabled = False
1499.          TabControl1.TabPages(1).Enabled = False
1500.          TabControl1.TabPages(3).Enabled = False
1501.          btnNexttab2.Enabled = False
1502.          btnPrevioustab2.Enabled = False
1503.          End Sub
1504.          Private Sub btnDisconnect1_Click(sender As Object, e As EventArgs) Handles btnDisconnect1.Click
1505.          serialportSyringepump1.Close()
1506.          serialportSyringepump2.Close()
1507.          cmbboxSyringepump1.Items.Clear()
1508.          btnDisconnect1.Enabled = False
1509.          TabControl1.TabPages(0).Enabled = False
1510.          TabControl1.TabPages(1).Enabled = False
1511.          TabControl1.TabPages(3).Enabled = False
1512.          btnNexttab2.Enabled = False
1513.          btnPrevioustab2.Enabled = False
1514.          lbllistparameterspump1.Hide()
1515.          lblparameterspump1.Hide()
1516.          btnclearallports.Enabled = True
1517.          MsgBox("Clear all ports, then scan all ports in order to reestablish communication.")
1518.          cmbboxBaudratepump1.Enabled = True
1519.          cmbboxSyringepump1.Enabled = True
1520.          lbllistparameterspump1.Text = ""
1521.          End Sub
1522.          Private Sub btnSend1sendcommands_Click(sender As Object, e As EventArgs) Handles
               btnSend1sendcommands.Click
```

```
1523.         lblOutput1sendcommands.Text = ""
1524.         serialportSyringepump1.Write(txtboxInput1sendcommands.Text & vbCrLf)
1525.         txtboxInput1sendcommands.Clear()
1526.         lblOutput1sendcommands.Text = serialportSyringepump1.ReadLine()
1527.         End Sub
1528.         Private Sub btnSend2sendcommands_Click(sender As Object, e As EventArgs)
1529.         End Sub
1530.         Private Sub txtboxDesorptiontimeauto_KeyPress(sender As Object, e As KeyPressEventArgs) Handles
             txtboxDesorptiontimeauto.KeyPress
1531.         If e.KeyChar <> ControlChars.Back Then
1532.         e.Handled = Not (Char.IsDigit(e.KeyChar))
1533.         End If
1534.         End Sub
1535.         Private Sub txtboxwashtime_KeyPress(sender As Object, e As KeyPressEventArgs) Handles
             txtboxWashtime.KeyPress
1536.         If e.KeyChar <> ControlChars.Back Then
1537.         e.Handled = Not (Char.IsDigit(e.KeyChar))
1538.         End If
1539.         End Sub
1540.         Private Sub txtboxWashflowrate_KeyPress(sender As Object, e As KeyPressEventArgs) Handles
             txtboxWashflowrate.KeyPress
1541.         If e.KeyChar <> ControlChars.Back Then
1542.         e.Handled = Not (Char.IsDigit(e.KeyChar))
1543.         End If
1544.         End Sub
1545.         Private Sub txtboxSuctiontime_KeyPress(sender As Object, e As KeyPressEventArgs)
1546.         If e.KeyChar <> ControlChars.Back Then
1547.         e.Handled = Not (Char.IsDigit(e.KeyChar))
1548.         End If
1549.         End Sub
1550.         Private Sub txtboxNumwashes_KeyPress(sender As Object, e As KeyPressEventArgs)
1551.         If e.KeyChar <> ControlChars.Back Then
1552.         e.Handled = Not (Char.IsDigit(e.KeyChar))
1553.         End If
1554.         End Sub
1555.         Private Sub txtboxNumwashesDatacollection_KeyPress(sender As Object, e As KeyPressEventArgs)
1556.         If e.KeyChar <> ControlChars.Back Then
1557.         e.Handled = Not (Char.IsDigit(e.KeyChar))
1558.         End If
1559.         End Sub
1560.         Private Sub txtboxInput1sendcommands_KeyPress(sender As Object, e As KeyPressEventArgs) Handles
             txtboxInput1sendcommands.KeyPress
1561.         End Sub
1562.         Private Sub txtSuctiontimedatacollection_KeyPress(sender As Object, e As KeyPressEventArgs)
1563.         If e.KeyChar <> ControlChars.Back Then
1564.         e.Handled = Not (Char.IsDigit(e.KeyChar))
1565.         End If
1566.         End Sub
1567.         Private Sub btnSubmit1_Click(sender As Object, e As EventArgs) Handles btnSubmit1.Click
1568.         If cmbboxSyringeselect1.SelectedItem = "Hamilton 1750" Then
1569.         serialportSyringepump1.Write("syrm hm3 500 ul" & vbCrLf)
1570.         ElseIf cmbboxSyringeselect1.SelectedItem = "Hamilton 1005" Then
1571.         serialportSyringepump1.Write("syrm hm2 5 ml" & vbCrLf)
1572.         End If
1573.         serialportSyringepump1.Write("force " & cmbboxForce1.SelectedItem & vbCrLf)
1574.         If cmbboxSyringeselect1.SelectedItem = "Infuse" Then
1575.         serialportSyringepump1.Write("irate " & txtboxRate1.Text & " " & cmbboxRate1.SelectedItem.ToString &
             vbCrLf)
1576.         ElseIf cmbboxSyringeselect1.SelectedItem = "Withdraw" Then
1577.         serialportSyringepump1.Write("wrate " & txtboxRate1.Text & " " & cmbboxRate1.SelectedItem.ToString &
             vbCrLf)
1578.         End If
```

```
1579.  serialportSyringepump1.Write("tvolume " & txtboxTargetvolume1.Text & " " &
       cmbboxTargetvolume1.SelectedItem.ToString & vbCrLf)
1580.  End Sub
1581.  Private Sub cmbboxSyringeselect1_SelectedIndexChanged(sender As Object, e As EventArgs) Handles
       cmbboxSyringeselect1.SelectedIndexChanged
1582.  cmbboxForce1.Items.Clear()
1583.  cmbboxRate1.Items.Clear()
1584.  cmbboxTargetvolume1.Items.Clear()
1585.  If cmbboxSyringeselect1.SelectedItem = "Hamilton 1750" Then
1586.  cmbboxForce1.Items.Add("30")
1587.  cmbboxRate1.Items.Add("ul/hr")
1588.  cmbboxRate1.Items.Add("ul/min")
1589.  cmbboxRate1.Items.Add("ul/sec")
1590.  cmbboxTargetvolume1.Items.Add("ul")
1591.  ElseIf cmbboxSyringeselect1.SelectedItem = "Hamilton 1005" Then
1592.  cmbboxForce1.Items.Add("50")
1593.  cmbboxRate1.Items.Add("ml/hr")
1594.  cmbboxRate1.Items.Add("ml/min")
1595.  cmbboxRate1.Items.Add("ml/sec")
1596.  cmbboxRate1.Items.Add("ul/hr")
1597.  cmbboxRate1.Items.Add("ul/min")
1598.  cmbboxRate1.Items.Add("ul/sec")
1599.  cmbboxTargetvolume1.Items.Add("ml")
1600.  cmbboxTargetvolume1.Items.Add("ul")
1601.  End If
1602.  End Sub
1603.  Private Sub txtboxRate1_KeyPress(sender As Object, e As KeyPressEventArgs) Handles
       txtboxRate1.KeyPress
1604.  If e.KeyChar <> ControlChars.Back Then
1605.  e.Handled = Not (Char.IsDigit(e.KeyChar) Or e.KeyChar = ".")
1606.  End If
1607.  End Sub
1608.  Private Sub txtboxTargetvolume1_KeyPress(sender As Object, e As KeyPressEventArgs) Handles
       txtboxTargetvolume1.KeyPress
1609.  If e.KeyChar <> ControlChars.Back Then
1610.  e.Handled = Not (Char.IsDigit(e.KeyChar) Or e.KeyChar = ".")
1611.  End If
1612.  End Sub
1613.  Private Sub txtboxRate2_KeyPress(sender As Object, e As KeyPressEventArgs)
1614.  If e.KeyChar <> ControlChars.Back Then
1615.  e.Handled = Not (Char.IsDigit(e.KeyChar) Or e.KeyChar = ".")
1616.  End If
1617.  End Sub
1618.  Private Sub txtboxTargetvolume2_KeyPress(sender As Object, e As KeyPressEventArgs)
1619.  If e.KeyChar <> ControlChars.Back Then
1620.  e.Handled = Not (Char.IsDigit(e.KeyChar) Or e.KeyChar = ".")
1621.  End If
1622.  End Sub
1623.  Private Sub btnNewmethod_Click(sender As Object, e As EventArgs) Handles btnClearall.Click
1624.  cmbboxInfusewithdraw1.Items.Clear()
1625.  cmbboxSyringeselect1.Items.Clear()
1626.  cmbboxForce1.Items.Clear()
1627.  cmbboxRate1.Items.Clear()
1628.  txtboxRate1.Clear()
1629.  cmbboxTargetvolume1.Items.Clear()
1630.  txtboxTargetvolume1.Clear()
1631.  End Sub
1632.  Private Sub btnSavemethod_Click(sender As Object, e As EventArgs) Handles btnSavemethod.Click
1633.  Dim savemethod As String
1634.  savemethod = Microsoft.VisualBasic.InputBox("Enter the file name: ", "Save method", "", 500, 700)
1635.  If savemethod = "" Then
1636.  Exit Sub
```

```
1637.          End If
1638.          MessageBox.Show("Disabled at the moment ... enable at the end")
1639.          End Sub
1640.          Private Sub btnLoadMethod_Click(sender As Object, e As EventArgs) Handles btnLoadMethod.Click
1641.          Dim loadmethod As String
1642.          loadmethod = Microsoft.VisualBasic.InputBox("Enter the method name you wish to load: ", "Load method",
               "", 500, 700)
1643.          If loadmethod = "" Then
1644.          Exit Sub
1645.          End If
1646.          Dim counter1 As String = ""
1647.          Dim counter3 As String = ""
1648.          Dim counter4 As String = ""
1649.          Dim counter7 As String = ""
1650.          Dim counter8 As String = ""
1651.          Dim counter9 As String = ""
1652.          Dim counter11 As String = ""


1653.          cmbboxInfusewithdraw1.Items.Clear()
1654.          cmbboxSyringeselect1.Items.Clear()
1655.          cmbboxForce1.Items.Clear()
1656.          cmbboxRate1.Items.Clear()
1657.          txtboxRate1.Clear()
1658.          cmbboxTargetvolume1.Items.Clear()
1659.          txtboxTargetvolume1.Clear()
1660.          MessageBox.Show("Disabled at the moment ...")
1661.          End Sub
1662.          Private Sub Button3_Click(sender As Object, e As EventArgs) Handles btnPreviousMethods.Click
1663.          TabControl1.SelectTab(3)
1664.          End Sub
1665.          Private Sub btnDisconnect2_Click(sender As Object, e As EventArgs)
1666.          btnscanforports.Enabled = False
1667.          btnclearallports.Enabled = True
1668.          End Sub
1669.          Private Sub txtboxDesorptionTime_KeyPress(sender As Object, e As KeyPressEventArgs)
1670.          If e.KeyChar <> ControlChars.Back Then
1671.          e.Handled = Not (Char.IsDigit(e.KeyChar))
1672.          End If
1673.          End Sub
1674.          Private Sub DesorptionTimer_Tick(sender As Object, e As EventArgs) Handles DesorptionTimer.Tick
1675.          timeleft = timeleft - DesorptionTimer.Interval
1676.          lblDesorptiontimer.Text = timeleft.ToString
1677.          If timeleft = 0 Then
1678.          DesorptionTimer.Stop()
1679.          End If
1680.          End Sub
1681.          Private Sub btnstartauto_Click(sender As Object, e As EventArgs) Handles btnStartauto.Click
1682.          GroupBox1.Enabled = False
1683.          GroupBox4.Enabled = False
1684.          grpboxSaveloadmethodMS.Enabled = False
1685.          btnNexttab1.Enabled = False
1686.          TabControl1.TabPages(2).Enabled = False
1687.          TabControl1.TabPages(3).Enabled = False
1688.          TabControl1.TabPages(4).Enabled = False
1689.          txtboxDesorptiontimeauto.Enabled = False
1690.          txtboxdesorptionvolume.Enabled = False
1691.          txtboxWashflowrate.Enabled = False
1692.          txtboxWashtime.Enabled = False
1693.          lblreadingPI1_1.Text = "4.4"
1694.          lblreadingPI2_1.Text = "0"
1695.          btnStartauto.Enabled = False
```

```
1696.          btnStopauto.Enabled = True
1697.          btnStopcollectionchart.Enabled = False
1698.          If txtboxDesorptiontimeauto.Text = "" Or txtboxdesorptionvolume.Text = "" Then
1699.          MessageBox.Show("Enter values for desorption time (ms) and desorption volume (uL)")
1700.          Exit Sub
1701.          End If
1702.          MessageBox.Show("Press OK when ready for desorption.", "Important Message")
1703.          DesorptionTimerauto.Stop()
1704.          desorptiontimestopwatch.Reset()
1705.          desorptiontimestopwatch.Start()
1706.          DesorptionTimerauto.Start()
1707.          End Sub
1708.          Private Sub DesorptionTimerauto_Tick(sender As Object, e As EventArgs) Handles
               DesorptionTimerauto.Tick
1709.          elapseddesorptiontime = desorptiontimestopwatch.ElapsedMilliseconds()
1710.          lblDesorptiontimer.Text = elapseddesorptiontime.ToString
1711.          If elapseddesorptiontime >= Convert.ToInt32(txtboxDesorptiontimeauto.Text) Then
1712.          DesorptionTimerauto.Stop()
1713.          desorptiontimestopwatch.Reset()
1714.          btnDrainauto_Click(btnDrainauto, New EventArgs())
1715.          End If
1716.          End Sub
1717.          Private Sub btnDrainauto_Click(sender As Object, e As EventArgs) Handles btnDrainauto.Click
1718.          btnStartPI1_Click(btnStartPI1, New EventArgs())
1719.          serialportSyringepump1.Write("stop" & vbCrLf)
1720.          lblcurrentpumpflowrate.Text = "0"
1721.          watchPI1timer.Start()
1722.          suctiontimestopwatchPI1.Start()
1723.          washingulmin = Convert.ToInt32(txtboxWashflowrate.Text)
1724.          End Sub
1725.          Private Sub Timer2_Tick(sender As Object, e As EventArgs) Handles watchPI1timer.Tick
1726.          lblcurrentsuctiontime.Text = suctiontimestopwatchPI1.ElapsedMilliseconds.ToString
1727.          If Convert.ToDecimal(lblreadingPI1_1.Text) < 3.5 Then
1728.          btnStopPI1_Click(btnStopPI1, New EventArgs())
1729.          GroupBox1.Enabled = False
1730.          GroupBox4.Enabled = False
1731.          txtboxDesorptiontimeauto.Enabled = False
1732.          txtboxdesorptionvolume.Enabled = False
1733.          txtboxWashflowrate.Enabled = False
1734.          txtboxWashtime.Enabled = False
1735.          btnStartauto.Enabled = False
1736.          btnStopauto.Enabled = True
1737.          TabControl1.TabPages(2).Enabled = False
1738.          TabControl1.TabPages(3).Enabled = False
1739.          TabControl1.TabPages(4).Enabled = False
1740.          btnNexttab1.Enabled = False
1741.          suctionflowrate = Convert.ToDecimal(txtboxdesorptionvolume.Text) /
               suctiontimestopwatchPI1.ElapsedMilliseconds.ToString * 1000 * 60
1742.          lblbroken.Text = suctionflowrate.ToString
1743.          newpumpflowrate = suctionflowrate
1744.          watchPI1timer.Stop()
1745.          suctiontimestopwatchPI1.Reset()
1746.          serialportSyringepump1.Write("irate " & washingulmin & " uL/min" & vbCrLf)
1747.          serialportSyringepump1.Write("run" & vbCrLf)
1748.          lblcurrentpumpflowrate.Text = Convert.ToString(txtboxWashflowrate.Text)
1749.          washing200ulmintime = 0
1750.          washingtimer200ulmin.Start()
1751.          washing200ulminstopwatch.Reset()
1752.          washing200ulminstopwatch.Start()
1753.          End If
1754.          End Sub
1755.          Private Sub Timer6_Tick(sender As Object, e As EventArgs) Handles washingtimer200ulmin.Tick
```

```
1756.           washing200ulmintime = washing200ulminstopwatch.ElapsedMilliseconds
1757.           lblwash200ulmintimer.Text = washing200ulmintime.ToString
1758.           If washing200ulmintime >= Convert.ToInt32(txtboxWashtime.Text) Then
1759.           serialportSyringepump1.Write("irate " & suctionflowrate & " uL/min" & vbCrLf)
1760.           serialportSyringepump1.Write("run" & vbCrLf)
1761.           adjustmentpi2timer.Stop()
1762.           btnStopPI2_Click(btnStopPI2, New EventArgs())
1763.           GroupBox1.Enabled = False
1764.           GroupBox4.Enabled = False
1765.           txtboxDesorptiontimeauto.Enabled = False
1766.           txtboxdesorptionvolume.Enabled = False
1767.           txtboxWashflowrate.Enabled = False
1768.           txtboxWashtime.Enabled = False
1769.           btnStartauto.Enabled = False
1770.           TabControl1.TabPages(2).Enabled = False
1771.           TabControl1.TabPages(3).Enabled = False
1772.           TabControl1.TabPages(4).Enabled = False
1773.           btnNexttab1.Enabled = False
1774.           washingtimer200ulmin.Stop()
1775.           washing200ulminstopwatch.Reset()
1776.           btnstartauto_Click(btnStartauto, New EventArgs())
1777.           End If
1778.           End Sub
1779.           Private Sub Timer3_Tick(sender As Object, e As EventArgs) Handles adjustmentpi2timer.Tick
1780.           If Convert.ToDecimal(lblreadingPI2_1.Text) < 2.2 Then
1781.           currentpumpflowrate = Convert.ToInt32(lblcurrentpumpflowrate.Text)
1782.           ElseIf Convert.ToDecimal(lblreadingPI2_1.Text) >= 2.2 Then
1783.           End If
1784.           End Sub
1785.           Private Sub btnStartPI1_Click(sender As Object, e As EventArgs) Handles btnStartPI1.Click
1786.           physicalChannelComboBoxPI1.Enabled = False
1787.           minimumValueNumericPI1.Enabled = False
1788.           maximumValueNumericPI1.Enabled = False
1789.           samplesPerChannelNumericPI1.Enabled = False
1790.           rateNumericPI1.Enabled = False
1791.           btnStartPI1.Enabled = False
1792.           GroupBox4.Enabled = False
1793.           txtboxDesorptiontimeauto.Enabled = False
1794.           txtboxdesorptionvolume.Enabled = False
1795.           txtboxWashflowrate.Enabled = False
1796.           txtboxWashtime.Enabled = False
1797.           btnStartauto.Enabled = False
1798.           btnStopauto.Enabled = False
1799.           TabControl1.TabPages(2).Enabled = False
1800.           TabControl1.TabPages(3).Enabled = False
1801.           TabControl1.TabPages(4).Enabled = False
1802.           btnNexttab1.Enabled = False
1803.           grpboxSaveloadmethodMS.Enabled = False
1804.           My.Computer.FileSystem.DeleteFile("D:\Emir Desktop\MOI photometric\Flow Control (MS)_v6 -
                2022_03\Exported data\test PI 1.txt")
1805.           If runningTask Is Nothing Then
1806.           Try
1807.           myTask = New Task()
1808.           myTask.AIChannels.CreateVoltageChannel(physicalChannelComboBoxPI1.Text, "",
1809.           CType(-1, AITerminalConfiguration), Convert.ToDouble(minimumValueNumericPI1.Value),
1810.           Convert.ToDouble(maximumValueNumericPI1.Value), AIVoltageUnits.Volts)
1811.           myTask.Timing.ConfigureSampleClock("", Convert.ToDouble(rateNumericPI1.Value),
1812.           SampleClockActiveEdge.Rising, SampleQuantityMode.ContinuousSamples, 1000)
1813.           myTask.Control(TaskAction.Verify)
1814.           runningTask = myTask
1815.           analogInReader = New AnalogMultiChannelReader(myTask.Stream)
1816.           analogCallback = New AsyncCallback(AddressOf AnalogInCallback)
```

```
1817.  InitializeDataTable(myTask.AIChannels, dataTable)
1818.  acquisitionDataGrid.DataSource = dataTable
1819.  analogInReader.SynchronizeCallbacks = True
1820.  analogInReader.BeginReadWaveform(Convert.ToInt32(samplesPerChannelNumericPI1.Value),
       analogCallback, myTask)
1821.  ChartingtimerPI1.Stop()
1822.  ChartingtimerPI1.Start()
1823.  TabControl1.TabPages(2).Enabled = False
1824.  TabControl1.TabPages(3).Enabled = False
1825.  TabControl1.TabPages(4).Enabled = False
1826.  channelParametersGroupBoxPI1.Enabled = False
1827.  timingParametersGroupBoxPI1.Enabled = False
1828.  Catch exception As DaqException
1829.  MessageBox.Show(exception.Message)
1830.  runningTask = Nothing
1831.  myTask.Dispose()
1832.  End Try
1833.  End If
1834.  End Sub
1835.  Private Sub AnalogInCallback(ByVal ar As IAsyncResult)
1836.  Try
1837.  If (Not (runningTask Is Nothing)) AndAlso runningTask Is ar.AsyncState Then
1838.  data = analogInReader.EndReadWaveform(ar)
1839.  dataToDataTable(data, dataTable)
       analogInReader.BeginMemoryOptimizedReadWaveform(Convert.ToInt32(samplesPerChannelNumericPI1.V
       alue), analogCallback, myTask, data)
1840.  End If
1841.  Catch ex As DaqException
1842.  MessageBox.Show(ex.Message)
1843.  runningTask = Nothing
1844.  myTask.Dispose()
1845.  End Try
1846.  End Sub
1847.  Private Sub dataToDataTable(ByVal sourceArray As AnalogWaveform(Of Double)(), ByRef dataTable As
       DataTable)
1848.  Dim currentLineIndex As Integer = 0
1849.  For Each waveform As AnalogWaveform(Of Double) In sourceArray
1850.  Dim dataCount As Integer = 0
1851.  If waveform.Samples.Count < 10 Then
1852.  dataCount = waveform.Samples.Count
1853.  Else
1854.  dataCount = 10
1855.  End If
1856.  For sample As Integer = 0 To (dataCount - 1)
1857.  dataTable.Rows(sample)(currentLineIndex) = waveform.Samples(sample).Value
1858.  lblreadingPI1.Text = waveform.Samples(sample).Value
1859.  lblreadingPI1_1.Text = lblreadingPI1.Text
1860.  lblgraphreadingPI1.Text = lblreadingPI1.Text
1861.  file = My.Computer.FileSystem.OpenTextFileWriter("D:\Emir Desktop\MOI photometric\Flow Control
       (MS)_v6 - 2022_03\Exported data\test PI 1.txt", True) 'ili dodati C:\path\test.txt'
1862.  file.WriteLine(lblreadingPI1.Text)
1863.  file.Close()
1864.  lblreadingPI1.Text = ""
1865.  Next
1866.  currentLineIndex += 1
1867.  Next
1868.  End Sub
1869.  Public Sub InitializeDataTable(ByVal channelCollection As AIChannelCollection, ByRef data As DataTable)
1870.  Dim numOfChannels As Int16 = channelCollection.Count
1871.  data.Rows.Clear()
1872.  data.Columns.Clear()
1873.  dataColumn = New DataColumn(numOfChannels) {}
```

```
1874.          Dim numOfRows As Int16 = 10
1875.          Dim currentChannelIndex As Int16 = 0
1876.          Dim currentDataIndex As Int16 = 0
1877.          For currentChannelIndex = 0 To (numOfChannels - 1)
1878.          dataColumn(currentChannelIndex) = New DataColumn
1879.          dataColumn(currentChannelIndex).DataType = System.Type.GetType("System.Double")
1880.         dataColumn(currentChannelIndex).ColumnName = channelCollection(currentChannelIndex).PhysicalName
1881.          Next
1882.          data.Columns.AddRange(dataColumn)
1883.          For currentDataIndex = 0 To (numOfRows - 1)
1884.          Dim rowArr As Object() = New Object(numOfChannels - 1) {}
1885.          data.Rows.Add(rowArr)
1886.          Next
1887.          End Sub
1888.         Private Sub btnStartPI2_Click(sender As Object, e As EventArgs) Handles btnStartPI2.Click
1889.          physicalChannelComboBoxPI2.Enabled = False
1890.          minimumValueNumericPI2.Enabled = False
1891.          maximumValueNumericPI2.Enabled = False
1892.          samplesPerChannelNumericPI2.Enabled = False
1893.          rateNumericPI2.Enabled = False
1894.          btnStartPI2.Enabled = False
1895.          GroupBox1.Enabled = False
1896.          btnStartauto.Enabled = False
1897.          btnStopauto.Enabled = False
1898.          txtboxDesorptiontimeauto.Enabled = False
1899.          txtboxdesorptionvolume.Enabled = False
1900.          txtboxWashflowrate.Enabled = False
1901.          txtboxWashtime.Enabled = False
1902.          TabControl1.TabPages(2).Enabled = False
1903.          TabControl1.TabPages(3).Enabled = False
1904.          TabControl1.TabPages(4).Enabled = False
1905.          btnNexttab1.Enabled = False
1906.          grpboxSaveloadmethodMS.Enabled = False
1907.         My.Computer.FileSystem.DeleteFile("D:\Emir Desktop\MOI photometric\Flow Control (MS)_v6 -
              2022_03\Exported data\test PI 2.txt")
1908.          If runningTaskPI2 Is Nothing Then
1909.          Try
1910.          myTaskPI2 = New Task()
1911.          myTaskPI2.AIChannels.CreateVoltageChannel(physicalChannelComboBoxPI2.Text, "",
1912.         CType(-1, AITerminalConfiguration), Convert.ToDouble(minimumValueNumericPI2.Value),
1913.          Convert.ToDouble(maximumValueNumericPI2.Value), AIVoltageUnits.Volts)
1914.          myTaskPI2.Timing.ConfigureSampleClock("", Convert.ToDouble(rateNumericPI2.Value),
1915.          SampleClockActiveEdge.Rising, SampleQuantityMode.ContinuousSamples, 1000)
1916.          myTaskPI2.Control(TaskAction.Verify)
1917.          runningTaskPI2 = myTaskPI2
1918.          analogInReaderPI2 = New AnalogMultiChannelReader(myTaskPI2.Stream)
1919.          analogCallbackPI2 = New AsyncCallback(AddressOf AnalogInCallbackPI2)
1920.          InitializeDataTablePI2(myTaskPI2.AIChannels, dataTablePI2)
1921.          acquisitionDataGridPI2.DataSource = dataTablePI2
1922.          analogInReaderPI2.SynchronizeCallbacks = True
1923.         analogInReaderPI2.BeginReadWaveform(Convert.ToInt32(samplesPerChannelNumericPI2.Value),
              analogCallbackPI2, myTaskPI2)
1924.          ChartingtimerPI2.Stop()
1925.          ChartingtimerPI2.Start()
1926.          channelParametersGroupBoxPI2.Enabled = False
1927.          timingParametersGroupBoxPI2.Enabled = False
1928.          Catch exception As DaqException
1929.          MessageBox.Show(exception.Message)
1930.          runningTaskPI2 = Nothing
1931.          myTaskPI2.Dispose()
1932.          End Try
1933.          End If
```

```
1934.  End Sub
1935.  Private Sub AnalogInCallbackPI2(ByVal ar As IAsyncResult)
1936.  Try
1937.  If (Not (runningTaskPI2 Is Nothing)) AndAlso runningTaskPI2 Is ar.AsyncState Then
1938.  dataPI2 = analogInReaderPI2.EndReadWaveform(ar)
1939.  dataToDataTablePI2(dataPI2, dataTablePI2)
       analogInReaderPI2.BeginMemoryOptimizedReadWaveform(Convert.ToInt32(samplesPerChannelNumericPI
       2.Value), analogCallbackPI2, myTaskPI2, dataPI2)
1940.  End If
1941.  Catch ex As DaqException
1942.  MessageBox.Show(ex.Message)
1943.  runningTaskPI2 = Nothing
1944.  myTaskPI2.Dispose()
1945.  End Try
1946.  End Sub
1947.  Private Sub dataToDataTablePI2(ByVal sourceArrayPI2 As AnalogWaveform(Of Double)(), ByRef
       dataTablePI2 As DataTable)
1948.  Dim currentLineIndexPI2 As Integer = 0
1949.  For Each waveformPI2 As AnalogWaveform(Of Double) In sourceArrayPI2
1950.  Dim dataCountPI2 As Integer = 0
1951.  If waveformPI2.Samples.Count < 10 Then
1952.  dataCountPI2 = waveformPI2.Samples.Count
1953.  Else
1954.  dataCountPI2 = 10
1955.  End If
1956.  For samplePI2 As Integer = 0 To (dataCountPI2 - 1)
1957.  dataTablePI2.Rows(samplePI2)(currentLineIndexPI2) = waveformPI2.Samples(samplePI2).Value
1958.  lblreadingPI2.Text = waveformPI2.Samples(samplePI2).Value
1959.  lblreadingPI2.Text = lblreadingPI2.Text
1960.  lblreadingPI2_1.Text = lblreadingPI2.Text
1961.  lblgraphreadingPI2.Text = lblreadingPI2.Text
1962.  file = My.Computer.FileSystem.OpenTextFileWriter("D:\Emir Desktop\MOI photometric\Flow Control
       (MS)_v6 - 2022_03\Exported data\test PI 2.txt", True) 'ili dodati C:\path\test.txt'
1963.  file.WriteLine(lblreadingPI2.Text)
1964.  file.Close()
1965.  lblreadingPI2.Text = ""
1966.  Next
1967.  currentLineIndexPI2 += 1
1968.  Next
1969.  End Sub
1970.  Public Sub InitializeDataTablePI2(ByVal channelCollectionPI2 As AIChannelCollection, ByRef dataPI2 As
       DataTable)
1971.  Dim numOfChannelsPI2 As Int16 = channelCollectionPI2.Count
1972.  dataPI2.Rows.Clear()
1973.  dataPI2.Columns.Clear()
1974.  dataColumnPI2 = New DataColumn(numOfChannelsPI2) {}
1975.  Dim numOfRowsPI2 As Int16 = 10
1976.  Dim currentChannelIndexPI2 As Int16 = 0
1977.  Dim currentDataIndexPI2 As Int16 = 0
1978.  For currentChannelIndexPI2 = 0 To (numOfChannelsPI2 - 1)
1979.  dataColumnPI2(currentChannelIndexPI2) = New DataColumn
1980.  dataColumnPI2(currentChannelIndexPI2).DataType = System.Type.GetType("System.Double")
1981.  dataColumnPI2(currentChannelIndexPI2).ColumnName =
       channelCollectionPI2(currentChannelIndexPI2).PhysicalName
1982.  Next
1983.  dataPI2.Columns.AddRange(dataColumnPI2)
1984.  For currentDataIndexPI2 = 0 To (numOfRowsPI2 - 1)
1985.  Dim rowArr As Object() = New Object(numOfChannelsPI2 - 1) {}
1986.  dataPI2.Rows.Add(rowArr)
1987.  Next
1988.  End Sub
1989.  Private Sub btnStopPI1_Click(sender As Object, e As EventArgs) Handles btnStopPI1.Click
```

```
1990.          physicalChannelComboBoxPI1.Enabled = True
1991.          minimumValueNumericPI1.Enabled = True
1992.          maximumValueNumericPI1.Enabled = True
1993.          samplesPerChannelNumericPI1.Enabled = True
1994.          rateNumericPI1.Enabled = True
1995.          btnStartPI1.Enabled = True
1996.          GroupBox4.Enabled = True
1997.          btnStartauto.Enabled = True
1998.          btnStopauto.Enabled = True
1999.          txtboxDesorptiontimeauto.Enabled = True
2000.          txtboxdesorptionvolume.Enabled = True
2001.          txtboxWashflowrate.Enabled = True
2002.          txtboxWashtime.Enabled = True
2003.          TabControl1.TabPages(2).Enabled = True
2004.          TabControl1.TabPages(3).Enabled = True
2005.          TabControl1.TabPages(4).Enabled = True
2006.          btnNexttab1.Enabled = True
2007.          grpboxSaveloadmethodMS.Enabled = True
2008.          ChartingtimerPI1.Stop()
2009.          If Not (runningTask Is Nothing) Then
2010.          runningTask = Nothing
2011.          myTask.Dispose()
2012.          channelParametersGroupBoxPI1.Enabled = True
2013.          timingParametersGroupBoxPI1.Enabled = True
2014.          End If
2015.          lblreadingPI1_1.Text = "0"
2016.          lblgraphreadingPI1.Text = "0"
2017.          End Sub
2018.          Private Sub btnStopPI2_Click(sender As Object, e As EventArgs) Handles btnStopPI2.Click
2019.          physicalChannelComboBoxPI2.Enabled = True
2020.          minimumValueNumericPI2.Enabled = True
2021.          maximumValueNumericPI2.Enabled = True
2022.          samplesPerChannelNumericPI2.Enabled = True
2023.          rateNumericPI2.Enabled = True
2024.          btnStartPI2.Enabled = True
2025.          GroupBox1.Enabled = True
2026.          btnStartauto.Enabled = True
2027.          btnStopauto.Enabled = True
2028.          txtboxDesorptiontimeauto.Enabled = True
2029.          txtboxdesorptionvolume.Enabled = True
2030.          txtboxWashflowrate.Enabled = True
2031.          txtboxWashtime.Enabled = True
2032.          TabControl1.TabPages(2).Enabled = True
2033.          TabControl1.TabPages(3).Enabled = True
2034.          TabControl1.TabPages(4).Enabled = True
2035.          btnNexttab1.Enabled = True
2036.          grpboxSaveloadmethodMS.Enabled = True
2037.          ChartingtimerPI2.Stop()
2038.          If Not (runningTaskPI2 Is Nothing) Then
2039.          runningTaskPI2 = Nothing
2040.          myTaskPI2.Dispose()
2041.          channelParametersGroupBoxPI2.Enabled = True
2042.          timingParametersGroupBoxPI2.Enabled = True
2043.          End If
2044.          lblreadingPI2_1.Text = "0"
2045.          lblgraphreadingPI2.Text = "0"
2046.          End Sub
2047.          Private Sub btnStopPI3_Click(sender As Object, e As EventArgs)
2048.          ChartingtimerPI3.Stop()
2049.          If Not (runningTaskPI3 Is Nothing) Then
2050.          runningTaskPI3 = Nothing
2051.          myTaskPI3.Dispose()
```

```
2052.         End If
2053.         End Sub
2054.         Private Sub ChartingtimerPI2_Tick(sender As Object, e As EventArgs) Handles ChartingtimerPI2.Tick
2055.         ChartingtimerPI2.Interval = 1000 'miliseconds'
2056.         chartPI2.Series(0).Points.Clear()
2057.         For Each line As String In IO.File.ReadAllLines("D:\Emir Desktop\MOI photometric\Flow Control (MS)_v6
              - 2022_03\Exported data\test PI 2.txt")
2058.         Dim points() As Double = Array.ConvertAll(line.Split(" "c), Function(s) CDbl(s))
2059.         chartPI2.Series(0).Points.AddY(points(0))
2060.         chartPI2.Series(0).XValueMember = "Time (ms)"
2061.         chartPI2.Series(0).YValueMembers = "Voltage (V)"
2062.         Next
2063.         End Sub
2064.         Private Sub ChartingtimerPI1_Tick(sender As Object, e As EventArgs) Handles ChartingtimerPI1.Tick
2065.         ChartingtimerPI1.Interval = 1000 'miliseconds'
2066.         chartPI1.Series(0).Points.Clear()
2067.         For Each line As String In IO.File.ReadAllLines("D:\Emir Desktop\MOI photometric\Flow Control (MS)_v6
              - 2022_03\Exported data\test PI 1.txt")
2068.         Dim points() As Double = Array.ConvertAll(line.Split(" "c), Function(s) CDbl(s))
2069.         chartPI1.Series(0).Points.AddY(points(0))
2070.         chartPI1.Series(0).XValueMember = "Time (ms)"
2071.         chartPI1.Series(0).YValueMembers = "Voltage (V)"
2072.         Next
2073.         End Sub
2074.         Private Sub btnStopauto_Click(sender As Object, e As EventArgs) Handles btnStopauto.Click
2075.         GroupBox1.Enabled = True
2076.         GroupBox4.Enabled = True
2077.         grpboxSaveloadmethodMS.Enabled = True
2078.         btnNexttab1.Enabled = True
2079.         TabControl1.TabPages(2).Enabled = True
2080.         TabControl1.TabPages(3).Enabled = True
2081.         TabControl1.TabPages(4).Enabled = True
2082.         btnNexttab1.Enabled = True
2083.         txtboxDesorptiontimeauto.Enabled = True
2084.         txtboxdesorptionvolume.Enabled = True
2085.         txtboxWashflowrate.Enabled = True
2086.         txtboxWashtime.Enabled = True
2087.         btnStartauto.Enabled = True
2088.         btnStopauto.Enabled = False
2089.         GroupBox1.Enabled = True
2090.         GroupBox4.Enabled = True
2091.         btnStopcollectionchart.Enabled = True
2092.         DesorptionTimerauto.Stop()
2093.         watchPI1timer.Stop()
2094.         washingtimer200ulmin.Stop()
2095.         adjustmentpi2timer.Stop()
2096.         desorptiontimestopwatch.Reset()
2097.         suctiontimestopwatchPI1.Reset()
2098.         washing200ulminstopwatch.Reset()
2099.         lblDesorptiontimer.Text = "..."
2100.         lblbroken.Text = "..."
2101.         lblcurrentpumpflowrate.Text = "..."
2102.         lblcurrentsuctiontime.Text = "..."
2103.         lblwash200ulmintimer.Text = "..."
2104.         btnStopPI1_Click(btnStopPI1, New EventArgs())
2105.         btnStopPI2_Click(btnStopPI2, New EventArgs())
2106.         newpumpflowrate = 0
2107.         End Sub
2108.         Private Sub btnStopcollectionchart_Click(sender As Object, e As EventArgs) Handles
              btnStopcollectionchart.Click
2109.         btnStopPI1_Click(btnStopPI1, New EventArgs)
2110.         btnStopPI2_Click(btnStopPI2, New EventArgs)
```

```
2111.  End Sub
2112.  Private Sub Button2_Click(sender As Object, e As EventArgs) Handles btnLoadMS.Click
2113.  Dim loadmethodMS As String
2114.  loadmethodMS = Microsoft.VisualBasic.InputBox("Enter the method name you wish to load: ", "MS Load
       method", "", 500, 700)
2115.  If loadmethodMS = "" Then
2116.  MessageBox.Show("Did not enter method name!")
2117.  Exit Sub
2118.  End If
2119.  Dim counter2 As String = ""
2120.  Dim counter5 As String = ""
2121.  Dim counter6 As String = ""
2122.  Dim counter12 As String = ""
2123.  Dim counter10 As String = ""
2124.  txtboxDesorptiontimeauto.Clear()
2125.  txtboxdesorptionvolume.Clear()
2126.  txtboxWashflowrate.Clear()
2127.  txtboxWashtime.Clear()
2128.  counter2 = System.IO.File.ReadAllLines("D:\Emir Desktop\MOI photometric\Flow Control (MS)_v6 -
       2022_03\MS Methods\" & loadmethodMS)(0)
2129.  txtboxDesorptiontimeauto.Text = Convert.ToInt32(counter2)
2130.  counter5 = System.IO.File.ReadAllLines("D:\Emir Desktop\MOI photometric\Flow Control (MS)_v6 -
       2022_03\MS Methods\" & loadmethodMS)(1)
2131.  txtboxdesorptionvolume.Text = Convert.ToInt32(counter5)
2132.  counter6 = System.IO.File.ReadAllLines("D:\Emir Desktop\MOI photometric\Flow Control (MS)_v6 -
       2022_03\MS Methods\" & loadmethodMS)(2)
2133.  txtboxWashflowrate.Text = counter6
2134.  counter12 = System.IO.File.ReadAllLines("D:\Emir Desktop\MOI photometric\Flow Control (MS)_v6 -
       2022_03\MS Methods\" & loadmethodMS)(3)
2135.  txtboxWashtime.Text = counter12
2136.  End Sub
2137.  Private Sub btnSaveMS_Click(sender As Object, e As EventArgs) Handles btnSaveMS.Click
2138.  Dim savemethodMS As String
2139.  savemethodMS = Microsoft.VisualBasic.InputBox("Enter the file name: ", "Save method", "", 500, 700)
2140.  If savemethodMS = "" Then
2141.  MessageBox.Show("Enter method name to save a method!")
2142.  Exit Sub
2143.  End If
2144.  Dim methodparametersMS As String
2145.  methodparametersMS = txtboxDesorptiontimeauto.Text + vbCrLf + txtboxdesorptionvolume.Text + vbCrLf
       +  txtboxWashflowrate.Text + vbCrLf + txtboxWashtime.Text
2146.  Using file = My.Computer.FileSystem.OpenTextFileWriter("D:\Emir Desktop\MOI photometric\Flow
       Control (MS)_v6 - 2022_03\MS Methods\" & savemethodMS, False)
2147.  file.WriteLine(methodparametersMS)
2148.  file.Close()
2149.  savemethodMS = ""
2150.  End Using
2151.  End Sub
2152.  End Class
```